INFORMATION TO USERS

This manuscript has been reproduced from the microfilm master. UMI films the text directly from the original or copy submitted. Thus, some thesis and dissertation copies are in typewriter face, while others may be from any type of computer printer.

The quality of this reproduction is dependent upon the quality of the copy submitted. Broken or indistinct print, colored or poor quality illustrations and photographs, print bleedthrough, substandard margins, and improper alignment can adversely affect reproduction.

In the unlikely event that the author did not send UMI a complete manuscript and there are missing pages, these will be noted. Also, if unauthorized copyright material had to be removed, a note will indicate the deletion.

Oversize materials (e.g., maps, drawings, charts) are reproduced by sectioning the original, beginning at the upper left-hand corner and continuing from left to right in equal sections with small overlaps. Each original is also photographed in one exposure and is included in reduced form at the back of the book.

Photographs included in the original manuscript have been reproduced xerographically in this copy. Higher quality 6" x 9" black and white photographic prints are available for any photographs or illustrations appearing in this copy for an additional charge. Contact UMI directly to order.

UMI

A Bell & Howell Information Company
300 North Zeeb Road, Ann Arbor MI 48106-1346 USA
313/761-4700 800/521-0600

Investigation on New Low Cost Electronically Controlled Fuel Metering Systems for Small Gas Turbine Engines

Seyed Saeid Mohtasebi

A Thesis

in

The Department

of

Mechanical Engineering

Presented in Partial Fulfilment of the Requirements

for the Degree of Doctor of Philosophy at

Concordia University

Montreal, Quebec, Canada

February 1997

ABSTRACT

Investigation on New Low Cost Electronically Controlled Fuel Metering Systems for Small Gas Turbine Engines

Seyed Saeid Mohtasebi, Ph.D.

Concordia University, 1997

This work introduces two new low cost, electronically controlled fuel metering systems for small gas turbine engines, particularly applicable in remotely piloted vehicles. The first one incorporates a diaphragm operated flat-seat bypass valve to maintain a constant differential pressure across the metering valve, which is actuated by a digital linear actuator. In the second one, both the metering and the bypass valves are controlled by two independently operated digital linear actuators.

The mathematical models for the first fuel metering system, were created and used for computer simulation. Next, after preparing the experimental test set-up, the manufactured prototype was tested and the models for both the steady state and the dynamic response were validated. Three design optimization criteria, fuel flow linearity, low sensitivity to the design parameters changes and fast dynamic response were examined to improve the performance of the proposed fuel metering system. Finally, a multi-objective optimization technique was developed and implemented to obtain the best design parameters of the system.

For the second fuel metering system, first the mathematical models for both the steady state and dynamic response were developed. Next, due to the flexibility

offered by this system, different control strategies for controlling the digital linear actuators during the normal operation mode of the actuators and also during the back-up operation modes were introduced and investigated. Finally, to investigate the impact of different control strategies on the dynamic response of the engine, a dynamic model for the engine was also developed and used.

At the end, four available fuel metering systems, including the two new ones, were compared regarding their deviation from the fuel flow linearity, dynamic response and the cost.

ACKNOWLEDGEMENTS

The author would like to express his sincere and deep appreciation to Dr. T. Krepec for providing constant enthusiastic help and guidance leading to this dissertation. Thanks are also extended to Dr. H. Hong for his valuable support and advice.

Thanks are also due to the Ministry of Culture and Higher Education of Iran for its financial support without which the present work would not have been possible.

The author is also grateful to the technical staff of the machine shop for manufacturing several parts of the fuel metering system prototype and to Mr. John Elliott and Wesley Fitch for their help in instrumentation.

Finally, the author would like to dedicate this work to the members of his family who always stood behind him with great patience and encouragement.

TABLE OF CONTENTS

Page

CHAPTER 5

CHAPTER 6

CHAPTER 7

CHAPTER 8

CHAPTER 9

LIST OF FIGURES

NOMENCLATURE

A_{10}	Curtain Area Through Diaphragm Orifice (m^2)
A_{bv}	Bypass Valve Flow Area (m^2)
A_d	Diaphragm Effective Area (m^2)
A_{do}	Vibration Damping Orifice Flow Area (m^2)
A_{dv}	Diaphragm Valve Orifice Flow Area (m^2)
A_i	Nozzle Flow Area (m^2)
A_{mv}	Metering Valve Flow Area (m^2)
A_{mp}	Minimum Pressurizing Valve Flow Area (m^2)
A_n	Nozzle Manifold Inlet Cross Section Area (m^2)
B	Damping Coefficient (N.m/ s)
C	Compensation Factor for Fuel Momentum (%)
C_1	Pump Displacement (m^3/ s/ rpm)
C_2, C_4	Pump Leakage Coefficient (m^5/ s/ N)
C_3	Pump Displacement (m^3/ s/ Volt)
C_{dbv}	Flow Coefficient for Bypass Valve
C_{ddo}	Flow Coefficient for Damping Orifice
C_{ddv}	Flow Coefficient for Diaphragm Valve Orifice
C_{dmv}	Flow Coefficient for Metering Valve
C_{dmp}	Flow Coefficient for Minimum Pressurizing Valve
C_{dn}	Flow Coefficient for Nozzle Orifice
dQ_n	Change in Nozzle Flow (m^3/ s)
D_{bv}	Bypass Valve Diameter (m)
D_n	Nozzle Manifold Diameter (m)
f	Metering Valve Actuator Triggering Frequency (Hz)
f_{bv}	Bypass Valve Actuator Triggering Frequency (Hz)
F_{SP}	Spring Preload Force (N)
ITAE	Transient Response Index (%)

J_M Engine Moment of Inertia ($N.m.S^2$)

K Number of Simulation

K_S Spring Constant (N/ m)

LIN Variation of Differential Pressure Index (%)

M_d Diaphragm Mass (kg)

M_e Effective Diaphragm Mass (kg)

M_{mvf} Final Steady State Nozzle Flow (kg/ h)

M_{mvi} Nozzle Flow at the i-th Step of Simulation (kg/ h)

n_{sbv} Number of Bypass Valve Slits

n_{smv} Number of Metering Valve Slits

N Engine Speed (rpm)

N_{nom} Engine Nominal Speed (rpm)

N_P Pump Speed (rpm)

P_0 Ambient Pressure (N/ m^2)

P_1 Pump Pressure (N/ m^2)

P_2 Metering Valve Down Stream Pressure (N/ m^2)

P_C Compressor Pressure (N/ m^2)

P_{max} Engine Maximum Power (W)

P_n Nozzle Pressure (N/ m^2)

P_u Upper Diaphragm Valve Chamber Pressure (N/ m^2)

Q Constant Pump Flow (m^3/ s)

Q_{bv} Bypass Valve Flow (m^3/ s)

Q_{do} Damping Orifice Flow (m^3/ s)

Q_{dv} Diaphragm Valve Orifice Flow (m^3/ s)

Q_{mv} Metering Valve Flow (m^3/ s)

Q_{mp} Minimum Pressurizing Valve Flow (m^3/ s)

Q_n Nozzle Flow (m^3/ s)

Q_P Pump Flow (m^3/ s)

SENS Sensitivity Index (%)

t Running Simulation Time (s)

T_C Compressor Torque (N.m)

T_d Damping Torque (N.m)

T_l Load Torque (N.m)

T_{max} Engine Maximum Torque (N.m)

T_t Turbine Torque (N.m)

V Pump Input Voltage (Volt)

V_1 Volume of the High Pressure Chamber (m^3)

V_2 Volume of the Metering Valve Down Stream (m^3)

V_n Volume of Nozzle Manifold (m^3)

V_u Volume of Upper Diaphragm Valve Chamber (m^3)

w Width of Metering Valve Slits (m)

w_{bv} Width of Bypass Valve Slits (m)

wi Weight on Objective Function

X_{mv} Metering Valve Plunger Position (mm)

X_{bv} Bypass Valve Plunger Position (mm)

y Diaphragm or Bypass Valve Plunger Position (m)

y_{max} Diaphragm Maximum Displacement (m)

α Angular Acceleration (rad / s^2)

β Bulk Modules of Fuel (N/ m^2)

ΔP Differential Pressure Across the Metering Valve (N/ m^2)

ΔP_{mean} Average Differential Pressure over the Metering Valve Movement (N/ m^2)

ΔP_i Differential Pressure Observed over the Flow Schedule (N/ m^2)

Δt_i Current Time Step (s)

ΔX_{mv} Metering Valve Actuator Step Size (m)

ΔX_{bv} Bypass Valve Actuator Step Size (m)

ρ Fuel Density (kg/ m^3)

ω Angular Velocity (rad/ s)

1. INTRODUCTION

The contemporary trend in industry towards simplification and performance increase of mechanical systems with simultaneous cost reduction, as a result of the implementation of electronic controls, has its impact also in the area of small gas turbine engines for aircraft. However, unlike large civil and military aircraft, the smaller and less expensive airplanes, helicopters and drones cannot afford the implementation of expensive parallel multi-channel electronic control systems which are dictated by the reliability and safety requirements. Because the level of complexity and range of operation of the control systems for small and large aircraft is not much different, some new, original alternatives should be developed for the small aircraft to satisfy the conflicting requirements about performance, safety and cost of their fuel control systems.

The present electronic fuel control units (EFCU's) for small gas turbine engines do not differ much from their older hydromechanical predecessors (FCU's) regarding their principle of operation. The main modifications are in the use of electronic actuators instead of bellows for the fuel flow metering and in replacing the mechanical speed governor with an electronic one based on the measurement of engine rotational frequency by a simple magnetic pickup sensing the Hall-effect. These two main electronic components are improving the engine operational performance without changing much the mode of operation of the fuel control system. Therefore, the cost of the fuel control system with electronic control remains quite low as compared with the cost of the gas turbine engine.

To reduce more the cost of the modern fuel control system, further

simplification of its main components would be required, however, without compromising the engine performance and the aircraft safety. The components taken into consideration would be the fuel pump and the fuel metering system. The following discussion describes possible ways of lowering the cost of these two components.

A typical constant displacement fuel pump is usually driven by the engine, so its fuel delivery rate is closely proportional to the engine speed. However, the engine fuel consumption rate characteristic versus speed is highly nonlinear. This means that in the mid speed range, the pump is delivering an excess of fuel which has to be bypassed (spilled back) to the tank, resulting in some energy losses and making the fuel metering system more complicated. A possible solution is to use a fuel pump with a variable displacement volume; however, such a pump is more complicated and expensive. Therefore, the ideal solution would be to have a pump which delivers only as much fuel as it is required by the engine; such a pump could be driven by a variable speed electric motor under electronic control. In this case, the fuel pump drive arrangement is simpler and less expensive.

The fuel metering system is usually based on two components: a metering valve and a bypass valve or a differential pressure valve. The metering valve is controlling the area of the fuel flow and the bypass valve or the differential pressure valve is maintaining a constant differential pressure across the metering valve. This constant pressure drop feature is providing the fuel metering system with linear fuel flow in response to the metering valve travel and is independent of the nozzle pressure. Thus, the system is designed to be less sensitive to the changes in the flow area of the fuel nozzle orifices in case of possible carbon deposit accumulation during

the service time of the engine. However, the metering valve usually requires machining of complicated shapes to maintain its linear fuel delivery schedule and the bypass valve can be also quite complicated in design.

Regarding the fuel metering system, there are following options for improvement:

1. It could be made less expensive by using a low cost linear digital actuator which is able to overcome a possible "jammed" metering valve.
2. It could be made less costly by simplifying the design of the bypass valve.
3. It could be improved by integrating the action of the metering valve with the bypass valve both equipped with independent linear digital actuators, without maintaining the principle of constant pressure drop across the metering valve; this could provide a faster dynamic response of the system in a transient process.
4. Regarding the possibility of a backup operation of the system, in case of failure of one of the components mentioned in item 3, there would be a possibility to use the second component only to schedule the fuel flow as required for the engine operation. The fuel delivery accuracy, particularly at transient operations, would suffer; however, the objective is to return the aircraft to its base.

It is anticipated that the above assumptions are feasible; they are based on the present state of the art of the electronic fuel control systems. This will be confirmed in the following literature review.

2. LITERATURE REVIEW

From the beginning of the jet era, hydromechanical technology has been predominant in the fuel supply control of gas turbine engines [1]. However, presently conventional hydromechanical fuel controls could not keep up with advances in modern aircraft propulsion systems and thus, analog and later digital electronic controls became a viable alternative in responding to the requirements of modern gas turbine engines. The importance and potential benefits of the increased flexibility offered by microelectronics with digital controls and their rapid improvement, have made practical the engine-mounted electronic fuel controls for different types of airplanes and helicopters. The capabilities of microelectronics for use in gas turbine engines were investigated by several researchers. Already in 1965, Peck [2] described the advantages of a microelectronics fuel control in meeting the requirements of an airborne propulsion turbine engine and Falk [3] demonstrated a logical method through which electronics might be successfully applied for the same purpose.

In 1974, the AiResearch Manufacturing Company of Arizona, a division of the Garret Corporation reported the development of a full authority electronic fuel control system for a small gas turbine engine [4]. The basic objective was to create an integrated fuel control and propeller governor system fully compatible with engine characteristics so that optimum engine performance would be attained during all ground and flight processes within the engine operating envelope. The control system employed electronic, hydraulic, pneumatic, and mechanical components which resulted in enhanced performance and reliability characteristics. The controller was developed for use in the Garret model TFE731-2 turboprop engine and its computer

was an analog device using operational amplifiers. The control system completed the qualification requirements and entered the production phase in August 1972; throughout the engine development program, 19,000 engine operating hours were accumulated. In addition, 3000 in-flight hours on the Dassault Falcon 10 Aircraft and on the Gates Learjet 35/36 Aircraft were logged.

As a result of the experience gained with the AiResearch TFE731-2 in 1981, the Garrett Turbine Engine Company, also a division of the Garrett Corporation developed and certified a similar electronic control system for use in the Model TPE331 turboprop engine manufactured by Garrett [5]. Many of the circuits developed and proven in service for the TFE were used directly in the TPE331 system with little or no modification. The new system provided automatic engine starting, engine speed switching functions, accelerating fuel scheduling, speed governing, overspeed protection, isochronous propeller governing, and monitoring functions.

In both of the above systems, the computer used was an analog device and it received inputs from various sensors mounted on the engine and from the fuel control unit. It performed complex computations and produced output signals to drive actuating devices like torque motors [6]. Finally, the Garrett research program resulted in the development of the TFE731-5 digital electronic controller for use in executive jet aircraft [7].

In early 1970's, the incorporation of the digital computer made a "quantum jump" in the computational and logical capabilities of the engine controls. The digital electronics is distinct from an analog control in that all input data are acted upon sequentially in the digital domain, rather than continuously, as in an analog system. Data processing is performed at very high speed in relation to the process being

controlled. It is also capable of detecting and taking alternative action in response to erroneous or missing data. The analog electric controls had computational limitations, performing one function for each module. The flexibility of digital electronic controls allowed the requirements for many applications to be met with similar hardware, providing a positive impact on a large part of the General Aviation Market [8].

In late 1960's, a program for use in a F-100 military engine was initiated in which a digital minicomputer was introduced in a supervisory role to assist the hydromechanical control in performing the increasingly complex power management function. This program has resulted in the successful development of the first engine mounted digital controller to enter military operational service [9].

As a result of the outstanding success of the above program, a digital supervisory control program was launched in 1972, for the commercial JT10D engine. This control system represented a quantum jump in commercial engine control performance. During 1974-1975, Boeing, Pratt and Whitney and Hamilton Standard conducted a joint demonstration program of this propulsion control system with the objective of evaluating the potential benefits of a fully electronic configuration. The program showed that the self-diagnostic capability of the digital machines would permit design of future control systems with higher operational reliability than any available engine controls [9].

In 1976, a multi-mode propulsion control system concept was developed for the remotely piloted research vehicle (RPRV) of the NASA Highly Manoeuvrable Aircraft Technology (HiMAT) program [10]. The overall purpose was the flight evaluation of advanced technology concepts for fighter aircraft, through the use of a low-cost, unmanned, remotely piloted, land recoverable vehicle. The HiMAT system

consisted of RPRV, the B52 launch aircraft, the NASA/DFRC ground control station, and the airborne backup control station [11].

In 1975, Bussell of Marconi-Elliott Avionic Systems Ltd., described the design of an engine mounted, digital fuel control system for a twin coupled, helicopter engine configuration [12]. The system was described from the point of view of the failure survival requirements. He highlighted the contribution of the digital system to the implementation of these requirements and also the environmental design techniques adopted to achieve maximum reliability.

Aviation Electric Limited, in close collaboration with the Canadian National Research Council (NRC) through a technology program funded jointly by the Canadian Government and the Bendix Corporation, generated a detailed hybrid computer model of gas turbine propulsion system [13]. The object was to develop not only the design tool but also the methodology to adapt the tool to suit any engine type, i.e., turboshaft, turbofan, or turboprop. Subsequent to model generation, a supporting engine test program was established to provide validation data for the model. The system selected was the Pratt & Whitney PT6T-400 Twin-pac engine driving a Bell UH-1 helicopter rotor. The engine was controlled by Bendix DP-F2 fuel controller and due to availability of an original engine model [14], the first generation of Full Authority Digital Controller (FADC) was designed. The FADC was a microprocessor based controller composed of an electronic control unit (ECU) driving a mechanical flow body containing the fuel metering valve. All the computational functions previously performed in the controller were implemented at ECU. The essentially real time computing capability of the engine simulation permitted communication with the ECU directly. However, the flow body was

represented within the hybrid computer model.

A second generation of digital controllers with the acronym NDEC (Speed (N) based Digital Electronic Control) was also used to obtain the validation data [15]. In fact, its very existence as a viable controller places credibility in the engine model because the control modes were designed using the engine model directly. The NDEC featured a number of novel concepts and controlled the engine through gas generator acceleration scheduling, as opposed to fuel delivery ratio which is fuel mass flow over compressor pressure ($\dot{m}_f/P_C$). Moreover, in the above research, a fuel controller was designed which employed innovative control mode concepts using the engine model directly to define the control mode parameters.

Full Authority Digital Electronic Control (FADEC) has been increasingly used by various manufacturers for the control of aircraft engines or aircraft auxiliary power units. The configurations of the controllers differ from one application to another but in general, each control designer is trying to find an optimal solution to sometimes conflicting requirements. The advantage of FADEC control over classical hydromechanical control: its increased reliability, flexibility in accommodating a large range of requirements and reduction of pilot workload, were well acknowledged in references [16], [17].

In 1976, a FADEC program, sponsored by the Naval Air Systems Command, directed by the Naval Air Propulsion Centre and performed by Pratt & Whitney Aircraft, was initiated [18], [19]. The FADEC objective was to design, fabricate and test an engine-mounted, flight type, digital electronic control for advanced military aircraft gas turbine engines. This control was designed to satisfy increased engine functional and environmental requirements, reduce life cycle costs, and improve

reliability and maintainability. The FADEC system concept featured gas generator fail-operational fault tolerance capabilities through the use of redundant sensing, computation and command paths, parameter synthesis and self-test techniques. Incorporation of advanced electronic circuit technology and a reduction in the use of complex hydromechanical hardware resulted in more than a 43% reduction in acquisition cost, a 26% reduction in weight, and a 130% improvement in piece part reliability on an overall control system basis, as compared with a system configured with the latest current production control technology. The engine selected for using the control was the General Electric Variable Cycle Engine; a uniquely configured F404. This engine was a low bypass ratio, variable compressor geometry twin spool turbofan with an after burner. The General Electric FADEC, was programmed to operate with standard F404 control strategy and upon external command to shift to a strategy producing automatic control of a Variable Cycle Technology (VCT) feature. The FADEC microprocessor was also programmed to provide Failure Indication and Corrective Action (FICA) that utilized a real time engine model to calculate and substitute replacement values for sensed values of fan speed, core speed, compressor discharge pressure, compressor inlet temperature, low-pressure turbine discharge temperature, and main engine fuel flow. Actuator Failure Indication and Corrective Action (AFICA) as well as adaptive starting fuel scheduling, were also demonstrated at the General Electric Company, Lynn, Massachusetts (sea level test), and at Naval Air Propulsion Centre (altitude test). The engine mounted FADEC accumulated over 134 hours of engine operation during the tests [20].

New FADEC systems have been designed to include a number of fault-tolerant features to enhance the operational reliability and maintainability. A Full Authority

Fault Tolerant Electronic Engine Control (FAFTEEC) program was sponsored by the U.S. Air Force to identify the basic redundancy requirements in the design architecture of control systems that provide very high levels of mission reliability [21]. The system reliability goal for the FAFTEEC program was specified in terms of a maximum acceptable level of 25 failures per million engine flight hours with a desired level of 2.5 failures per million engine flight hours. An additional goal for transfer to hydromechanical backup control was established at an order of magnitude less than that for the system reliability goal. The program combined the design expertise of Pratt & Whitney Aircraft (gas turbine Propulsion control system), Hamilton Standard (engine mounted digital electronic computers), and Charles Stark Draper Laboratories (fault tolerant control architecture and reliability modelling). This team configured several candidate FAFTEEC systems with varying levels of redundancy and then evaluated these systems to project system mission reliability, maintenance reliability, cost, weight, and cost of ownership.

In keeping with the general industry trend of applying FADEC technology to small gas turbine engines, Textron Lycoming and Chandler Evans Division of Coltec Industries [22] developed and qualified a single channel control system for use on the Textron Lycoming LF507-1F turbofan engine. The LF507-1F was the world's smallest FADEC-equipped airline turbofan engine and was the only FADEC-equipped turbofan developed and certified for the regional jetliner market. The used FADEC employed modern control algorithms to achieve surge-free operation over the flight envelope while providing rapid transient performance and crisp handling qualities. The control interfaced with the aircraft via ARINC 429 (Aeronautical Radio Incorporation [23]) data link to control each engine automatically to a desired power

setting. A simple hydromechanical backup control provided full dispatch capability in case of critical FADEC system failure. In addition, the FADEC included advanced diagnostics for fault identification to the line replaceable unit (LRU) level without specialized test equipment.

Similar research work has been done by other manufacturers. In 1991, Pratt & Whitney Canada reported that it had chosen to use FADEC control for its new PW305 turbofan engine in the 5000 lb (22.2 kN) thrust range [24]. The objective of the program was to provide the optimum engine operation within safe limits, reduced pilot workload and high reliability over the whole flight envelope.

In 1980, a full authority, dual channel, fault tolerant digital electronic control system for aircraft gas turbine engines was designed by the Bendix Energy Controls Division and flight-tested on the Boeing 747 research aircraft [25]. This effort was part of a cooperative program between Boeing Commercial Airplane Company, Pratt & Whitney Aircraft, Bendix Energy Control Division, and Hamilton Standard to demonstrate the improved capability of a totally Electronic Propulsion Control System (EPCS). The EPCS configuration incorporated two full authorities electronic control channels both of which responded to the airplane and engine in a completely redundant and independent manner. Two electronic computers were connected to the FCU and power to the electronic units was provided by two independent alternators driven from the engine gearbox. The electronic unit consisted of four major sections: input signal conditioning, multiplexing and digital conversion, processor and memory, and output drivers. The control used two microprocessors: a processor for data acquisition and a processor for control. The data acquisition processor handled all functions related to input data from A/D converter, speed, resolver angle, pressure

conversion, discrete digital signals, and ARINC/ data from the aircraft bus. The second processor performed the control calculation using data obtained from data acquisition processor and communication between processors was accomplished by direct memory access of the data acquisition processor's memory by the control memory. The CPU of each channel was implemented with two Texas Instruments TI-SBP 9900A IIL (Integrated Injection Logic) microprocessors in a dual processor architecture [26].

In 1982, Zuliani and Kline of Hamilton Standard reported the development of a new digital microprocessor based electronic control system for small gas turbine engine applications [27]. The Hamilton Standard multi-application control system (MACS) combined the computing power of a modern digital microprocessor with the reliability of hydromechanical control unit which was also used as a manual backup. The basic design concept allowed the control system to be applied to turboprop, turboshaft, and turbofan applications with only minor modifications. The microprocessor-based ECU was designed to have a high degree of hardware commonality among all three engine applications, to achieve the goal of cost-effective control. In this regard, the electronics within the ECU contained one digital board which was common to all applications and an analog board which changed with each application. The ECU contained a 8039 microprocessor with 128 words of internal RAM and 4096 words of external PROM. All analog signals were conditioned in their respective conditioning circuit and then multiplexed through an eight bit A/D converter. Moreover, all digital signals were processed by frequency to digital circuits prior to the use by the microprocessor and its software program [28].

For unmanned applications in missiles and remotely piloted vehicles (RPV's),

there has been a more general acceptance of full authority electronic computation in engine mounted fuel controls than in the case for man-carrying applications. This largely results from the fact that the same level of redundancy and/or backup modes, in case of a computer fault, is usually not considered necessary in the unmanned case [29]. Missile and RPV gas turbine engines are characterized by requirements for small size (usually less than 22 kN trust) and weight, short life and low cost. High reliability is also most important, both operational and for prolonged periods of storage. During 1973 and 1974, a program was conducted by Chandler Evans, under contract to the U. S. Air Force Aero Propulsion Laboratory (AFAPL), to investigate and develop control technology for 1976-1980 engines in the 4.4 kN thrust class [30]. The program was aimed particularly at the development of control components and high speed pump technology for future missile and RPV systems. In this program, mostly analog computation was used because at that time, digital computation was still expensive and was not as reliable as the analog system.

In 1989, Georgantas and Krepec [31, 32] presented a simple and low cost fuel metering system for the Garret ETJ 1081 turbojet engine applicable in a RPV. The proposed metering system consisted of only a metering valve operated by a digital linear actuator and controlled by an on-board microcomputer. It was the simplest and most less expensive solution for that type of engine, however, not feasible for longer engine service due to the fact that the fuel flow rate to the engine would be much dependent on the flow rate of the engine nozzles which are susceptible to contamination. Also, the accuracy of fuel delivery would be difficult to achieve at low flow rates. However, with the flexibility of the electronic control, this design was considered feasible, particularly for missile applications.

Continuing with the above research and in order to improve the performance of the above fuel metering system, Carrese et al in 1990 [33] proposed a new simple and inexpensive electronically controlled metering system for small gas turbine engines. The proposed system was partly based on the Bosch K-Jetronic [34] fuel injection system concept for gasoline spark ignition (SI) engines. In the original system, the metering valve was operated mechanically by an air-flow meter and the metered fuel flow was divided equally among engine cylinders, each having its own differential pressure valve. However, in the proposed system, the metering valve was operated electronically and there was only one large diaphragm valve to control the differential pressure across the valve. The new system required close to constant fuel supply pressure which could be assured either by a constant displacement pump with a pressure regulating valve or by a centrifugal pump driven by the engine.

To overcome the limitations of the above system, i.e. low fuel flow rate, and to reduce the sensitivity to the increase of the nozzle manifold pressure due to the build-up of the carbon deposits in the nozzles, a new design was presented by Georgantas et al [35]. In this system, the metering valve of Bosch K-Jetronic fuel injection system was interfaced with a bypass valve of the design used in the Bendix DP-F2 fuel control system [36]. The bypass valve spilled the excess of fuel discharged by the pump so that only this portion of fuel which was passing through the metering valve, was injected into the engine. The metering valve consisted of a plunger which changed the flow area by exposing four longitudinal slits on the valve barrel. With the plunger position proportional to the flow area, a constant differential pressure ensured linearity between the fuel delivery and the metering valve position. A damping orifice was also used to stabilize the bypass valve motion by restricting

the fuel flow from and to the top chamber of the bypass valve.

Due to the complexity of the plunger and barrel of the Bendix bypass valve presented above and its higher cost, a new concept was presented by Krepec et al [37] in 1991. It proposed a new design of the bypass valve based on the K-Jetronic differential pressure valve. However, it was not controlling the fuel flow to the nozzle but the return bypass flow to the tank. This design seems to be the simplest and cheapest one of all being analyzed; however, it requires further investigation.

The feasibility of electronic fuel control unit operating both metering and bypass valves was investigated by Krepec et al [38] in 1991. The analysis was a direct follow-up to the investigation of the electronic fuel control unit in which only the metering valve was under microprocessor control. The concept assumed the use of two digital electronic actuators which operated the metering valve and the bypass valve independently. The flexibility of this configuration offered a possibility to perform functions not possible by conventional fuel control units or by the single actuator electronic unit already discussed. A unique backup capability was also possible and in case of the failure of one valve, the other valve could perform fuel scheduling. Moreover, to evaluate the performance of the proposed fuel control unit and to establish an appropriate control strategy, the interaction between the fuel control unit and the engine was studied by forming a mathematical model for the entire system. The acceleration and maximum speed governing processes were investigated by simulating the engine speed transition from idle to maximum speed.

In electronic fuel control systems, it is very important to choose properly the parameters of the digital controllers. Thus, to overcome problems encountered in the design of controllers, three different configurations, the classical PD controller, the

Smith predictor and the Dahlin algorithms were analyzed and implemented by Georgantas et al [39]. An integral term was not included in the PD controller, since the stepper motor used in the system was of low inertia and integrated the executed steps. A model for the fuel control unit was needed for the two latter control structures, therefore, a first order model with a delay was used. Finally it was concluded that the Smith predictor and the Dahlin algorithms were superior to the conventional PD controller and performed better in the presence of the system transport delays.

Research and development on low cost electronic control systems for small gas turbine engines of remotely piloted vehicles was also performed by other companies. In this regard, the U.S. Air Force initiated an Integrated Reliable Fault Tolerant Control (IRFTC) for expandable turbine engines. The program was named INTERFACE II and the purpose was to develop and demonstrate the technology base needed by advanced, low cost, non man-rated turbine engine control systems. The major goal of the program was to significantly reduce the cost, size, and weight of the control system. In response to the requirements of the INTERFACE II program, Teledyne CAE designed a new low cost, light weight digital electronic control system applicable to the wide variety of drones, RPV's and missiles. The control system was successfully demonstrated on an engine in an altitude chamber at Teledyne. All components of the system, such as, fuel pump and metering device, actuators, engine sensors, and electronic hardware were thoroughly investigated and evaluated [40].

In 1993, engineers at Allied Signal Fluid Systems [41] introduced three valves which offered new approaches to fuel metering and control for medium gas turbine engines. The design approaches used for these valves incorporated several innovative

technologies, including high-temperature elastomeric seals, high-pressure shut-off capabilities, high-temperature brushless DC motor actuators, fibber-optic rotary output position sensor, no moving parts oscillating-jet flowmeter, high temperature rapid solidification aluminum alloy and closed-loop electronic fuel flow metering. All three were direct-drive, brushless dc motor actuated valves and used closed-loop position control or flow control. Depending on the design, one or two actuators was employed to effect position control via rotary variable differential transformer (RVDT) feedback to an electronic control unit. Furthermore, there was only one electric/electronic channel to control the metering element. However, it would be a straight forward improvement to provide a second electrical/electronic control channel that would significantly improve reliability. In 1992, the first design was successfully used to operate a JTAGG (Joint Turbine Advanced Gas Generator) for 51.5 h and 51 starts.

Summarizing this review, it has to be acknowledged that, despite the long and infinitive period of research, development, and implementation, the electronic fuel controls are still not fully accepted regarding their reliability. This is being overcome in larger aircrafts by the use of multichannel systems. However, the electronic fuel control systems are increasingly more recognized as improving the gas turbine engine performance due to their flexibility and accuracy [6].

3. LITERATURE REVIEW SUMMARY AND THESIS OBJECTIVES

The literature review of electronic fuel control systems confirmed the validity of the initial assumptions made in the introductory chapter, regarding the possibility of lowering the cost of fuel control systems for small gas turbine engines and thus the main areas of research have been also determined. In general, the modern electric/ electronic technology will be employed, since there is no doubt that such systems will prevail in the future.

3.1 Possible Solutions for Low Cost Fuel Metering Systems

There are several possibilities of improvement in the low cost fuel metering systems found in the literature; some of them will be presented below and discussed.

3.1.1 Metering Valve Only

Figure 3.1 shows a schematic of a simple and inexpensive metering valve configuration [31]. It is operated by a digital linear actuator and controlled by an on board microcomputer. However, its simplicity results in significant variations of the differential pressure across the metering orifice and, therefore, in high sensitivity to the potential changes in the nozzle flow area; which can occur due to the partly clogging of the nozzle orifices caused by carbon deposits. This valve is also providing a poor fuel scheduling resolution at lower flow range. However, this can be, to some extent, improved by proper shaping of the metering orifice, as shown in figure 3.2 [32].

The use of this simple metering valve would be recommended only in such remotely piloted vehicles which will be destroyed after short time of operation (missiles); in this case, the carbon deposits would not have enough time to develop in the nozzle orifice.

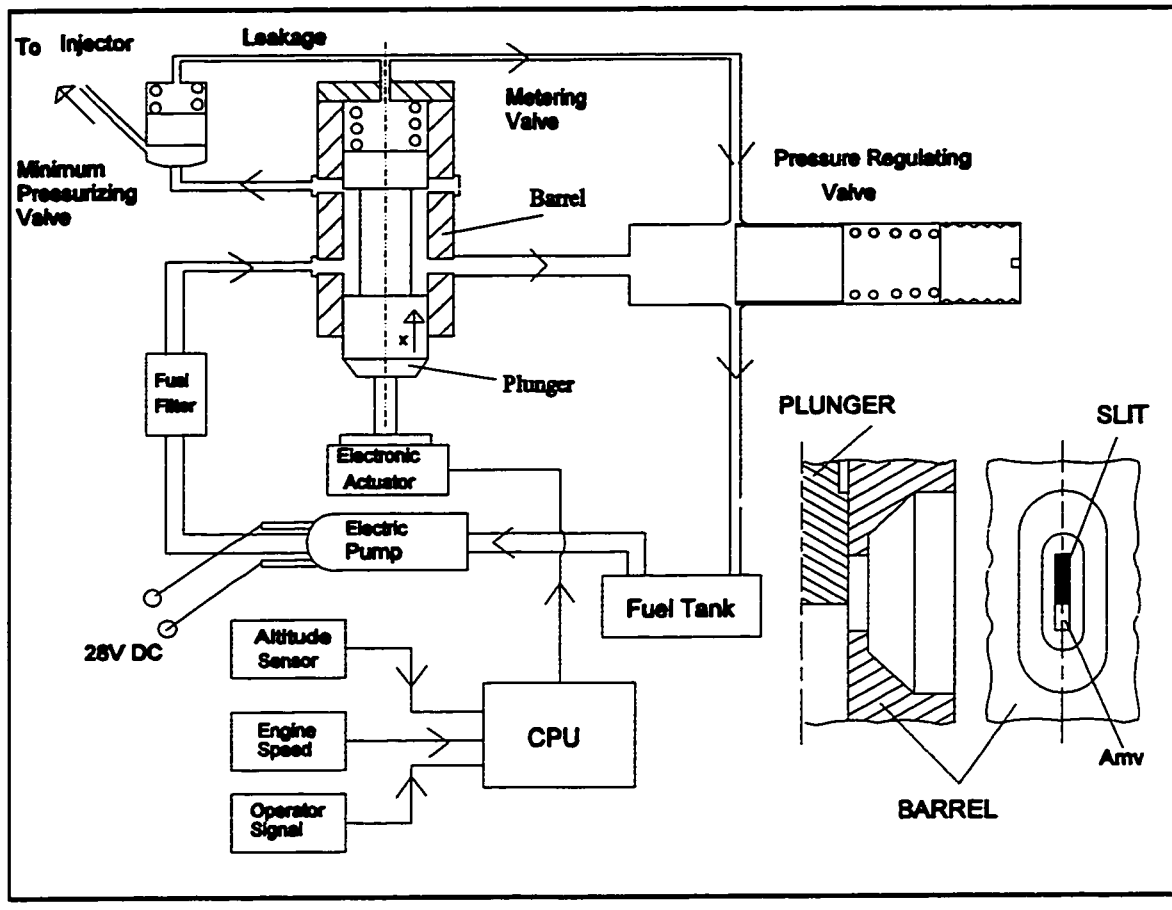

Figure 3.1 Schematic of a Metering Valve Only

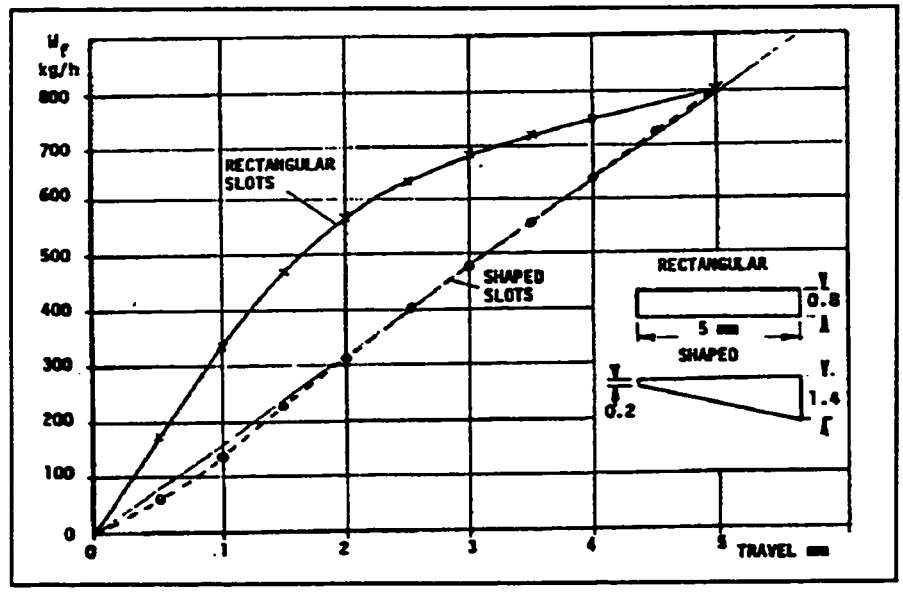

Figure 3.2 Fuel Flow vs. Metering Valve Travel Using Different Slit Shapes [32]

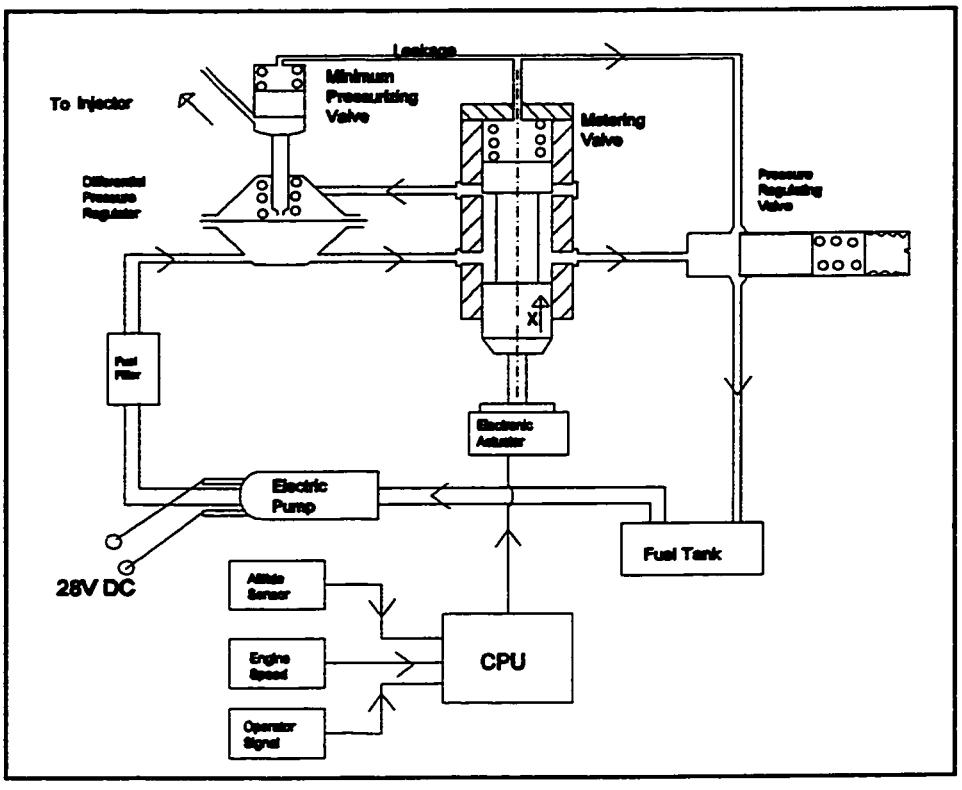

Figure 3.3 Schematic of a Metering Valve with Differential Pressure Flat-Seat Valve

3.1.2. Fuel Metering System with Differential Pressure Flat-Seat Valve and Constant Supply Pressure (Configuration 2)

Figure 3.3 shows a schematic of the metering valve with a differential pressure flat-seat valve configuration [33]. Similar metering and flat-seat valves are used in Bosch K- Jetronic fuel injection systems for automotive spark ignition engines [34]. A pressure regulating valve is maintaining a constant pressure in the fuel supply line and the differential pressure flat-seat valve is providing a constant differential pressure across the metering valve. Such a fuel metering system has all the features required for satisfactory fuel scheduling, including the close to linear relationship between the metering valve travel and the nozzle fuel flow rate; however the fuel flow rate is rather limited to small flow rates. This fuel metering system has reduced sensitivity to the nozzle orifice contamination by the carbon deposits and is simple and inexpensive, as compared with other valves used for similar purposes.

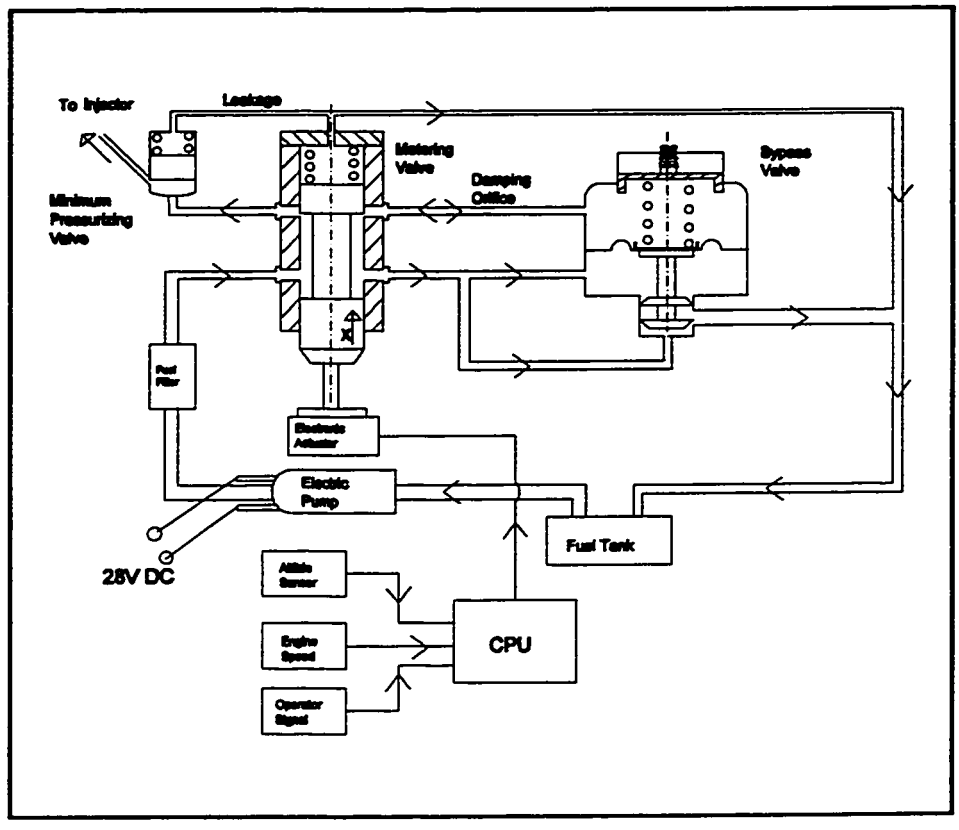

Figure 3.4 Schematic of a Metering Valve with Bendix Bypass Valve

3.1.3 Fuel Metering System with Bendix Bypass Valve and Varying Supply Pressure (Configuration 3)

Figure 3.4 shows a schematic of the metering valve with a plunger-type bypass valve configuration [35]. Such bypass valve is used in Bendix DP-F2 fuel control units [36]. The pressure in the metering valve is changing according to the nozzle pressure which depends on the fuel flow rate to the combustor and on the combustor pressure. This valve is more complicated and expensive to manufacture due to the complex design of its plunger-stem and barrel. It is used in thousands of DP-F2 fuel control units for small gas turbine engines which are some of the most popular fuel control units in the world.

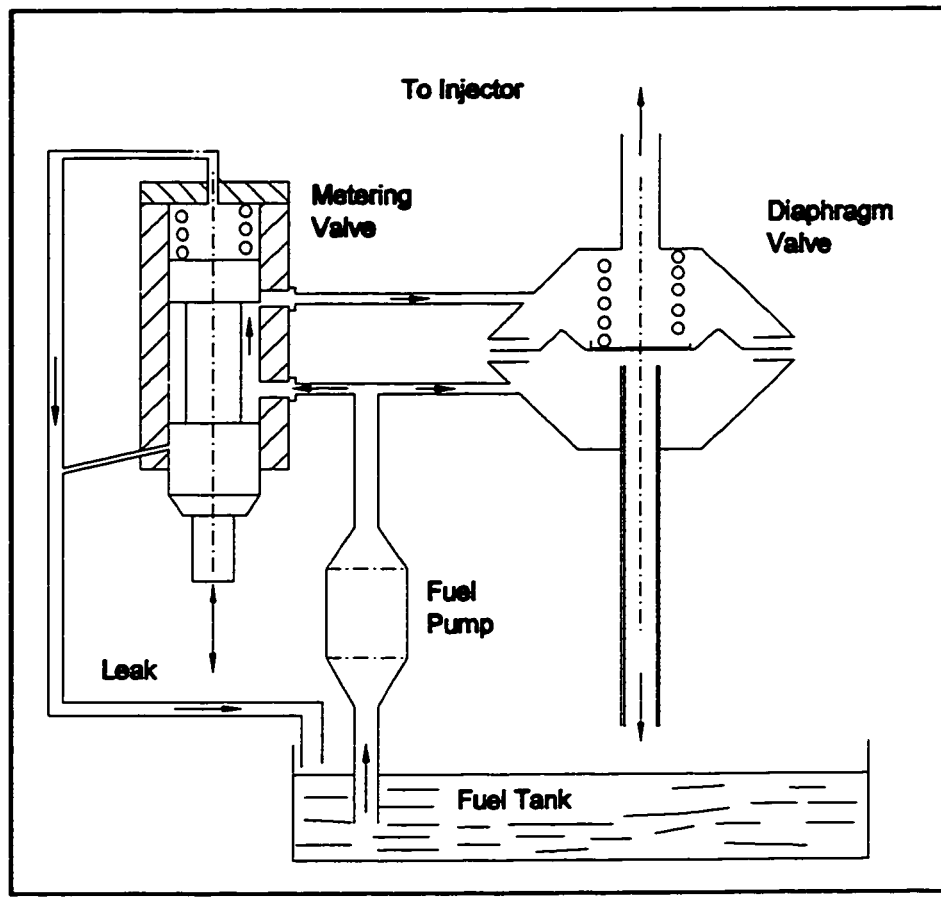

Figure 3.5 Schematic of a Metering Valve with the Diaphragm Flat-Seat Bypass Valve

3.1.4 Fuel Metering System with Diaphragm Flat-Seat Bypass Valve and Varying Supply Pressure (Configuration 1)

Figure 3.5 shows a schematic of a metering valve with a diaphragm flat-seat bypass valve configuration [37]. This is a new concept of the bypass valve which is worth to be fully investigated. It operates with a system pressure which varies depending on the fuel flow rate to the combustor and on the combustor pressure. It represents a low cost approach and a promise of adequate performance, while replacing the more expensive configuration of the Bendix bypass valve (figure 3.4).

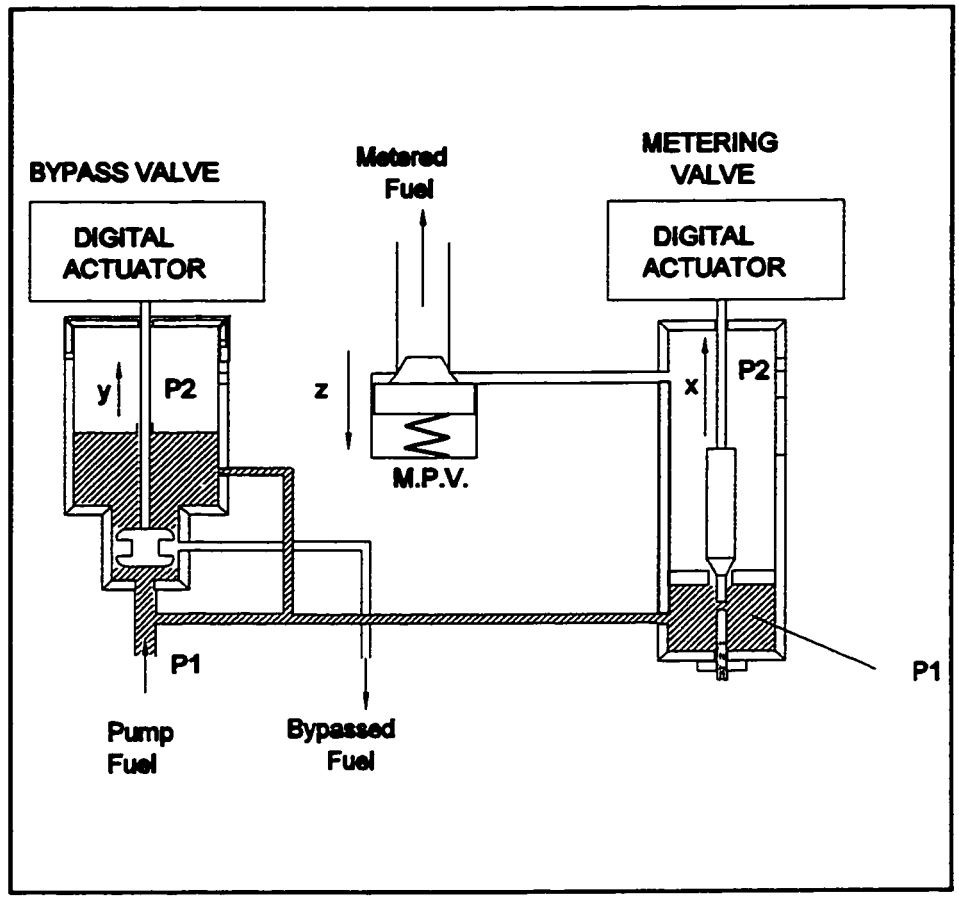

Figure 3.6 Schematic of a Double Valve Fuel Metering System

3.1.5 Double Valve Fuel Metering System with Varying Differential Pressure Across the Metering Valve

Figure 3.6 shows a schematic of a Bendix metering system consisting of a metering valve interfaced with a bypass valve both operated by two independent digital linear actuators [38]. The metering valve is controlling the fuel flow to the engine nozzles and the bypass valve is spilling the excess of fuel back to the tank. However, the pressure across the metering valve is not kept constant. It is regulated in such a manner that during a transient process, the fuel flow increases and decreases much faster, as compared with a conventional fuel system which is maintaining a constant differential pressure across the metering valve.

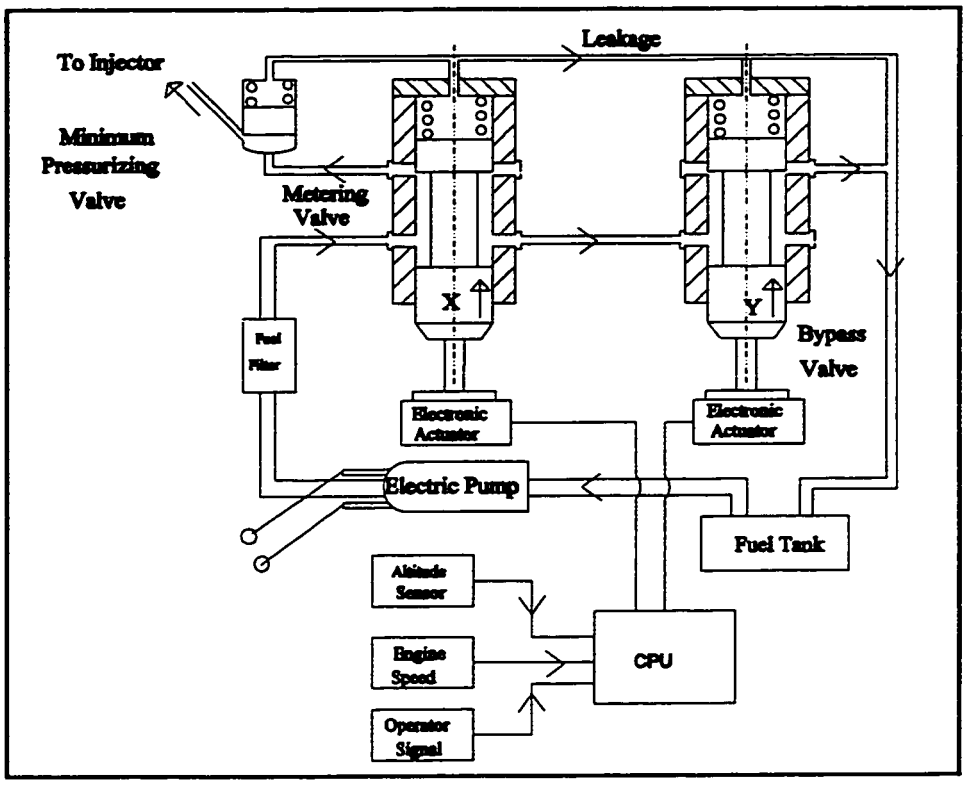

Figure 3.7 Schematic of a Double Barrel, Double Plunger Fuel Metering System

3.1.6 Double Barrel, Double Plunger Fuel Metering System with Varying Differential Pressure Across the Metering Valve and Backup Configurations (Configuration 4)

Figure 3.7 shows the schematic of a double barrel, double plunger fuel metering system operated by two digital linear actuators [32]. A metering plunger is controlling the fuel flow to the nozzles and a bypass plunger is spilling the excess of fuel back to the tank. Thus, the pressure across the metering valve plunger is not constant and is controlled in such a way that, during the engine transient process the rate of the fuel flow change be much faster than that of conventional fuel metering systems.

This fuel metering system includes a back-up feature. If one of the plungers fails to operate, the second plunger takes over and provides the fuel flow to the engine so that the aircraft will be able to return home. This is a new concept of a fuel metering system and should be further investigated.

3.2 Thesis Objectives

Two of the above presented fuel metering systems which are new, have been chosen for further design analysis and simulation: the metering valve with diaphragm flat-seat bypass valve and varying system pressure (configuration 1 as described in 3.1.3) and the double barrel, double plunger fuel metering system with back-up capabilities (configuration 4 as described in 3.1.5). These two novel fuel metering systems are quite simple and represent low cost solutions. The first one can be considered as a low cost alternative to the bypass valves in many existing fuel metering systems like the Bendix DP-F2 fuel control unit, maintaining constant differential pressure across the metering valve. The second one offers a faster engine transient response with the use of low cost components similar to those in the first four above mentioned fuel metering systems. Additionally, it offers an improvement in the aircraft safe operation without recurring to the expensive use of parallel components, as it is done in many existing electronic fuel systems. Both systems will be also analyzed regarding the impact of different fuel pumps.

4. THESIS RESEARCH PROGRAM AND METHODOLOGY

An explanation is due to the reader regarding the discussed different design configurations of the electronic fuel metering systems (EFMS) which have their industrial implications. The second and the third configurations of low cost EFMS's have been developed for Bendix Avelex in Montreal as the result of a cooperative research with Concordia University. The second configuration was, to some extent using the concept from Bosch K-Jetronic fuel injection system and incorporated some of its components. The third configuration was a combination of a Bosch K-Jetronic metering valve and Bendix DP-F2 bypass valve. The research was also proposing a concept of a double barrel, twin actuator system for further research.

The research presented in this thesis, is a follow-up to the previous work, which has the following merits:

1. It proposes and investigates a novel electronic fuel metering system, with a design simplicity comparable to that of the second configuration, however, without the need of a pressure regulator which operates as a bypass valve. Moreover, it can replace the much more expensive, Bendix bypass valve in the DP-F2 fuel control unit due to its simplified bypass valve design.
2. It proposes and investigates a simplified design of a single barrel, twin actuator EFMS with additional features improving the performance and safety of a small gas turbine engine operation.

The thesis research program listed below should provide the answers to several questions being relevant to the research topic. Some of the most important questions could be formulated as follows:

1. Is the proposed low cost diaphragm type flat-seat bypass valve providing adequate control of constant differential pressure across the metering valve, i.e. an acceptable linear relationship between the fuel flow rate and the metering valve travel?
2. What kind of control strategy should be used to manage the double plunger fuel metering valve at both steady state and transient operations?
3. Are both fuel metering configurations providing adequate dynamic response during the fast engine transient processes?
4. What are the double valve fuel delivery characteristics during the back-up operations? Are they adequate?
5. What is the impact of different types of fuel pumps on the delivery characteristics of the fuel metering valves?
6. How do these new fuel metering valves compare in cost with those used presently?

To answer these questions, the following research methodology was applied:

1. The system principles and operations were analyzed and determined, regarding their applications to the small gas turbine engines used in the drones, missiles and other remotely piloted vehicles (chapters 5 and 10).

2. Mathematical models were derived for the new proposed fuel metering systems, including also configurations 2 and 3 which were presented in chapter 3, in order to compare and investigate the steady state and dynamic responses of different fuel metering systems (chapter 6).
3. Prototype of the first proposed fuel metering system (configuration 1) was designed, manufactured and tested to validate its model; to perform the experiments, special test facilities with required instrumentations have been developed (chapter 7).
4. The first configuration was computer simulated and its mathematical model was validated by the comparison between the simulated results and experimental data (chapter 8).
5. The optimization techniques were used to improve the performance of the first proposed fuel metering system regarding the nozzle flow linearity, low sensitivity to the design parameters changes and the short dynamic response time. Finally, the best design parameters for the first configuration were obtained by developing a multi-objective optimization technique (chapter 9).
6. The feasibility of the second proposed fuel metering system (configuration 4) was investigated (chapter 10).
7. Due to the flexibility offered by the configuration 4, different control options which are used during the transient processes were presented and investigated (chapter 10).
8. A dynamic model for a small gas turbine engine was developed and was used to evaluate the impacts of different control options on the engine transient responses (chapter 10).

9. The comparison of all four design configurations was done, regarding the steady state, dynamic response processes and cost (chapter 10).
10. Conclusions were drawn regarding the investigated systems (chapter 11).
11. Recommendations were made for further research work (chapter 11).

5. SYSTEM DESCRIPTION AND OPERATION OF CONFIGURATION 1 (NEW)

Before modelling of the design configurations presented in chapter 3, it is necessary to discuss their principles of designs. However, due to the fact that the operation of all four fuel metering systems has some similarities, therefore, the first configuration was chosen to be specifically discussed in terms of its system description and operation. This description will be used as a base for the modelling of all design configurations. More details about the system descriptions and operations of the second and the third configurations are available in references [33] and [35] respectively. The details about the fourth configuration will be presented in chapter 10. Therefore, in this chapter, the description of the first proposed fuel metering system and its function is presented and then, the operation of each individual component comprising of the whole system is described.

5.1 Description of the Proposed Fuel Metering System

The schematics of the proposed fuel metering system and its assembly drawing are shown in figures 5.1 and 5.2 respectively. Depending on the design, fuel is supplied to the entrance of the fuel metering system by either an electric pump or an engine operated gear pump which is driven at a fraction of (1/6) of the engine speed. The fuel metering system consists of two main sections; the metering valve and the diaphragm flat-seat bypass valve.

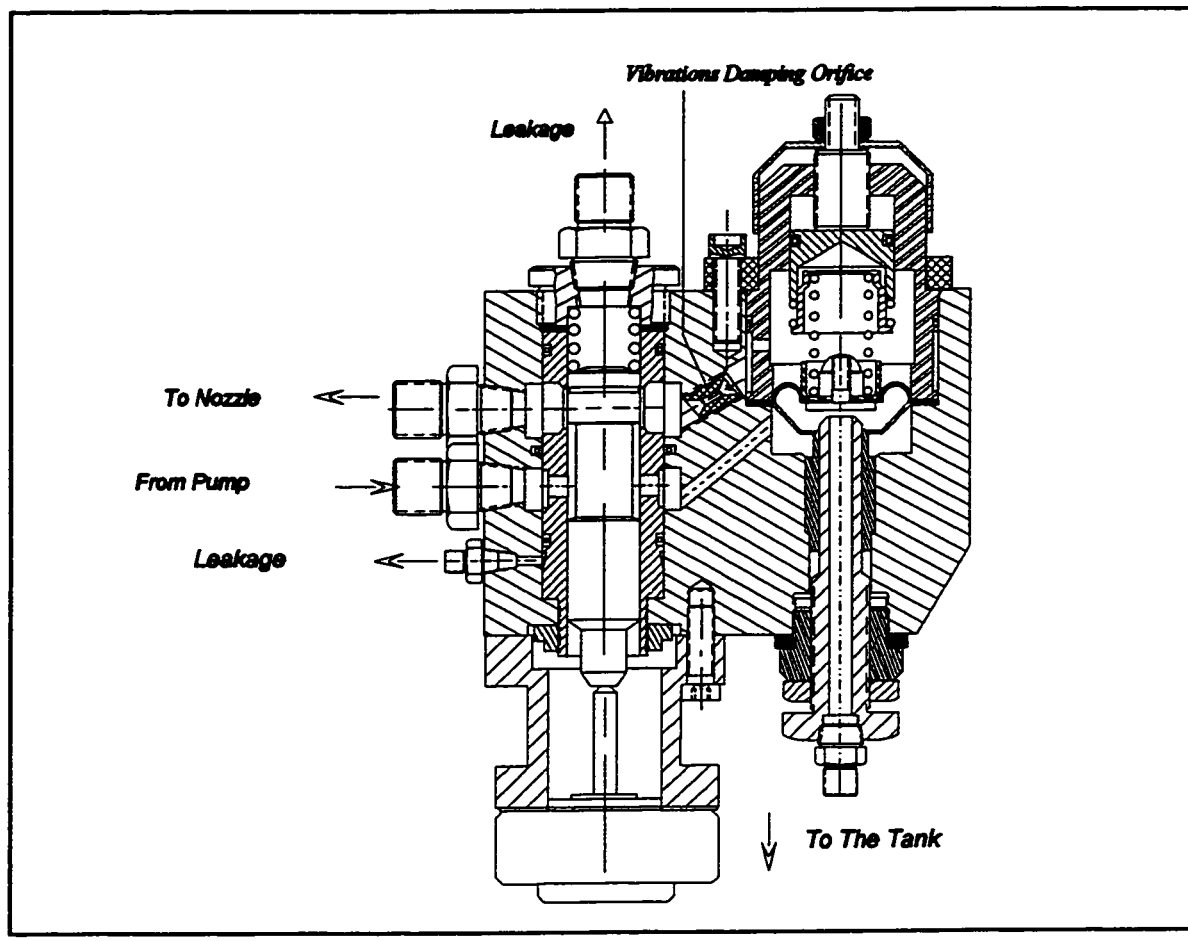

Figure 5.1 Fuel Metering System Prototype

The metering valve concept is taken from Bosch K-Jetronic fuel injection system for spark ignition engines and modified for higher fuel flow. It consists of a plunger and a barrel with six slits which are cut by electro-discharge machining (see figure 3.1). Depending on the longitudinal position of the plunger exposing the slits in the barrel, the fuel flow rate to the engine is determined. The diaphragm flat-seat bypass valve concept is also based on Bosch K-Jetronic design, but is modified to conform to the fuel metering requirement of a gas turbine engine. Since the flat-seat type bypass valve maintains an essentially constant differential pressure across the

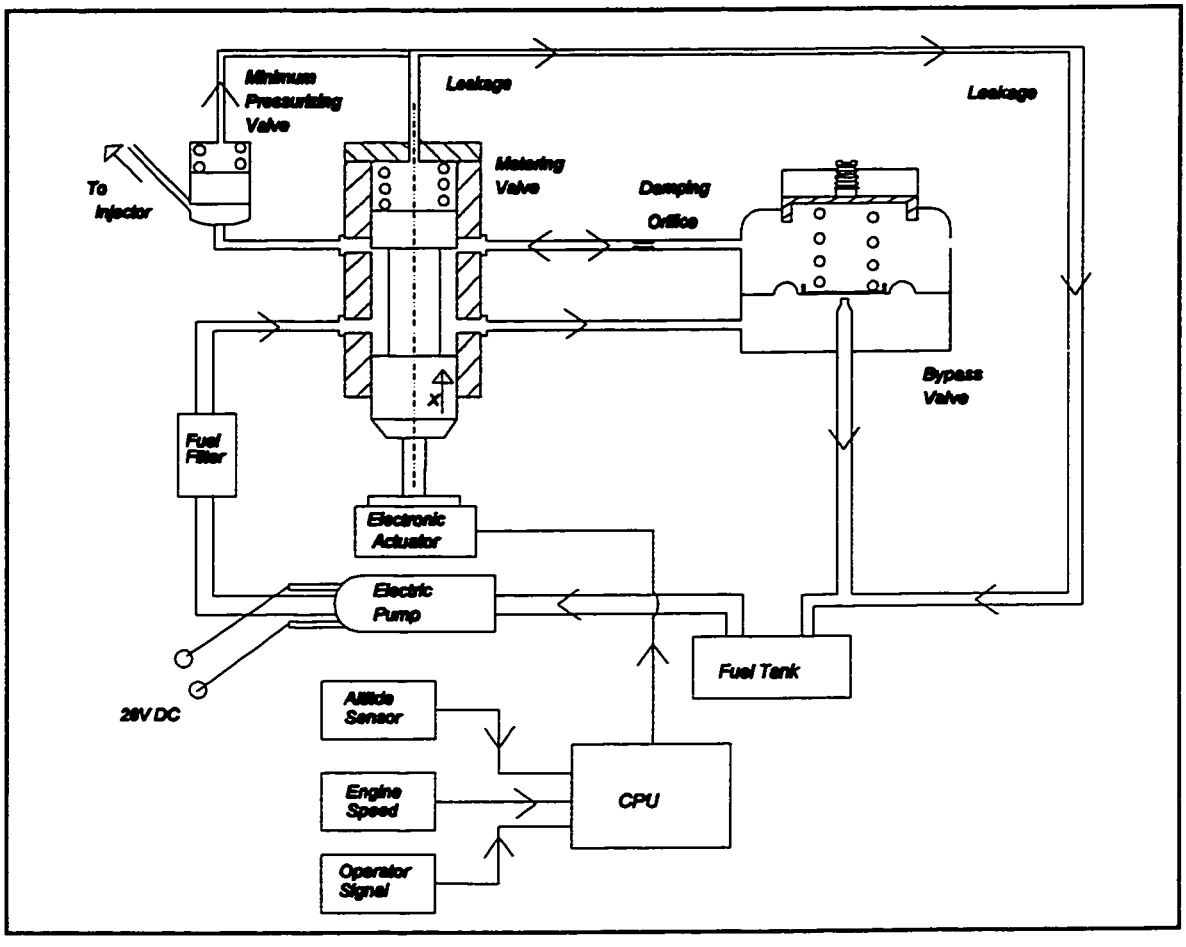

Figure 5.2 Hydraulic Schematic of the First Proposed Fuel Metering System

metering valve, regardless of variations in the inlet or exit fuel pressures, the fuel flow rate is essentially a function of the metering valve position and the fuel discharged by the pump in excess of engine requirement, is returned to the pump inlet. The metering valve is actuated by a linear digital actuator and a spring is used to return the plunger and to maintain a connection between the barrel and the stepper motor shaft during retraction.

The diaphragm flat-seat bypass valve is connected in parallel with the metering valve and is used to maintain a constant differential pressure across the metering valve

by releasing back to the tank the excess fuel delivered by the pump. In test prototype the upper chamber of the diaphragm bypass valve was taken from a Bendix DP-F2 fuel control unit [34]. However, the bottom chamber has a design completely different from the Bendix one and consists of a manifold pipe with a flat-seat valve which bypass the fuel flow to the tank.

The face of the manifold orifice is parallel to the diaphragm and the clearance between the inlet pipe circumference and the diaphragm surface determines the effective flow area through the diaphragm flat-seat valve.

A vibrations damping orifice stabilizes the diaphragm motion by restricting the fuel passage between the metering valve and the top chamber of the bypass valve. The position of the diaphragm during a steady state process depends on the balance between the pressure difference force across the diaphragm and the spring force.

5.2 Components Description

In this section, each component of the proposed fuel metering system is briefly discussed, as shown in figure 5.2.

The *minimum pressurizing valve* is located between the fuel metering valve and the nozzle and is used to cut-off the fuel flow to the engine combustor while the engine is not operating. Its second function is to maintain adequate fuel pressure in the system, particularly during low engine speed and at high altitudes, to assure continuous fuel flow to the engine.

The precise components of the fuel metering system are protected against the possible contaminating particles by a *paper filter* installed before the metering valve. The solid particles having a size greater than 6 μm are being retained from the system [42].

Both, the engine driven gear pump and a pump driven with an electric motor at constant speed could be used to maintain the required fuel delivery for the engine. These pumps will be fully discussed in the next chapter.

The fuel metering system prototype is operated by the K92211-P2 *digital linear actuator* manufactured by Airpax. This actuator is a stepper motor that has been modified by incorporating an internally threaded rotor fitted with a lead screw shaft. Applying digital pulses to the unit's coils in proper sequence causes the threaded rotor to turn in linear increments of 0.025 mm per pulse and the shaft to move like a screw. This design not only provides a high shaft moving force, but also the actuator shaft remains in a locked position when the torque is removed. It has a maximum travel of 22.2 mm and generates a maximum force of 20.9 N. The maximum pull-out and pull-in stepping rates are 700 and 500 steps per second

respectively [43].

Series SAA1027 *stepper motor driver* is used to operate the digital linear actuator. The SAA is a 16-pin dual-in-line plastic package complete IC stepper driver which is capable of driving a 4 coil, two-phase stepper motor. The pulses are supplied to a single input and the direction of travel is controlled by a voltage level applied to a gate input. A single 12 V DC power supply operates both the IC driver and the actuator [43].

The *altitude sensor* is used to provide a required signal for the Processor (CPU) to act for different ambient air pressures and to change the fuel flow to the engine according to the engine requirements.

An electronic microcontroller is one of the essential parts of an electronic fuel control unit. It is used as data acquisition and control unit, i.e. to:

I. Collect digital and analog data from sensors mounted on the engine.

II. Operate the digital linear actuator.

III. Communicate with air borne computer and peripheral equipment.

IV. Perform all calculating functions in real time and with the high speed required to follow the real processes.

V. Control the fuel control unit based on the program installed in its memory.

VI. Save data in memory for later investigations.

The proposed electronic controller design is based on the Intel 80C196KC 16-*bit Embedded Single Chip Microcontroller* operating at a reference frequency of 16 MHz. The controller is one part of the Intel EV80C196KC Evaluation board which

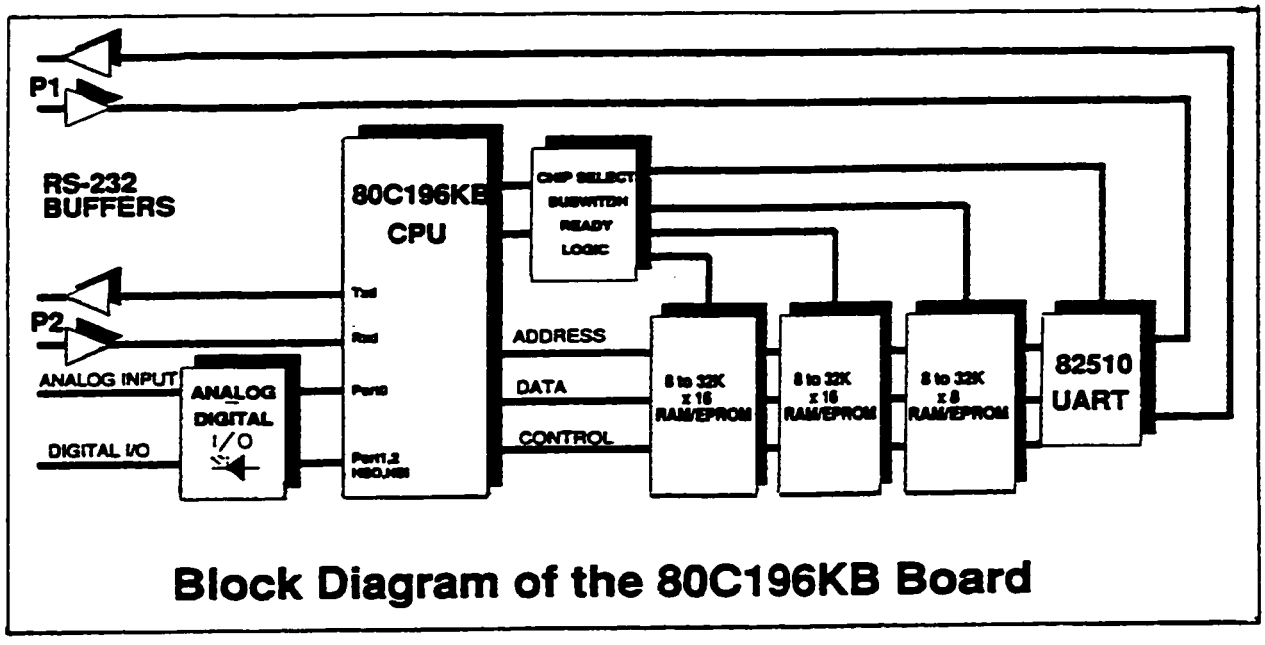

Figure 5.3 Block Diagram of the EV80C196KB (KC) Evaluation Board [45]

has its own software programming to simplify writing, saving and executing of the program [44]. The evaluation board consists of the 80C196KC CPU, 8K-word 8K - bytes of user code/data memory, a Universal Asynchronous Receiver/ Transmitter (UART) for host communications and an analog input filtering with a precision voltage reference. There are six main sections of the EV80C196KC Evaluation board: Processor, Memory, Host interface, Digital I/O, Analog inputs and Decoding. A block diagram of the EV80C196KC Evaluation board is shown in figure 5.3 [45].

The Intel 80C196KC family is a CHMOS branch of the MCS-96 family of high performance, 16-bit microcontrollers. All of the MCS-96 components share a common instruction set and architecture. However, the CHMOS components have enhancements to provide higher performance and lower power consumption. The

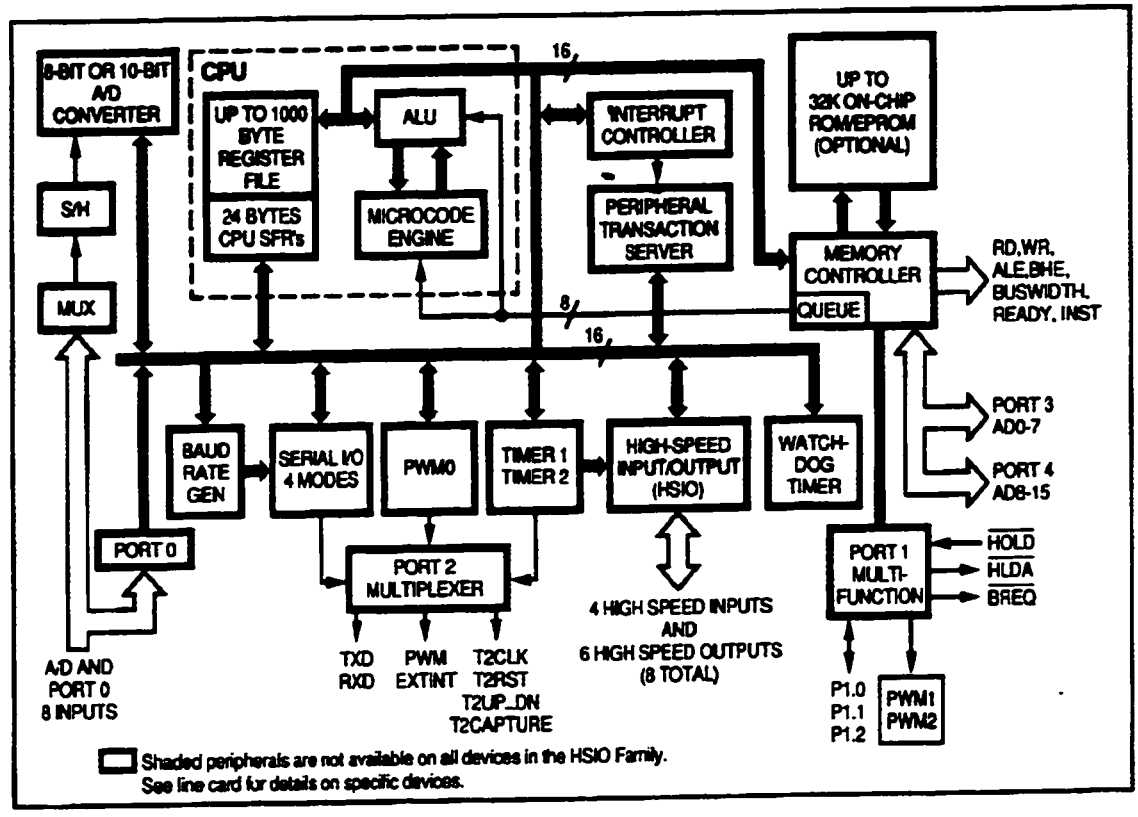

Figure 5.4 Functional Block Diagram of the 80C196KC [46]

MCS-96 family is a register to register architecture, so it eliminates the accumulator bottleneck and most operations can be quickly performed from or to any of the 256 registers. In addition, the registers operations control the many peripherals which are available on the chips. These peripherals include a full-duplex Serial I/O (SIO) port, an 8-channel 8 or 10-bit resolution Analog to Digital (A/D) converter with programmable sample and conversion times, a Peripheral Transaction Server (PTS) which acts as a microcoded interrupt handler to greatly reduces CPU overhead during interrupt servicing, three hardware generated Pulse Width Modulators (PWM) outputs, up to 48 I/O lines and a High Speed I/O (HSOI) subsystem which has two

16-bit timer/counters as a base time, a 16-bit watchdog timer, an 8-level input capture FIFO and an 8-entry programmable output generator and 488 bytes of RAM and 16K of ROM/ EPROM. Figure 5.4 shows functional block diagram of microcontroller. More details about the microcontroller and its peripherals are given in references [45] and [46].

6. DESCRIPTION OF MATHEMATICAL MODELS OF DIFFERENT DESIGN CONFIGURATIONS

In this chapter, the mathematical model for the first proposed fuel metering system, i.e. *fuel metering system with diaphragm flat-seat bypass valve and varying supply pressure (configuration 1)*, is derived to predict and evaluate the behaviour of the system for both steady state and transient conditions. Computer simulation of the system is used as a proper design tool for optimizing the parameters of the fuel metering system in order to improve its performance and to compare with the other fuel metering systems described in chapter 3, which are:

1. Fuel metering system with differential pressure flat-seat valve and constant supply pressure (configuration 2).
2. Fuel metering system with plunger type (Bendix) bypass valve and varying supply pressure (configuration 3).
3. Double plunger fuel metering system with varying differential pressure across the metering valve and back-up configurations (configuration 4).

The mathematical models of these three metering systems are also derived based on the sample description of the first configuration presented in chapter 5, with consideration of the necessary changes depending on the particular design. It has to be mentioned here that these models are developed for the fuel metering systems operating on a test bench, where the nozzle is substituted by a needle valve . This is done to validate the mathematical models to compare with experiments.

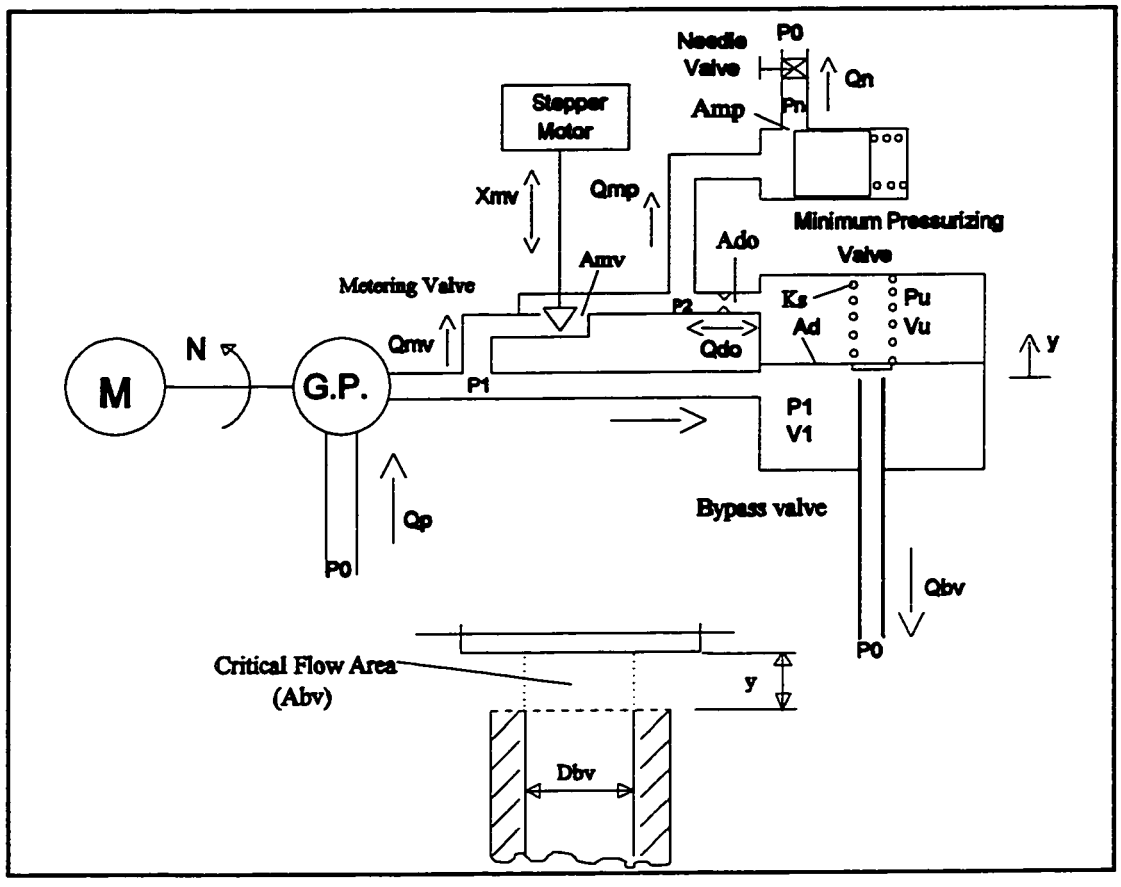

Figure 6.1 Schematic of the Fuel Metering System with Diaphragm Flat-Seat Bypass Valve

6.1 Model for Fuel Metering System with a Diaphragm Flat-Seat Bypass Valve and Varying Supply Pressure (Configuration1)

A schematic diagram of the fuel metering system is shown in figure 6.1, and the equations describing the different parts of the system are presented in the following sections.

6.1.1 Fuel Flow Rate Equations

Fuel Delivery Using Different Pumps

a) Constant Displacement Pump Driven by the Engine

There are two basic types of constant displacement fuel pumps which are used in gas turbine engines, the piston pumps and the gear pumps [47]. Where lower pressures are required, the gear pump is preferred because of its lower cost and light weight. The constant displacement pump is driven by the engine gear train and its output is directly proportional to its speed. There is a flow leakage loss due to pressure gradients across the small clearances of the pump. The pump flow characteristic is not exactly linear at low differential pressures but at higher pressures it is assumed that the characteristic is fairly linear and it can be described by following equation:

$$Q_P = C_1 N_P - C_2 (P_1 - P_0) \tag{6.1}$$

where C_1 is the pump volumetric displacement, N is the pump speed and the $C_2 (P_1 - P_0)$ represents leakage flow losses as a function of differential pressure across the pump.

b) Constant Displacement Pump Driven by DC Electric Motor at Varying Speed

The output of an electric fuel pump depends heavily on the fuel discharge pressure, since at higher pressure the electric motor is more loaded and therefore, its speed decreases. There are two methods to use an electric fuel pump in a fuel metering system [31]:

1. Primary circuit maintains an almost constant pressure by using a pressure regulating valve which spills the excess fuel back to the tank. This method is used in the *fuel metering system with diaphragm flat-seat valve and constant supply pressure.*
2. Primary circuit produces a variable pressure which depends on the nozzle pressure. In this case the bypass valve spills the excess of fuel back to the tank. This method is used in the new proposed fuel metering system and also in the *fuel metering system with plunger type (Bendix) bypass valve and varying supply pressure.*

The pump characteristic of a constant displacement pump driven by a DC electric motor can be described by following equation:

$$Q_P = C_3 V - C_4 (P_1 - P_0) \tag{6.2}$$

where the first term is a function of pump supply voltage and the second term indicates the flow loss due to the increase in output back pressure and consequently decrease in the pump speed. This type of pump is inexpensive and is used in most automotive vehicles, mainly at low injection pressures.

c) Fuel Pump Driven by Constant Speed Electric Motor

In this type of pump, the motor speed is controlled by an electronic controller and is almost independent on the discharge pressure. In other words, the pump fuel flow is constant in all operating conditions. Here, it is supposed that a fuel pump with following characteristic is available:

$$Q_P = Q = Constant \tag{6.3}$$

Metering Valve Flow

The flow in the metering valve is described by the equation for the fuel discharge through a rectangular flow area A_{mv} :

$$Q_{mv} = C_{dmv} A_{mv} \sqrt{2 (P_1 - P_2)/ \rho} \qquad (6.4)$$

where $A_{mv} = n_{smv} X_{mv} W$, n_{smv} is the number of slits on the metering valve barrel and W is the width of the slits (see figure 3.1). P_1 and P_2 are pump and metering valve downstream pressures and C_{dmv} is the flow coefficient for the metering valve. Q_{mv} is the metering valve flow and ρ is the fuel density.

Diaphragm Flat-Seat Bypass Valve Flow

The excess fuel flow returned to the tank through the flat-seat bypass valve is given by:

$$Q_{bv} = C_{dbv} A_{bv} \sqrt{2 (P_1 - P_0)/ \rho} \qquad (6.5)$$

where:

$$A_{bv} = \pi D_{bv} y \qquad if \quad y \leq D_{bv} / 4$$
$$A_{bv} = \pi D_{bv}^2 /4 \qquad if \quad y > D_{bv} / 4$$

Q_{bv} , A_{bv} and D_{bv} are flow, flow area and diameter of the bypass valve respectively. y is the diaphragm flat-seat position.

Vibrations Damping Orifice Flow

The flow through the vibrations damping orifice is given by:

$$Q_{do} = C_{ddo} A_{do} \, sgn\,(P_2 - P_u) \sqrt{2|(P_2 - P_u)|/\rho} \tag{6.6}$$

The term $sgn\,(P_2 - P_u)$ is used to indicate the fuel flow in both directions during transient processes. P_u is the upper diaphragm chamber pressure and A_{do} is the flow area of the damping orifice.

Minimum Pressurizing Valve Flow

The flow through the minimum pressurizing valve is described by:

$$Q_{mp} = C_{dmp} A_{mp} \sqrt{2\,(P_2 - P_n)/\rho} \tag{6.7}$$

At high flow, A_{mp} is constant and acts as a fixed orifice. Note that, in order to simplify the simulation and experiment, the dynamics of the pressurizing valve will not be taken into consideration. P_n is the nozzle pressure.

Injector Nozzle Flow

The fuel flow through the injector nozzle is:

$$Q_n = C_{dn} A_n \sqrt{2\,(P_n - P_0)/\rho} \tag{6.8}$$

where A_n is the flow area of the injector orifice (needle valve flow area).

6.1.2 Continuity Equations

Metering Valve Upstream Volume

Pressure P_1 is a function of the volume included between the pump outlet and the diaphragm flat-seat bypass valve (V_1 as shown in figure 6.1), the effective bulk modulus of elasticity of the fuel (β) and the net influx of fuel to the volume:

$$\frac{dP_1}{dt} = \frac{\beta}{V_1}\left(Q_P - Q_{bv} - Q_{mv} - A_d \frac{dy}{dt}\right) \tag{6.9}$$

where A_d is the diaphragm effective area.

Metering Valve Downstream Volume

The pressure in the fuel manifold is given by:

$$\frac{dP_2}{dt} = \frac{\beta}{V_2}\left(Q_{mv} - Q_{do} - Q_{mp}\right) \tag{6.10}$$

Diaphragm Chamber Upper Volume

The pressure in the upper volume of the diaphragm flat-seat bypass valve is described by:

$$\frac{dP_u}{dt} = \frac{\beta}{V_u}\left(Q_{do} + A_d \frac{dy}{dt}\right) \tag{6.11}$$

Nozzle Manifold Volume

The pressure in the nozzle manifold volume is described by:

$$\frac{dP_u}{dt} = \frac{\beta}{V_u}(Q_{mp} - Q_u) \tag{6.12}$$

6.1.3 Valve Motion Equations

Diaphragm Flat-Seat Valve Motion

Forces acting on the diaphragm flapper valve during a transient process are mainly due to the pressure difference across the diaphragm, the diaphragm spring and its pre-load force and the inertia forces required to accelerate the diaphragm and the fuel on either side of the diaphragm. Damping forces can be neglected as compared to the spring and pressure forces. The motion equation for the diaphragm is given by:

$$M_e \frac{d^2y}{dt^2} = P_1(A_d - A_{bv}) - P_u A_d - K_y y - B\frac{dy}{dt} - F_{sp} \tag{6.13}$$

where $M_e = M_d + C\rho V_u$. M_d is the diaphragm mass and the second term on the right is due to the fluid momentum force. C is a coefficient to compensate for the fact that not all the fuel in volume V_u follows the movement of the diaphragm.

Metering Valve Plunger Motion

The metering valve plunger motion is incremental and is described by:

$$X_{mv} = \Delta X_{mv}\ INTEGER\ (\ ft\ ) \tag{6.14}$$

where f is the actuator triggering frequency and ΔX_{mv} is the actuator step size.

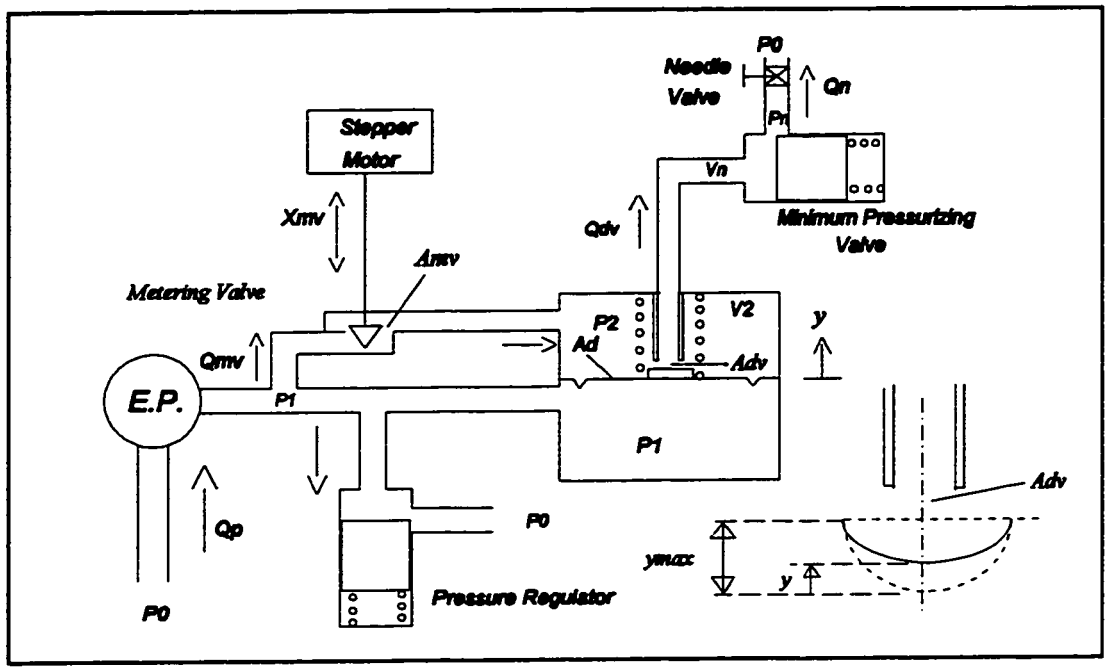

Figure 6.2 Schematic of the Fuel Metering System with Differential Pressure Flat-Seat Valve and Constant Supply Pressure

6.2 Model for Fuel Metering System with Differential Pressure Flat-Seat Valve and Constant Supply Pressure (Configuration 2)

In this section, the mathematical model of the *fuel metering system with differential pressure flat-seat valve and constant supply pressure* is derived. A schematic diagram of the fuel metering system is shown in figure 6.2. More details of the model are given in reference [33].

6.2.1 Fuel Flow Rate Equations

The equations describing the metering valve flow and the injector nozzle flow are given by Equations 6.4 and 6.8 respectively.

Diaphragm Valve Orifice

$$Q_{dv} = C_{ddv} A_{dv} \sqrt{2 (P_2 - P_n)/ \rho} \tag{6.15}$$

where:

$$A_{dv} = \pi D_n (y_{max} - y) \qquad \text{if} \quad y \geq y_{max}-D_n/4$$
$$A_{dv} = \pi D_n^2/4 \qquad \text{if} \quad y < y_{max}-D_n/4$$

6.2.2 Continuity Equations

Upper Chamber Volume

$$\frac{dP_2}{dt} = \frac{\beta}{V_2} (Q_{mv} - Q_{dv} + A_d \frac{dy}{dt}) \tag{6.16}$$

Nozzle Manifold Volume

$$\frac{dP_n}{dt} = \frac{\beta}{V_n} (Q_{dv} - Q_n) \tag{6.17}$$

6.2.3 Valve Motion Equations

Diaphragm Type Flat-Seat Valve Motion

$$M_e \frac{d^2y}{dt^2} = P_1 A_d - P_2 (A_d - A_n) - P_n A_n - K_s y - B\frac{dy}{dt} - F_{sp} \tag{6.18}$$

Metering valve plunger motion is described by equation 6.14.

In the above equations, P_1 , P_2 and P_n are the pump pressure, the upper diaphragm chamber pressure and the nozzle pressure respectively. V_2 *and* V_n are the volumes of the upper diaphragm valve chamber and the nozzle manifold. A_{dv} *and* A_n are the flow area through the diaphragm orifice and the nozzle manifold pipe inlet cross sectional areas.

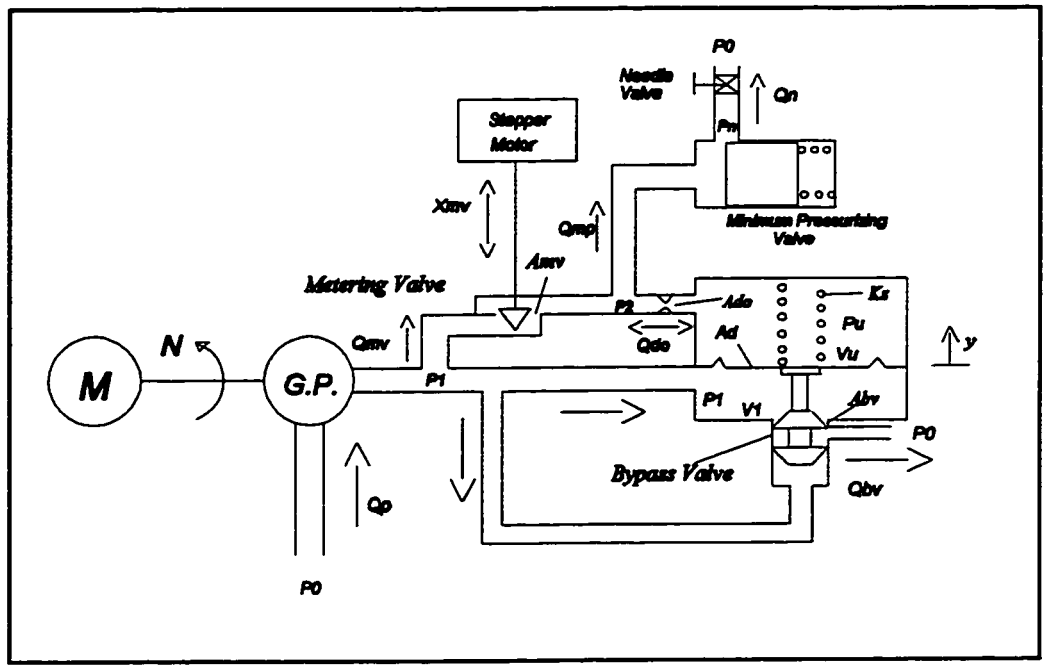

Figure 6.3 Schematic of the Fuel Metering System with Plunger Type (Bendix) Bypass Valve

6.3 Model for Fuel Metering System with Plunger Type (Bendix) Bypass Valve (Configuration 3)

In this section the mathematical model of *the fuel metering system with Bendix bypass valve and varying supply pressure* is presented. The schematic diagram of the system is shown in figure 6.3. More details of the system are given in reference [35].

6.3.1 Fuel Flow Rate Equations

The equations describing the pump delivery, metering valve, bypass valve , vibrations damping orifice, minimum pressuring valve and injector nozzle flows are given by equations 6.1 and 6.6 through 6.8 respectively.

Bypass Valve Flow

$$Q_{bv} = C_{dbv} A_{bv} \sqrt{2 (P_1 - P_0)/ \rho} \qquad (6.19)$$

where:

$$A_{bv} = b_1 y^2 + b_2 y + b_3$$

b_1, b_2 and b_3 are the bypass valve flow area constants.

6.3.2 Continuity Equations

Similarly, equations 6.9 through 6.12 are valid descriptions of the metering valve high and low pressures volumes, diaphragm chamber upper volume and nozzle manifold volume.

6.3.3 Valve Motion Equations

Bypass Valve Motion

The movement of the bypass valve is described by:

$$M_e \frac{d^2y}{dt^2} = (P_1 - P_u) A_d - K_y y - B\frac{dy}{dt} - F_{sp} \qquad (6.20)$$

Similarly the metering valve motion is described by equation 6.14.

In the above equations, P_1 , P_2 , *and* P_u are the pump pressure, the nozzle pressure and the upper diaphragm chamber pressure , V_1 , V_2 *and* V_u are the volumes of the metering valve high pressure and upper diaphragm valve chambers. A_{bv} , A_{do} , *and* A_n are the flow area of the bypass valve, the damping orifice and the nozzle manifold pipe inlet cross sectional areas respectively.

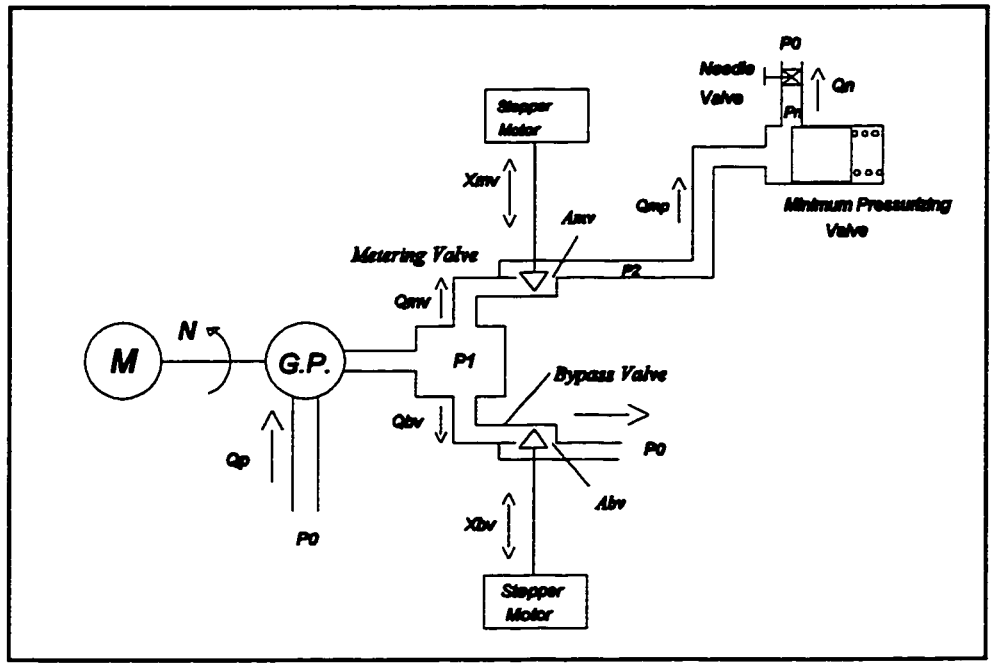

Figure 6.4 Schematic of the Double Plunger Fuel Metering System

6.4 Model for Double Plunger Fuel Metering System with the Varying Differential Pressure Across the Metering Valve and the Back-Up Configurations (Configuration 4)

In this section, the mathematical model of the system is derived similarly as described for the previous systems. A schematic diagram of the fuel metering system is shown in figure 6.4.

6.4.1 Fuel Flow Rate Equations

The equations describing the pump delivery, the metering valve flow, the minimum pressurizing valve flow and the injector nozzle flow are given by equations 6.1, 6.4, 6.7 and 6.8 respectively.

Bypass Valve Flow

The excess fuel flow returned to the tank through the bypass valve is given by:

$$Q_{bv} = C_{dbv} A_{bv} \sqrt{2 (P_1 - P_0)/ \rho} \qquad (6.21)$$

The flow area A_{bv}, is the combined area of the slits on the bypass valve barrel and is a function of the plunger position X_{bv} i.e. $A_{bv} = X_{bv} n_{sbv} w_{bv}$.

6.4.2 Continuity Equations

Metering Valve Volume

Pressure P_1 is a function of the volume included between the pump outlet and the metering valve restrictions, the effective bulk modulus of elasticity of the fuel and the net influx of fuel to the volume:

$$\frac{dP_1}{dt} = \frac{\beta}{V_1} (Q_P - Q_{bv} - Q_{mv}) \qquad (6.22)$$

Metering Valve Downstream Volume

The pressure in the metering valve downstream is given by:

$$\frac{dP_2}{dt} = \frac{\beta}{V_2} (Q_{mv} - Q_{mp}) \qquad (6.23)$$

Similarly the nozzle manifold volume is given by equation 6.12.

6.4.3 Valve Motion Equations

The equation describing the metering valve motion is given by equation 6.14.

Bypass Valve Motion

The bypass valve motion is incremental and is described by:

$$X_{bv} = \Delta X_{bv}\ INTEGER\ (f_{bv}\ t) \tag{6.24}$$

where f is actuator triggering frequency and ΔX_{bv} is step size of actuator.

7. EXPERIMENTAL INVESTIGATIONS OF CONFIGURATION 1 (NEW)

7.1 Design of the Fuel Metering System Prototype

To validate the mathematical models of the first fuel metering system by comparison of the simulated performance with the experimental results, first, the test prototype must be built and investigated before attempting the design optimization.

In order to reduce the cost of the prototype, its design was done in such a manner that a limited number of components had to be manufactured. It was found that several components from the Bosch K-Jetronic fuel injection system for automotive spark ignition engines, as well as from the Bendix bypass valve could be used for building of a new test prototype for the first configuration.

Figure 7.1 shows the prototype which is using the Bosch K-Jetronic metering valve and some components of Bendix DP-F2 fuel metering system such as flexible diaphragm, spring and etc. It has to be mentioned here that the slits of the Bosch metering valve used in the proposed design needed to be modified using electro-discharge machining to provide the required range of fuel flow rate controlled by its flow area. The new components have been manufactured in the Engineering Faculty Machine Shop and were assembled for experiment. Moreover, a digital linear actuator manufactured by AIRPAX, which is being used in several computerized systems was employed to operate the metering valve plunger. The stepper motor model is K92211-P2 with the step size of 0.025 mm and the maximum stepping rate of 700 steps/ s.

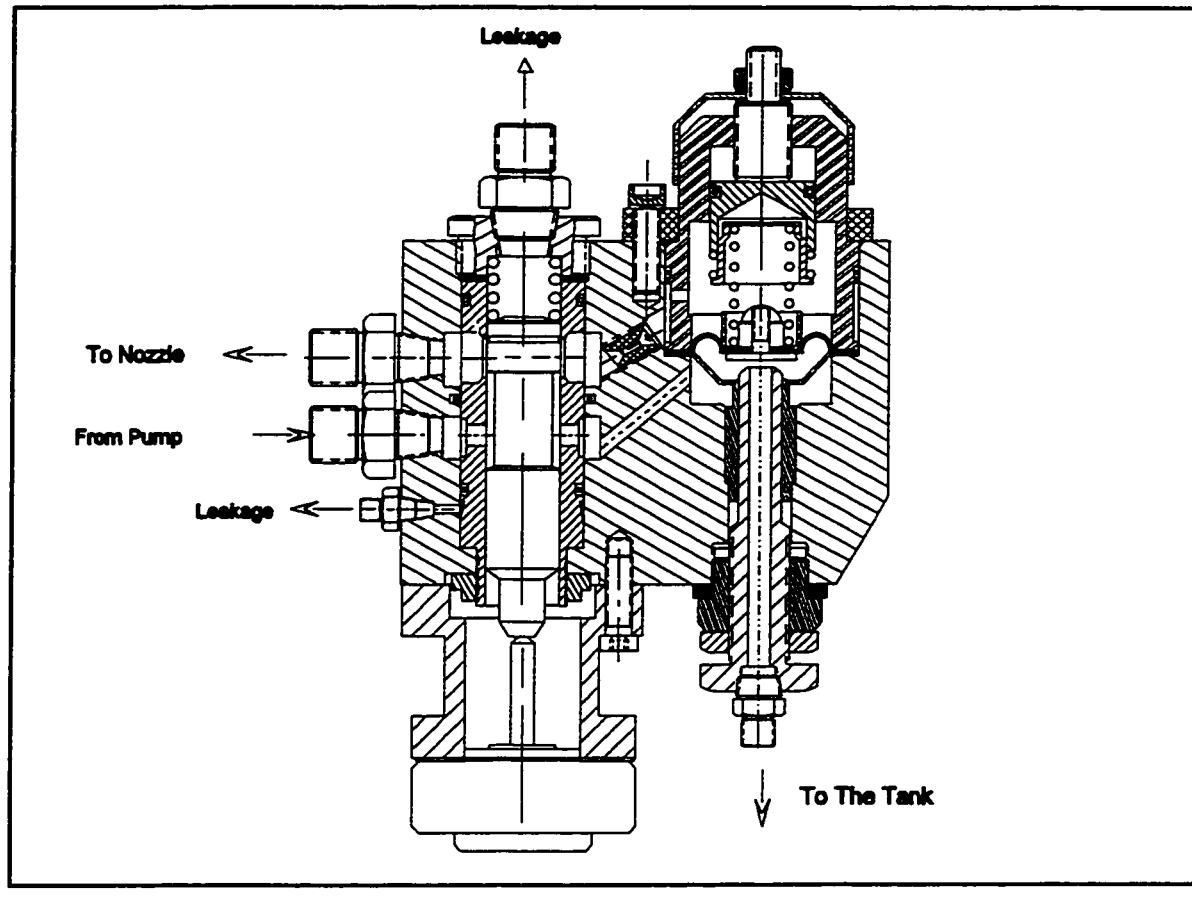

Figure 7.1 Fuel Metering System Prototype (Configuration 1)

7.2 Description of Test Facilities

The schematic diagram and some pictures of the fuel metering system with the fuel pump and measuring instruments are shown in figures 7.2 to 7.6. With reference to figure 7.2, a high pressure gear pump made by Sundstrand Aviation model 0255323-101-03, was run by an electric AC motor, Electromotors WEG S.A. model 184T, equipped with a variable speed controller, Reliance Electric model 1DB2005. It was used to supply fuel to the fuel metering system at different flow rates. A low pressure centrifugal pump and an electrically driven constant displacement pump were used to boost the fuel inlet pressure to the gear pump. A relief valve was also

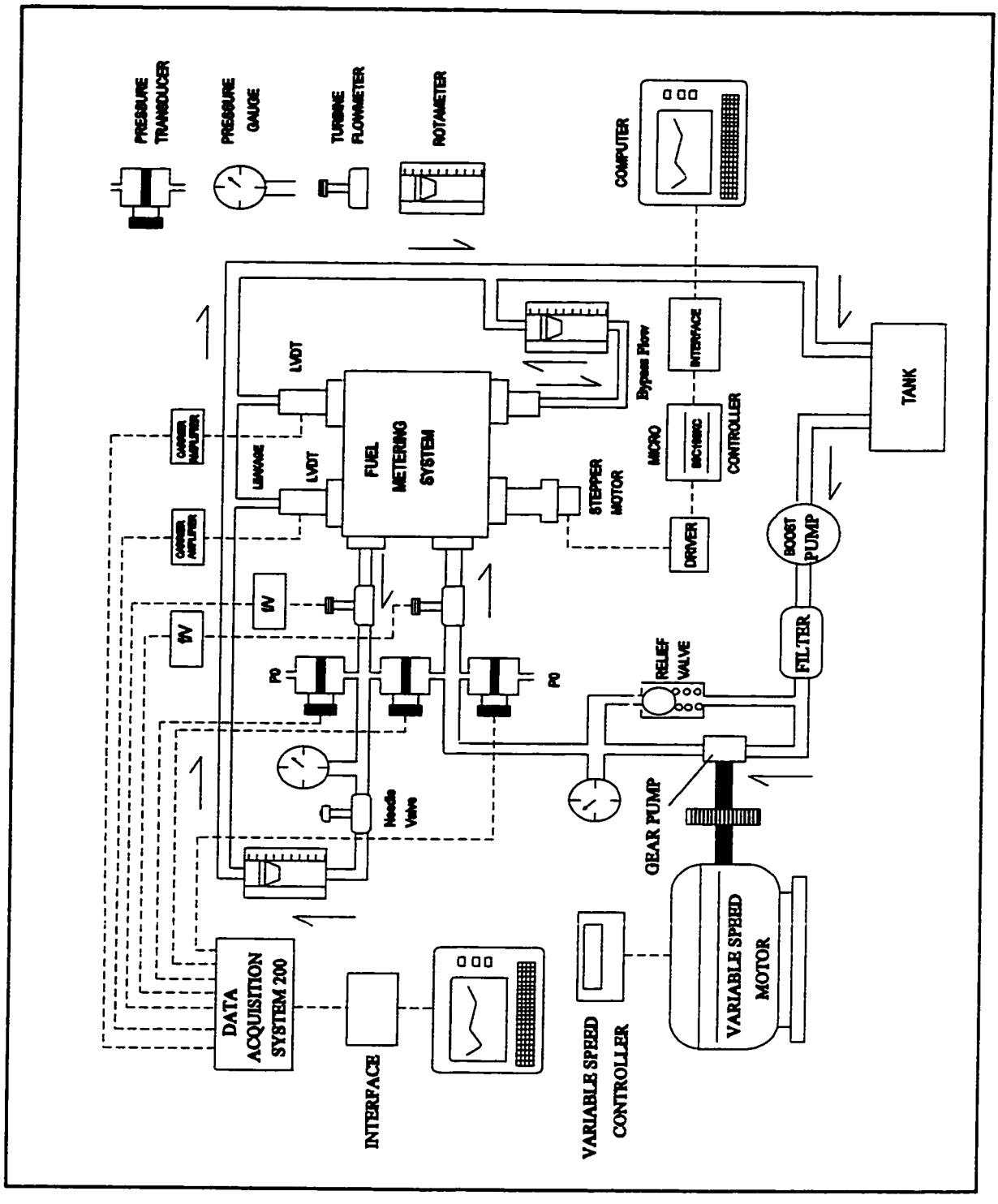

Figure 7.2 Schematic Diagram of the Experimental Set-Up

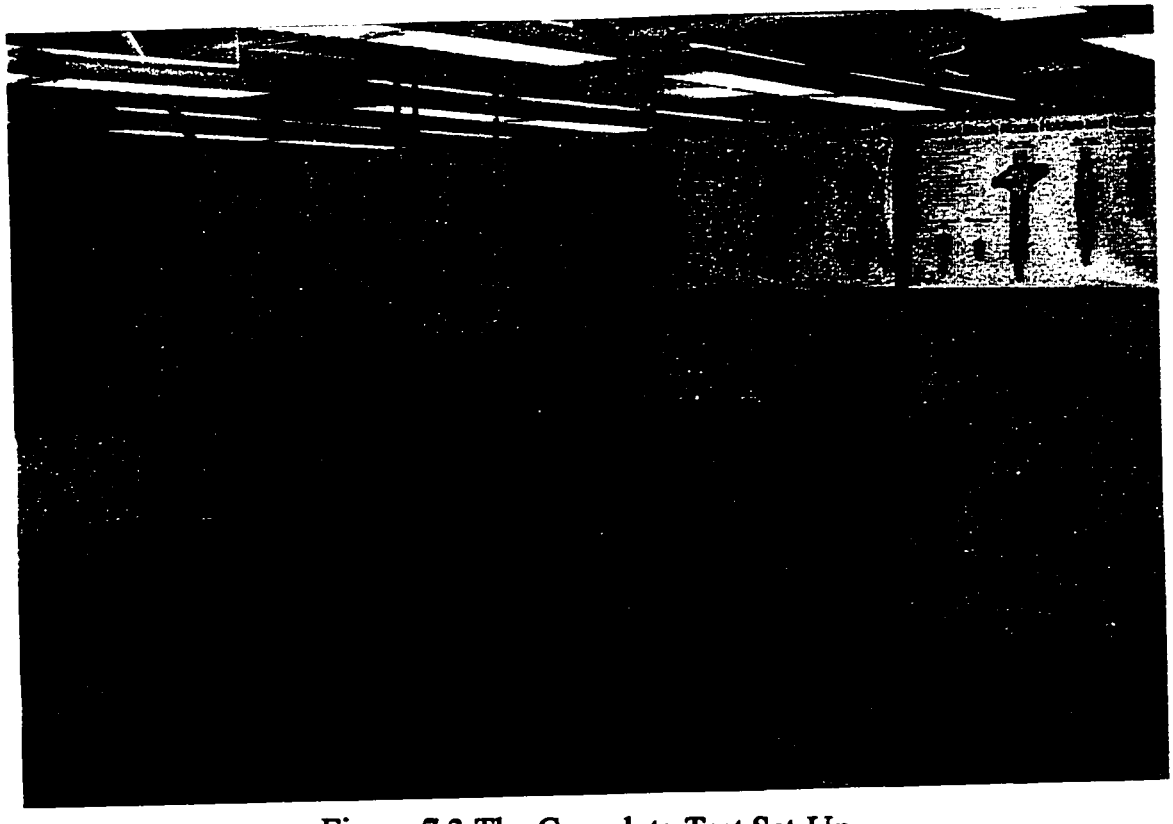

Figure 7.3 The Complete Test Set-Up

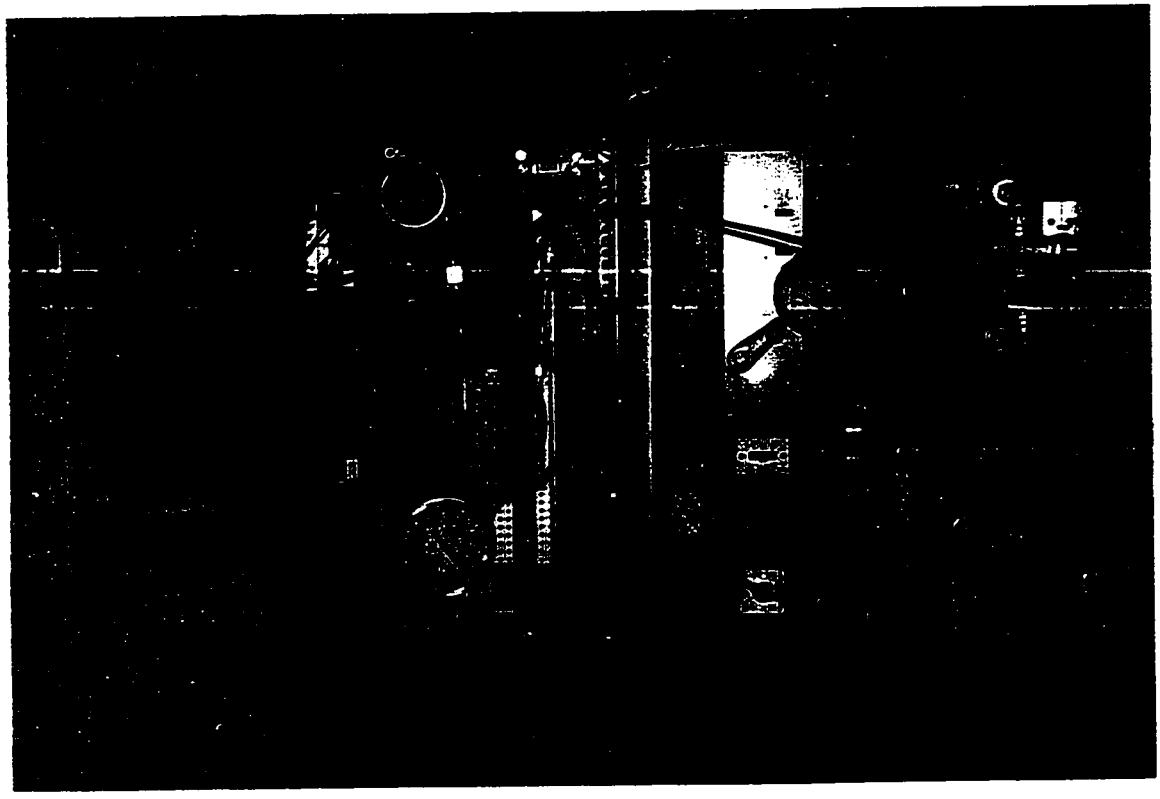

Figure 7.4 Gear and Boost Pumps, Electric AC Motor, Filters and Instrumentations

installed in order to protect the system from excessive high pressure. Two Bosch automotive filters (figure 7.4) with paper cartridge were used to trap any contaminating solid particles. Dial gauges indicated the pump and nozzle pressures. Two rotameters were used in order to measure the nozzle and the bypass flow rates and to record the data during the steady state and transient processes, two turbine flowmeters made by COX, models AN 8-4 and LF 6-1, providing a frequency signal from a magnetic pick-up, were installed in the test set-up to measure the pump flow and metered fuel flow with the aid of frequency to voltage converters.

The high pressure pump discharge pressure, the differential pressure across the metering valve and the nozzle pressure were measured by steel diaphragm pressure transducers, models DP15Tl and KP15, made by VALIDYNE. These transducers were equipped with indicator amplifiers, models CD12 and CD25.

The metering valve plunger and diaphragm flat-seat bypass valve displacements were measured by two LVDT travel transducers made by AVL model 425. Both LVDTs were equipped with carrier amplifiers, AVL model 3075-A02. Special modifications have been made to the test prototype housing to allow the installation of both travel transducers. Figure 7.7 shows the positioning of the LVDT's on the metering and bypass valves.

The liquid used for testing, was MIL-C-7024 calibrating fluid which has been designated for calibration of aircraft fuel systems. This fluid is less flammable than regular aircraft fuel, however, its main characteristics are almost the same as the fuel used in aircrafts. The specific gravity of the fluid is 772 kg/ m^3 at 32°C.

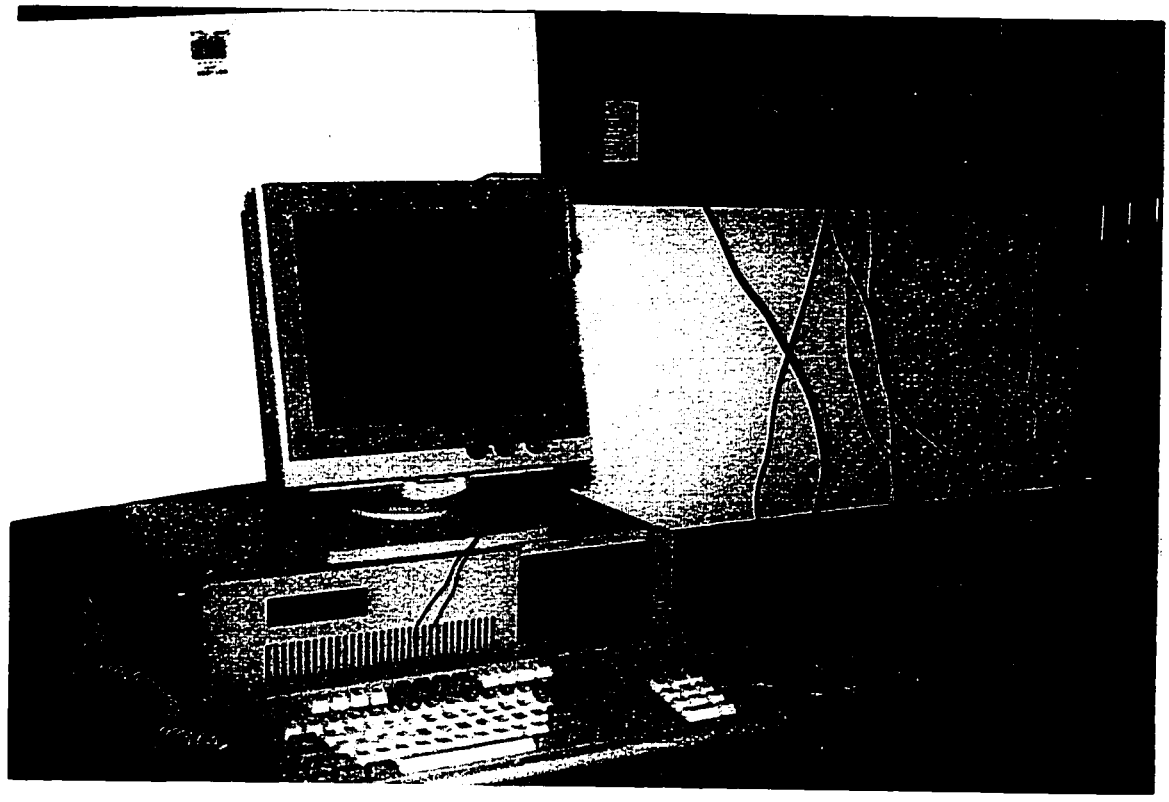

Figure 7.5 The Microcontroller and its Connections

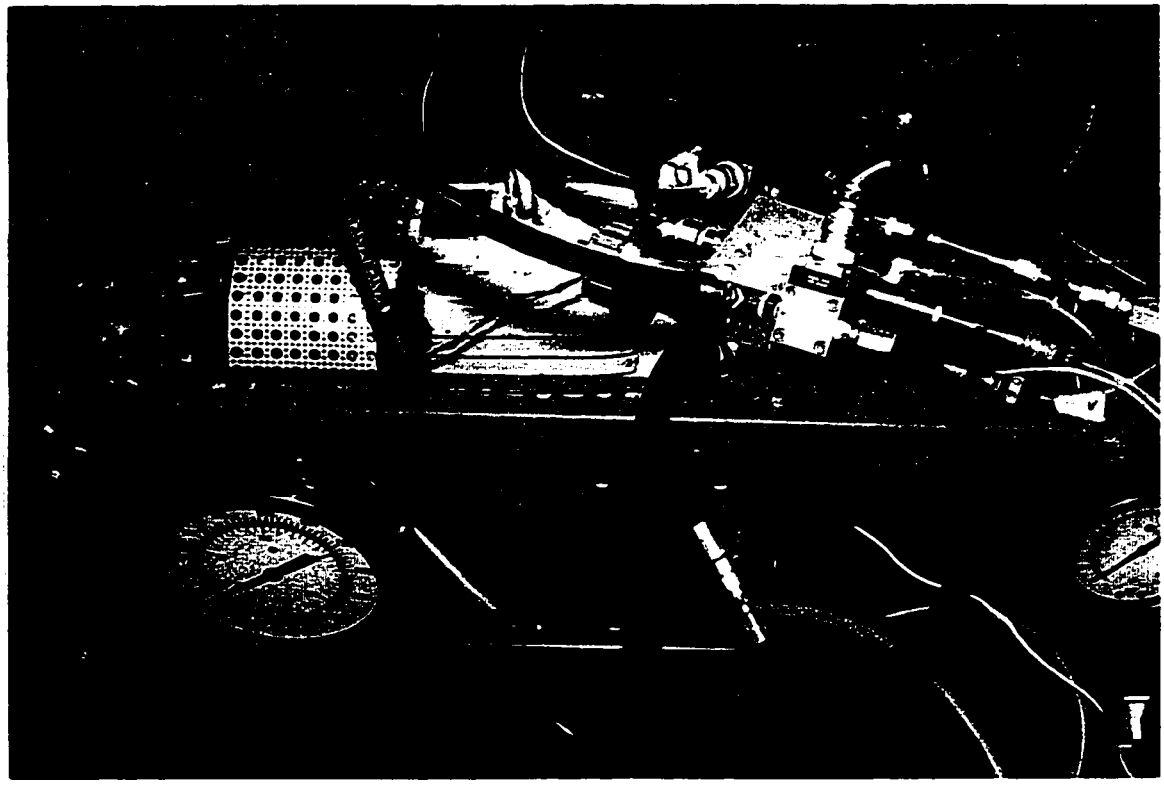

Figure 7.6 The Fuel Metering System Prototype Installed on the Test Bench

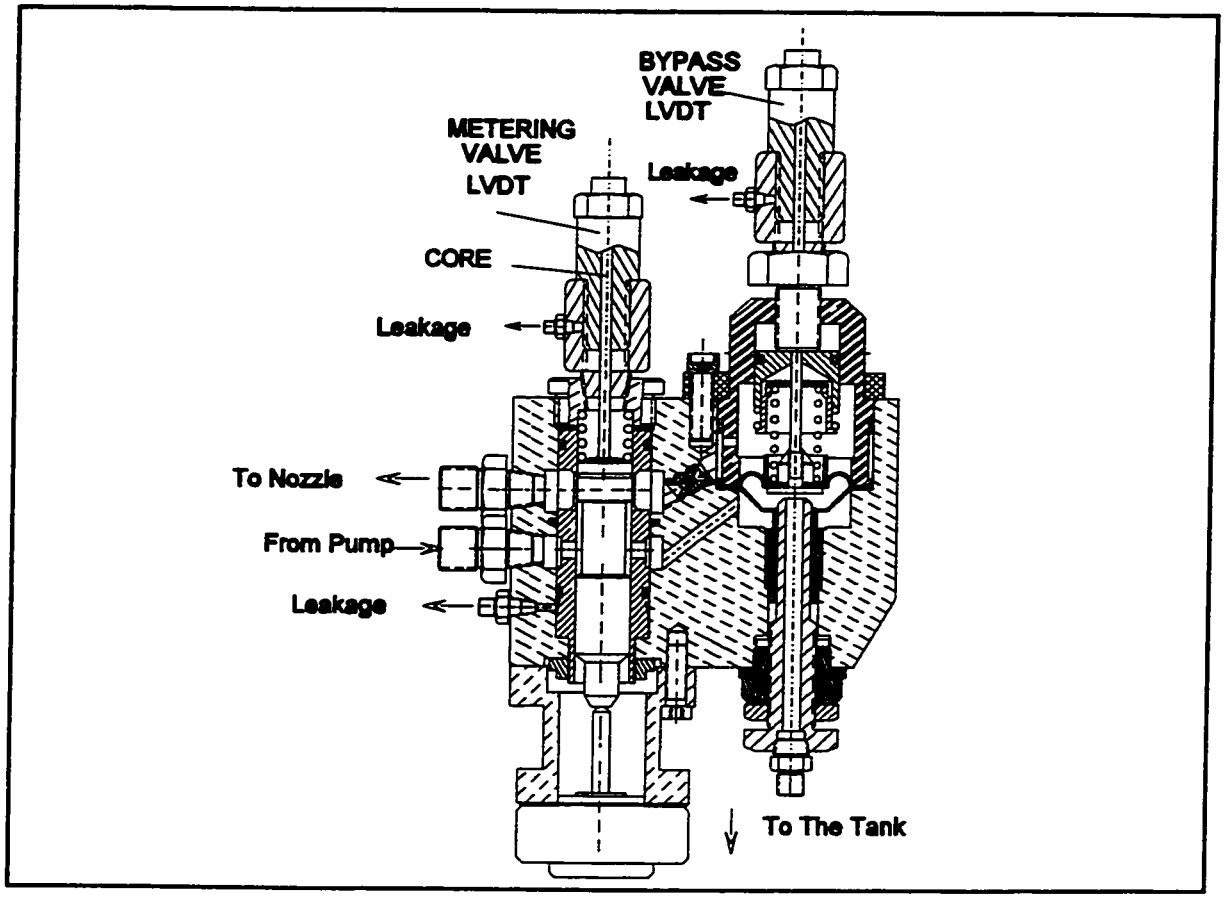

Figure 7.7 LVDT Travel Transducers Installed on the Prototype

The microcontroller chosen to control the stepper motor driver circuit was the 80C196KC as a part of the Intel EV80C196KC Evaluation Board. This board can be used with ASM 96 and ECM 96 software packages on a personal computer. The communication between microcontroller and PC was accomplished with a 82510 UART, Universal Asynchronous Receiver/ Transmitter, through the serial port of the PC. An assembly program was written to produce the required signals and pulses in order to control the stepper motor driver. The metering valve plunger demand position, the current position and the speed of the metering valve plunger were the inputs of the program. The current position of the metering valve plunger was sensed

by an LVDT connected to the microcontroller.

To record the steady state and transient responses, a data acquisition system, SYSTEM 200 manufactured by Sciemetric Instruments Incorporation was used. The SYSTEM 200 is a modular, general purpose, measurement and control system suited to different applications, including data acquisition and process control [48]. A working system is assembled by selecting the necessary I/O modules to support the desired application. The modules are connected to the host computer which can be either a personal computer or a SYSTEM 200 processor card. Software, GEN200, is then added to the system to support the control or measurement tasks. The GEN200 is designed as a general purpose software for data acquisition and control applications and is run on a Pentium machine or compatible [49]. The software offers many features that simplify the system automation and computer monitoring and control. It is fully menu driven, supports multi-tasking measurement and control applications and allows both, real time and historical graphics. It also allows the real-time modifications of the system set-up parameters such as scan rates, while the system is running.

7.3 Test Procedure

To obtain accurate results, first of all, the pressure transducers, LVDT's and COX flowmeters have been calibrated and then installed in the test set-up. The calibration results are shown in Appendix A. To obtain the steady state results, the metering valve position was incremented slowly and after the full travel of the metering valve was completed, the metering valve started to return to its original position at the same stepping rate. In both cases, sufficient time was allowed for the system to attain equilibrium. The stepping rate of the stepper motor was set at 1 step/s and the scanning and saving periods of the data acquisition were fixed at 0.1 and 0.5 second respectively.

It would be also possible to use a signal generator and an electric switch to operate the stepper motor driver instead of using the microcontroller and its software. The signal generator produces required pulses to operate the driver and the electric switch reverses the direction of the stepper motor. Due to the simplicity of the second method, it would be rather recommended for the steady state processes.

To obtain the transient responses of the system, the stepping rate of the stepper motor was increased to 90 steps/s and the scanning and saving time of data acquisition were set at 0.02 and 0.05 second respectively. Closed loop position control was used to set the final desired position of the metering valve to ensure the same ramp input at different conditions. This test ensured the repeatability of the experimental results. The results of the steady state and the dynamic processes were saved in different files for further investigation.

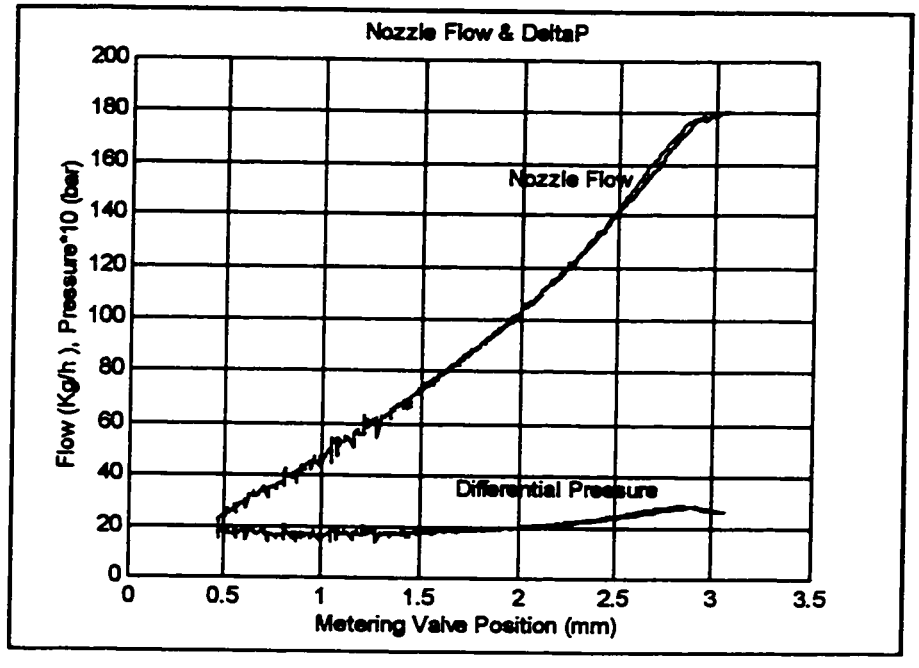

Figure 7.8 Experimental Steady State Results for the Nozzle Flow and the Differential Pressure Across the Metering Valve (Np= 4200 rpm)

7.4 Steady State Test Results

Figure 7.8 shows the fuel flow rate to the nozzle and the differential pressure across the metering valve versus the metering valve travel. It is seen that, there is a tendency for ΔP to increase with the fuel flow rate and consequently, to make the nozzle flow less linear. This can be explained as the impact of the unbalanced pressure force acting on the upper side of the diaphragm, due to the lower pressure inside the exit manifold acting on the bottom side of the diaphragm. According to the equilibrium equation for the diaphragm flat-seat valve, the differential pressure across the metering valve is equal to (see figure 7.9):

$$\Delta P = P_1 - P_u = (P_1 A_{bv} + K_s y + F_{sp}) / A_d \qquad (7.1)$$

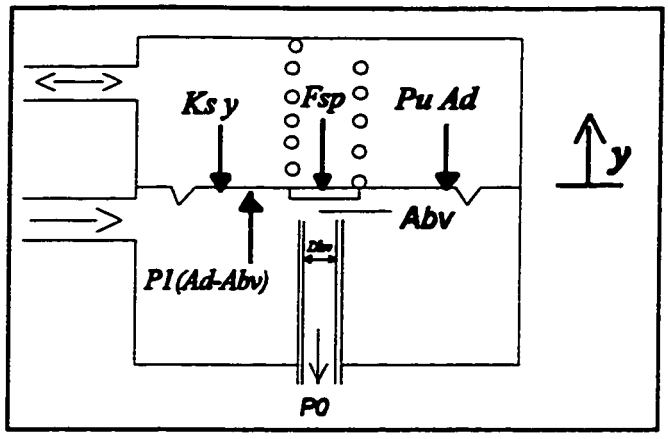

Figure 7.9 Schematic of Force Balance on the Diaphragm

To have a constant differential pressure not dependent on the flow rate, the term $P_1 A_{bv} + K_s y$ should remain constant. To partly obtain this goal, the increase of the pressure due to the higher flow rate, could be compensated with the spring force reduction. As it is shown in the figure 7.8, at the low fuel flow rate, less than 100 kg/ h, the differential pressure is almost constant, however, with the increase of the fuel flow, the $P_1 A_{bv}$ force is not compensated by the spring force and thus, the differential pressure is rising. This means that the bypass valve diameter and the spring constant must be chosen properly to have a constant differential pressure. Also a minimum value for the bypass valve flow area (A_{bv}) should be provided to avoid the saturation of the bypass flow during high flow rate. More investigation could be done to achieve an almost constant differential pressure, using the optimization methods.

As it is seen, there is a very small hysteresis loop in all characteristics. This might be due to the backlash of the lead screw of the linear actuator which converts the rotary motion of the digital actuator to the linear motion. There is also a second possibility that the characteristics of the high pressure gear pump during the loading and unloading is different.

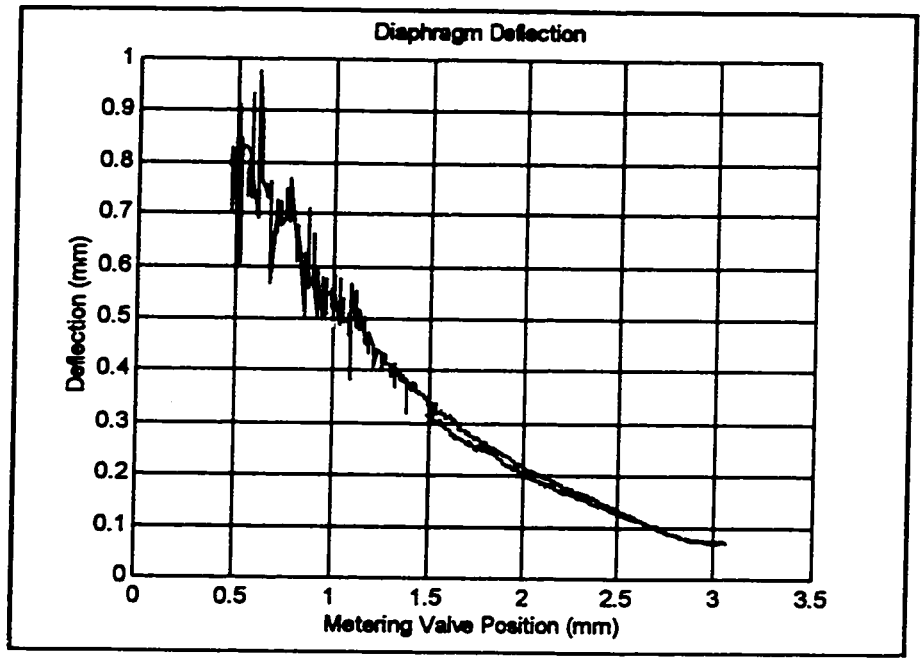

Figure 7.10 Experimental Steady State Results for the Diaphragm Deflection

Figure 7.10 shows the diaphragm flat-seat deflection. The diaphragm has maximum deflection during the initial metering valve travel and reaches its minimum displacement when the metering valve is completely open.

Figures 7.10 and 7.11 indicate that when the flat-seat valve is in its closed position, there is still some flow going through the bypass valve. This is due to a possible non-perpendicularity of the diaphragm flat-seat surface towards the exit manifold. Figure 7.12 shows the proposed design change to correct this situation. A guide bar can be used to pilot the diaphragm flat-seat valve perpendicularly to the bypass valve inlet face. This method was not used in the experiments due to the obstacle with installation of the bypass valve LVDT.

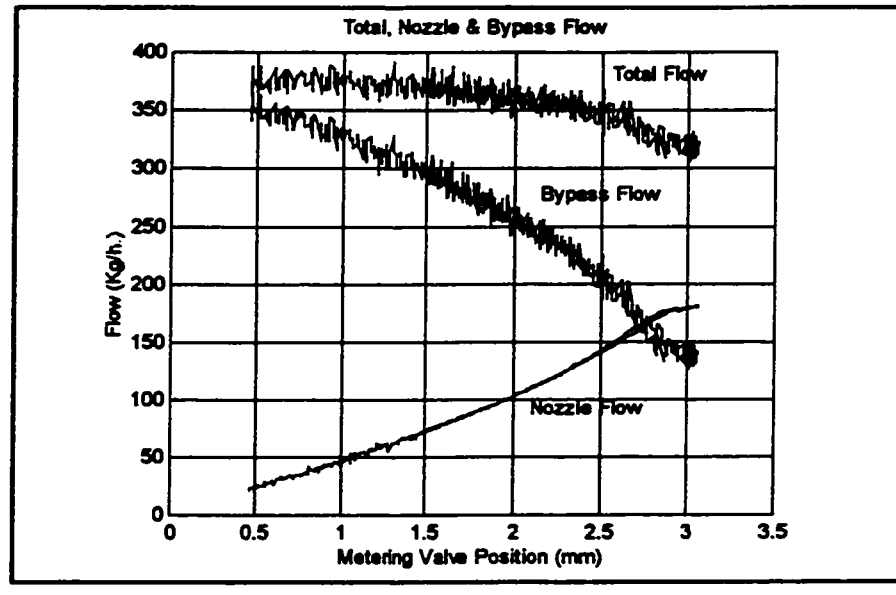

Figure 7.11 Experimental Steady State Results for Total, Bypass and Nozzle Flows

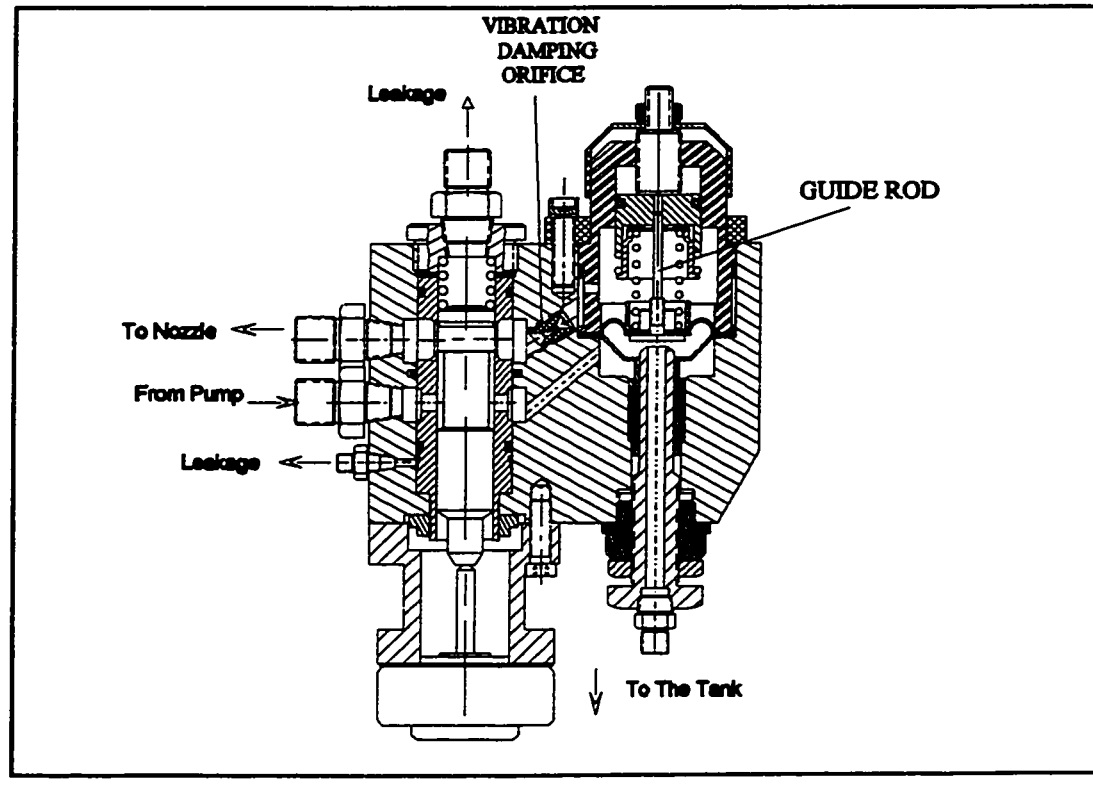

Figure 7.12 Prototype New Design with Guide Rod

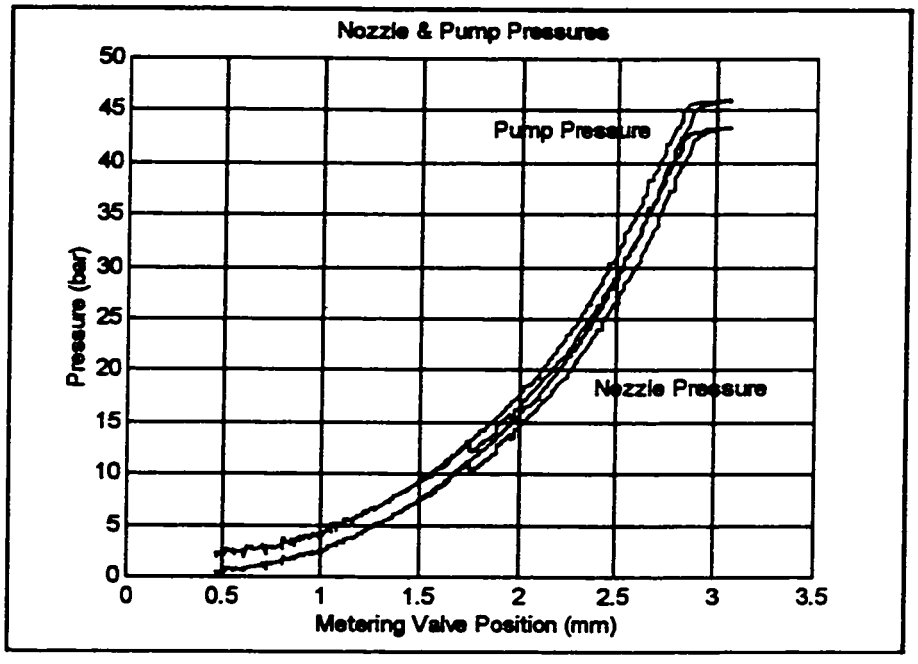

Figure 7.13 Experimental Steady State Results for Pump and Nozzle Pressures

Figure 7.13 shows the pump and the nozzle pressures versus the metering valve position. The figure also shows the effect of hysteresis on both pressures.

There are some fuel flow fluctuation shown in figure 7.11 which might be due to the high pressure pulsation from the gear type fuel pump. This phenomenon could be minimized by reducing the size of the vibration damping orifice (see figure 7.12). However, this might result in a slower transient response of the system and should be optimized.

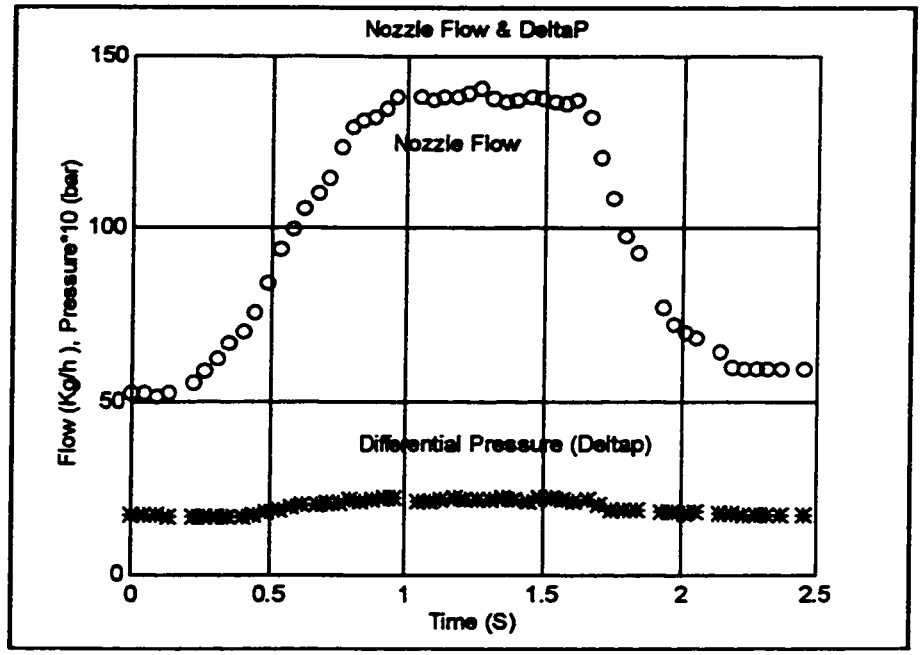

Figure 7.14 Experimental Transient Response of the Nozzle Flow and the Differential Pressure Across the Metering Valve

7.5 Transient Response Experimental Results

The experimental results of the dynamic response of the fuel metering system to a ramp movement of the metering valve plunger are shown in figures 7.14 to 7.17. The settling time of the nozzle flow is less than 0.8 sec. Since the ramp input actuation of the metering valve plunger is only 90 steps/ s, the system has a potential for much faster response. In the next chapter, computer simulation will be done for both steady state and transient processes and the results will be compared with the experimental data.

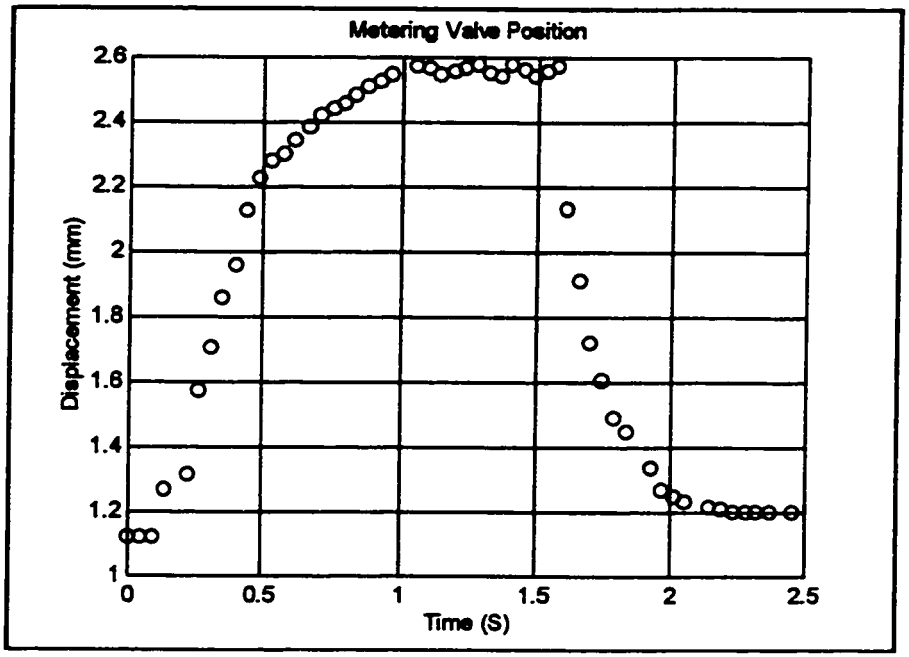

Figure 7.15 Experimental Transient Response of the Metering Valve Plunger Displacement

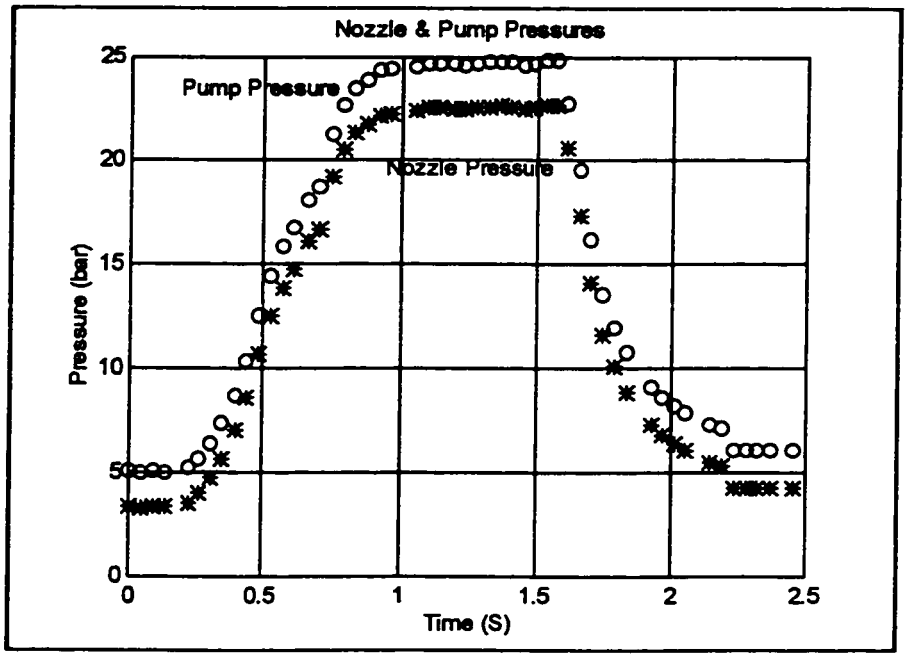

Figure 7.16 Experimental Transient Response of Nozzle and Pump Pressures

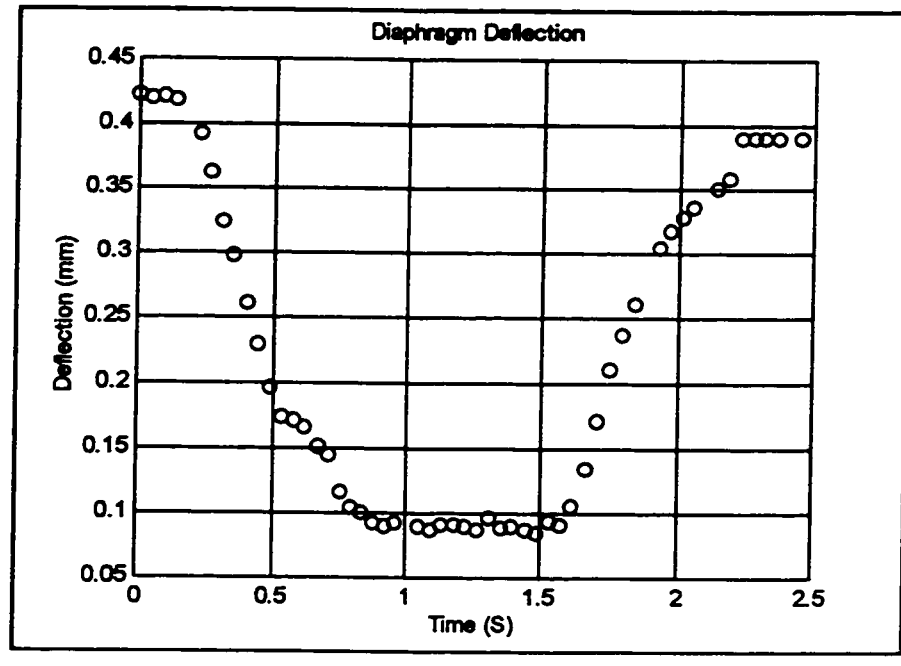

Figure 7.17 Experimental Transient Response of Diaphragm Deflection

8. COMPUTER SIMULATION OF PROCESSES FOR CONFIGURATION 1 (NEW)

A mathematical model for both the steady state and the transient response of the system was developed in chapter 5. In this chapter, a method to solve the model equations is presented and then the simulation results are investigated.

8.1 Simulation Methods

8.1.1 For Steady State

The steady state mathematical model is used to predict the behaviour of the system for the full travel of the metering valve with different pump types and at different speeds. The model is obtained by setting the transient terms $(\frac{d}{dt}, \frac{d^2}{dt^2})$ equal to zero. This results in a set of non-linear equations. Since some parameters such as $A_{bv}(y)$, y ,Q_P (P_1) are conditional and, depending on the solution, have different values, an accurate search technique based on trial and error method is used to solve the non-linear set of steady state equations. The following flowchart, figure 8.1, shows the search method. A program was written in MATLAB domain to perform the calculations, printing and plotting of the results. MATLAB which stands for *matrix laboratory*, is a high-quality programming software for numeric computation and visualization. It integrates numerical analysis, matrix computation, signal processing and graphics in an easy to use environment where problems and solutions are expressed just as they are written mathematically without traditional programming [50].

Nominal Parameters Values

$K_S = 6130$ N/m

$F_{SP} = 39.975$ N

$D_{bv} = 3.25$ mm

W= 1.3598 mm

$M_e = 12$ gr

$A_d = 270$ mm^2

$C_d = 0.6$ (for all)

$n_{xmv} = 6$

$\rho = 772$ kg/ m^3

$A_{do} = 0.04$ mm^2

$A_n = 1.08$ mm^2

$\beta = 4e8$ N/m^2

$V_1 = 4e\text{-}5$ m^3

$V_2 = 7.85e\text{-}6$ m^3

$$A_{eq} = \frac{C_{dbv} A_{xmv}}{C_{dn} A_n}$$

$$A_{eq1} = C_{dn} A_n \sqrt{\frac{2 A_{eq}}{(A_{eq}+1)\rho}} + C_{dbv} A_{bv} \sqrt{\frac{2}{\rho}}$$

$$\Delta = \sqrt{(2 C_2 C_1 - A_{eq1}^2)^2 - (2 C_2 C_1)^2}$$

$$P_1 = \frac{(-2 C_2 C_1 + A_{eq1}^2) - \Delta}{2 C_2^2}$$

C_1 and C_2 are pump coefficients.

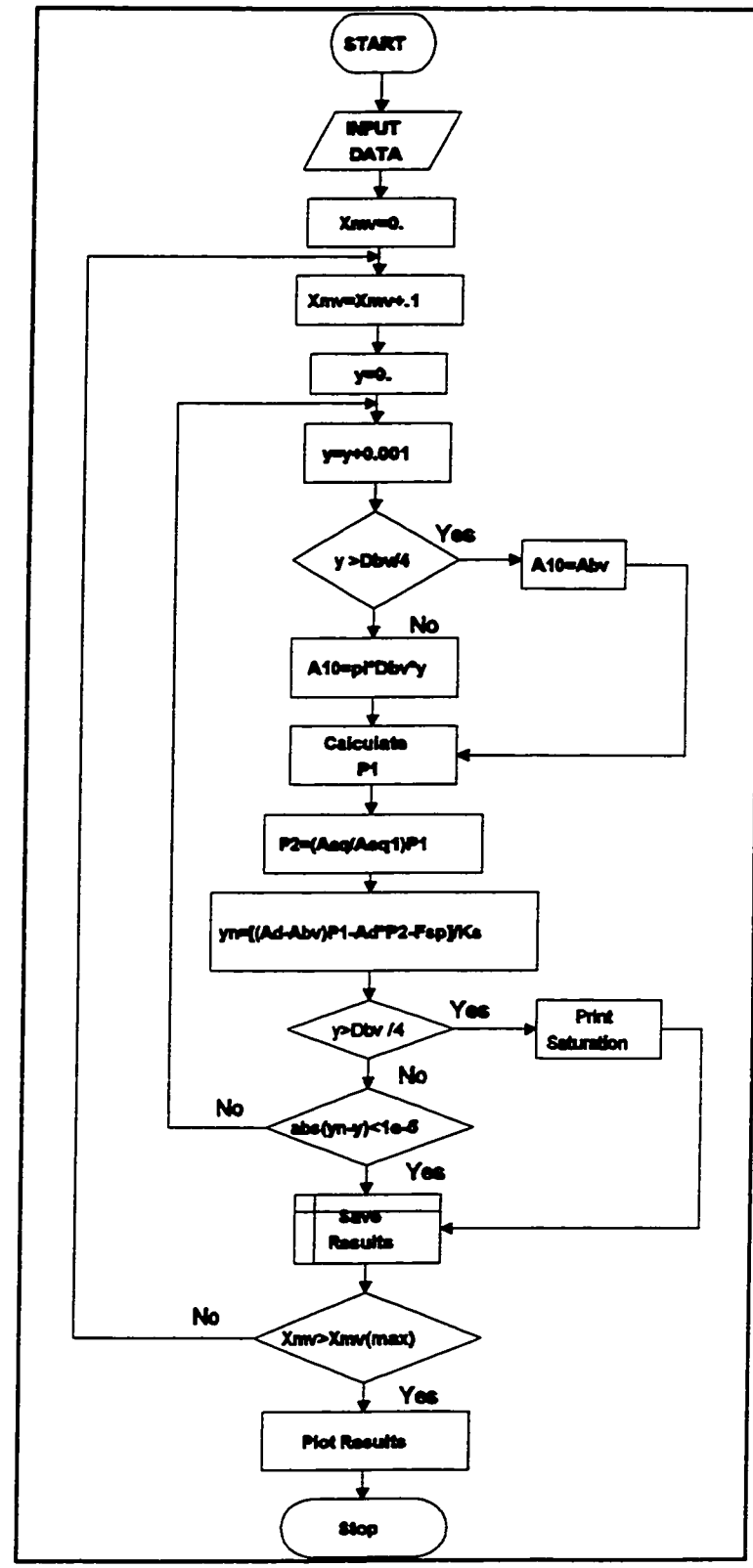

Figure 8.1 Flowchart for Calculation of Steady State Results

8.1.2 For Dynamic Response

The dynamic model is implemented on a digital computer using SIMULINK Dynamic System Simulation Software. This software is a program for simulating a dynamic system and is an extension to MATLAB. SIMULINK adds many features specific to the dynamic systems, while retaining all of MATLAB's general purpose functionality [51].

SIMULINK has different types of integration algorithms such as third and fifth order Runge-Kutta, Euler, Gear, Adams and others. The Runge-Kutta methods are good general purpose methods that work well for a large range of problems [52]. The third order method uses a second order method for step size control and takes three steps to generate one output point. The fifth order one uses a forth order method for step size control and it takes six unevenly spaced points between the output points. Although the fifth order Runge-Kutta is generally faster and more accurate than third order one, it produces fewer output points; therefore, the third order is a preferred choice for smoother plots and consequently, it was chosen as integration algorithm.

8.2 Simulation of Steady State Processes

Figures 8.2 to 8.6 show some steady state simulation results for the full travel of the metering valve for nominal design variable setting. Figures 8.2 and 8.3 shows the steady state simulation results at different pump speeds by using a constant displacement pump driven by the engine. The figure 8.2 shows that the metered fuel output varies almost linearly with the metering valve movement at low metering valve opening. As the system demands more fuel flow and the metering valve opening increases, the diaphragm flat-seat valve starts to close to reduce the flow through the

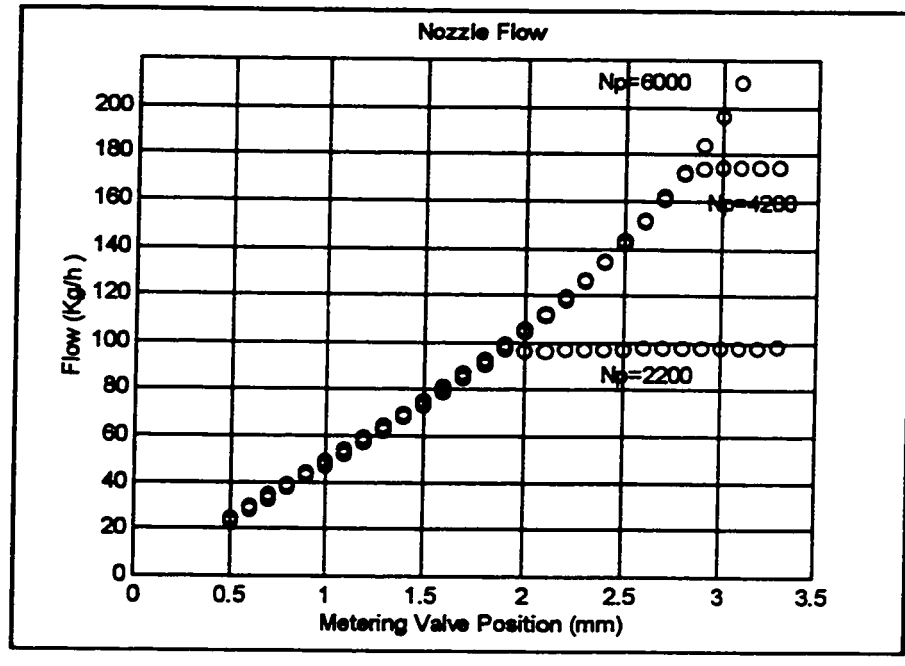

Figure 8.2 Steady State Simulation Result for the Nozzle Fuel Flow with Constant Displacement Pump Driven by the Engine

bypass valve. However, due to the increase of unbalanced forces acting on the diaphragm, the differential pressure across the metering valve increases providing the non-linearity of the nozzle flow versus the metering valve position.

Figure 8.2 also shows that at some higher metering valve openings, the nozzle flow rate might not follow the metering valve travel. This is due to the fact that at those metering valve positions, the pump which is running at lower speed, is not able to maintain the required flow for both the metering valve and the bypass valve. In this case, the diaphragm flat-seat valve is at its closed position and thus, all the pump flow passes through the metering valve. By opening more the metering valve orifice, the nozzle flow increases slightly, however, the differential pressure decreases, as shown in figure 8.3.

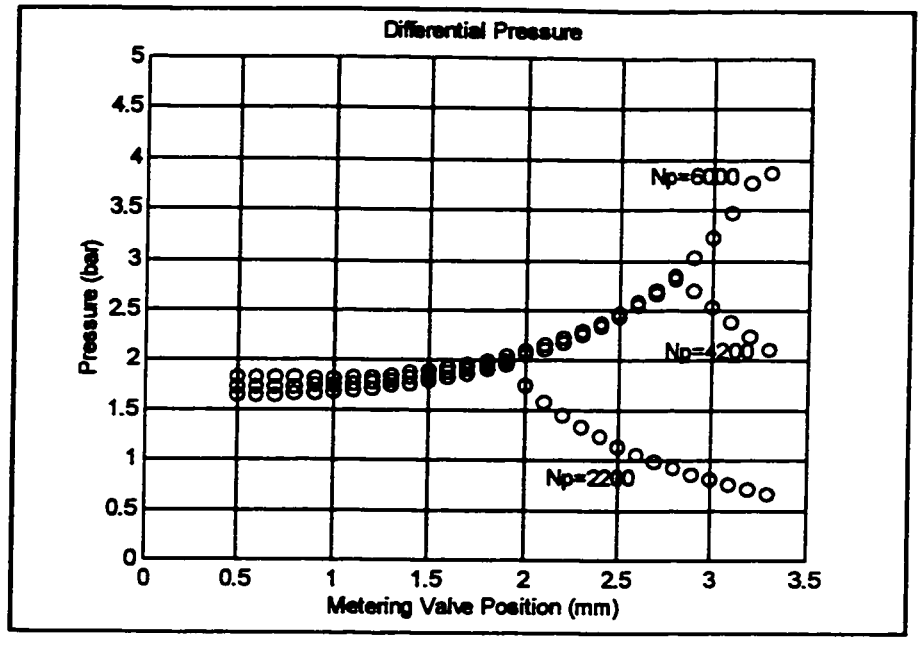

Figure 8.3 Steady State Simulation Result for the Differential Pressure Across the Metering Valve with Constant Displacement Pump Driven by the Engine

Figure 8.4 shows the steady state simulation results for the nozzle flow when the fuel metering system is supplied by a constant displacement pump driven by a DC electric motor at varying pressures. As it is shown in figure 8.5, the pump flow declines by about 40% as the pump discharge pressure reaches its maximum value. This is due to the fact that the motor driving the pump, is torque sensitive and by increasing the load (nozzle pressure), the pump speed decreases. However, the pump flow rate is still high enough as compared with the value which is required for a linear relation between the metering valve movement and the nozzle flow. This means that the proposed metering system is not sensitive to the flow decline due to the nozzle back pressure. The behaviour of such a system is almost the same as in the previous case for the engine driven pump.

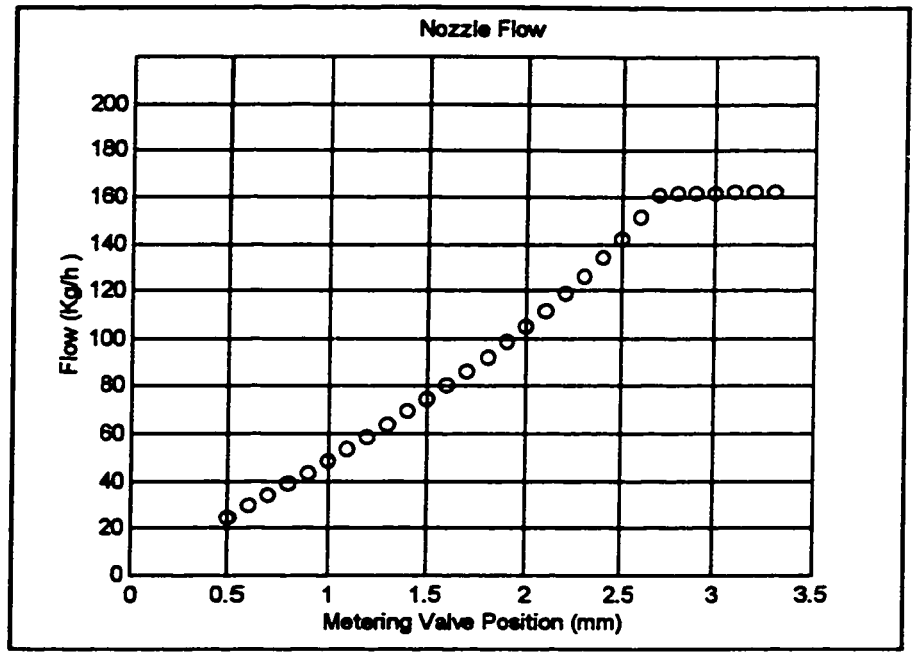

Figure 8.4 Steady State Simulation Result for the Nozzle Flow with a Constant Displacement Pump Driven by a DC Electric Motor

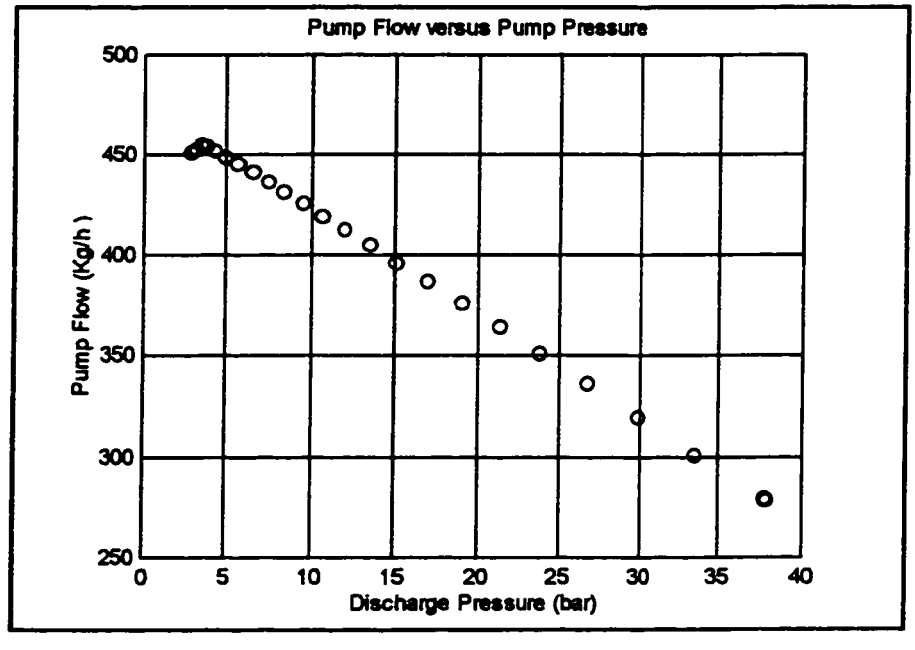

Figure 8.5 The Pump Flow Versus the Pump Pressure for a Pump Driven by a DC Electric Motor

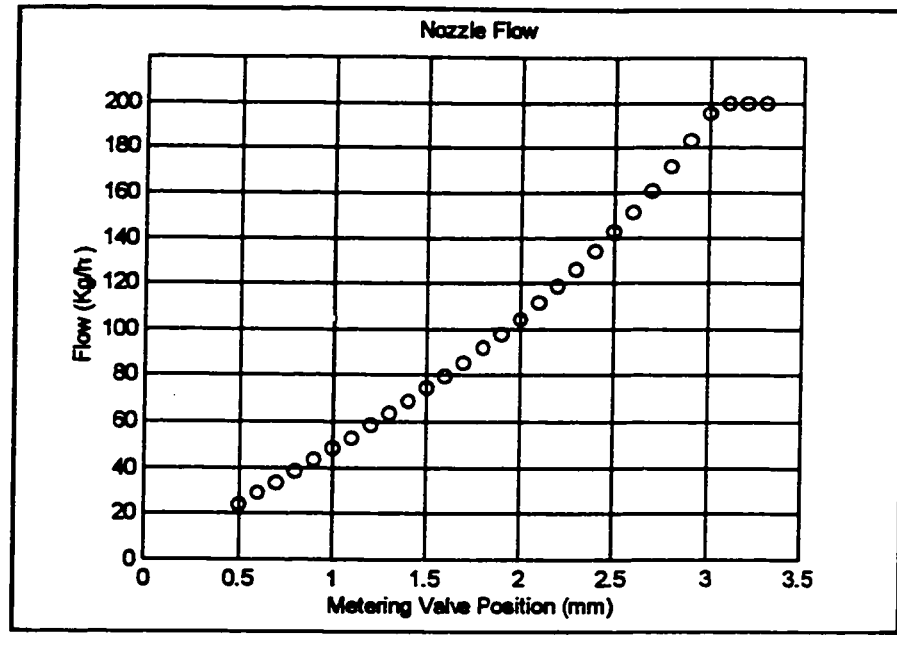

Figure 8.6 Steady State Simulation Result for the Pump Driven by a Constant Speed Electric Motor

Figure 8.6 shows the steady state simulation results for a constant displacement fuel pump which is driven by a constant speed electric motor. In this case, the pump flow output is independent on the nozzle pressure and is almost constant. Similar to the previous cases, due to the diaphragm type differential pressure bypass valve characteristics, at high metering valve opening, the non-linearity increases.

Finally, the above simulation results confirmed that the proposed fuel metering system is applicable with different fuel pump types; however, the parameters of the system should be optimized in order to provide the best linear relation between the metering valve movement and the nozzle flow. This design analysis will be done in the next chapter.

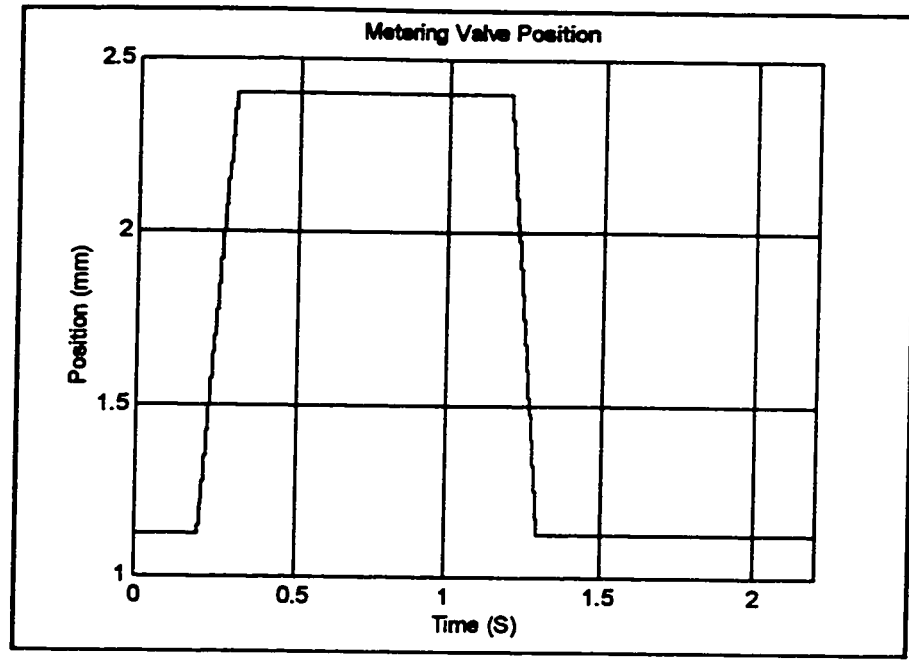

Figure 8.7 Metering Valve Plunger Position Versus Time (Simulation)

8.3 Simulation of Dynamic Response

The investigation of the transient response of the fuel metering system is performed when the metering valve is moving with a large stepping rate. This provides a ramp input to the control system. Figure 8.7 shows the positive and negative ramp inputs when the metering valve moves from the initial position of 1.1 mm to 2.4 mm and then returns to its initial position. The step size and the stepping rate is .025 mm and 450 steps/ s respectively and the actuation time is about 100 ms.

Figure 8.8 shows the nozzle flow transient response to a positive and a negative ramp input. As seen, the settling time is 0.8 s and 0.62 s respectively. This means that the system has a faster response when lowering the fuel flow demand.

Figure 8.9 shows the diaphragm deflection transient. The diaphragm moves down to close the diaphragm orifice in order to accommodate a larger nozzle flow

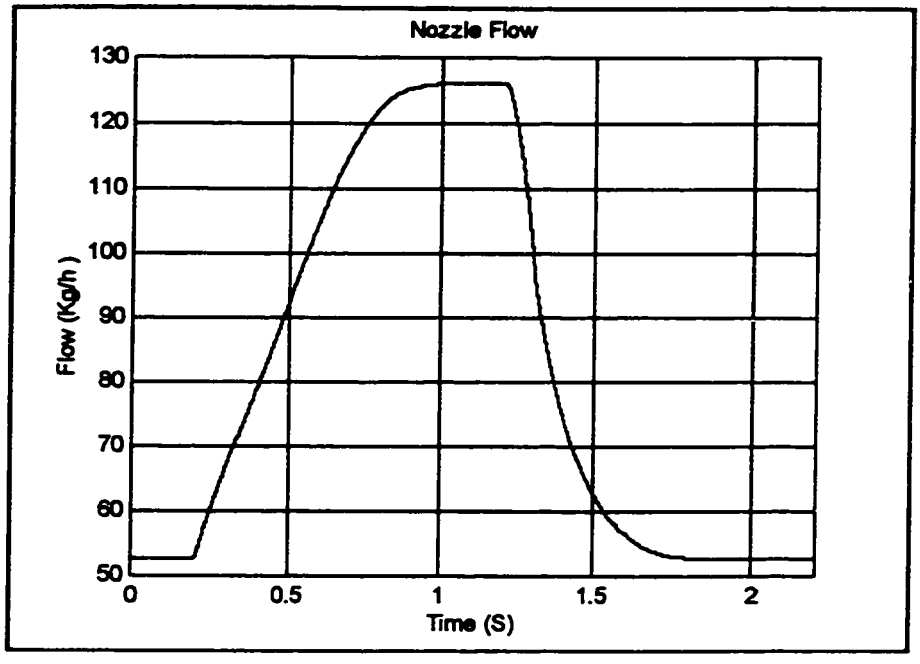

Figure 8.8 Nozzle Flow Transient (Simulation)

during a positive metering valve ramp input. During a negative ramp input the diaphragm moves up to let more bypass flow pass through the diaphragm bypass valve and consequently, the nozzle flow decreases.

Figure 8.10 shows the pump output. As it is seen, the pump flow declines as the pump pressure increases. This is due to the fact that as the back pressure (load) on the pump increases, the leakage across the pump gears also increases.

Figure 8.11 shows the differential pressure across the metering valve. Due to the fast opening of the metering valve, instantly the differential pressure slightly decreases, until the metering valve reaches its final position and stops. Next, the differential pressure recovers by moving the diaphragm down. Similar scenario repeats for the metering valve closing, as a negative metering valve ramp input is applied. In this case, also the differential pressure instantly increases as the metering

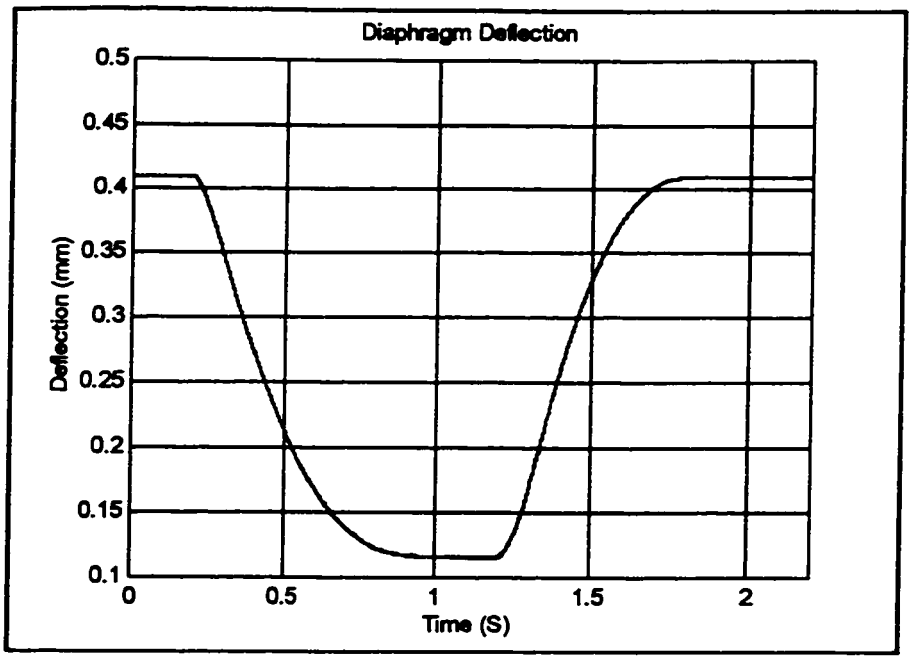

Figure 8.9 Diaphragm Deflection Transient (Simulation)

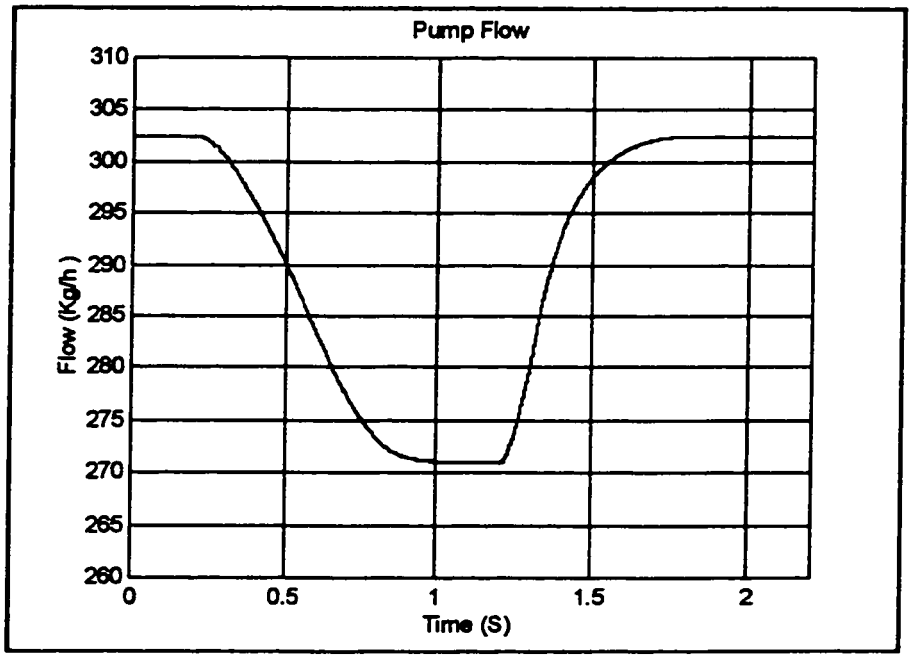

Figure 8.10 Pump Flow Transient (Simulation)

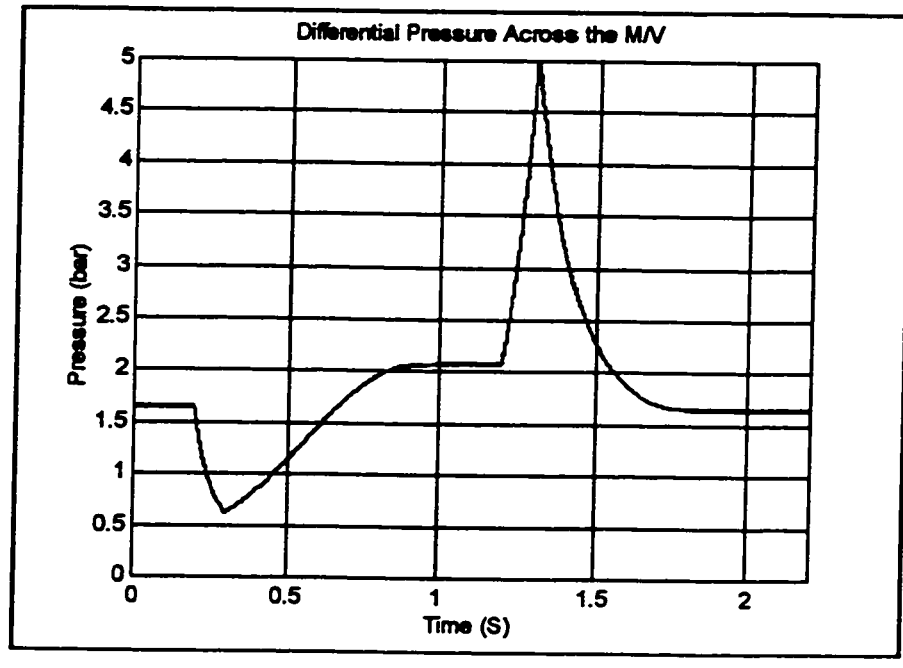

Figure 8.11 Differential Pressure Transient (Simulation)

valve returns to its initial position and next, the differential pressure decreases due to the opening of the diaphragm flat-seat valve.

8.4 Validation of the Mathematical Model

In this section, the experimental results are used to validate the mathematical model described in chapter 5.

8.4.1 Steady State Model Validation

Figures 8.12 to 8.15 show both the steady state simulation and the experimental results. As seen, the model accurately predicts experimental results for steady state conditions. The differential pressure remains almost constant over small opening of the metering valve but it rises gradually with further metering valve opening. During the first period of the metering valve opening, the diaphragm flat-seat valve opens by a significant amount in an attempt to maintain the differential pressure. As shown in figure 8.14, the fuel pump delivery drops at higher opening of the metering valve due to the rise in the nozzle pressure. However, the pump output is sufficient to maintain the required flow for both the metering and the diaphragm flat-seat bypass valves and therefore, the metered flow varies semi-linearly with the metering valve position. It is anticipated that the parameters of the system should be optimized to improve the linearity of the metering valve characteristic.

Figure 8.13 shows that the diaphragm fluctuates at low output of the metering valve. It might be related to the pressure pulsation as the result of the gear pump output fluctuation. This phenomenon is disappearing at higher pump speed.

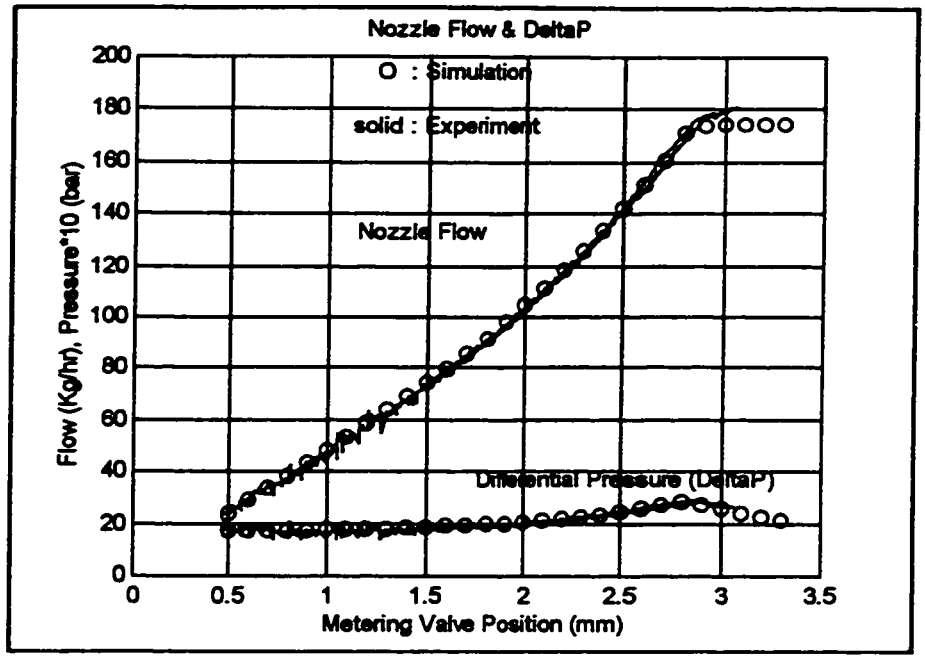

Figure 8.12 Experimental and Simulation Steady State Results for the Nozzle Flow and the Differential Pressure Across the Metering Valve

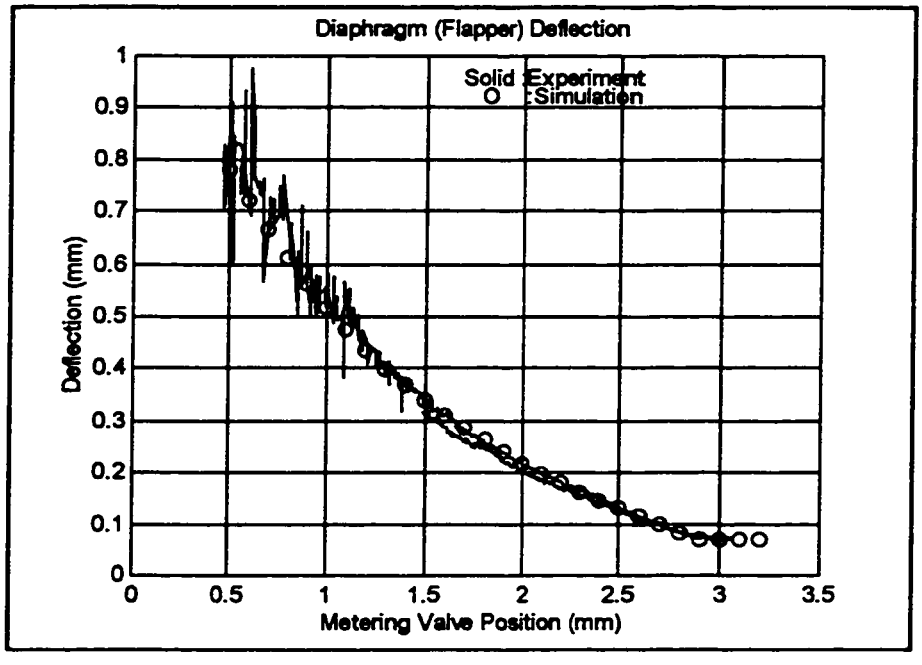

Figure 8.13 Experimental and Simulation Steady State Results for the Diaphragm Deflection

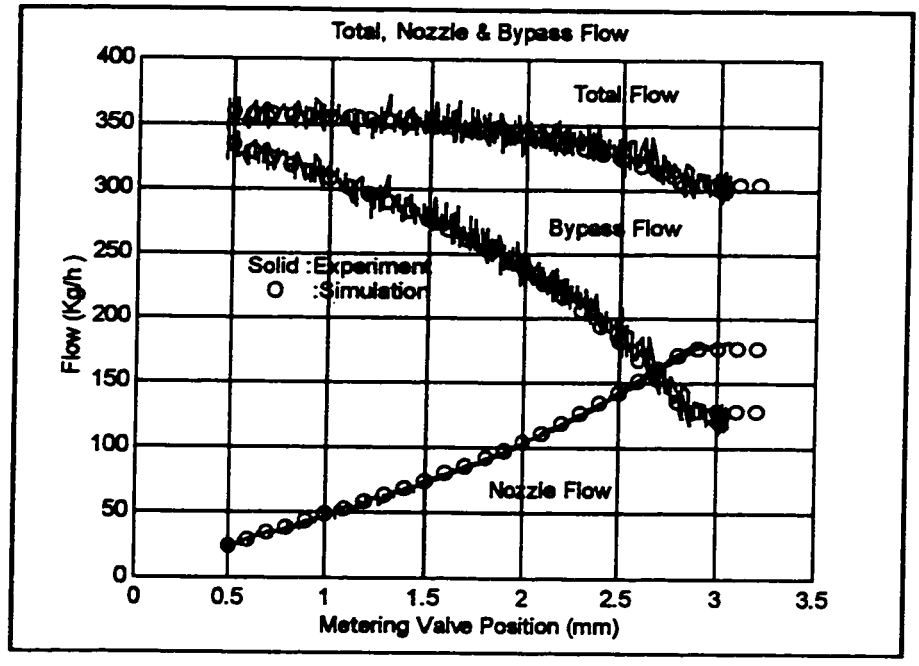

Figure 8.14 Experimental and Simulation Steady State Results for the Total, Bypass and Nozzle Flows

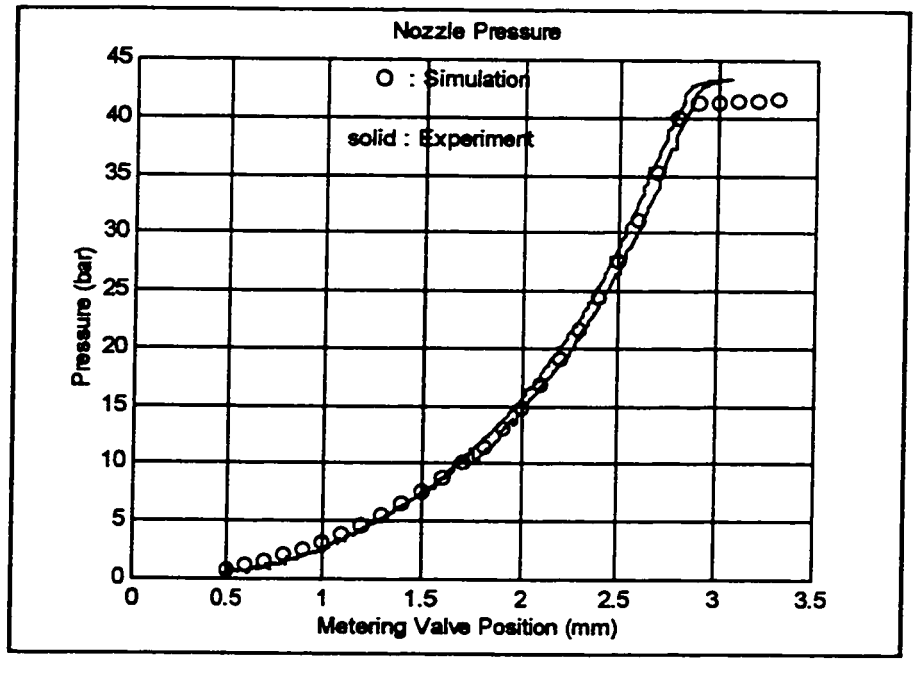

Figure 8.15 Experimental and Simulation Steady State Results for the Nozzle Pressure

8.4.2 Dynamic Model Validation

Figures 8.16 to 8.21 compare the simulated and experimental transient responses of the system to an 80 steps/s ramp input of the metering valve where it moves from 1.1 mm to 2.6 mm. The simulated transient response of the metered fuel flow, the diaphragm deflection, the nozzle and pump pressure, the differential pressure across the metering valve and the diaphragm agree quite well with the experiments. Some visible discrepancies between simulation and experiments are mainly due to the inaccuracies in the estimation of the fuel modulus of elasticity, the volume of various chambers within the fuel metering system and piping and also the prediction of the pump fuel delivery.

In general, the model predicts the steady state and transient behaviours of the system quite accurately and could be used for design optimization.

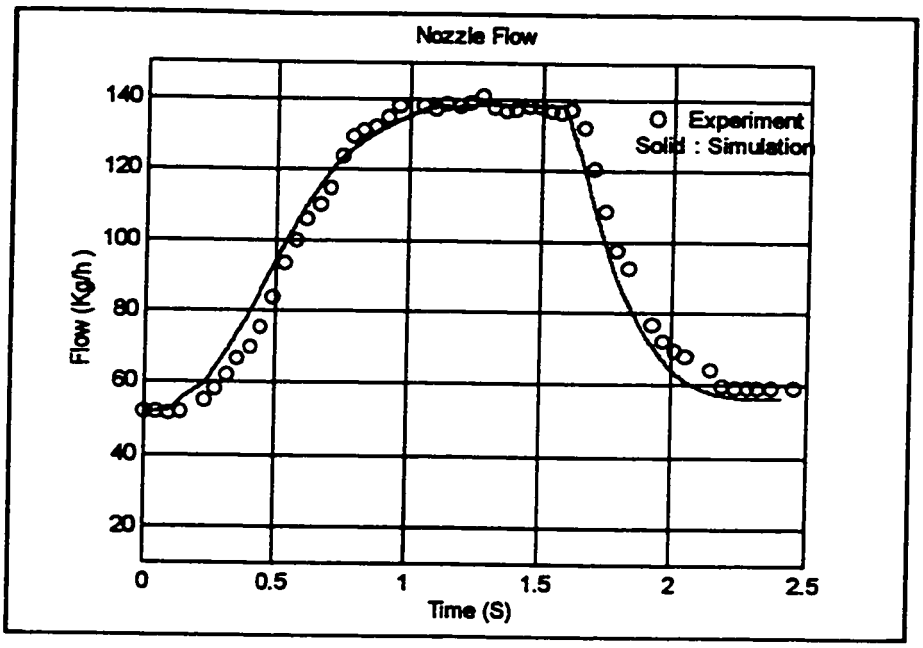

Figure 8.16 Experimental and Simulation Transient Results for the Nozzle Flow

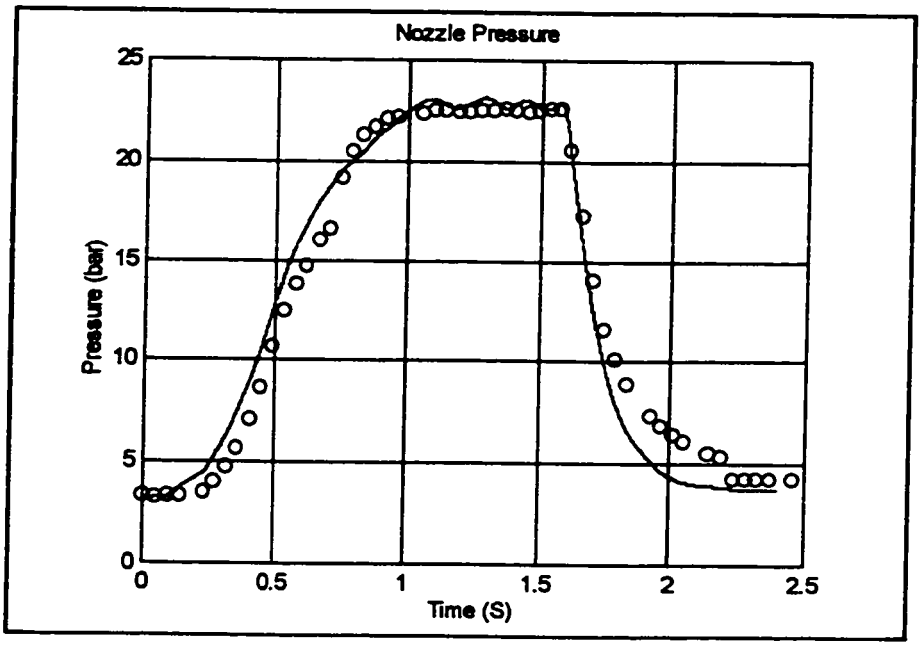

Figure 8.17 Experimental and Simulation (solid line) Transient Results for the Nozzle Pressure

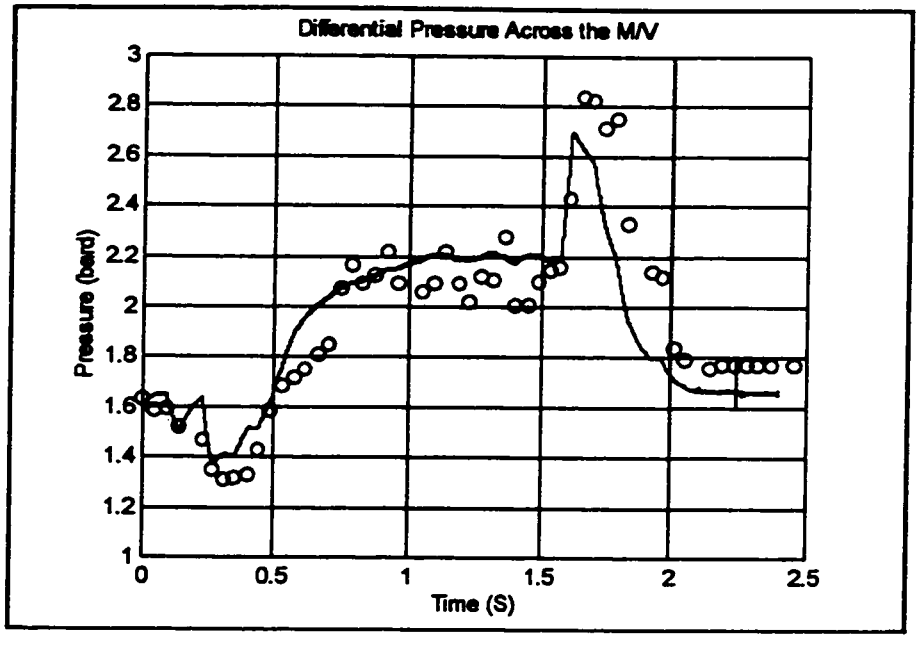

Figure 8.18 Experimental and Simulation (Solid Line) Transient Results for the Differential Pressure Across the Metering Valve

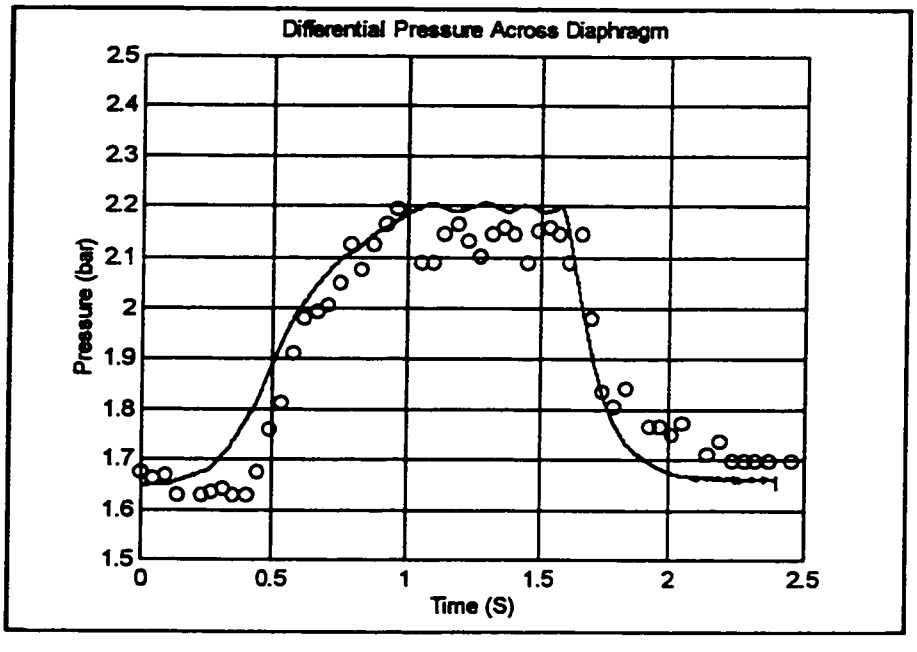

Figure 8.19 Experimental and Simulation (Solid Line) Transient Results for the Differential Pressure Across the Diaphragm

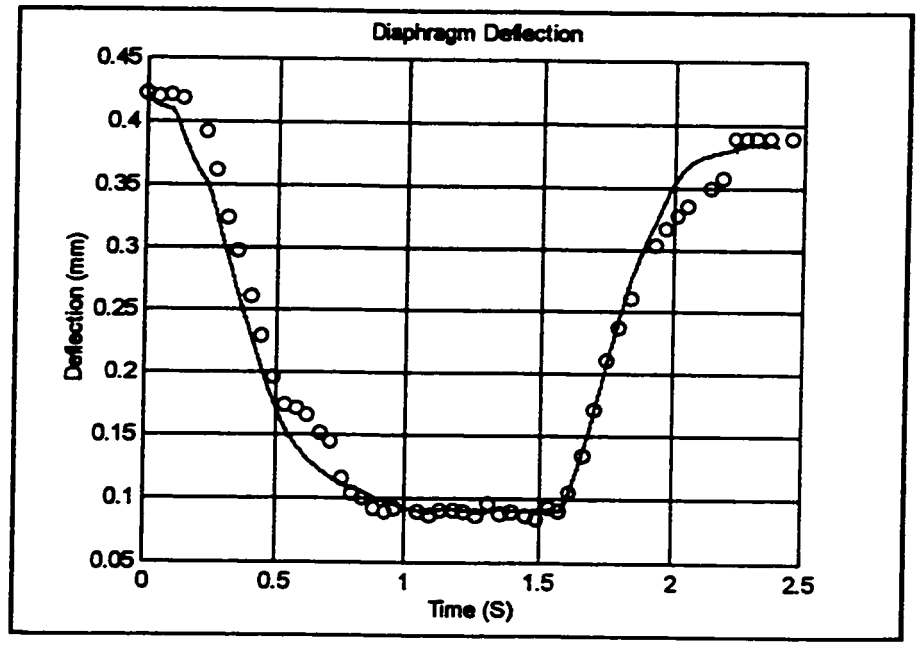

Figure 8.20 Experimental and Simulation (Solid line) Transient Results for the Diaphragm Deflection

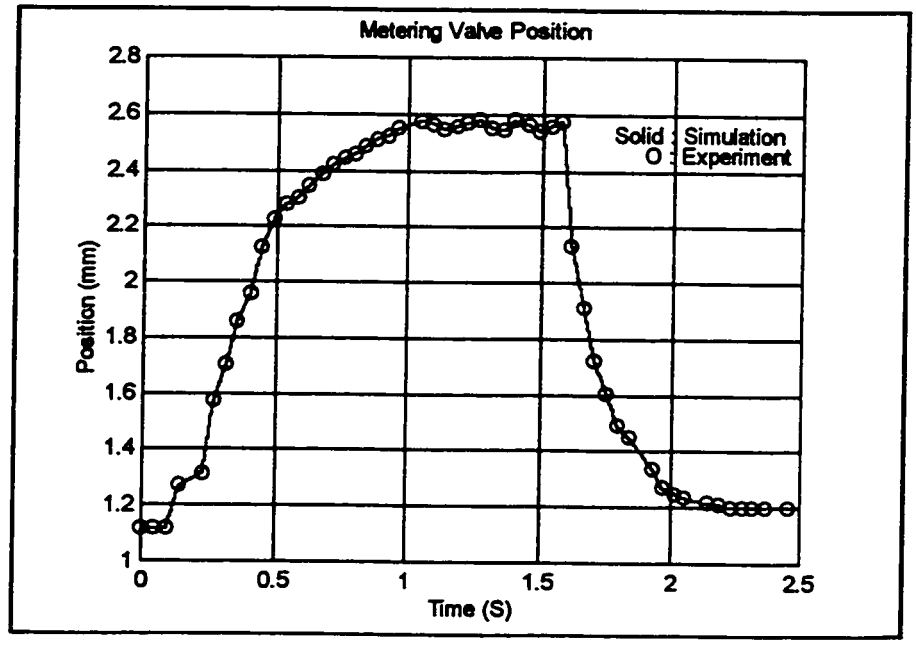

Figure 8.21 Experimental and Simulation (Solid line) Transient Results for the Metering Valve Position

9. OPTIMIZATION OF CONFIGURATION 1(NEW)

The purpose of this chapter is to optimize the design of the fuel metering system. As it was explained in Chapter 1, for a fuel metering system, it is beneficial to maintain a constant differential pressure across the metering valve, so that the metered fuel flow rate would be proportional to the metering valve flow area, i.e., to the plunger travel. However, Chapter 8 showed that there is some non-linearity in differential pressure across the metering valve due to the unbalanced pressure forces acting on the diaphragm. To have a closer constant differential pressure across the metering valve and also to improve the performance of the system, three design optimization objectives were identified and investigated as follows:

1. Minimize the variation in the differential pressure across the metering valve over the full fuel flow operating range. This is also a measure of the linearity of the nozzle flow versus the metering valve travel.
2. Speed up the transient response.
3. Make the system less sensitive to the possible nozzle orifice contamination, to the spring preload and spring constant changes and also to the variations of the bypass valve orifice diameter (sensitivity analysis).

These three criteria have been arbitrarily determined for the proposed fuel metering system and the full optimization procedure will be described in the next sections. Finally, these criteria will be unified in a multi-objective optimization scheme.

9.1 The First Optimization Criterion; Linearity:

To have a linear metering valve fuel flow schedule, the differential pressure across the metering valve should be kept close to constant. In this section, the validated model, as presented in chapter 6 is used to design the system with the lowest change of differential pressure across the metering valve over the full fuel flow schedule. It is also possible to maintain a constant differential pressure across the metering valve by taking advantage of the abilities offered by an electronic controller. However, due to the complicated software required for this purpose and also to the need of additional sensors, a linear metering valve is preferred by customers due to its simplicity.

The sources of variation of the differential pressure across the metering valve can be identified from a force balance equation on the diaphragm flat-seat valve at the steady state condition. By setting the transient terms (d/dt, d^2/dt^2) equal to zero in the equation (6.13), the following force balance equation is found (see figure 7.9):

$$P_1(A_d - A_{bv}) - P_u A_d - K_s y - F_{sp} = 0 \qquad (9.1)$$

Expressing the forces in terms of differential pressure ($P_1 - P_u$), the equation can be rearranged as follows:

$$P_1 - P_u = \frac{F_{sp}}{A_d} + \frac{P_1 A_{bv}}{A_d} + \frac{K_s y}{A_d} \qquad (9.2)$$

The spring preload force, the first term, has a constant value and does not change during the metering valve movement. Therefore, it does not have any direct

impact on the regulated differential pressure variation. However, changing of the spring preload force, results in the differential pressure change.

As it is seen, the signs of the second and the third terms are positive. This means that these terms can not eliminate each other so that the differential pressure remains only a function of the preload force.

The second term indicates that the differential pressure is rising as the pump pressure is increasing. This means that the pump pressure has a direct effect on differential pressure. To lower its effect, the bypass orifice flow area (A_{bv}) should be as small as possible. However, the minimum bypass flow area is determined by the maximum bypass flow rate passing through the bypass valve.

The third term indicates that the differential pressure tends to increase as the diaphragm moves up. This effect can be amplified with the use of a stiffer spring.

It should be noted here that the effects of the second and the third terms act in opposite directions with respect to the nozzle flow. This indicates a possibility to design the diaphragm flat-seat valve so that these effects compensate (neutralize) each other as much as possible.

It seems that there is also another possible solution for linearity improvement by increasing the preload force, so that the first term dominates equation 9.2. However, there are three disadvantages. First, it decreases the resolution of the system, i.e. one step of the stepper motor will correspond to a larger flow change. The second is that by using a higher differential pressure, a higher pump pressure is required which needs a more powerful pump, resulting in higher cost of the fuel system. Finally, by increasing the pump pressure, the second term will be changed and therefore the differential pressure will still not be constant.

9.1.1 The Impact of Design Variables on the Differential Pressure

In this section, first, a performance index is defined as the maximum variation of the differential pressure from its average value over the full flow schedule. This index is defined as LIN,

$$LIN = 100 \frac{\max \mid \Delta P_i - \Delta P_{mean} \mid}{\Delta P_{mean}} \tag{9.3}$$

where ΔP_i is the value of the differential pressure observed over the flow schedule, and ΔP_{mean} is the average differential pressure over the metering valve schedule.

The effect of each variable on the LIN index is examined by parametrically varying it, while all other design variables are kept constant.

A program in MATLAB domain is written to calculate the LIN index. First, all the data required from steady state simulations are given. Then for a particular design variable i.e. K_S ,with the other design variables kept fixed, the program is run several times to find ΔP_i for each case and for different values of K_S. Finally, by calculating the LIN index in percentage, the results are plotted. This procedure is repeated for all design variables.

9.1.2 Simulation Results

The results of the simulation exercises of design variables on the LIN index are shown in figures 9. 1 to 9.4. Figure 9.1 shows the effect of the spring preload on the differential pressure variation. As seen, by increasing the preload force, the change in differential pressure is less significant, however it is still increasing. This means

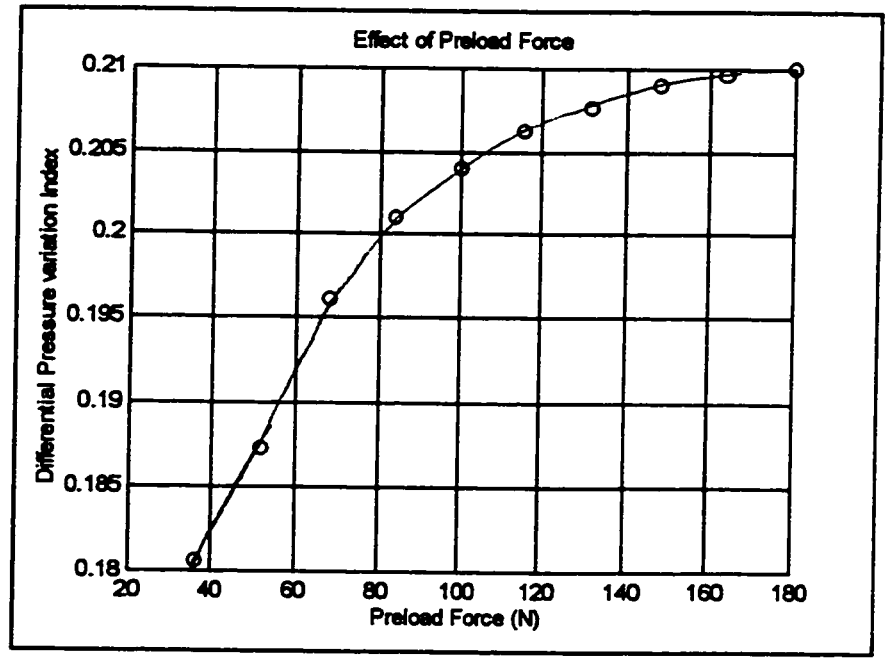

Figure 9.1 Effect of the Preload Force on the LIN Index

that for the proposed fuel metering system, it is not necessary to increase the nominal value of the spring preload force to obtain better linearity. This figure also confirms that by increasing the preload force, the differential pressure increases. The reason is that by increasing the preload force, the pump must deliver the same flow with a higher pressure. This higher pressure increases the unbalance force on the bottom side of the diaphragm and therefore, the differential pressure increases.

Figure 9.2 shows the effect of the spring constant on the LIN index. It shows that there is an optimum spring constant value of about 98 N/mm. With such a spring, the variations in differential pressure will be minimized. The reason is that, for a low spring constant, the force variation due to the $K_s\ y$ term, as compared to $P_1\ A_{bv}$ term in equation 9.2, is very small. By increasing the spring constant, during initial movement of the metering valve, the first term dominates the second term but

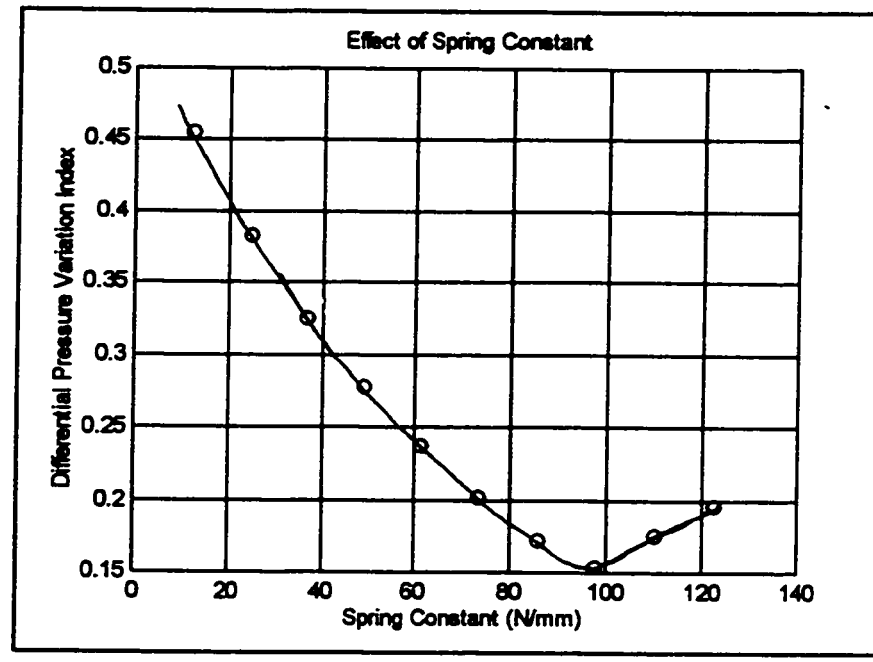

Figure 9.2 Effect of the Spring Constant on the LIN Index

gradually the first term decreases and the second term increases. At K_S=98 N/mm, both terms compensate each other very well during the full movement of the metering valve. After the increase over the optimum value, the change of the first term will be bigger than the second term and therefore, the change in differential pressure increases.

Figure 9.3 shows the effect of the bypass orifice diameter on the LIN index. It shows that the differential pressure variation increases as the diameter increases. This can be explained as follows. For a given flow range, by increasing the bypass orifice diameter, the P_1 A_{bv} force increases. With the increase of this force, the force balance in equation 9.2 will be changed and, therefore, the differential pressure will be increased.

Figure 9.4 shows the effect of the nozzle contamination. It is well known that

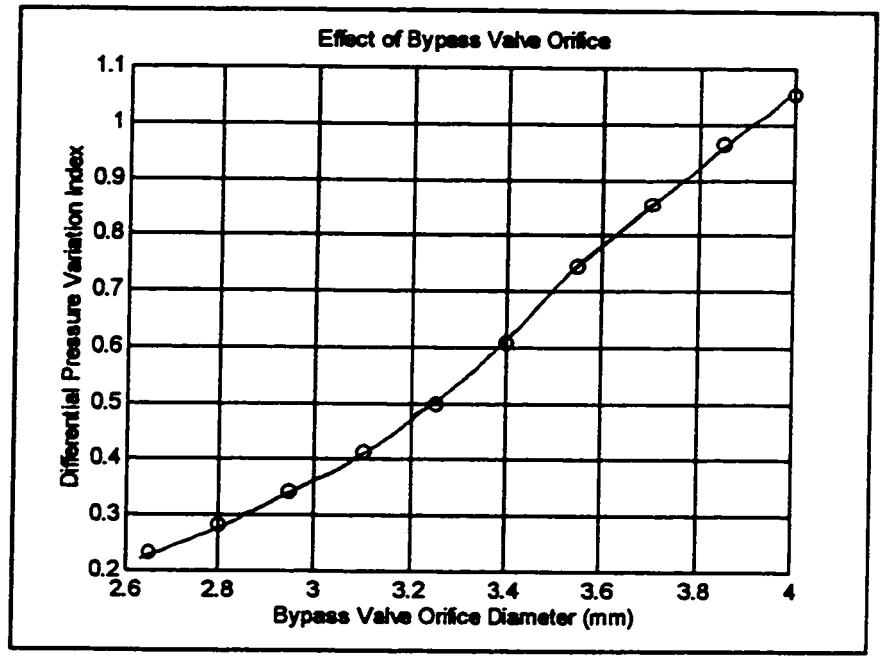

Figure 9.3 Effect of the Bypass Valve Orifice Diameter on the LIN Index

carbon deposits are the major causes of injector flow rate change in gas turbine engines. Contamination reduces the effective flow area of the nozzle. A well designed fuel injection system should be, to some extent, insensitive to the flow area changes of the nozzle. A small, about 1.5 percent increase is observed in the differential pressure as the nozzle flow area decreases by 1 percent. This deviation seems to be acceptable. The reason for the impact of the nozzle contamination on the differential variation index is given as follows. By decreasing the nozzle flow area, the pressure P_2 and the pump pressure increase to such extent that the same fuel flow before contamination would enter the combustor. By increasing the pump pressure, the term $P_1 \ A_{bv}$ in equation 9.2 increases, therefore, a wider variation of differential pressure is produced.

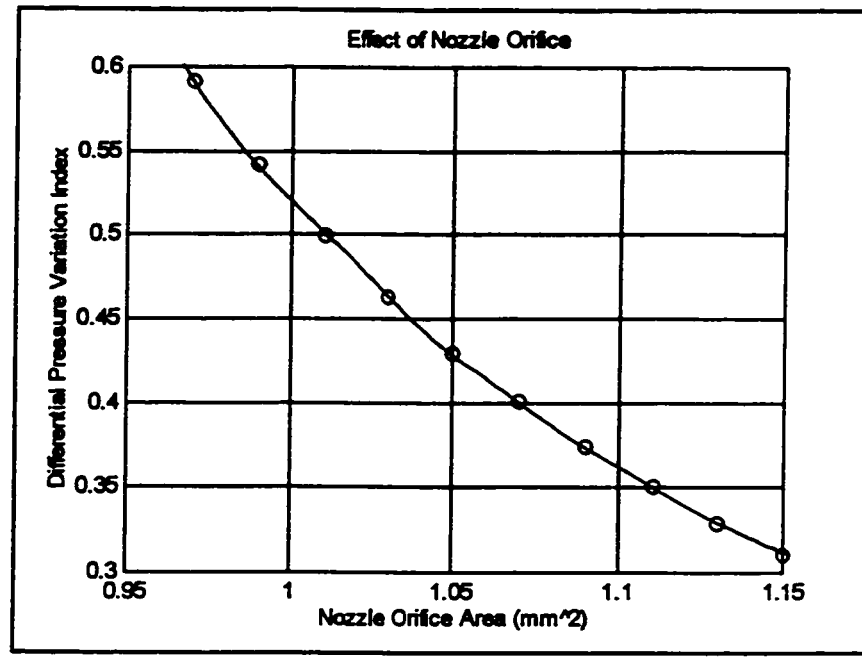

Figure 9.4 Effect of the Nozzle Flow Area on the LIN Index

Finally, to have a linear relation between the metering valve position and nozzle flow, it is recommended that the spring constant be 98 N/mm and the bypass valve diameter is chosen as small as possible. The ultimate values will be determined during the multi-objective optimization.

9.2 The Second Optimization Criterion;

Transient Response Performance:

In this section, the effect of design variables on the transient response of the system is presented. Since a fast transient response of the fuel metering system is required, a transient performance index must be defined. The performance index chosen to evaluate the transient response is ITAE , Integral of the Absolute Value of the Error multiplied by Time, and is defined as follows:

$$ITAE = \sum_{i=1}^{K} \frac{| Mmv_f - Mmv_i |}{Mmv_f} \; t \; \Delta t_i \qquad (9.4)$$

where:

Mmv_f : is the final steady state nozzle flow

Mmv_i : is the nozzle flow at the i-th step of the simulation

t : is the running simulation time

Δt_i : is the current time step

K : is the number of simulations

The ITAE index has such a characteristic that in the unit step response of the system, a large initial error is weighted lightly, and errors occurring late in the transient response are penalized heavily. Other indices commonly used in control theory such as Integral Square Error (ISE), Integral of Time multiplied Square Error (ITSE) and Integral of Absolute Error (IAE) indices could also be used. However, the ITAE index is the best performance index for optimization of an overdamped response. More details about different indices and their application is given in reference [53].

A particular program was written to find the dynamic response of the model for different operating conditions. This was done by using Simulink Toolbox of MATLAB. A ramp input was created as a reference input by selecting a very high stepping rate in the simulation program to provide a suitable criterion for differentiating a fast design from a slow one.

Consideration should be given to the fact that not all simulation time steps, Δt_i, are equal, since Simulink uses an adaptive step size technique. However, it was found that the steps taken were still small enough to create negligible integration errors in calculation of the index. The simulation was done for 1.25 s and the average step size is 0.1 ms.

9.2.1 Simulation Results

Figures 9.5 to 9.8 show the effect of design variables on the transient response. The effect of all variables is investigated in sequence with all other variables fixed at nominal settings. Only the feasible design range is investigated.

Figure 9.5(a) shows the effect of the spring preload force on the performance index. It indicates that increasing the spring preload force increases the speed of the transient response. It is concluded that with a larger differential pressure, a smaller change in metering valve flow area is required to achieve the same change in fuel flow. Thus, the stepper motor has to push the plunger for a shorter distance and, therefore, it speeds up the response of the system. However, by increasing the differential pressure, the resolution of the fuel metering system is reduced. Figure 9.5(b) shows two typical transient responses for a low spring preload and a high preload forces, indicating the improvement in the performance index due to the increase in the spring preload force.

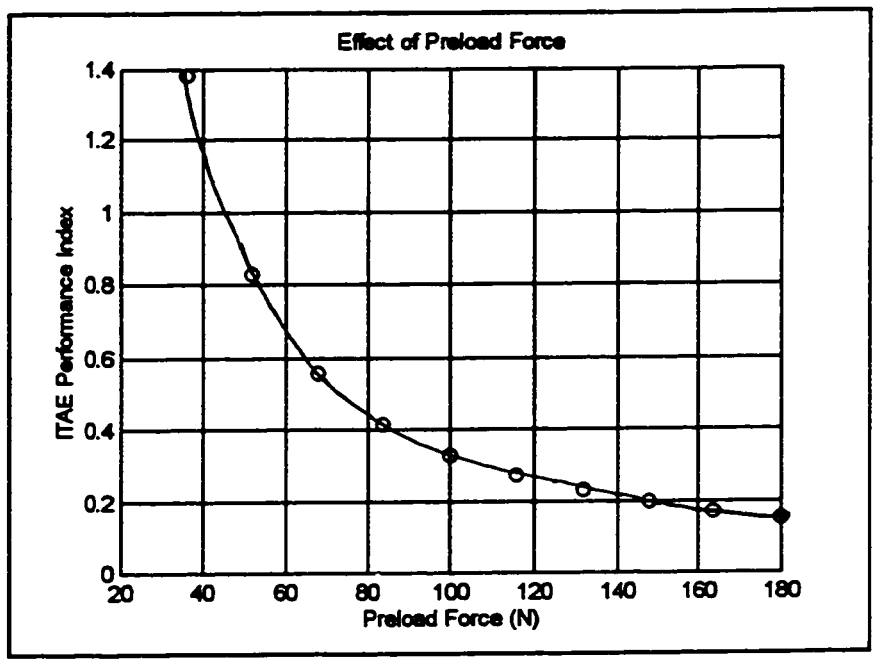

Figure 9.5(a) Effect of the Preload Force on the ITAE Index

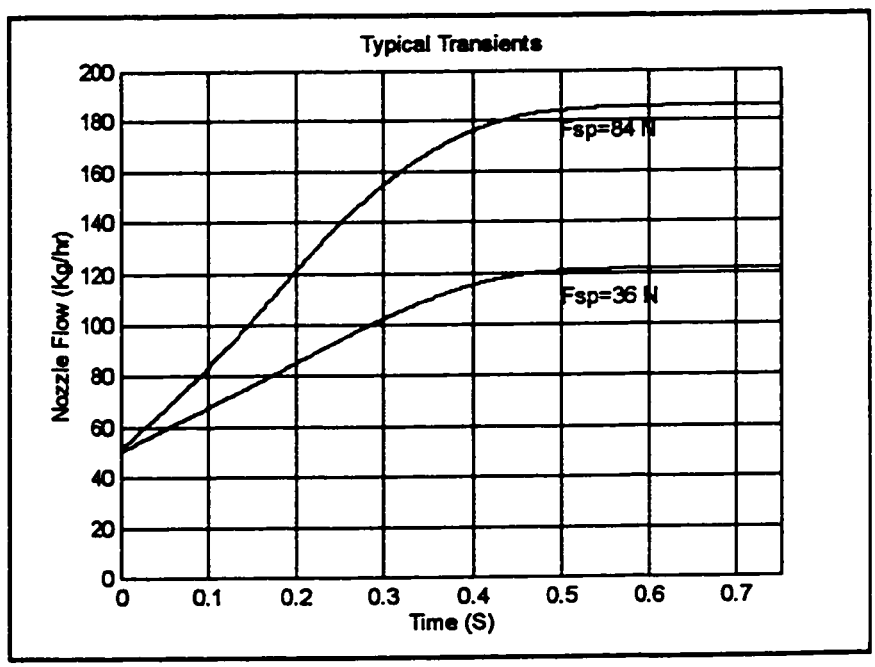

Figure 9.5(b) Effect of the Preload Force on the Transient Response

Figure 9.6(a) shows the effect of the spring constant on the ITAE index. A higher constant gives a faster response. The effect can be understood, first by examining the dynamic force balance. With a higher spring constant, a higher differential pressure is achieved. As in the previous case, increasing the differential pressure speeds up the response. There is also second reason for explaining the effect. By increasing the spring constant, the displacement of the diaphragm decreases. Therefore, the time to fill the upper chamber of the diaphragm decreases and the upper chamber pressure reaches its steady state faster. Figure 9.6(b) shows two typical transients, one with a low spring constant, and the other one with a high spring constant, demonstrating the improvement in ITAE index due to the increased spring constant value.

Figures 9.7(a) and (b) show that for the range considered, the diaphragm mass has a negligible effect on the transient response. This indicates that the pressure forces dominate and the model can be reduced from a fifth order to a third order system.

Figures 9.8(a) show the effect of bypass orifice diameter on the ITAE index. A larger diameter gives a faster response. Figure 9.8(b) shows that by increasing the bypass orifice diameter, the nozzle flow increases. This is despite the fact that with a bigger bypass orifice diameter, the bypass flow has to increase and, therefore, less fuel flow goes to the nozzle. This fact can be understood again by examining the dynamic force balance. The bypass orifice diameter has a direct effect on the differential pressure and by increasing the bypass valve diameter, the differential pressure increases. There is also a second reason. By increasing the orifice diameter, the pressure exerted on the bottom side of the diaphragm decreases, therefore the diaphragm moves down and less fuel passes through the bypass valve; as a result the nozzle flow increases.

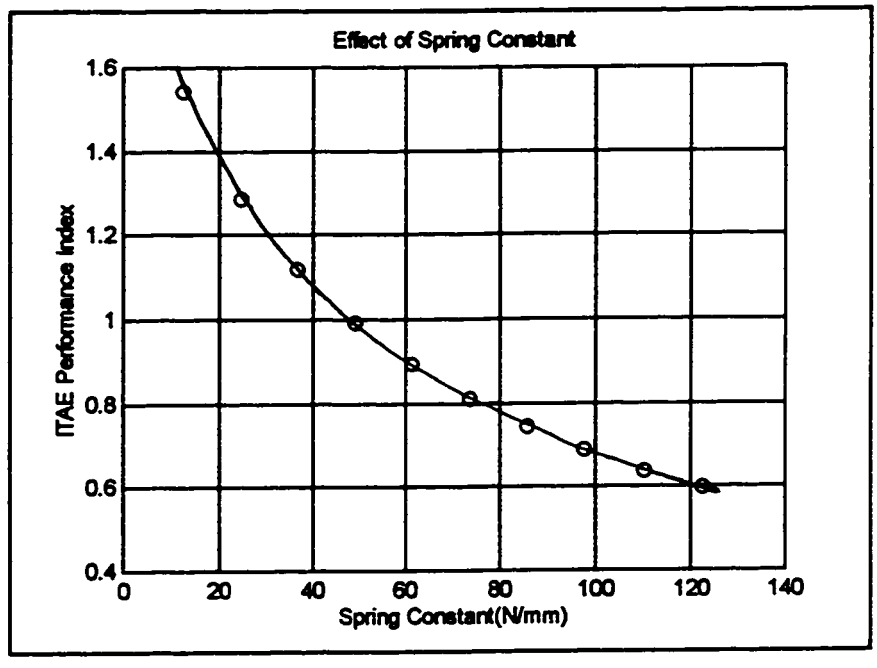

Figure 9.6(a) Effect of the Spring Constant on the ITAE Index

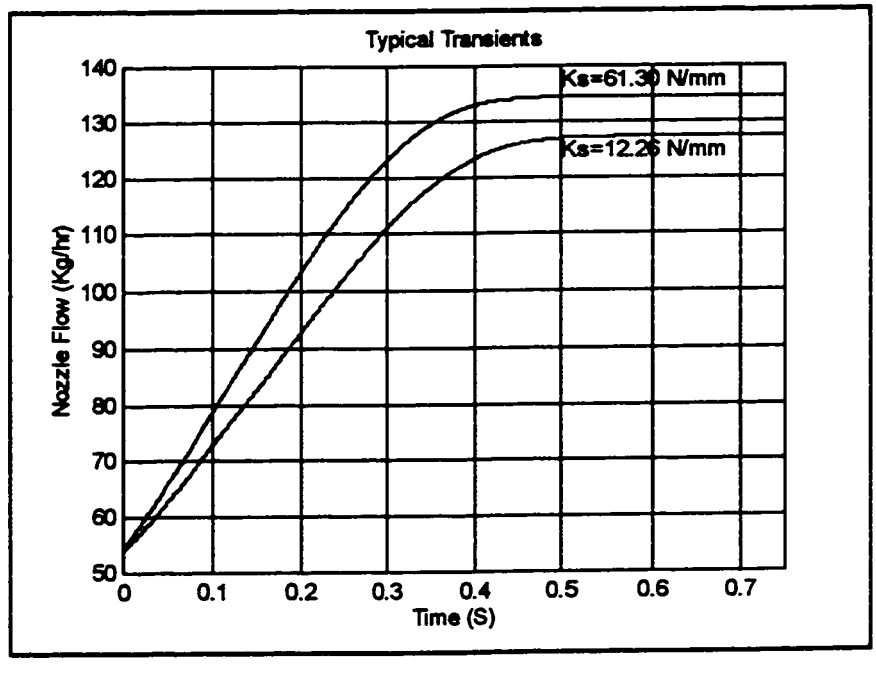

Figure 9.6(b) Effect of the Spring Constant on the Transient Response

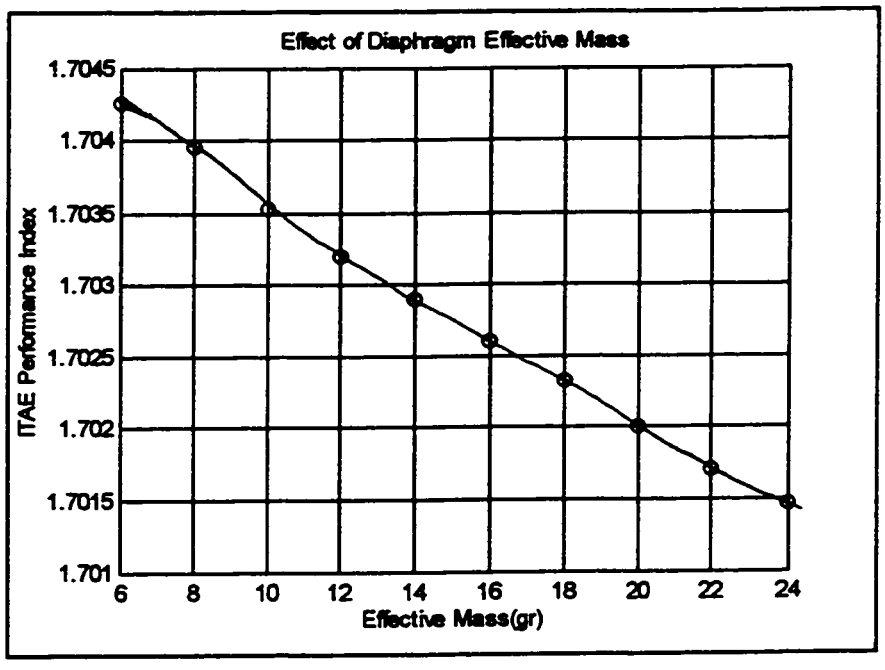

Figure 9.7(a) Effect of the Effective Mass on the ITAE Index

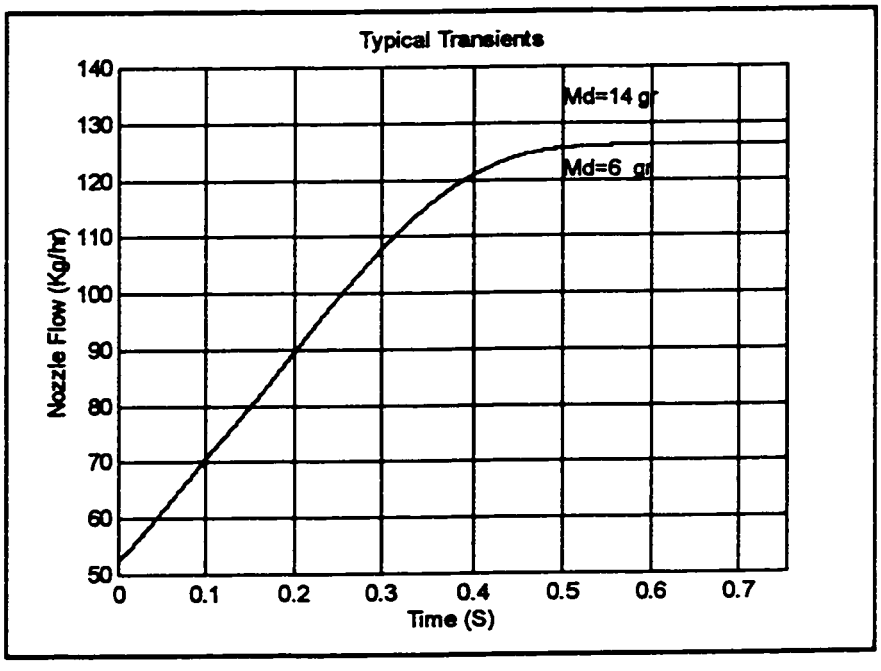

Figure 9.7(b) Effect of the Effective Mass on the Transient Response

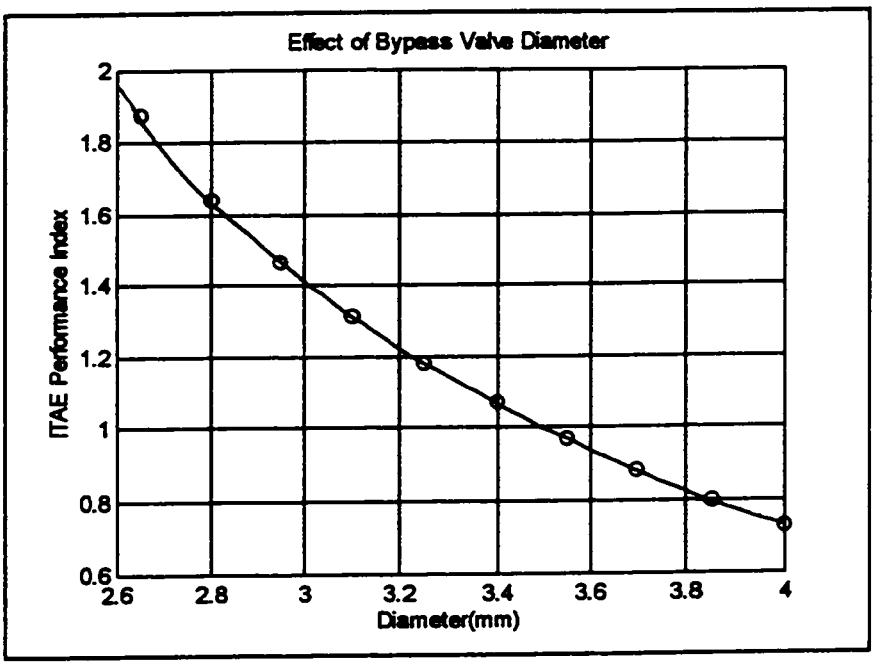

Figure 9.8(a) Effect of Bypass Valve Diameter on the ITAE Index

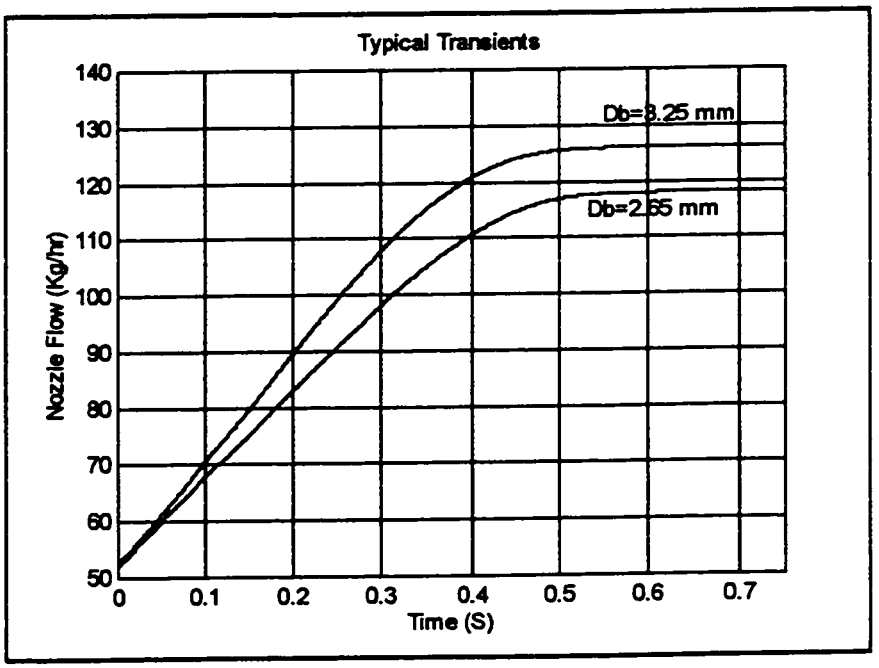

Figure 9.8(b) Effect of Bypass Valve Diameter on the Transient Response

9.3 The Third Optimization Criterion; Sensitivity Analysis

Sensitivity considerations are important since the behaviour of a control system varies with the changes in the component values or system parameters. These changes can be caused by temperature, pressure, wear, contamination or other environmental factors. Systems must be built so that the expected changes do not degrade its performance beyond some specified bound. A sensitivity analysis can yield the percent of the change in a specification, as a function of a change in a system parameter. One of the designer's goal, then, is to build a system with minimum sensitivity over an expected range of the environmental changes.

In control systems, the primary purpose of using a feedback is to reduce the sensitivity of the system to the parameter variations and unwanted disturbances. If we intend to construct a suitable open-loop control system as the proposed fuel metering system, we must select all the design parameters very carefully so that they respond accurately.

As it was mentioned before, for the proposed fuel metering system, it is very important to make *the metering valve flow schedule* less sensitive to the design parameters changes. This means that a selected metering valve position should give the same flow despite the carbon deposit contamination of the nozzle orifice or other environmental changes.

Finally, to apply the sensitivity analysis, the definition of sensitivity has to be formalized [54]. That is:

$$S_{F:P} = \lim_{\Delta P \to 0} \frac{\textit{Fractional change in the function, } F}{\textit{Fractional change in the parameter, } P} \qquad (9.5)$$

$$= \lim_{\Delta P \to 0} \frac{\Delta F/F}{\Delta P/P} = \lim_{\Delta P \to 0} \frac{P\Delta F}{F\Delta P}$$

which reduces to

$$S_{F:P} = \frac{P}{F}\frac{\delta F}{\delta P} \tag{9.6}$$

9.3.1 Sensitivity Calculation

For the proposed fuel metering system, five design parameters are considered as subjects to change:

1. The nozzle flow area, A_n, which can vary due to the carbon deposits contaminating the nozzle.
2. The spring preload force, F_{sp}, which can change due to the thermal expansion of the diaphragm valve housing and other factors, as well as to the time-related spring deformation.
3. Spring constant, K_s, which can change in time and also tolerances can be significant due to manufacturing.
4. Metering valve flow area, A_{mv}, which can change due to the contamination of the metering valve and also to the unreliable stepper motor control (lost steps).
5. Bypass orifice exit diameter, D_{bv}, which can change due to the contamination of the bypass valve and to the impact of the diaphragm contacting the exit manifold face.

Now it is desired to calculate the variation of the nozzle flow with respect to these parameters, i.e. $\frac{dQ_n}{dA_n}$, $\frac{dQ_n}{dF_{sp}}$, $\frac{dQ_n}{dK_s}$, $\frac{dQ_n}{dA_{mv}}$, $\frac{dQ_n}{dD_{bv}}$. To do this, first of all, from the steady state mathematical model, it is necessary to eliminate the state variables (P_1, P_2, P_n *and* y) except nozzle pressure P_2. This gives a single expression which contains only the state variable, P_2. Below, the required mathematical manipulations

are performed to calculate the sensitivity to nozzle contamination.

$$b_1 P_2 + b_2 M = c_1 - c_2 A_{eq} P_2 \tag{9.7}$$

where:

$$A_{db} = A_d - A_{bv}$$

$$A_{eq} = 1 + \left(\frac{A_n}{A_{mv}}\right)^2$$

$$b_1 = 0.5\, C_{dn} A_n \sqrt{\frac{2}{\rho P_2}}$$

$$b_2 = \frac{C_{dbv}\, \pi\, D_{bv}}{K_s} \sqrt{2 \frac{A_{eq}}{\rho}}$$

$$M = (A_{eq} A_{db} - A_d) P_2^{1.5} - F_{sp} P_2^{0.5}$$

The above equation can be implicitly differentiated to obtain the five derivatives of the upper diaphragm chamber pressure with respect to the five parameters of interest. Using calculus methods and taking the derivative with respect to the nozzle area A_n, and solving for dP_2 / dA_n,

$$\frac{dP_2}{dA_n} = - \frac{O}{N} \tag{9.8}$$

where:

$$O = C_{dn} \sqrt{2 \frac{P_2}{\rho}} + \frac{b_2 A_n M}{A_{eq} A_{mv}^2} + 2 b_2 \frac{A_i}{A_{mv}^2} A_{db} P_2^{1.5} + 2 c_2 \frac{A_n}{A_{mv}^2} P_2$$

$$N = b_1 + b_2 b_3 + c_2 A_{eq}$$

$$b_3 = 1.5 (A_{eq} A_{db} - A_d) P_2^{1.5} - 0.5 F_{sp} P_2^{-0.5}$$

Finally, the sensitivity of the nozzle flow to the nozzle orifice contamination

is obtained using the discharge equation (equation 6.8) and its derivative.

$$\frac{dQ_n}{dA_n} = C_{dn} \sqrt{2 \frac{P_2}{\rho}} + b_1 \frac{dP_2}{dA_n} \tag{9.9}$$

Similar relations for the sensitivity of the flow to the other four parameters of our interest can be derived. The results are given below.

$$\frac{dP_2}{dK_s} = \frac{b_2 M}{N K_s} \tag{9.10}$$

$$\frac{dQ_n}{dK_s} = b_1 \frac{dP_2}{dK_s}$$

$$\frac{dP_2}{dF_{sp}} = \frac{b_2}{N} P_2^{0.5} \tag{9.11}$$

$$\frac{dQ_n}{dF_{sp}} = b_1 \frac{dP_2}{dF_{sp}}$$

$$\frac{dP_2}{dA_{mv}} = \left(\frac{1}{N}\right) \left(\frac{b_2 A_n^2 M}{A_{eq} A_{mv}^3} + 2 b_2 \frac{A_n^2}{A_{mv}^3} A_{db} P_2^{1.5} + 2 c_2 \frac{A_n^2}{A_{mv}^3} P_2\right) \tag{9.12}$$

$$\frac{dQ_n}{dA_{mv}} = b_1 \frac{dP_2}{dA_{mv}}$$

$$\frac{dP_2}{dD_{bv}} = \frac{- b_2 M}{N D_{bv}} \tag{9.13}$$

$$\frac{dQ_n}{dD_{bv}} = b_1 \frac{dP_2}{dD_{bv}}$$

In general, the above equations are a function of the operating point and also of the nominal design parameters. Here, a flow of 91 kg/ h which, corresponds to the metering valve position of 1.8 mm, is chosen as an operating point. A program is written in MATLAB domain to calculate the sensitivity equations according to the desired operating point and also to the nominal design parameters. The results are plotted in the sensitivity histogram of figure 9.9.

As it is shown in the figure, the nozzle flow has maximum sensitivity to the metering valve flow area. This is due to the fact that the metering valve flow which is equal to the nozzle flow during a steady state condition, is proportional to the metering valve displacement. This means that the sensitivity should be 100%, however due to the increase in differential pressure resulting from the increase in metering valve flow, the sensitivity is more than 100%.

A change in the spring preload force setting has also a significant impact on the sensitivity. This means that the thermal expansion of the diaphragm valve housing which has an effect on the preload force, can change the differential pressure. Therefore, the nozzle flow is changed indirectly.

As it is shown in figure 9.9, the flow sensitivity to the nozzle contamination is about 20%. The negative sign indicates that as the nozzle orifice becomes contaminated (the nozzle flow area decreases), the nozzle pressure increases. This is due to the fact that by decreasing the nozzle flow area, the nozzle pressure and upper chamber pressure should be increased to have the same flow rate as before nozzle orifice contamination. In this case, the diaphragm valve moves down and less flow passes through the bypass valve. Therefore, more fuel passes through the nozzle orifice.

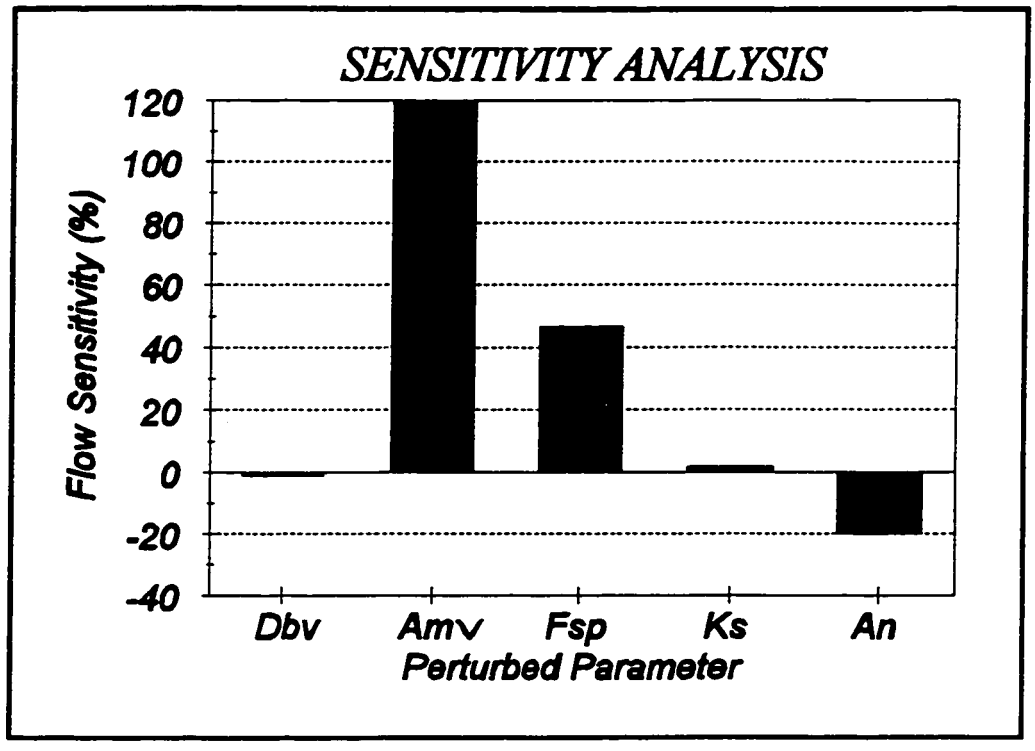

Figure 9.9 Sensitivity Histogram

Also figure 9.9 shows that the sensitivities of the nozzle flow rate due to the changes of the spring constant and bypass valve diameter are very low (less than 1%) and, therefore the system can be considered as not sensitive to these parameter changes.

A numerical example can be used to clarify the interpretation of the sensitivity index. If the nominal flow is 91 kg/ h and the nominal nozzle area is 1.01 mm^2 and if contamination reduced the nozzle area to 0.9 mm^2 (about 10%), the sensitivity index can be used to determine the change in flow dQ_n due to the contamination.

$$dQ_n = (-0.20426)\ \frac{(0.9\ -1.01)}{1.01}\ 91 = 2.0244\ kg/\ h \qquad (9.14)$$

This means that the expected nozzle flow variation is about 2% of the nominal flow.

For the multi-objective optimization scheme, it is necessary to define a single index as a measure of the overall system sensitivity. This index is found by taking a weighted sum of the normalized derivation of the fuel flow with respect to each of the defined design parameters. These weights should reflect the likelihood and severity of each parameter. Therefore, the overall sensitivity index is defined as follows:

$$SENS = w1 \left|\frac{dQ_n}{dA_n}\left(\frac{A_n}{Q_n}\right)\right| + w2 \left|\frac{dQ_n}{dK_s}\left(\frac{K_s}{Q_n}\right)\right| + w3 \left|\frac{dQ_n}{dF_{sp}}\left(\frac{F_{sp}}{Q_n}\right)\right| + w4 \left|\frac{dQ_n}{dD_{bv}}\left(\frac{D_{bv}}{Q_n}\right)\right| \quad (9.15)$$

The weights (w1, w2, w3, w4) are subjectively assigned by the designer. For example, carbon deposits contaminating the nozzle orifice is an unavoidable phenomenon, and therefore, sensitivity to nozzle contamination is given a strong weight in the sensitivity index. The value chosen for w1 is 50%.

It is considered relatively improbable that the helical spring constant and the bypass orifice diameter will change significantly during the operation life of the fuel metering system. Therefore, a small value of 10% is chosen for both of them.

The sensitivity of the system response to the preload force changes is given a weight of 30%. This is due to the fact that the thermal expansion of the valve housing, resulting from the ambient temperature changes is inevitable.

Two programs have been written to perform the optimization for sensitivity analysis. The first program was used to calculate and plot the sensitivity histogram. In this program, an operating point was chosen, i.e. metering valve position was set on 1.8 mm, and the sensitivity equations were solved using nominal design parameters (K_S=6130 N/m, A_n=1.01 mm^2, F_{SP}=39.975 N and D_{bv}=3.25 mm).

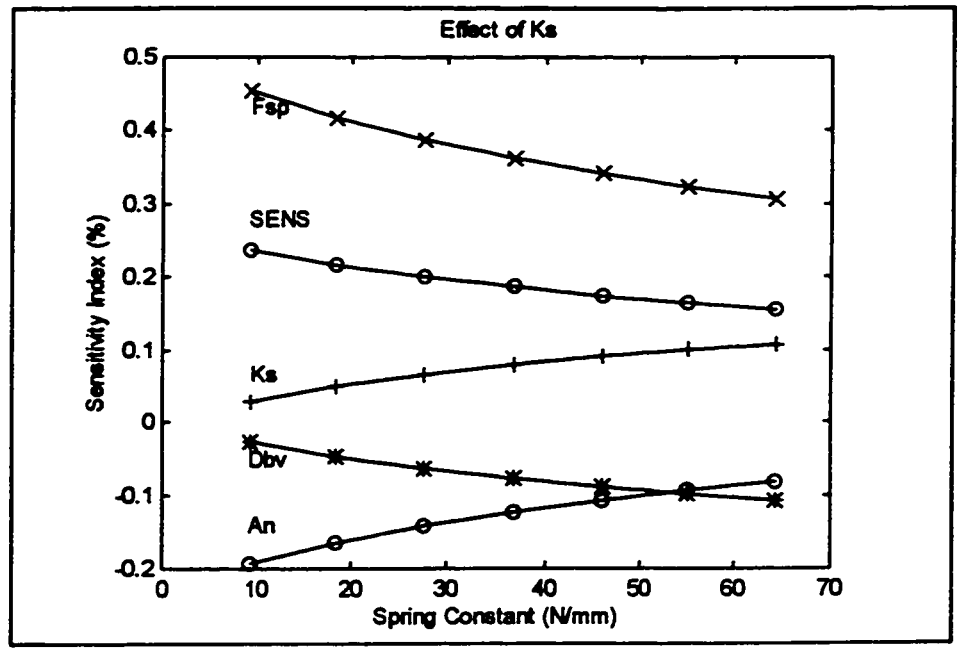

Figure 9.10 Effect of the Spring Constant on the Fuel Flow Sensitivity

In the second program, the impact of each design variable such as F_{SP}, K_S, A_n, and D_{bv} on the combined sensitivity index as well as on the individual sensitivity indices were investigated and the results were plotted. This means that each design variable changes several times, with the other variables kept fixed while the sensitivity indexes were calculated for each case.

9.3.2 Simulation Results

Figure 9.10 shows that a large spring constant results in a better composite (overall) sensitivity index (SENS). This means that increasing the spring constant decreases the overall sensitivity index. This result is expected because the spring force should compensate the P_1 A_{bv} term in the force balance equation, especially when the pump pressure is high. Moreover, the figure shows the impact of the spring

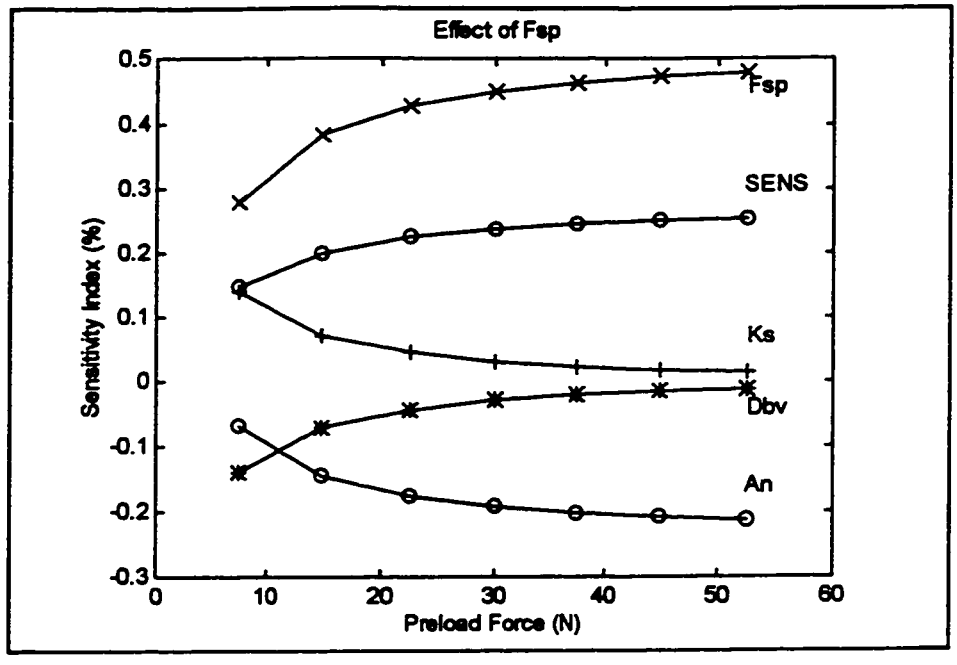

Figure 9.11 Effect of the Preload Force on the Fuel Flow Sensitivity

constant on the individual sensitivities for which the relationship is negatively monotonic (recall that negating a function reverses the monotonicity) except, for the spring constant and bypass valve diameter sensitivity indices. However, these components have low weights in the composite index, therefore, it has little impact on the overall trend shown in the figure.

Figure 9. 11 shows that a low preload force gives the best composite sensitivity index. The reason is that by increasing the preload force, the differential pressure increases and, therefore, the nozzle flow increases. Also the figure shows the impact of the preload force on the individual sensitivities. Similar to the previous figure, the relationship is positive monotonic except for the spring constant and bypass valve diameter.

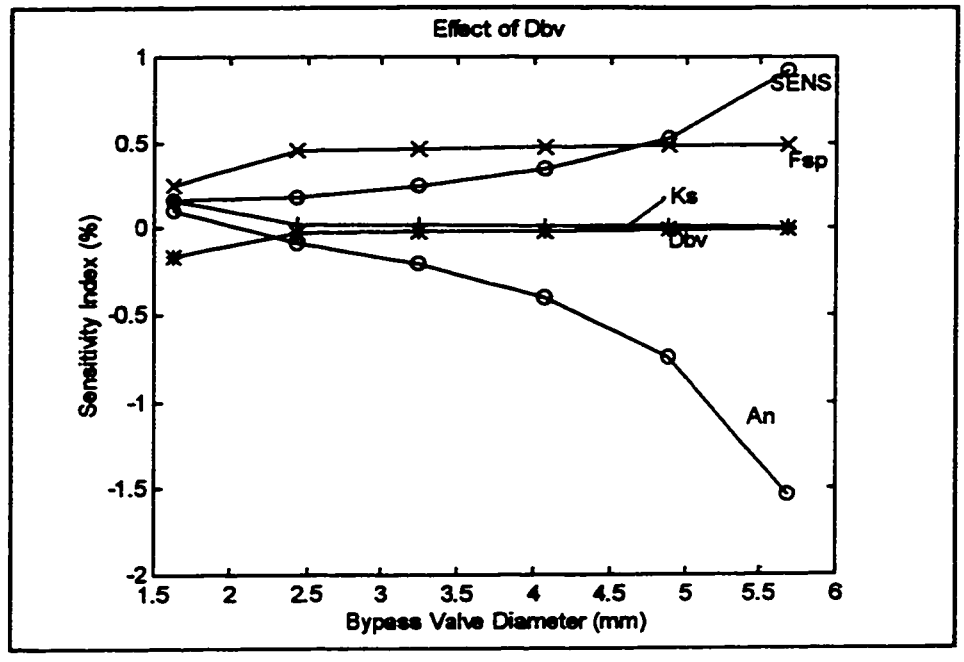

Figure 9.12 Effect of Bypass Valve Diameter on the Fuel Flow Sensitivity

Figure 9.12 shows the effect of the bypass orifice diameter on the overall sensitivity index and also on the individual sensitivities. This figure shows that a small bypass valve diameter should be used from the sensitivity point of view, because by increasing the diameter, the differential pressure increases, and therefore, the nozzle flow increases.

The small decrease in the sensitivity to the nozzle flow area changes as shown in figure 9.13, is also due to the fact that the increase in the nozzle orifice diameter results in a decrease in the nozzle pressure and upper chamber pressure in the bypass valve. Therefore, the diaphragm moves up and less fuel flow passes through the nozzle. However, the flow changes are almost negligible. This means that the proposed fuel metering system is less sensitive to the possible nozzle contamination.

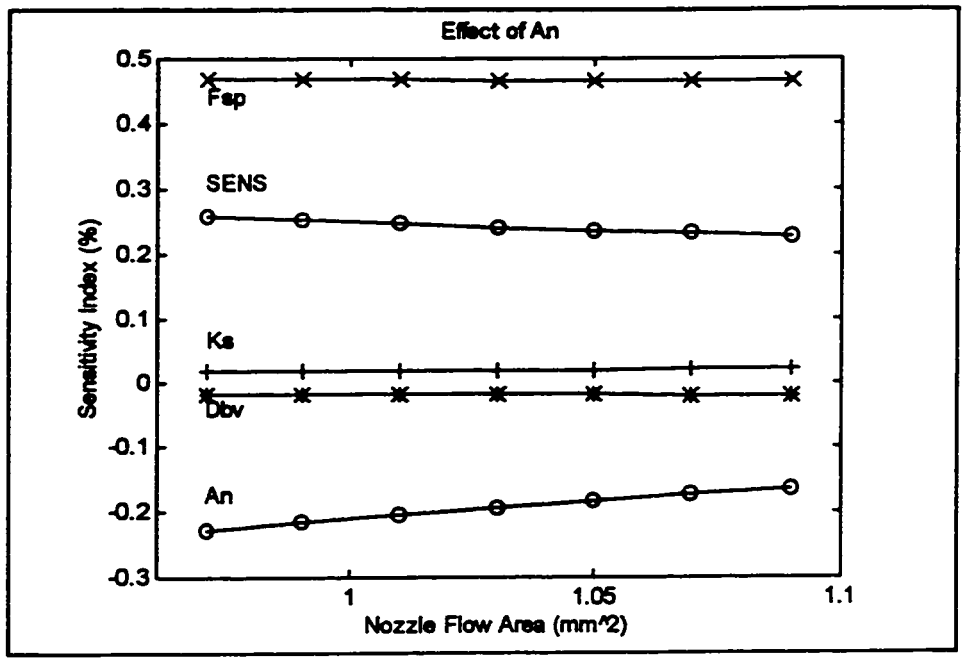

Figure 9.13 Effect of the Nozzle Flow Area on the Fuel Flow Sensitivity

It is concluded from this analysis that a larger spring constant and nozzle flow area, and a smaller bypass orifice diameter and preload force are decreasing the sensitivity index.

The purpose of the next section, is to combine all three criteria; speed of transient response, fuel flow linearity and sensitivity to design parameters variations, in a unified optimization scheme that will consider the three criteria simultaneously. This study is very important for choosing the design variables of the fuel metering system and it will be performed in the next section.

9.4 Multiple Objective Optimization

The purpose of a single-objective optimization procedure is to search for the optimum of a function, or an object of one or several variables, which may be subjected to some constraints. However, for a practical design problem, rarely does a single objective, with several hard constraints, adequately represent the problem being faced. More often there is a vector of objectives which must be traded off in some way, and as the number of objectives increases, trade-offs are likely to become complex and less easily quantified. A general formulation of a multi-objective optimization problem is defined as follows:

$$\begin{aligned} &\textit{minimize} \quad f(x) \\ &x \in \Omega \ (\textit{feasible region}) \\ &\textit{subject to following constraints:} \\ &g_i(x) = 0 \quad i = 1,\ldots,m_e \\ &g_i(x) \le 0 \quad i = m_e+1,\ldots,m \\ &x_l \le x \le x_u \end{aligned} \tag{9.16}$$

where f(x) is a vector of objectives which is subjected to a number of constraints or bounds and must be minimized. Note that since f(x) is a vector, then if any of the components of f(x) are competing , there is no unique solution to this problem and it may be impossible to minimize all objectives simultaneously. This means that instead of seeking a single optimal solution, a set of *nondominated solutions* [56] (also called noninferiority [57] and Pareto optimality [58]) is sought. A nondominated solution is one in which an improvement in one object requires a degradation of another one and is a subset of the feasible region. The main characteristic of the nondominated set

of solutions is that for each solution outside the set, there is a nondominated solution for which all objective functions are unchanged or improved (decrease) and at least one which is strictly improved (decreased). A formal definition of the set of nondominated solutions is presented as follows.

Definition [55]: A point $x^* \in \Omega$ for which Ω is a nondominated region and, therefore, a subset of feasible region, is a nondominated solution if for some neighbourhood of x^*, there does not exist a Δx such that $(x^* + \Delta x) \in \Omega$ and

$$\begin{aligned} f_i(x^* + \Delta x) &> f_i(x^*) \qquad i=1,\ldots,m \\ f_j(x^* + \Delta x) &\geq f_j(x^*) \qquad \textit{for some } j \neq i \end{aligned} \tag{9.17}$$

Thus, it is evident from the definition that as one moves from one nondominated solution to another nondominated solution, as one objective function improves, then one or more of the other objectives must increase in value. Moreover, any point in the feasible region that is not a nondominated point represents a point in which degradation can be attained in all the objectives, however, it is clear that such a point is of no value. Therefore, the multi-objective optimization is concerned with the generation and selection of nondominated points. However, once the entire nondominated set of solutions is found, the designer picks up the final design from this set, based on his subjective evaluation of the relative importance of the criteria.

In general, for the multi-objective optimization case, an *optimum* can only be found once the priority or preference among the objectives has been determined by the designer. This means that in multi-objective optimization, the designer must decide which objective or objectives are preferred and by how much. In this case, it is possible to find one optimum solution for the problem.

The techniques for multi-objective optimization are wide and varied. However, three of them, are presented in the following section.

9.4.1 Methods of Solution

There are several multi-objective analysis techniques for finding the set of nondominated solutions for a multi-objective optimization problem. The main difference between them lies in how the decision maker inputs his subjectivity into the analysis. In general, the simplest method is to convert the problem to a form that can be numerically solved using single criterion mathematical programming optimization techniques.

Weighted Sum Method

The weighted sum strategy is the simplest way to solve the multi-objective optimization. It converts the multi-objective problem of minimizing the vector f(x) into a scalar one by constructing a weighted sum of all the objectives:

$$\textit{minimize} \quad F(x) = \sum_{i=1}^{m} w_i f_i(x) \qquad (9.18)$$

$$\textit{and}$$

$$\sum_{i=1}^{m} w_i = 1$$

The problem can then be optimized using a standard optimization algorithm. In general, the entire nondominated sets is found by parametrically varying the weights between zero and one and solving the resulting single criterion optimization each time. It seems the method is very simple. However, the parametric variation of

weights in discrete steps, is very expensive computationally. In addition, this method provides less insight into the design optimization than other methods and the assignment of the preferred weighting of objectives by the designer can be very subjective and difficult to justify. Also, there is another problem that all the objectives can not be measured with comparable units. This makes the task of assigning weights even harder. Therefore, this method will not be used in this analysis.

ϵ- Constraint Method

This method [55] is more applicable than the weighting method due to the fact that the designer's subjective input is in the form of proposed limits to each objective function rather than to the relative worth or weights. This is usually much easier to do. In general, this method involves minimizing of an objective and expressing the other objectives in the form of inequality constraints.

$$\begin{aligned} &\textit{minimize} \quad f_p(x) \\ &\textit{subject to} \\ &f_i(x) \leq \epsilon_i \quad i=1,\ldots,m, \; i \neq p \end{aligned} \tag{9.19}$$

The advantage of this method is that it gives the designer, the goal achievement for each of the objectives. In other words, it reveals how much each objective is achieved, as compared to the maximum achievable. However, the user must specify the maximum and minimum acceptability for each objective (ϵ) and then, by varying each ϵ between its upper and lower limits and solving the problem each time, a nondominated set could be generated. This means that this method does not give any

unique solution for the problem and ultimately, the designer must pick up the final set according to his preference.

Goal Attainment Method [58]

This method which was presented by Gembicki [59], involves expressing a set of design goals, $f^* = \{ f^*_1, f^*_2, ..., f^*_m \}$, which is associated with a set of objectives, $f(x) = \{ f_1(x), f_2(x), ..., f_m(x) \}$. The problem formulation allows the objectives to be under-or over-achieved, enabling the designer to be relatively imprecise about initial design goals. The relative degree of under-or-over achievement of the goals is controlled by a vector of weighting coefficients, $w = \{ w_1, w_2, ..., w_m \}$ and is expressed as a standard optimization problem using the following formulation:

$$\begin{aligned} &\textit{minimize} \quad \gamma \\ &\gamma \in \Re \ , \ x \in \Omega \ (\textit{feasible region}) \\ &\textit{subject to:} \\ &f_i(x) - w_i \gamma \le f_i^* \qquad i = 1,...,m \end{aligned} \tag{9.20}$$

The term $w_i \gamma$ introduces an element of slackness into the problem which otherwise imposes that the goals be rigidly met. The weighting vector, w, enables the designer to express a measure of the relative trade-offs between the objectives. This method provides a convenient intuitive interpretation of the design problem, which is solvable using standard optimization procedures.

9.4.2 Problem Formulation and Description

In this section, the objective functions and the design constraints imposed on the design variables are presented. The problem can be formulated as follows:

$$
\begin{aligned}
&\textit{minimize} \quad F(x) = [\, LIN(x),\ SENS(x),\ ITAE(x) \,] \\
&\textit{subject to the following constraints:} \\
&LIN(x) \le 0.14 \\
&ITAE(x) \le 1e\text{-}2 \\
&SENS(x) \le 0.13 \\
&15\ N/mm \le Ks \le 55\ N/mm \\
&20\ N \le F_{sp} \le 40\ N \\
&2.5\ mm \le D_{bv} \le 3.6\ mm \\
&\pi\ D_{bv}\ y \le A_{bv} \\
&C_{dmv}\ s\ w\ n_s \sqrt{2\ \Delta P / \rho} \le 1.4 / (3600\ \rho)
\end{aligned}
\tag{9.21}
$$

It is desired to simultaneously minimize the three objectives. The first three constraints ensure that each objective is in an acceptable range and the final solution provides at least a minimum requirement. The second three constraints are side constraints which represent practical limits on the design variables. The seventh constraint ensures that the saturation in the bypass valve orifice does not occur in the operating range. This means that the area between the bypass valve and the diaphragm flat-seat valve must be smaller than the bypass valve flow area. The last constraint is a flow resolution constraint, which states that one step movement of the stepper motor should not cause a flow change of more than 1.4 kg/ h. This is due to the fact that the

fuel metering system must accurately meter fuel to the combustor during the engine operation and avoid stall or flameout of the engine.

Note that the design variables consist of the spring constant, the preload force and the bypass valve diameter. The diaphragm mass is not considered as a design variable. This is due to the fact that the diaphragm mass comes into the play only in the transients performance index and it was found in section 9.2, that the impact of it on the transient response is negligible.

9.4.3 The Numerical Search Techniques

In general, solving a multi-objective function with several constraints is very difficult and therefore, the first thing to do is to simplify the problem. From examining the effect of design variables on each objective function, it was found that increasing the spring constant improves all three objective functions. This means that the spring constant has to be made as high as possible. However, the last constraint, flow resolution constraint, limits the spring constant value by restricting the differential pressure across the metering valve which is a function of design variables. Therefore, it is not possible to set a final value for spring constant and then remove it from the design variables. For other design variables, it was found that reducing the preload force and the bypass valve diameter improves the linearity index and the sensitivity index. However, reducing the values of both of them degrades the transient performance index. This means that for this problem, no simplification can be made.

The side constraints show that the variation of each design variable is wide and, therefore, they must be restricted somehow to have a faster convergence of the solution. To do this, it was decided to find the feasible region of the problem at the

first step of the optimization. A direct search method was used to look for the feasible region. Each variable was varied from its minimum value to its maximum, while the other variables were fixed. Violating just one of the constraints stopped the search and the next search was started by choosing a new set of variables. The design variables which satisfied all the constraints were recorded. During the search, the sets of design variables which had bigger values than 44000 N/m for the spring constant, 34 N for preload force and 3 mm for the bypass valve diameter, were removed from the search due to the violation of the flow resolution constraint. Meanwhile, the sets of design variables which had a value smaller than (32000 N/m, 27 N and 2.7 mm) were mostly removed from the search due to the bypass valve saturation. Figure 9.14 shows the comparison between the feasible region and the side constraints. The figure also shows that some new limitations (upper and lower limits) for the design variables are necessary in order to have a faster convergence and less computational time. Therefore, new upper and lower limits which covers totally the feasible region, were finally chosen to be used in the optimization algorithms. Figure 9.15 shows the new side constraints and feasible region.

The optimization toolbox of MATLAB [58] was used to find the optimum design variables. There are two optimization algorithms of MATLAB that can be used in this investigation. The first one is *constr* algorithm which finds the minimum of a multi-variable function subjected to the inequality constrains. This algorithm can be used to find the minimum of each objective function, while the other two objective functions are restricted by the constraints described in the problem formulation.

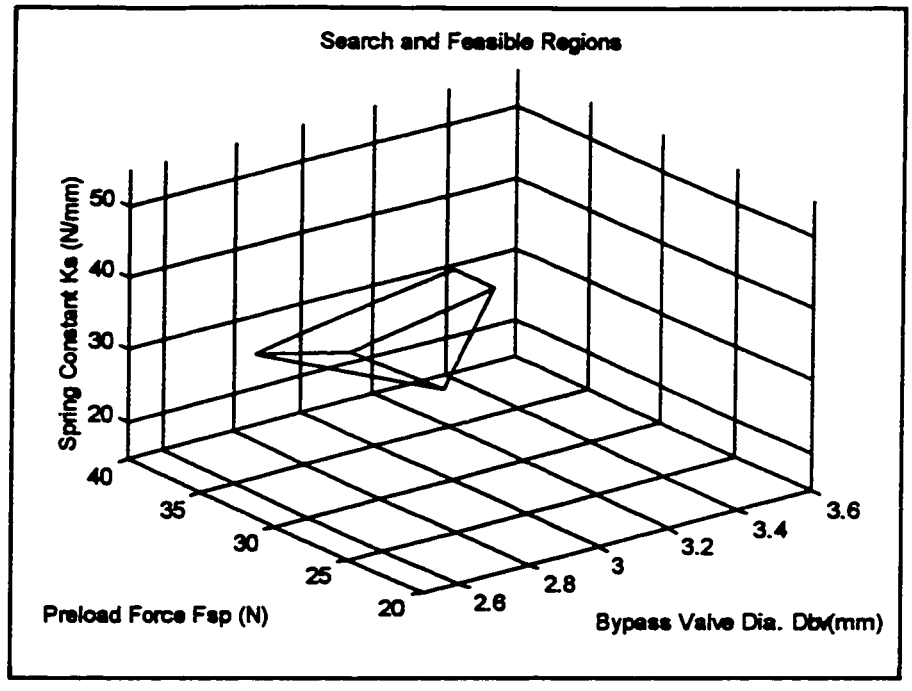

Figure 9.14 Search and Feasible Regions of the Problem

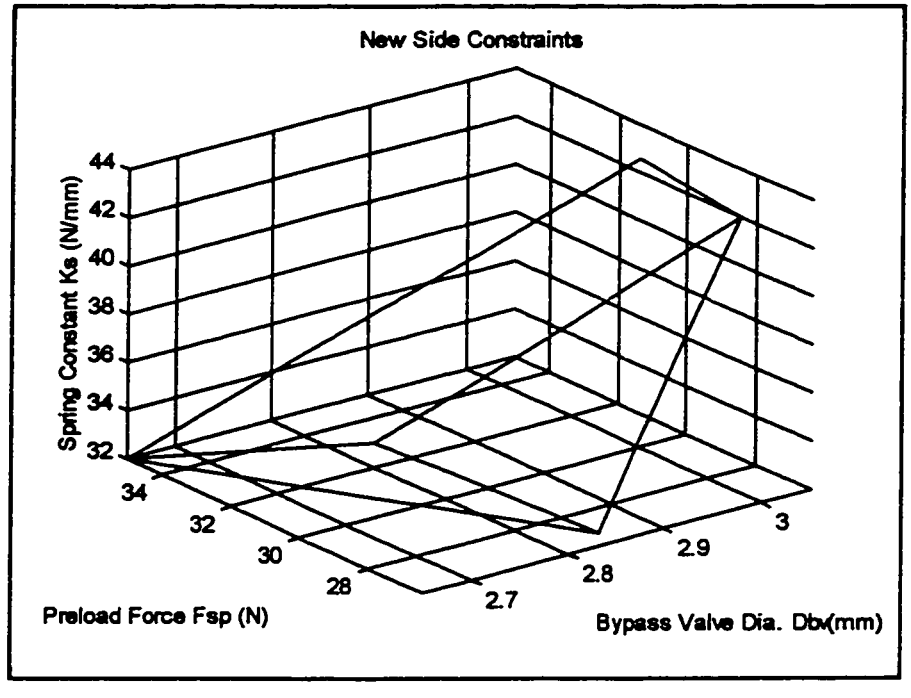

Figure 9.15 New Side Constraints and Feasible Region

The second algorithm is *attgoal* algorithm [58], Goal Attainment Method (equation 9.20), which solves multi-objective optimization problems by minimizing a set of object functions simultaneously. Due to the fact that for the proposed problem, there is no any unique solution, this method was used to find the nondominated sets of design variables.

9.4.4 Optimization Results

In this section, the results of computer optimization are presented. First, in optimizing of the linearity index (LIN) using constr algorithm, it was found that the minimum value of the LIN index was 0.082013 and the optimum spring constant, the preload force and the bypass valve diameter were 32750 N/m, 33.3 N and 2.68 mm respectively. With these values, the variation of differential pressure across the metering valve is minimized. The program was run several times with different starting points, in order to find the global minimum of the index. This means that each time a new optimum point (set of design variable) was found; it was used as a starting point for the next run and the optimization was finished as no improvement was seen in the LIN index.

Similar optimization was done for the transient performance index ITAE, and sensitivity index SENS, with the resulting optimums of 0.0068994 and 0.11057 respectively. The optimum design variables were:

$K_s = 44000\ N/m$, $Fsp = 30\ N$ *and* $D_{bv} = 3\ mm$

when optimizing for ITAE index and

$K_s = 43984\ N/m$, $Fsp = 26\ N$ *and* $D_{bv} = 2.9907\ mm$

when optimizing for SENS index. Figure 9.16 shows the locations of resulting

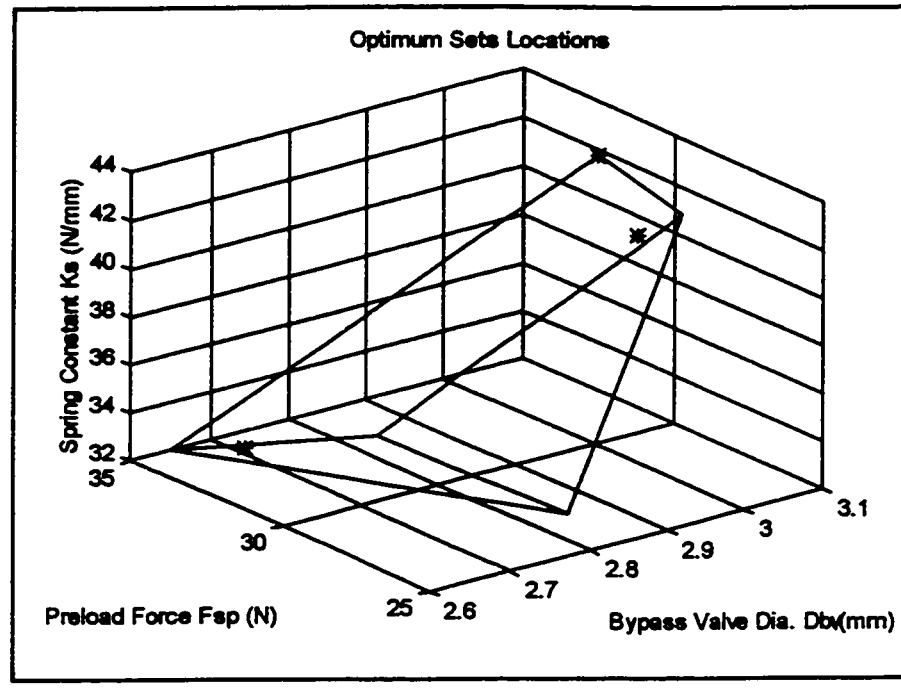

Figure 9.16 The Locations of the Optimum Sets of Each Objective Function

optimums of each objective function within the feasible region.

The results for the multi-objective optimization using the goal attainment method are shown in figure 9.17. As it was mentioned before, these sets of design variables are nondominated solutions and therefore no conclusion can be drawn which set is the optimum one. Moreover, those sets which were obtained during the minimization of each objective separately, were also nondominated solutions and are shown in figure 9.17. The (+) points on the figure shows some of the dominated solutions.

Finally, to choose the optimum solution among the nondominated solutions, a goal function must be defined. As it was mentioned before, the minimum of objective functions were not achieved simultaneously. However, they represent the best that could be achieved for one objective function if it were not limited by other

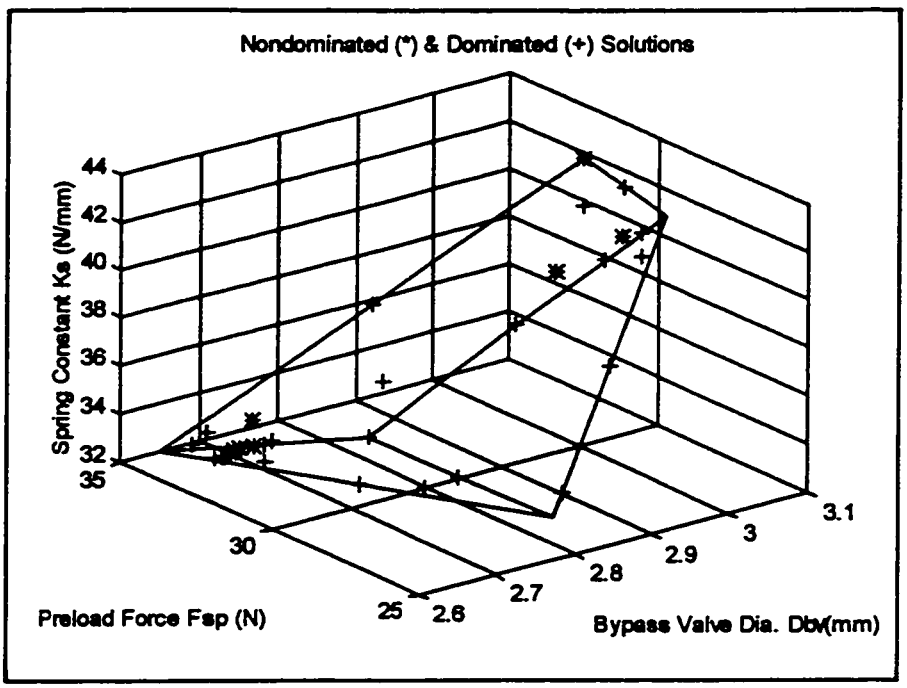

Figure 9.17 Dominated and Nondominated Sets of Solutions

objective functions. Therefore, the following goal function is defined:

$$GOAL\ (X) = \left[\frac{LIN\ (x)}{LIN_{min}} + \frac{ITAE\ (x)}{ITAE_{min}} + \frac{SENS\ (x)}{SENS_{min}} \right] \tag{9.22}$$

Note that the minimums of LIN, ITAE and SENS index are the values which were found during the minimization of each objective function. This means that each term in the goal function should be greater or equal to one and then, the minimum value of the goal function is 3. Values greater than 3, show the deviation from the ideal case. Due to the fact that the nondominated solutions were found before, it is not necessary to do the optimization again. Therefore, by examining the goal function for each nondominated sets, the final solution is found, that is:

$K_s = 42226\ N/m$, $Fsp = 29.722\ N$ and $D_{bv} = 2.8813\ mm$

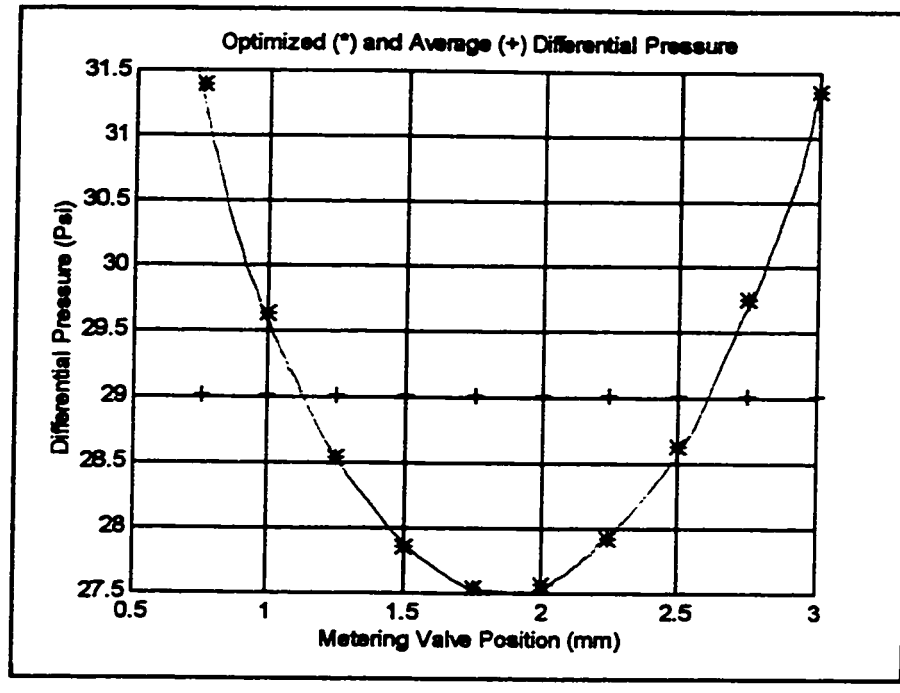

Figure 9.18 Differential Pressure Across the Metering Valve

The corresponding values of objective functions are:

LIN = 0.092654 , $ITAE$ = 0.0071471 *and* $SENS$ = 0.11557

Finally, the goal achievement for each objective function is computed as follows:

Goal achievement for LIN Index: [LIN_{min} / $LIN(x)$] = 0.082013 /0.092654 = 88.6%

Goal achievement for ITAE Index:

[$ITAE_{min}$ / $ITAE(x)$] = 0.006899 /0.0071471 = 96.5%

Goal achievement for SENS Index: [$SENS_{min}$ / $SENS(x)$] = 0.11057 /0.11557 = 99.7%

Note that this is only one of many possible solutions. For example, if the point to find is the best linearity based on the given constraints, then, the corresponding values of objective functions are:

LIN = 0.082013 , $ITAE$ = 0.0082469 *and* $SENS$ = 0.12386 and the

Goal achievement for LIN Index: [LIN_{min} / $LIN(x)$] = 0.082013 /0.082013 = 100 %

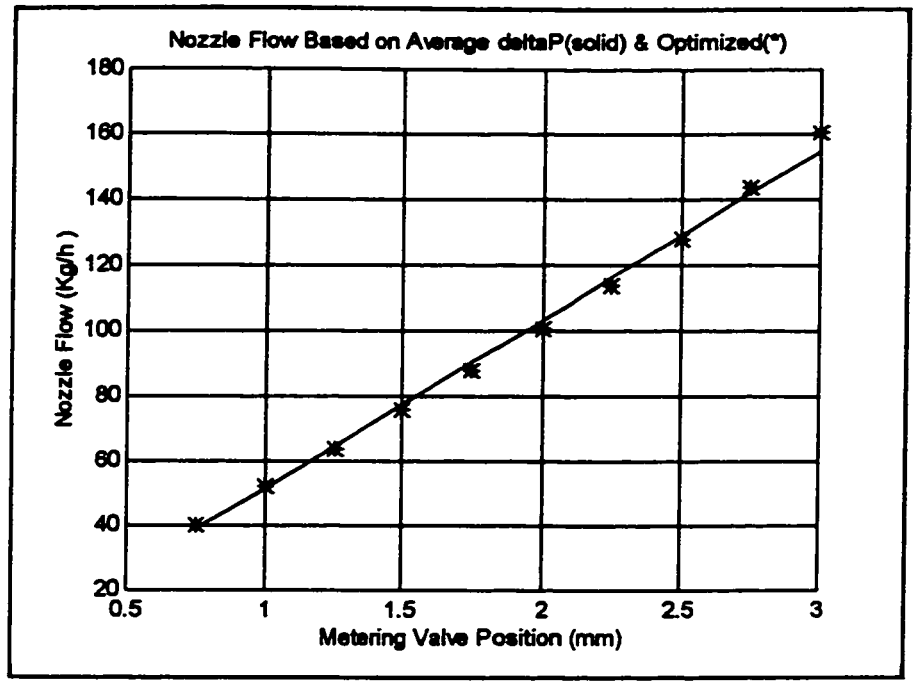

Figure 9.19 Optimized Nozzle Flow

and the Goal achievement for ITAE Index:

$[\ ITAE_{min} / ITAE(x)] = 0.006899 / 0.008247 = 83.65\%$

and the Goal achievement for SENS Index:

$[\ SENS_{min} / SENS(x)] = 0.11057 / 0.12386 = 89.3\%$

In conclusion, it is recommended that the spring constant be 42230 N/m, the preload force be 29.7 N and the bypass valve exit diameter be 2.9 mm. Figure 9.18 shows the change of the differential pressure across the metering valve based on the optimum design variables. As seen, the differential pressure has a concave form so that the deviation from the average differential pressure can be minimized. Next, the figure 9.19 shows the nozzle flow versus the metering valve position. The star (*) curve shows the nozzle flow based on the optimum design variable and the solid line is the desired nozzle flow with a constant (average) differential pressure. This figure

shows clearly the improvement of the linearity (as compared to figure 8.12), obtained as the result of the optimization. In the end of the next chapter, the first configuration based on the optimized design variables will be compared with other three configurations which were presented in the thesis objectives (Chapter 3).

10. SYSTEM DESCRIPTION AND OPERATION OF CONFIGURATION 4

10.1 Single Barrel Double Plunger Fuel Metering System Concept

In this chapter, the feasibility of a double plunger fuel metering system is investigated. As explained in the thesis objectives (section 3.1.6), this system originally employed two parallel barrels with plungers; now this system has been simplified to make it smaller, lighter and cheaper. The plungers have been located in only one barrel and are moving in opposite directions. They are operated by two linear digital actuators simultaneously but independently, as shown schematically in figure 10.1. This means that this system is able to keep a constant differential pressure across the first metering valve at steady state condition and vary the differential pressure during the transient flow condition, in order to speed up the dynamic response of the engine. This is due to the fact that both the metering valve and the bypass valve plungers are operated under the electronic control management. Moreover, this system has also a back-up feature which means that if one of the plungers fails to operate, the second one takes over and provides the fuel flow to the engine so that the aircraft would be able to return home safely. This feature will be fully investigated in the following sections.

Following the above description, first, the steady state response of the system based on the mathematical model, which was presented in section 6.4, is investigated. Then, the transient response of the system is described. Because several control options can be chosen for this system, which have a direct impact on the transient response of the system, therefore, some of them have been presented and their

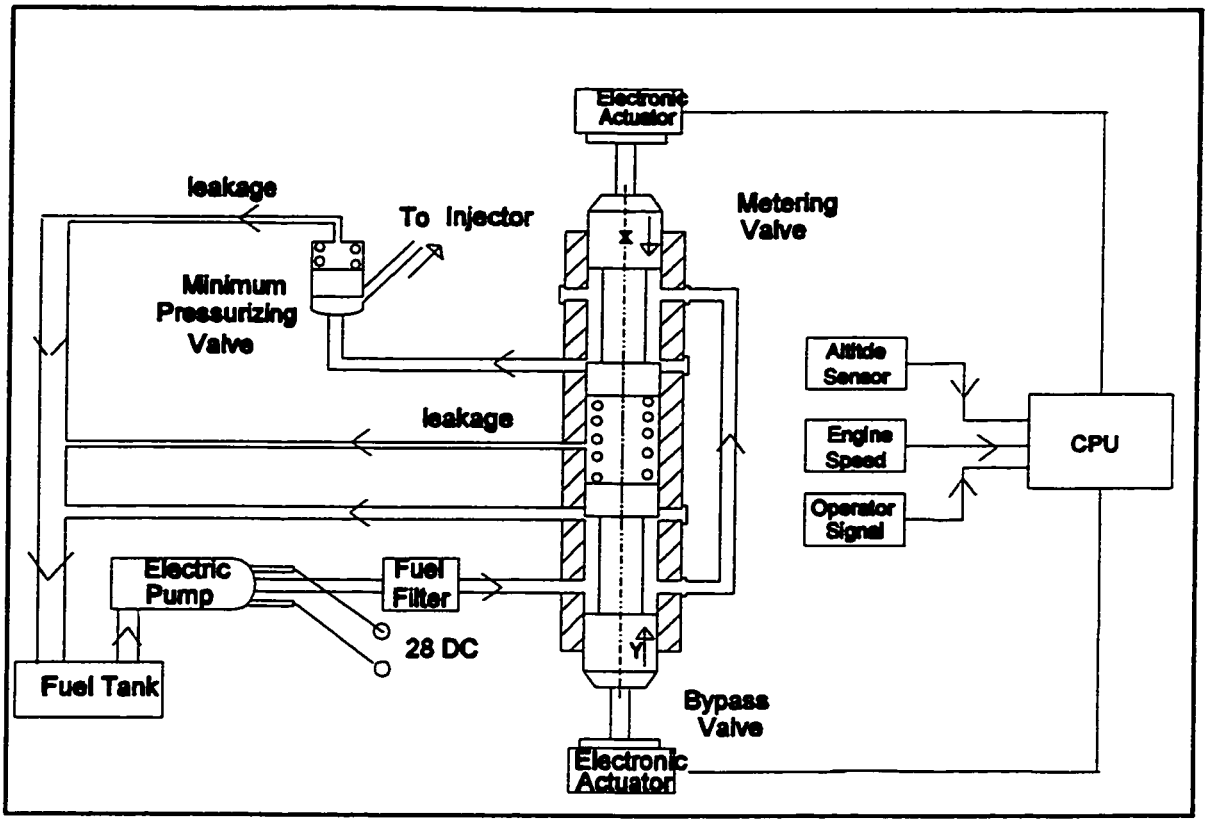

Figure 10.1 Schematic of a Single Barrel, Double Plunger Fuel Metering System

impacts on the performance of the system are investigated. To compare these options and to show the impact of them on the whole system including the engine, a simple dynamic model for the gas turbine engine will be developed and analyzed. Finally, the different fuel metering configurations which were presented in the thesis objectives, are compared regarding both the steady state and the dynamic response conditions and the conclusions will be drawn.

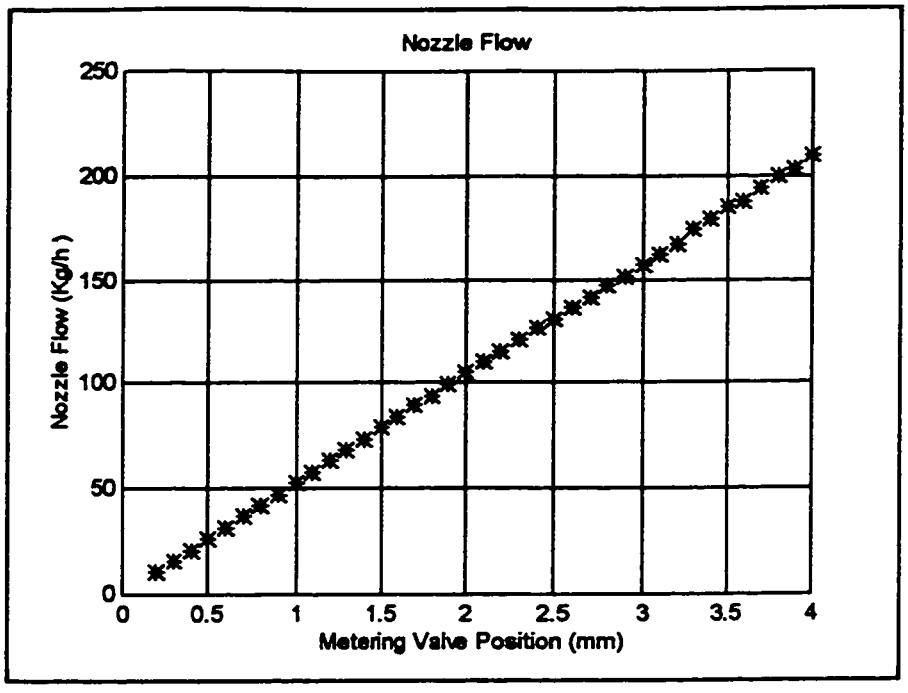

Figure 10.2 Steady State Simulation Results for the Nozzle Flow

10.2 Simulation of Steady State Processes

Equations presented in section 6.4 were used in order to describe the mathematical model of configuration 4. The model for steady state is obtained by setting the transient terms $(\frac{d}{dt}, \frac{d^2}{dt^2})$ equal to zero. This results in a set of nonlinear equations which are solved for the full travel of the metering valve. The step sizes and the maximum of the stepping rate of the stepper motors for both, the metering and the bypass plungers, are considered equal and are set at 0.025 mm and 500 steps / s respectively.

Figure 10.2 shows the simulation results for the nozzle fuel flow versus the metering valve position. The results confirm that, the metered fuel flow varies linearly with respect to the metering valve movement. This is due to the fact that the differential pressure across the metering valve is kept constant by the bypass valve.

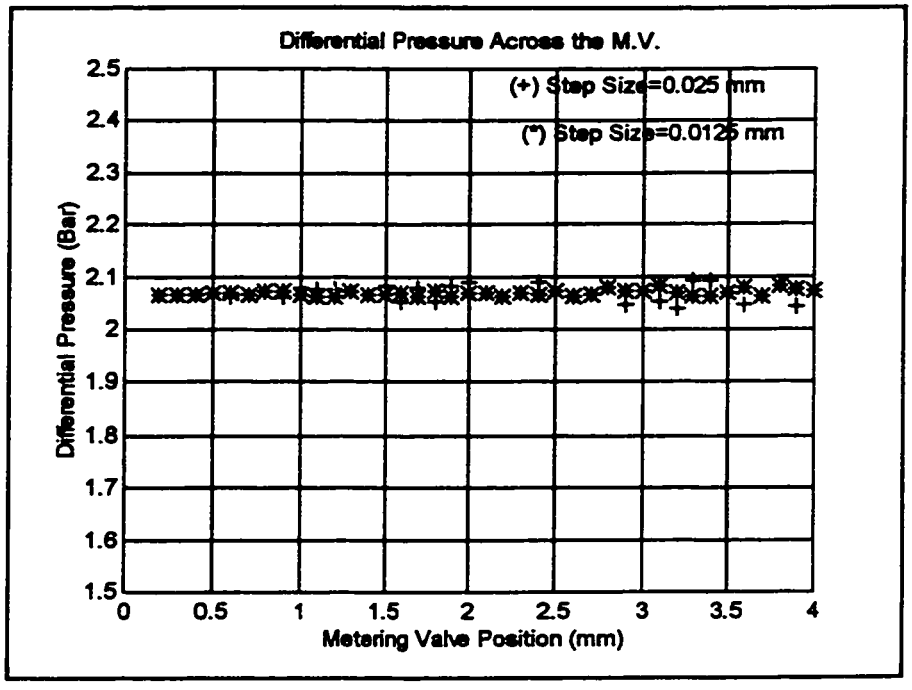

Figure 10.3 Effect of the Stepper Motor Step Size on the Differential Pressure

Figure 10.3 shows the differential pressure across the metering valve. There is a small fluctuation around the average differential pressure due to the incremental movement of the stepper motor. Choosing a smaller step size reduces the magnitude of the fluctuation and the nozzle fuel flow varies less. However, a smaller step size would increase the settling time of the dynamic response. In the following sections, the situation resulting from the failure of the bypass valve or the metering valve is investigated.

10.2.1 Bypass Valve Failure

The schematic diagram of a single barrel, double plunger fuel metering system is shown in figure 10.4. During the normal operation of the system, the metering valve controls the nozzle fuel flow and the bypass valve spills the excess of fuel back

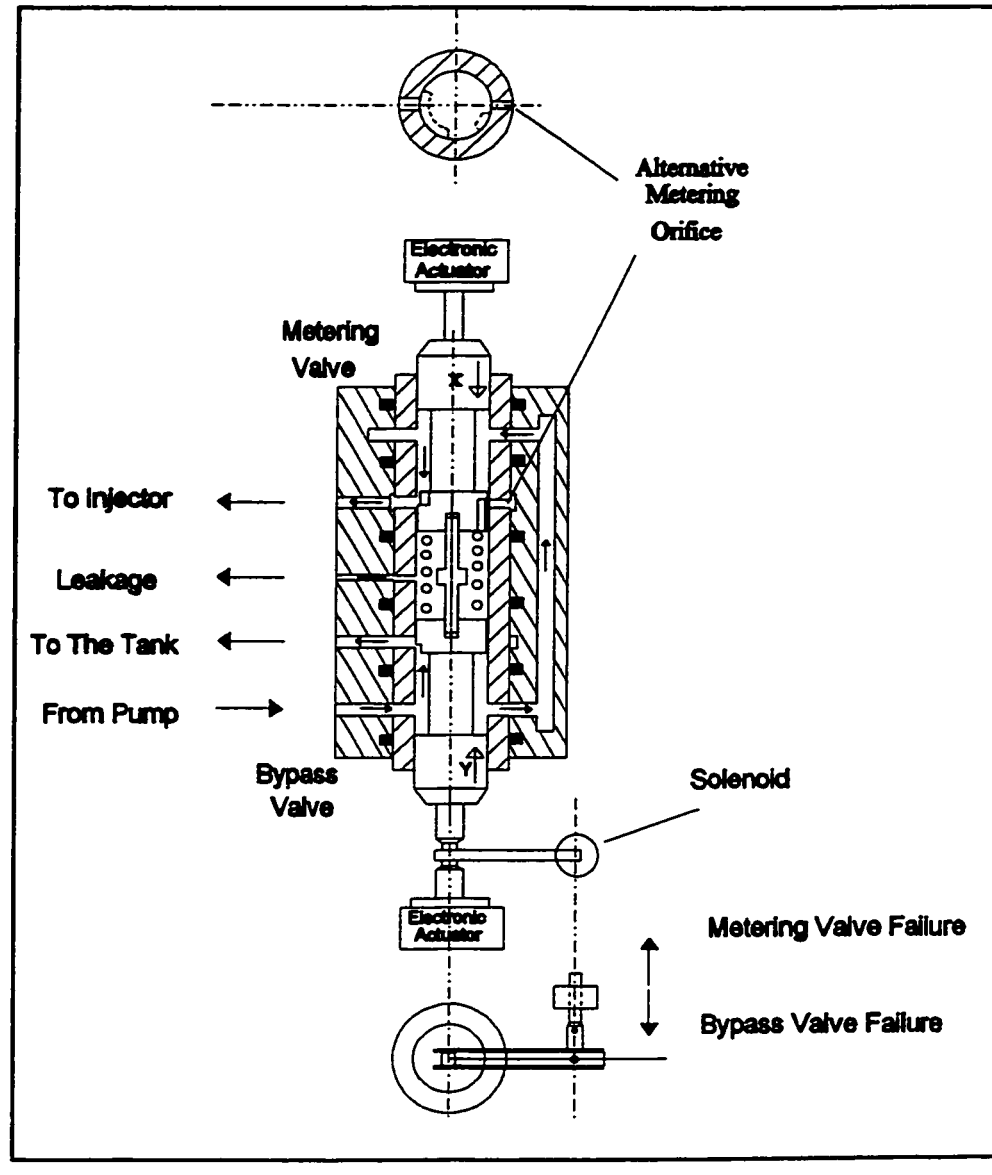

Figure 10.4 Schematics of the Single Barrel and Double Plunger Assembly

to the tank. However, as shown in the figure, during the back-up operation due to failure of the bypass valve, a double stroke on-off solenoid which actuates a radial lever connected to the plungers, is used to rotate both plungers. As the bypass valve fails, the plungers are rotated clockwise. As a result, the bypass port is closed, however, the metering valve still operates , as shown in figure 10.5. After the bypass

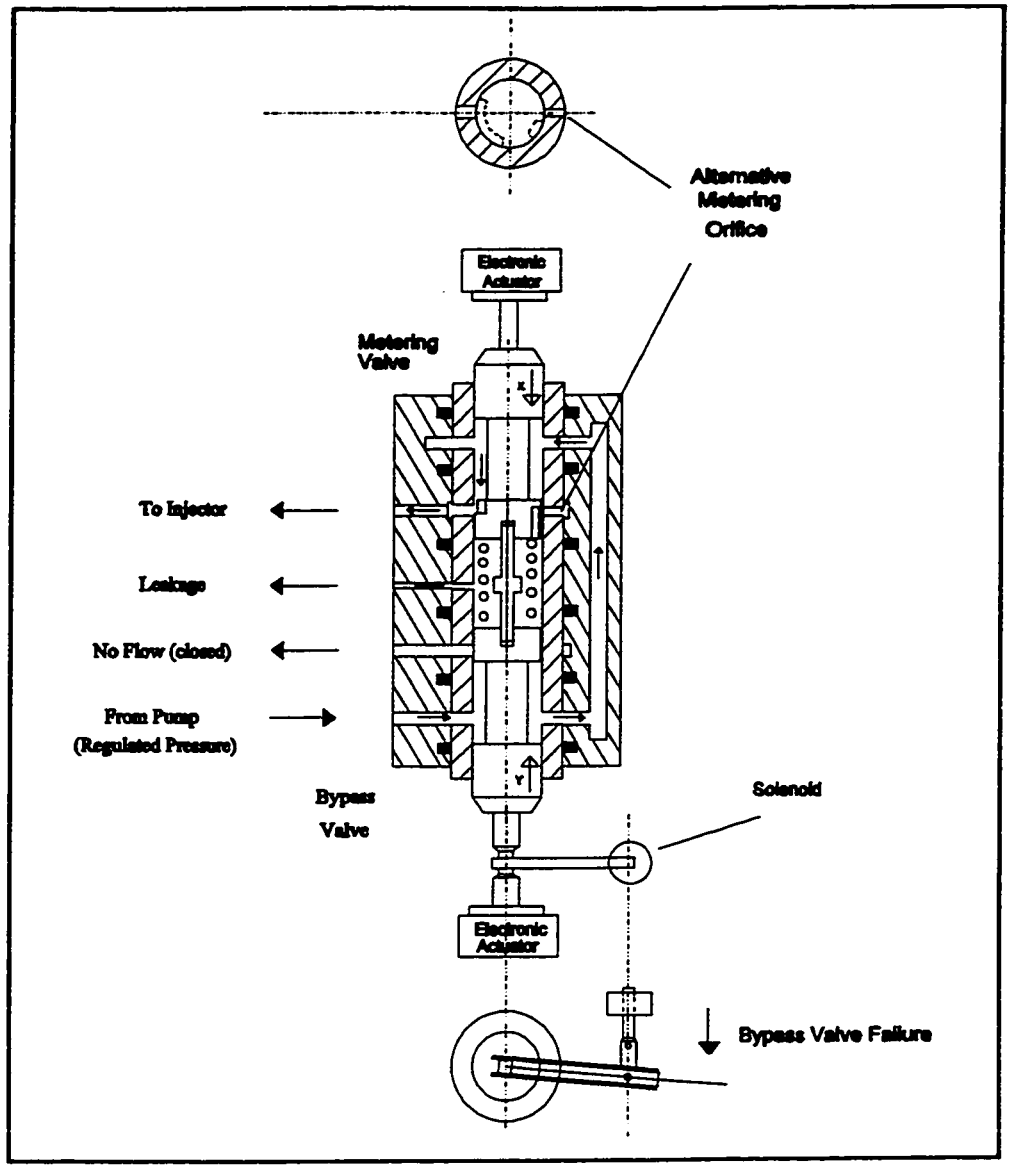

Figure 10.5 Schematic of the Fuel Metering System During the Bypass Valve Failure

flow closes, the fuel pressure increases and thus opens a relief valve in front of the pump, which is set for a higher constant pressure. This relief valve is originally used to protect the system from excessive pressure. Figure 10.6 shows the simulation result for the bypass valve failure. The relief valve is set at 55 bar pressure. As it is seen, the nozzle flow is no longer varying linearly and this is due to the fact that the differential

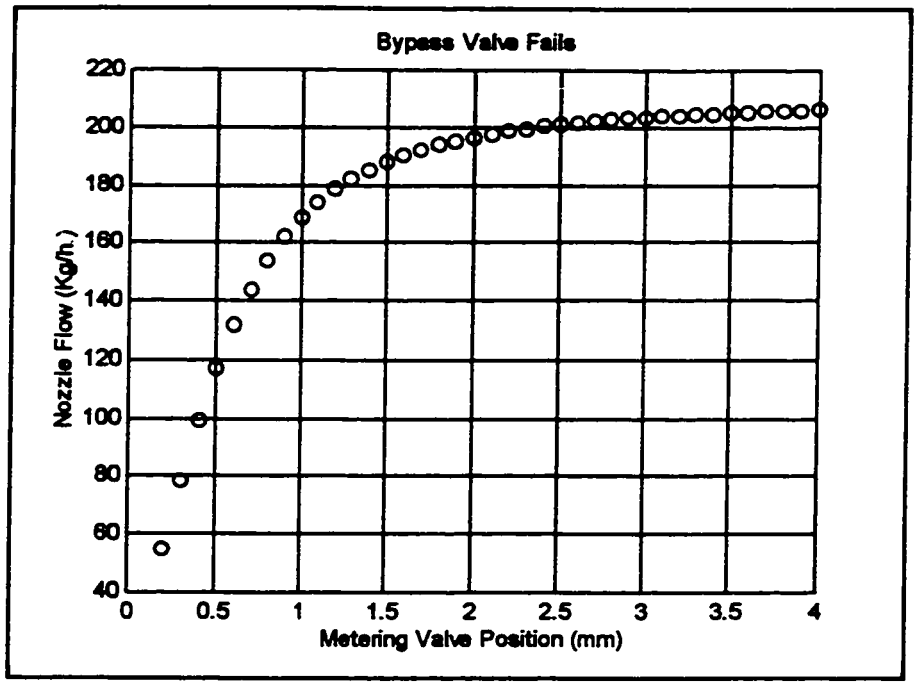

Figure 10.6 Simulation Results for the Bypass Valve Failure

pressure across the metering valve increases with the higher nozzle flow rate. The situation is similar to that with the metering valve only configuration , as described in section 3.1.1. However, even in this case, the metering valve is still able to maintain the nozzle flow required for the engine and can return the aircraft to home safely.

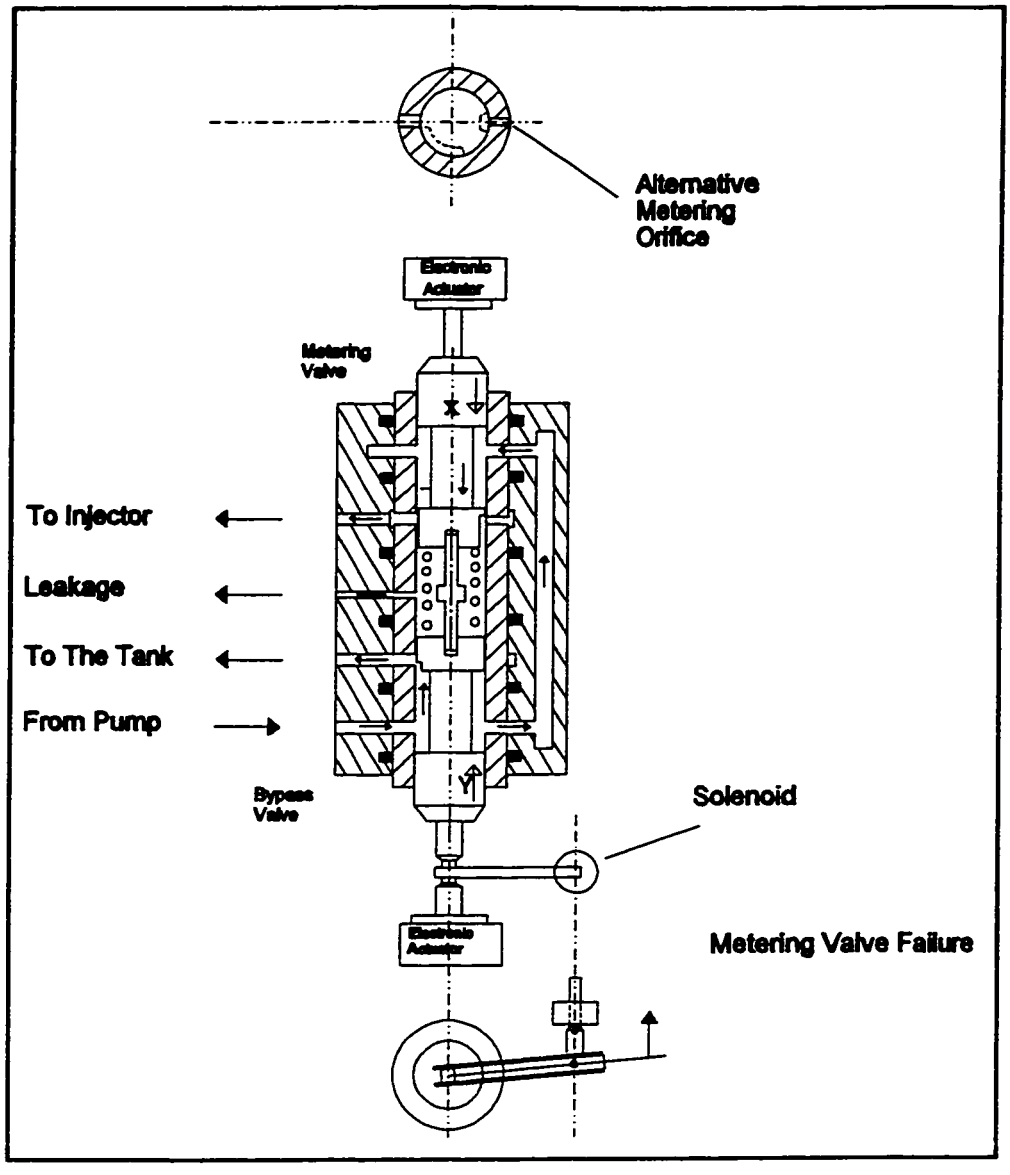

Figure 10.7 Schematic of the Fuel Metering System During the Metering Valve Failure

10.2.2 Metering Valve Failure

As the metering valve fails, both the valves are rotated counterclockwise by the solenoid. In this case, the metering valve is closed, however, at the same time, a fixed orifice in the barrel is opened to allow the fuel flow to the nozzle, as shown in figure 10.7. This means that the bypass valve controls the differential pressure across the

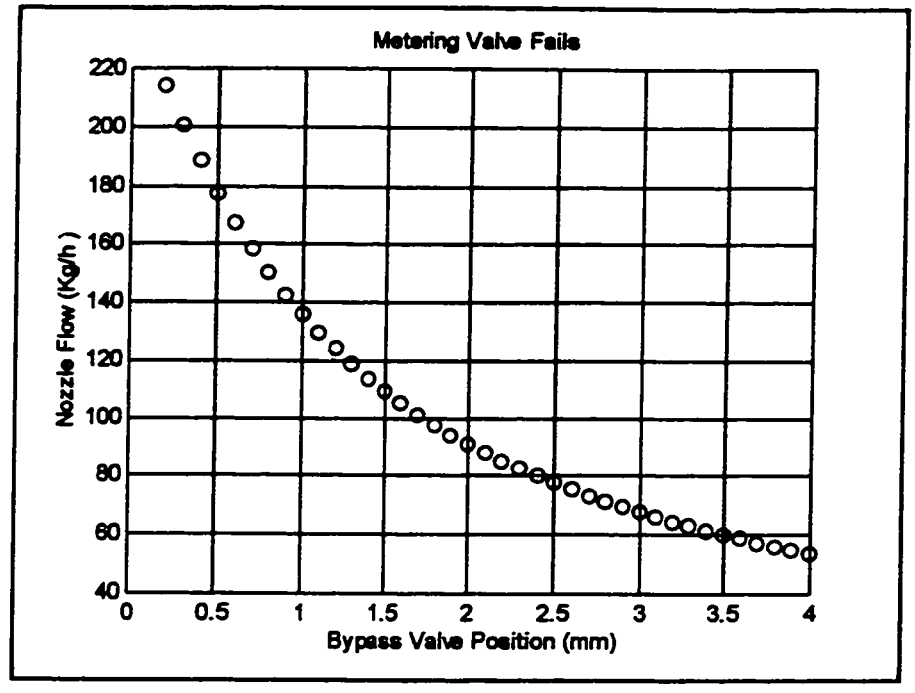

Figure 10.8 Simulation Results for the Metering Valve Failure

fixed orifice by spilling the excess flow of the pump back to the tank. Figure 10.8 shows the simulation results for the nozzle flow versus the full travel of the bypass valve plunger.

It has to be mentioned here that, at both back-up operation modes, the fuel metering system is not operating as per the best performance of the engine. However, in both cases, the objective is to supply the engine with an adequate fuel flow rate, allowing the aircraft to fly.

10.3 Dynamic Simulation Results

In this section, the transient response of the fuel metering system, based on the mathematical model described in section 6.4, is investigated. Due to the flexibility of this configuration, different control options can be presented. This is due to the fact that both, the metering valve and the bypass valve are under independent electronic control and, therefore, it is possible to provide a constant or variable differential pressure across the metering valve. Moreover, since different control options have different impacts on the dynamic response of the system, therefore, the dynamic response of the system with each option is first presented and the results of all the control options are next compared to determine the most advantageous one for the proposed fuel metering system.

Figure 10.9 shows the block diagram of the first control option. As it is seen, the error e_1, which is a difference between the demanded and the actual fuel flow, acts on the first digital controller to produce a voltage signal. Meanwhile, the second error e_2, which is the difference between the desired and the actual differential pressure, acts on the second digital controller. In both cases, the voltage signals enter two voltage to frequency converters to produce the rectangular waveforms. These rectangular waveforms are used to trigger the stepper motor drivers which send a sequence of pulses to drive the actuators of the first and the second stepper motors in proper directions and thus, increase or decrease the fuel flow and the differential pressure across the metering valve, respectively. Note that the controllers output voltages are limited to the maximum values which are provided by the stepper motors manufacturers to ensure that the actuators produce a linear force high enough to drive the valve when the controller outputs are very high.

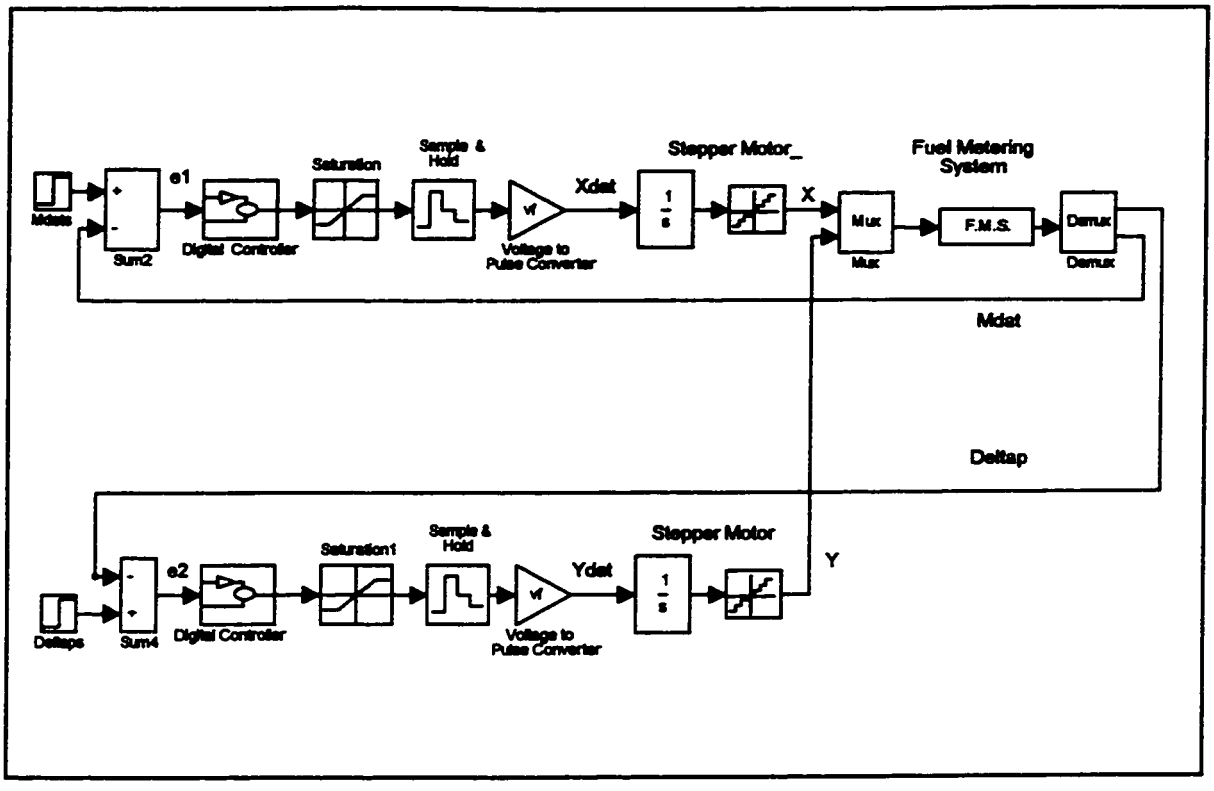

Figure 10.9 The Block Diagram of the First Control Option

In general, the purpose of this option is to keep a constant differential pressure across the metering valve, even during the transient period. This ensures that the relation between the metering valve position and the fuel flow is linear and unique and is not changing during the operation.

Figures 10.10 to 10.12 show the typical dynamic responses of the system to a request for an abrupt change in the fuel flow rate from the initial value of 83.5 kg/h to the final value of 183.5 kg/ h. Next, after 2 seconds, the fuel flow rate is commanded to return to its initial value of 83.5 kg/ h. Meanwhile, the differential pressure must be kept constant by the second actuator. The step sizes and the maximum stepping rates of the both stepper motors are 0.025 mm and 500 steps /s respectively.

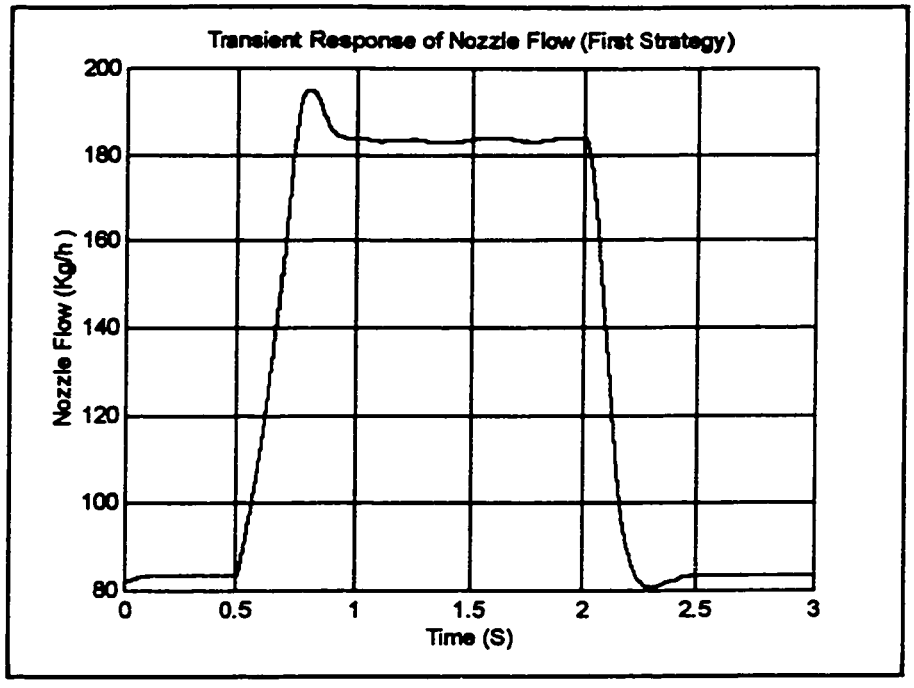

Figure 10.10 The Dynamic Response of the Metered Fuel Flow for the First Control Option

At the start of the transient process, the error e_1 is very large, therefore, the output of the first controller is saturated and the metering valve moves at its maximum stepping rate. With the opening of the metering valve, the differential pressure across the metering valve drops suddenly and therefore, the bypass valve moves back with its maximum rate trying to keep a constant differential pressure.

It has to be mentioned here that at steady state operation, the positions of both valves may fluctuate about their final values, as shown in the figures. This is due to the fact that the metered fuel flow is a function of the differential pressure and the opening of the metering valve. This means that around steady state, the deviation of the first actuator from its final value results in the deviation of the second actuator and, therefore, both actuators never stop at their final values and fluctuate around them. These fluctuations depends on the gains of the controllers and the step size of

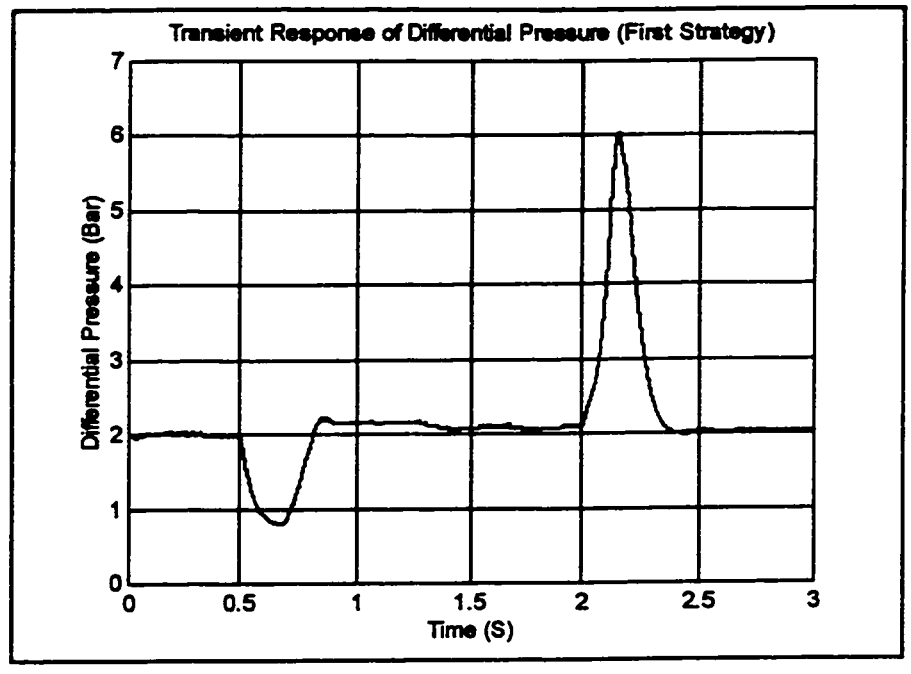

Figure 10.11 The Transient Response of the Differential Pressure for the First Control Option

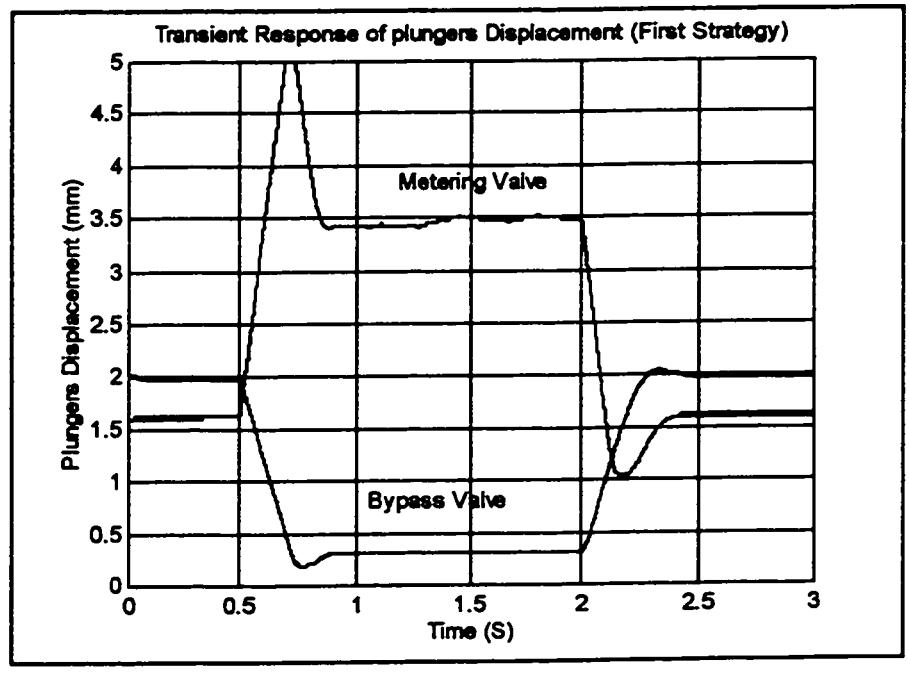

Figure 10.12 The Dynamic Responses of the Actuators Displacement for the First Control Option

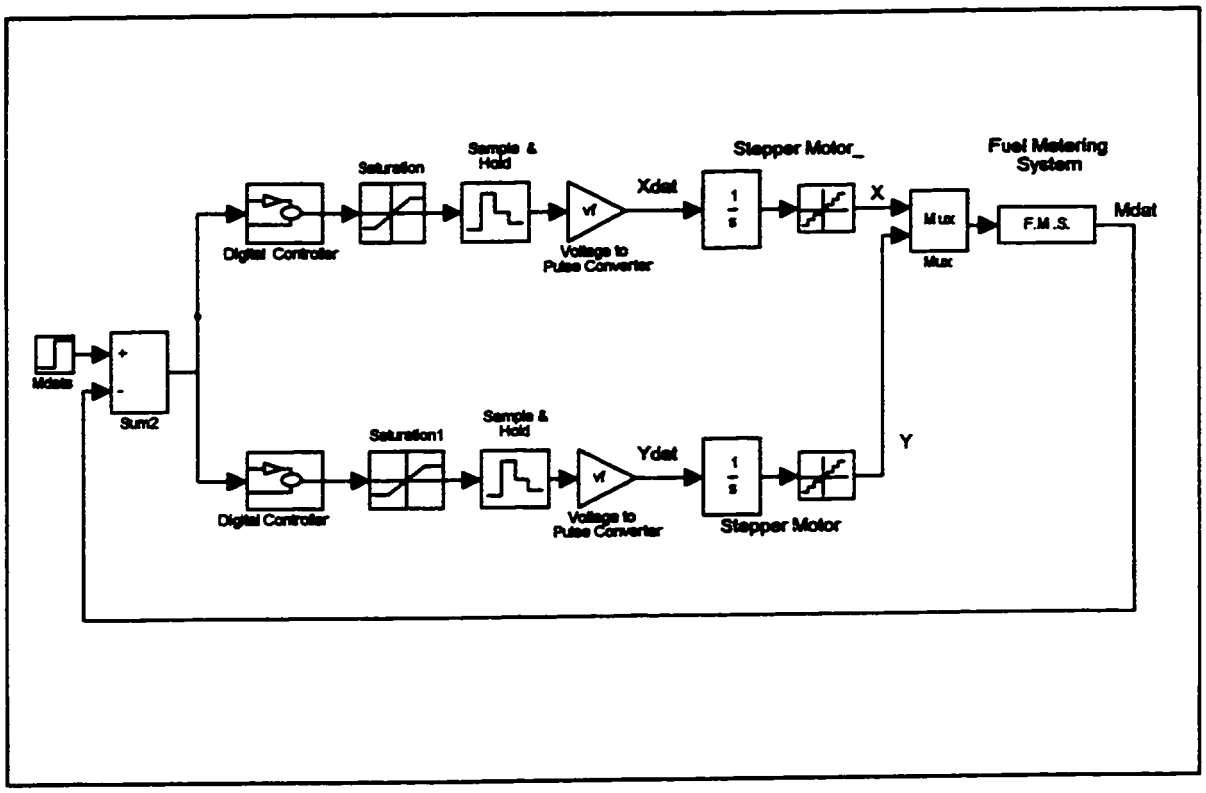

Figure 10.13 The Block Diagram for the Second Control Option

the stepper motors and, to some extend, can be eliminated by deactivation of the controllers when the errors are smaller than a minimum value.

In the **second control option,** figure 10.13, the error e_1, which is the difference between the demanded and the actual fuel flow, acts on both digital controllers. In other words, in this control option, the fuel flow rate is controlled by varying both the metering valve flow area and the bypass valve flow area which indirectly changes the differential pressure across the metering valve. If both, the metering valve and the bypass valve actuators move in appropriate directions so as to synchronously increase or decrease the fuel flow rate, then it is possible to have a faster transient response.

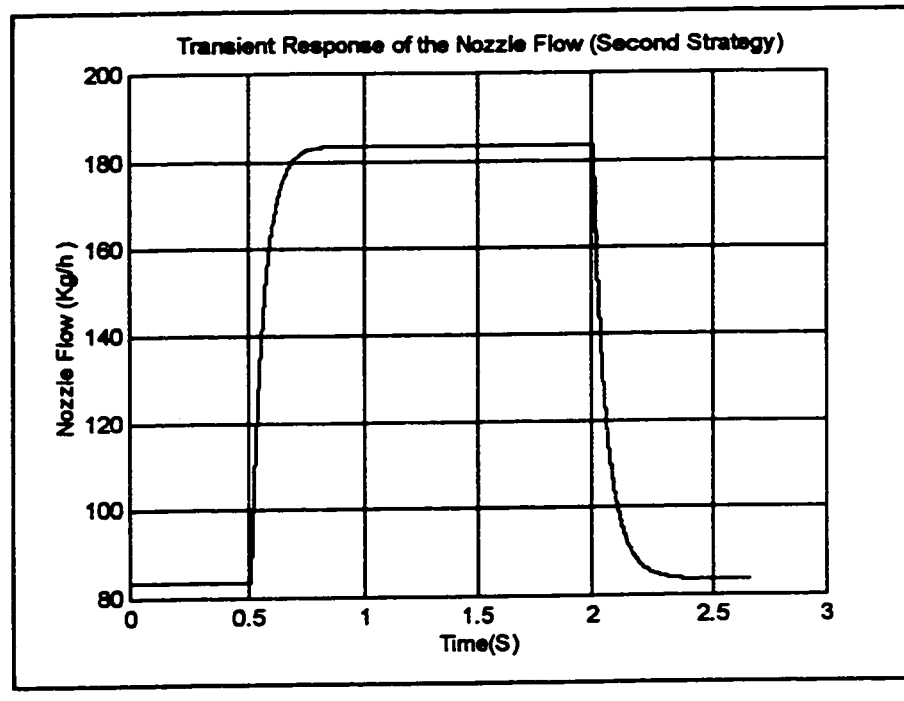

Figure 10.14 The Dynamic Response of the Metered Fuel Flow for the Second Control Option

Figures 10.14 to 10.16 show the simulation results obtained for the second control option. At the beginning of the transient, the metering valve plunger moves forward with its highest speed to open the metering valve and to let more fuel flow to the nozzle. Meanwhile, the bypass valve actuator moves back with its highest speed to close the bypass valve and increase the differential pressure. This provides an initial boost in the fuel flow rate change. However, when the error is reduced, both plungers move more slowly and the differential pressure decreases.

Because in this control option, the differential pressure is not kept constant, therefore, there are several positions of the valves which meet the required fuel flow. In other words, many position combinations of the valves can produce the same fuel flow rate. The transient response of the system based on this strategy, is a function of the initial positions of the plungers and therefore, the behaviour of the system is not predictable during operation.

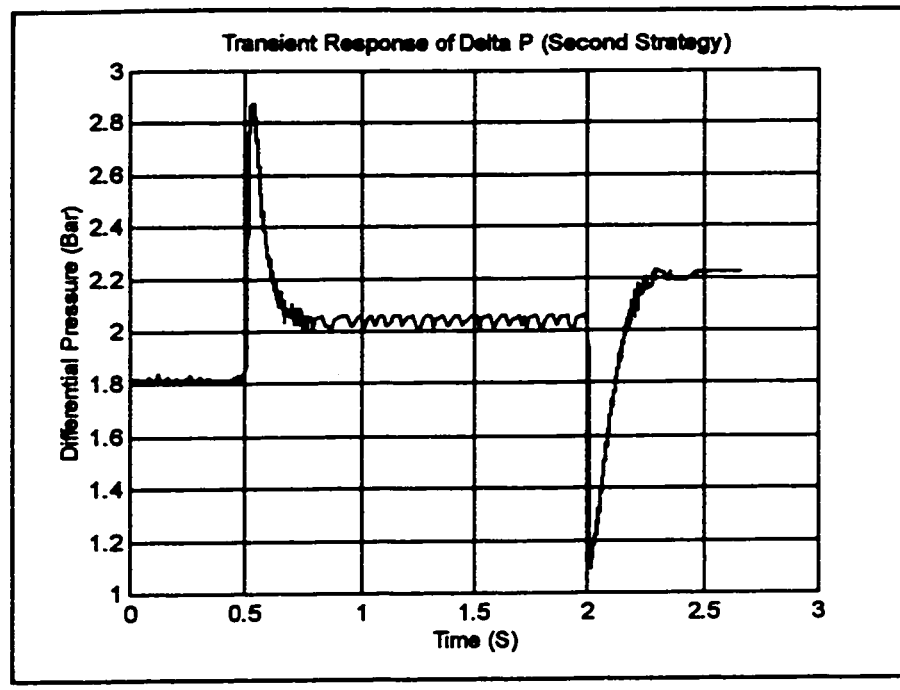

Figure 10.15 The Transient Response of the Differential Pressure for the Second Control Option

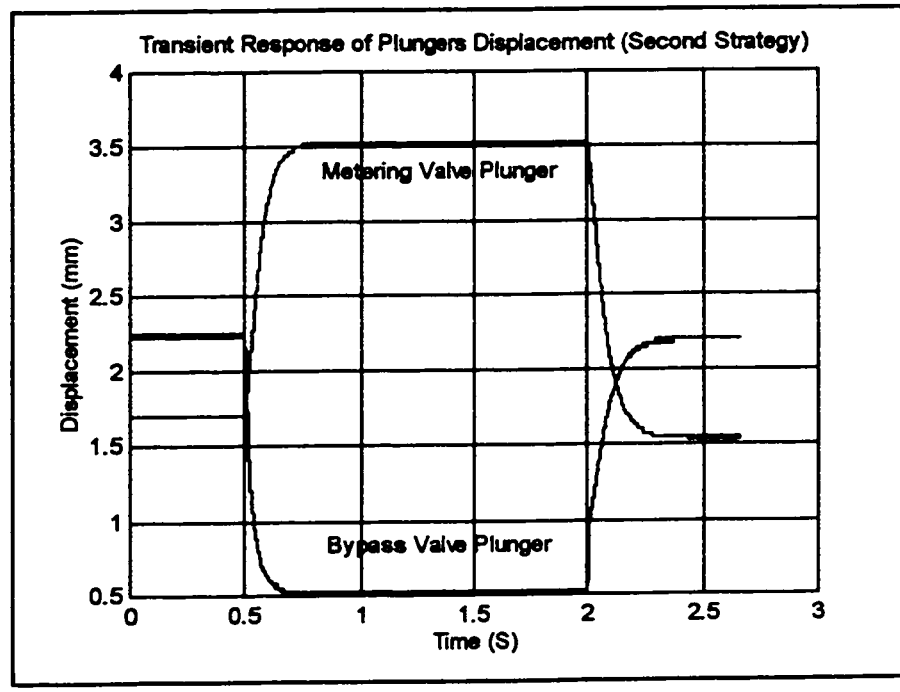

Figure 10.16 The Dynamic Responses of the Actuators Displacements for the Second Control Option

In general, the transient response of the system based on this control option is faster than the response based on the first control option. However, due to the unpredictable positioning of the actuators, the second option is less applicable in practice.

To improve the transient processes over those obtained with the first and the second control options, a new **control strategy (third control option)** is presented. In this strategy, the main advantage is that the differential pressure across the metering valve changes only during the transient part of the response and then, it returns to its initial value during the steady state part. Figure 10.17 shows the block diagram of this control strategy. According to this strategy, when higher fuel flow rate is demanded by the engine, the differential pressure is set to a higher value and therefore, the response is faster. After the nozzle flow reaches 85% of its final value, the differential pressure returns to its steady state value and from this moment the response is slower. However, this ensures that there is just one positioning of the actuators. When a nozzle flow decline is required, the differential pressure is set to its lower value as long as the nozzle flow is more than 15% of the final value and then the differential pressure returns to its steady state value.

Figure 10.18 shows the transient response of the metered fuel flow. As seen, the response is very fast as long as the flow is less than 85% of its final value. This is due to the fact that, as the metering valve moves forward, the differential pressure is also increasing, as shown in figure 10.19. However, when the nozzle flow reaches 85% of the final value, the differential pressure starts to return to its steady state value and thus the response is slower.

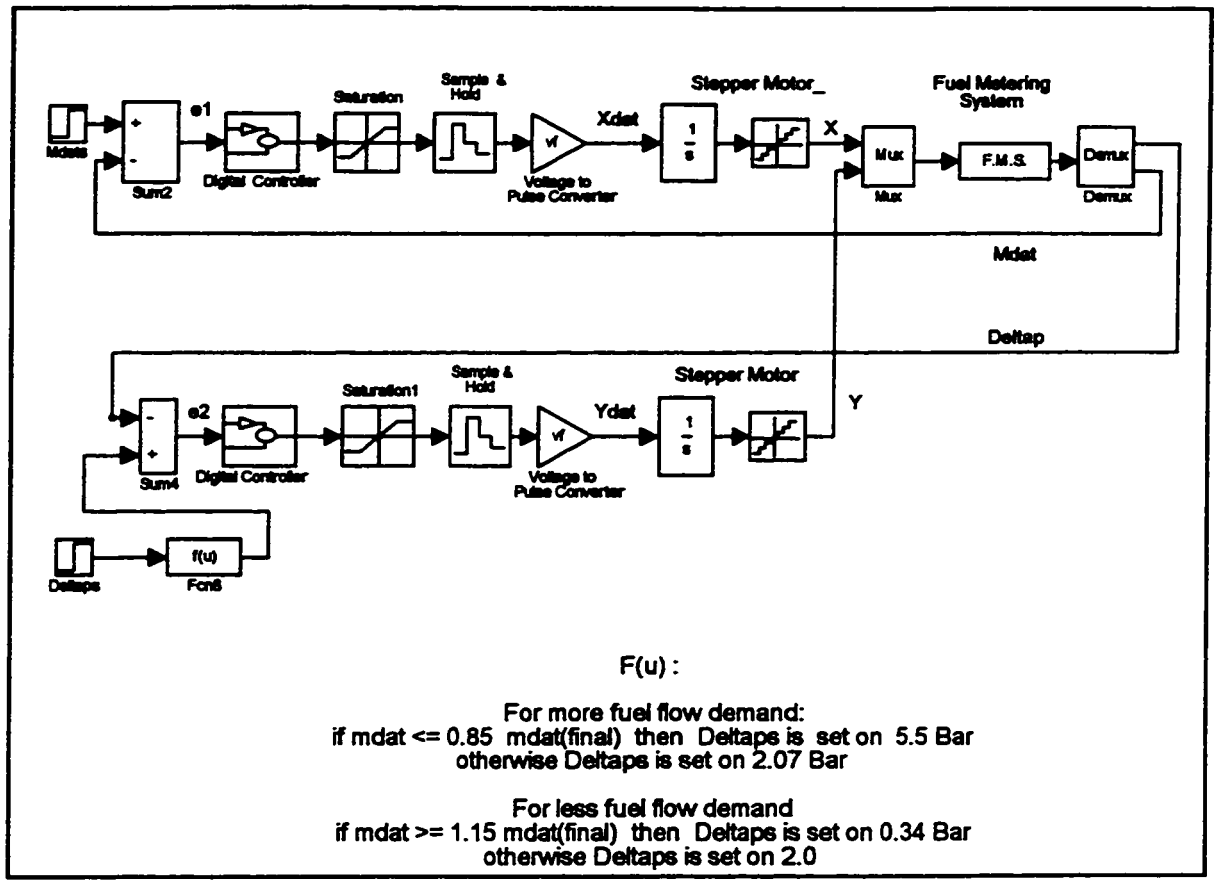

Figure 10.17 The Block Diagram for the Third (New) Control Option

Figure 10.20 shows the differential pressure setting plotted from the simulation. As it is seen, the maximum and the minimum of the differential pressure is 5.5 and 0.34 bar respectively. This means that the gain of the second controller is not constant and varies during the transient part of the response.

The comparison of the results for the different control options and the choice of the best option is done in the next section after including the engine model in the system.

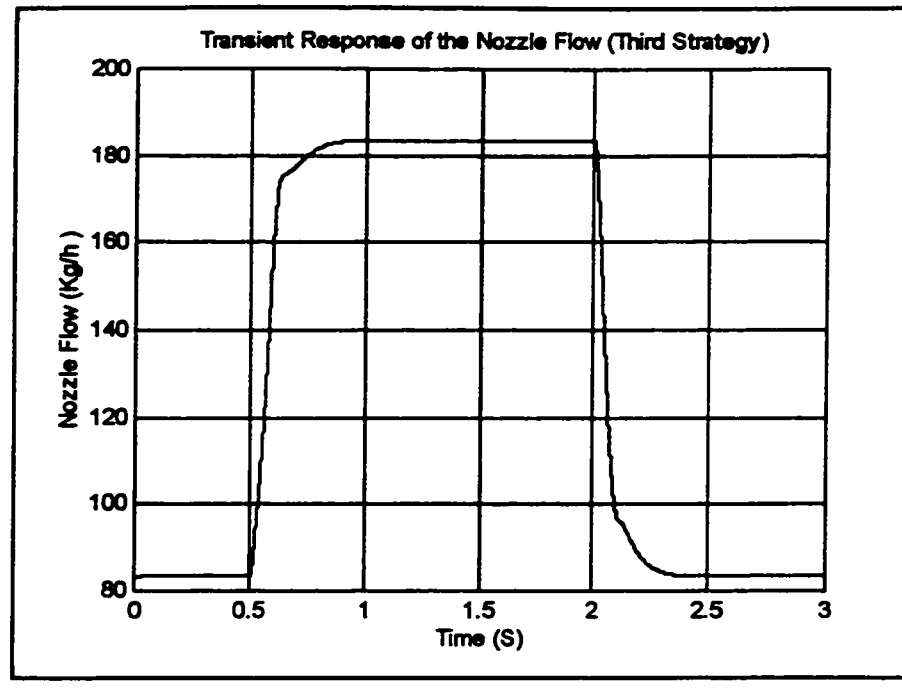

Figure 10.18 The Dynamic Response of the Metered Fuel Flow for the Third (New) Control Option

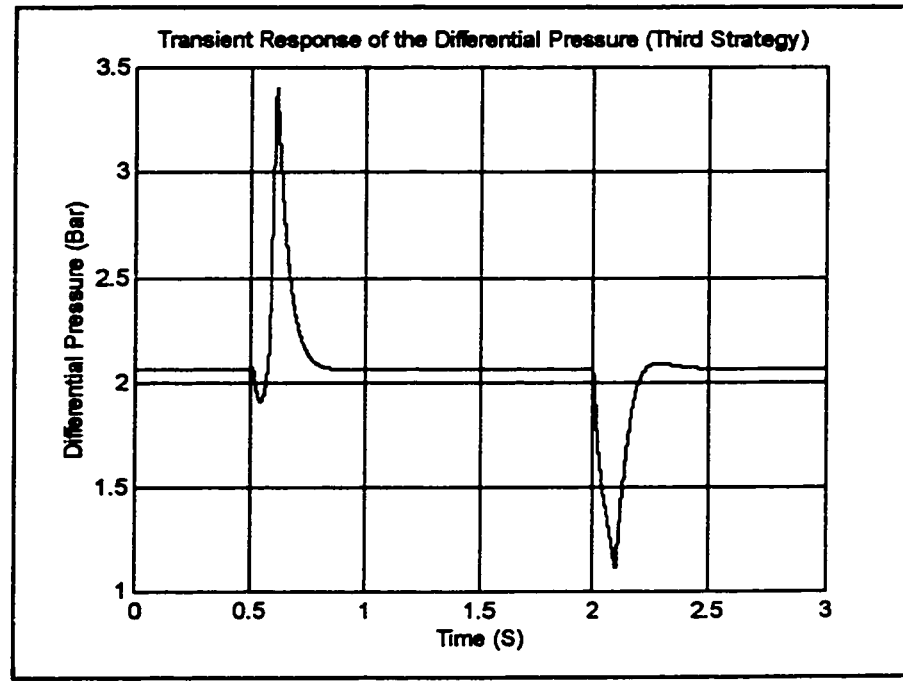

Figure 10.19 The Simulated Transient Response of the Differential Pressure for the Third (New) Control Option

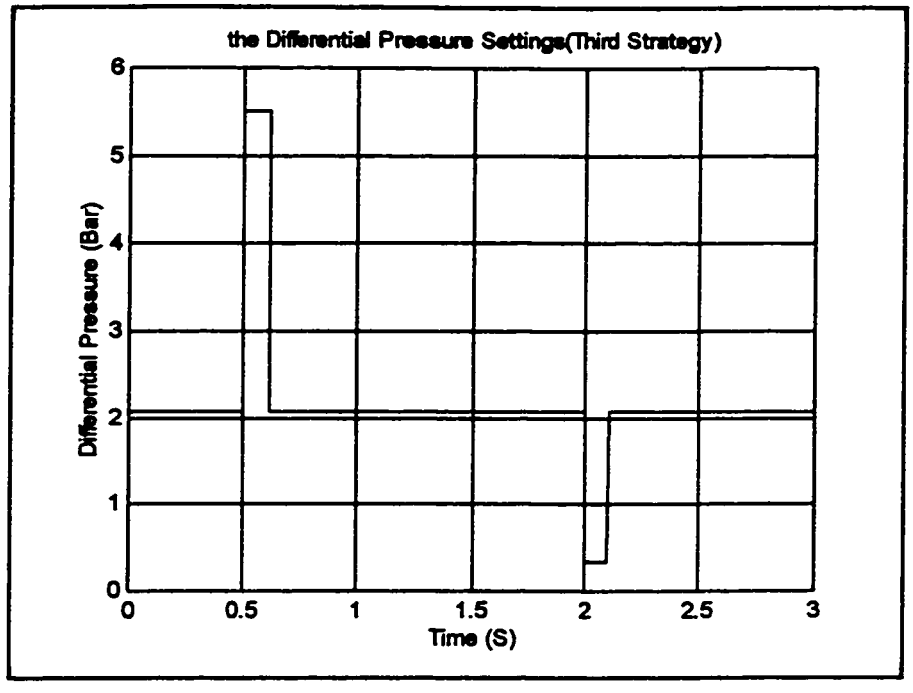

Figure 10.20 The Differential Pressure Setting Plotted from the Simulation Results for the Third (New) Control Option

In the **back-up mode configuration**, when there is a failure in the metering valve or the bypass valve controller, a double stroke on-off solenoid changes the angular position of the plungers. When there is a failure in the bypass valve controller, the solenoid rotates the valves clockwise to cover the bypass port. Consequently, by closing the bypass port, the pump delivery pressure increases and thus a relief valve in the system is opened to limit the pump delivery pressure. This means that during the bypass valve failure, the bypass valve flow area is zero and the pump pressure is set at maximum level by the relief valve. These values are considered in the simulation of the dynamic response of the system.

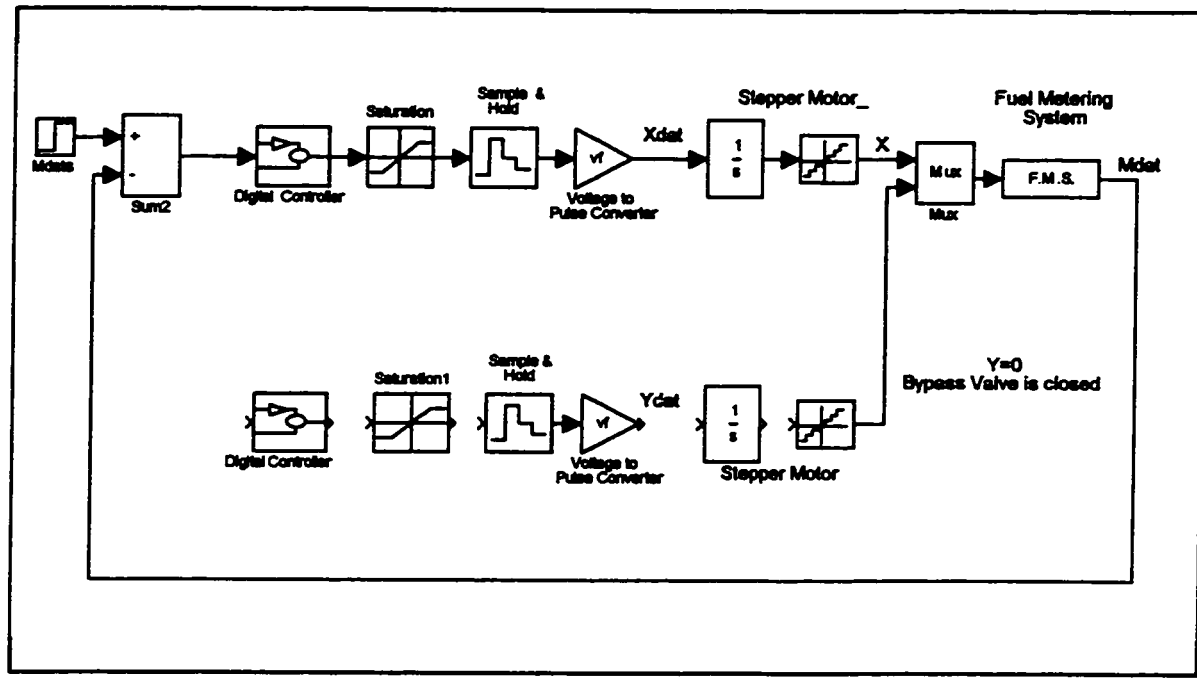

Figure 10.21 The Block Diagram of Control System During Bypass Valve Failure

If the metering valve fails, both plungers are rotated counterclockwise and thus a fixed metering valve orifice in the barrel is indexed with the metering valve slit. This means that the metering valve flow area is constant during the metering valve failure.

Figure 10.21 shows the block diagram of control system which is used during the bypass valve controller failure. As it was mentioned before, during the bypass valve failure, the bypass valve orifice is closed and a relief valve protects the system from excessive pressure. In this case, the relief valve is set at 55 bar.

Figures 10.22 and 10.23 show the simulation results for different fuel flow rate demands. Figure 10.22 illustrates that the transient fuel response of the system is ensured to be very fast, and that the system operation even during the failure is satisfactory. However, as shown in figure 10.23, the relief valve is set for a higher

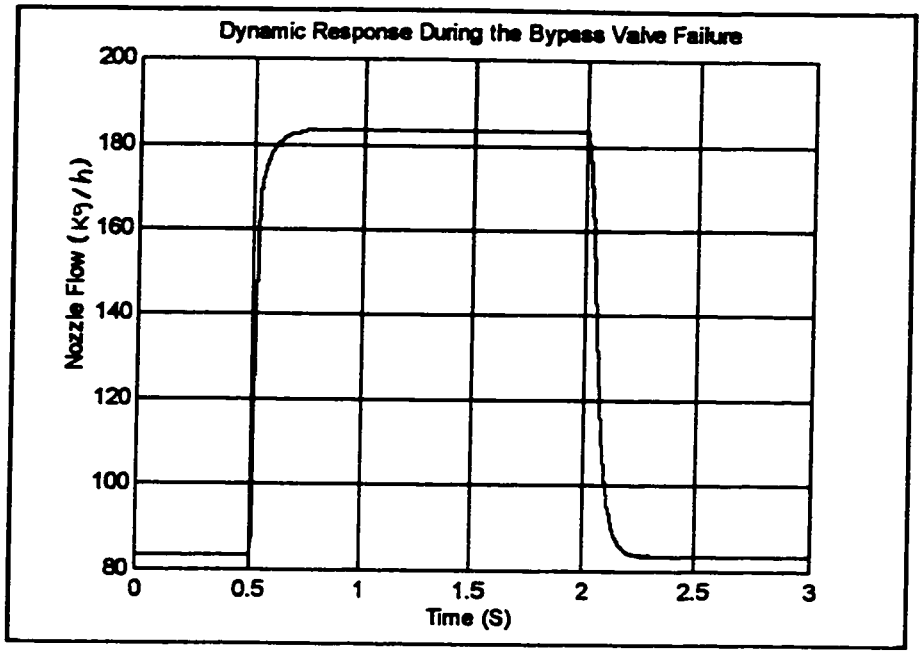

Figure 10.22 Dynamic Response of the Metered Fuel Flow During the Bypass Valve Failure

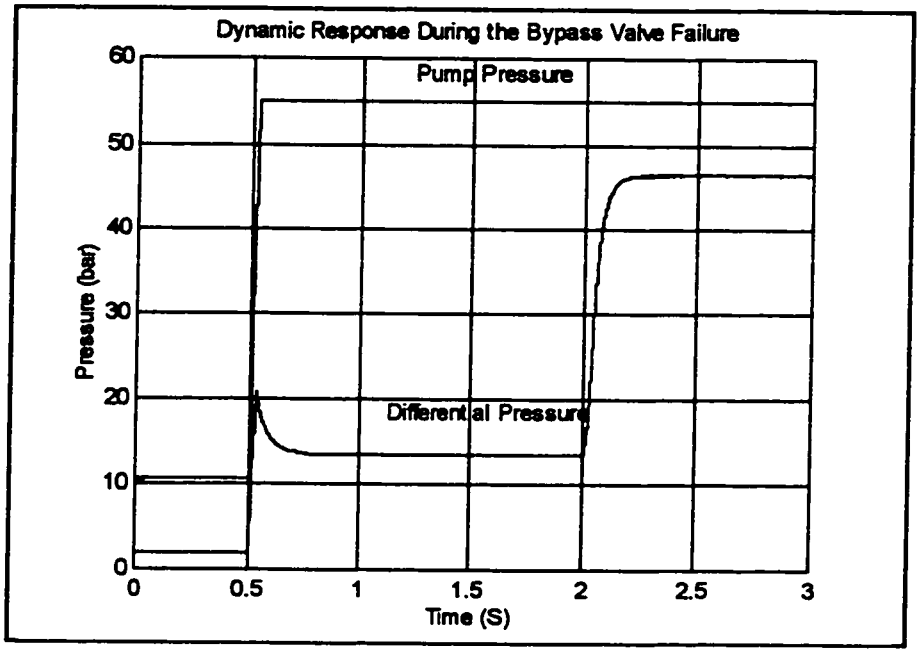

Figure 10.23 Dynamic Responses of the Pump Pressure and Differential Pressure across the Metering Valve During the Bypass Valve Failure

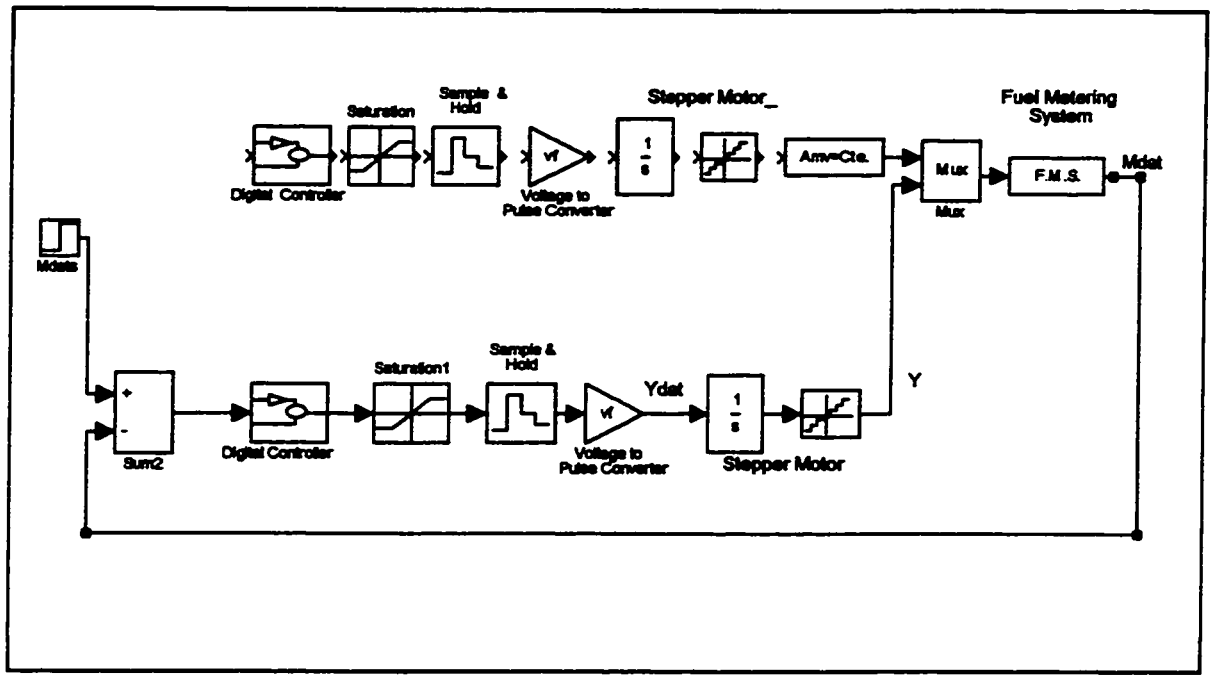

Figure 10.24 The Block Diagram of the Control System During the Metering Valve Failure

pump delivery pressure, and the differential pressure across the metering valve is also high. This means that the pump is operating with a higher load which might not be acceptable for the long time extensive operation.

Figure 10.24 shows the block diagram of the control system which is used during the metering valve failure. As seen, the metering valve controller is not operating and the bypass valve is acting solely on the error which is the difference between the fuel flow demand and the actual fuel flow. This part is the same as that one which was explained in the second control option. Note that, contrary to the second control option, the system has just one unique solution. This is due to the fact that the metering flow area is constant and does not change during the operation.

Figures 10.25 and 10.26 show the dynamic response of the system for different nozzle flow demands. As seen, the response is very fast despite the fact that the

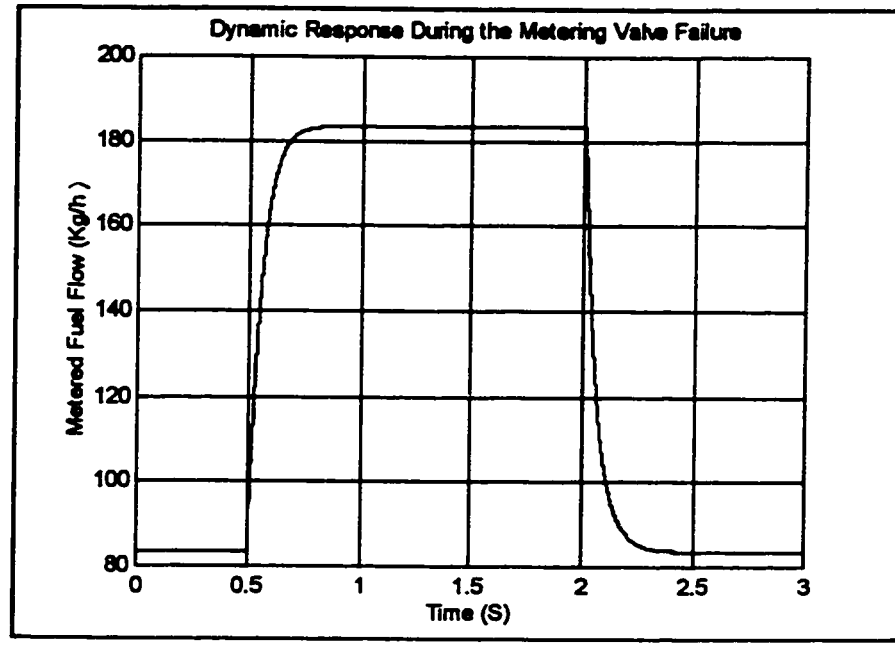

Figure 10.25 Dynamic Response of the Metered Fuel Flow During the Metering Valve Failure

metering valve is not operating. This is due to the fact that the differential pressure across the metering valve is not constant and is varying by the bypass valve controller to speed up the response. These figures ensure that the proposed fuel metering system has a satisfactory response, even during the metering valve failure.

In general, both back-up modes ensure that the proposed fuel metering system is operating quite well during the back-up conditions and therefore, it can be recommended to be used in small gas turbine engines to improve their reliability and safety. In the next section, the engine model is presented to be used as a tool for comparison of different control options discussed earlier.

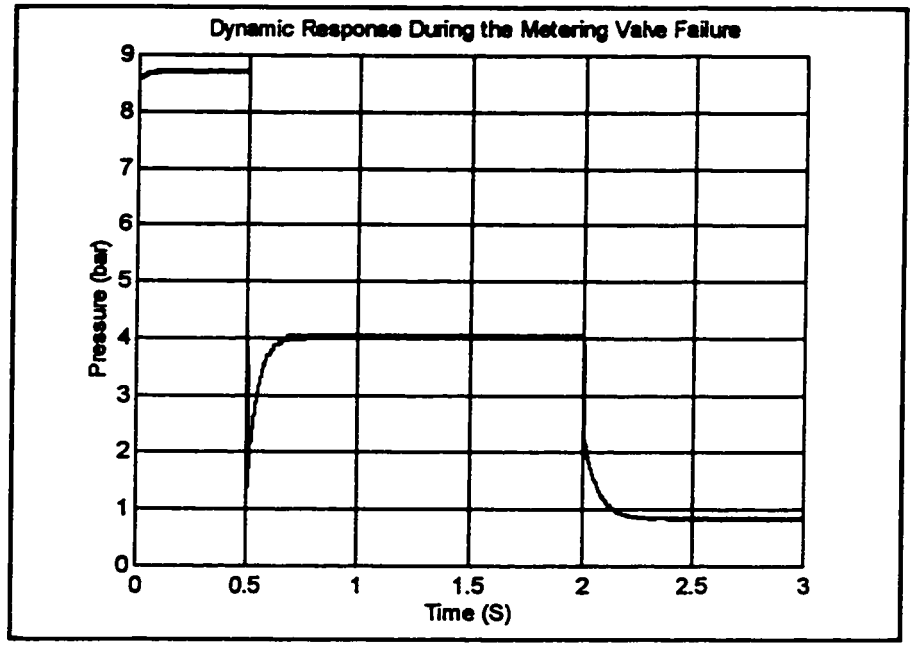

Figure 10.26 Dynamic Response of the Differential Pressure across the Metering Valve During the Metering Valve Failure

10.4 Engine Model

Due to the fact that a fuel metering system is interfacing the engine, therefore, the investigation of the dynamic response of the system including the gas turbine engine is recommended, in order to properly evaluate the behaviour of the complete system. However, to achieve the real time control, engine model has to be simplified. Therefore, a dynamic analysis was used to obtain the transfer function describing the response of the engine to the fuel flow changes. It was supposed that the fuel metering system is mounted on the gas generator shaft of a gas turbine engine. The data for this simulation were taken from descriptive notes for PT6A-27 turboprop engines [60]. The fuel delivery schedule for this engine is shown in figure 10.27.

Engine Maximum Torque at Steady State Condition

The maximum engine torque for steady state condition is calculated from the maximum engine power and the corresponding nominal speed:

P_{max} = 715 HP = 533.2 kW at N_{nom} = 33000 rpm

Then:

$$T_{max} = \frac{P_{max}}{(2\pi N) \ / \ 60} = \frac{533200}{(2\pi 33000) \ / \ 60} = 154.29 N.m$$

Fuel Flow Rate

The maximum fuel flow is 200 kg/h, which is considered for the maximum value of the fuel schedule. Therefore, the fuel flow at the nominal steady state power of 533.2 kW at 100% engine speed is assumed to be 10% lower, to allow for overcoming of the momentary load increase when running at governing mode. Then

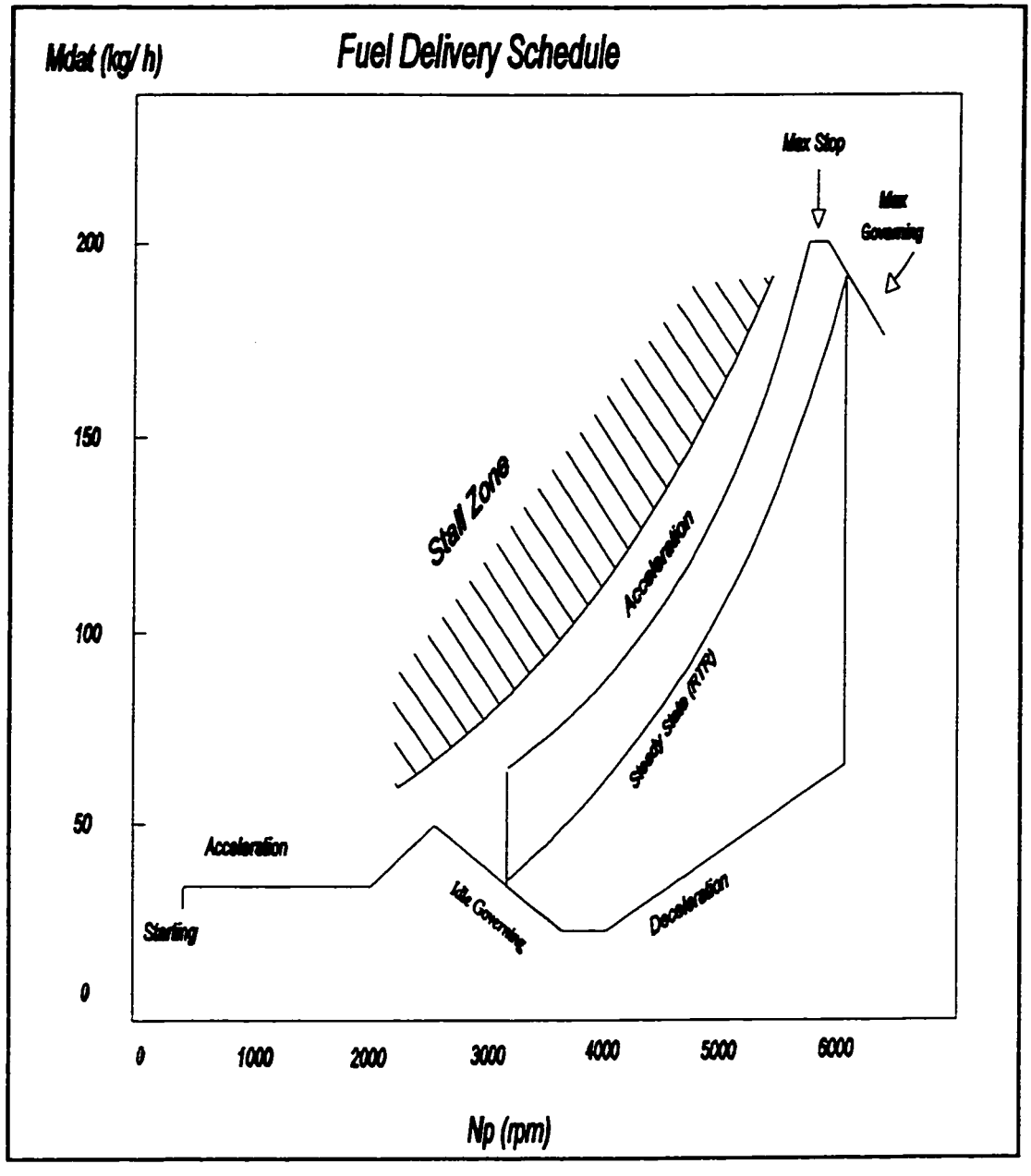

Figure 10.27 Fuel Delivery Schedule for PT6-A27

at 533.2 kW the fuel flow is:

$$\dot{m_f} = \frac{200}{1.1} = 181.82 \ kg/h$$

and the specific fuel consumption is:

$$SFC = \frac{\dot{m}_f}{P_{max}} = \frac{181.82}{533.2} = 0.3410 \ \frac{kg}{kW.h}$$

Torque to Fuel Flow Ratio at Maximum Governing Speed Range

For the purpose of simplifying the dynamic simulation, the ratio of fuel flow to torque at maximum governing is assumed constant and is not affected by the speed change in the narrow speed range of the maximum governing engine operation.

$$SFC = \frac{\dot{m}_f}{P} = \frac{\dot{m}_f}{T\omega}$$

then

$$T = \frac{1}{SFC}\frac{\dot{m}_f}{\omega} = 1.056*10^7 \ \frac{\dot{m}_f \ (kg/s)}{\omega \ (rad/s)} \ N.m$$

Evaluation of the Moment of Inertia

The moment of inertia for the PT6-A27 engine is calculated from following equation:

$$J_M = \frac{T}{\alpha}$$

It is assumed that the torque (T) and the angular acceleration (α) are average and also it takes 3 second for the engine to accelerate from the ground idle (GI) to the maximum power (MP). The angular velocities of the engine at GI and MP are 1738 and 3455 (rad/s) respectively. Therefore, the average angular acceleration is found as

follows:

$$\alpha_{ave} = \frac{(\omega_{MP} - \omega_{GI})}{3} = 576.96 \ \frac{rad}{s^2}$$

And finally, assuming that a 10% surplus of maximum torque over steady state torque causes the engine to accelerate at the above calculated acceleration rate, and thus the moment of inertia is calculated to be:

$$J_M = 2.68 \ 10^{-2} \ N.m.s^2$$

Dynamic Model of the Engine

The dynamic balance of the torques is found as follows:

$$T_t - T_c - T_d - T_l = J \ \dot{\omega}$$

and

$$T_d = B \ \omega$$

where subscripts t, c, d and l stand for turbine, compressor, damping and load. Taking the Laplace transform and simplifying the equation:

$$\frac{\omega}{(T_t - T_c) - T_l} = \frac{1}{JS + B}$$

and

$$T_t - T_c = 1.056 \ 10^7 \ \frac{\dot{m_f}}{\omega}$$

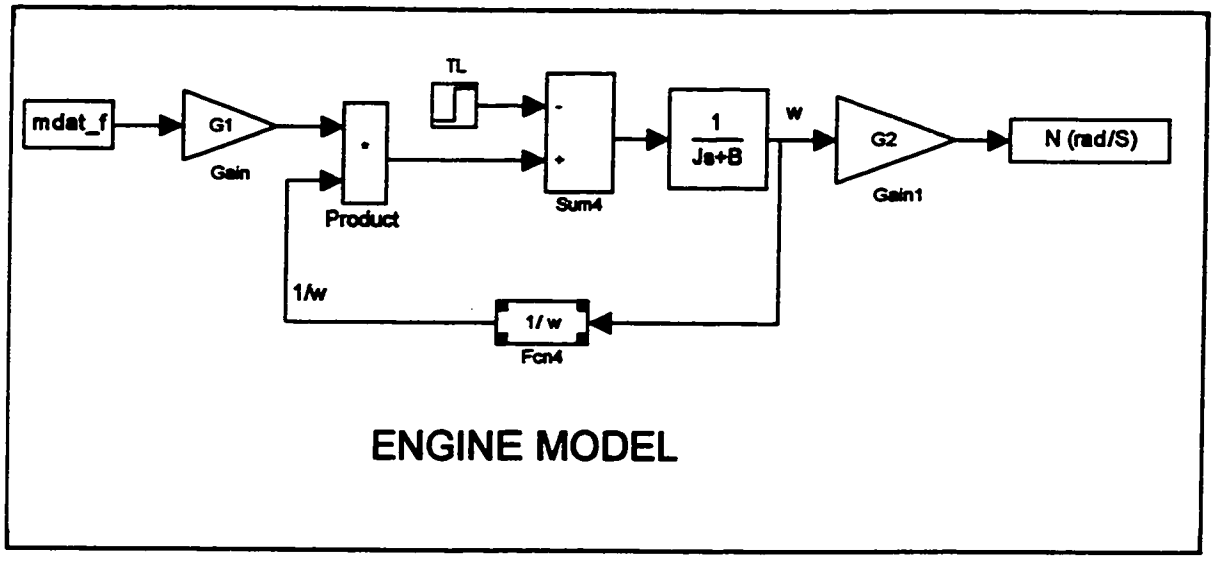

Figure 10.28 The Block Diagram of the Engine Model

Figure 10.28 shows the dynamic model of the engine. This model is linked with the fuel metering system model in order to investigate the impact of different control options on the complete system model.

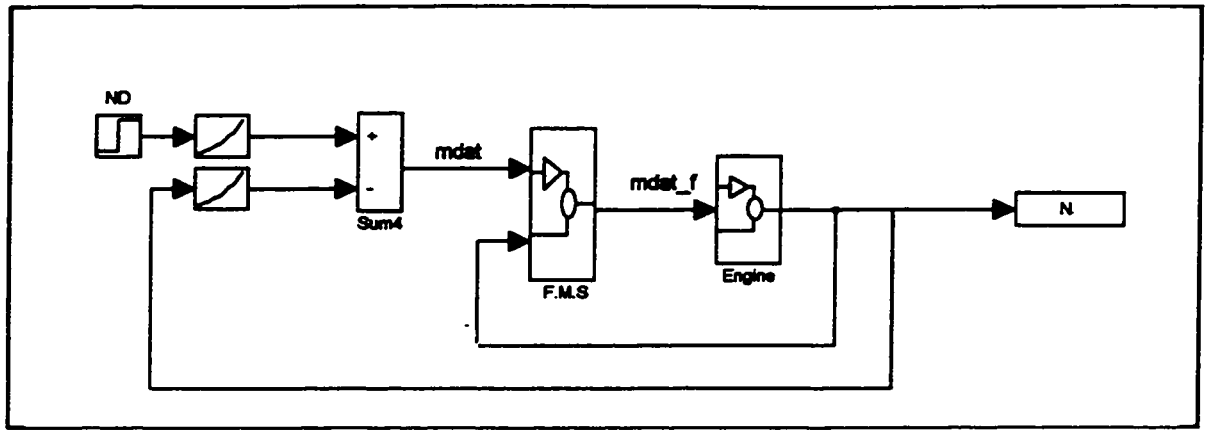

Figure 10.29 The Block Diagram of the Complete System Model

10.5 Comparison of Different Control Options

In this section, the dynamic response of the whole system with the engine speed feedback is investigated in order to evaluate the behaviour of the complete system when different control strategies are applied. Figure 10.29 shows the complete system model. As seen, the demand and the actual feedback engine speed are compared and the error is generated. Note that the controllers gains were obtained based on the fuel flow feedback, therefore, for the current system, the error should be evaluated based on the fuel flow. To do this, the engine speeds are converted to their equivalent fuel flow based on the fuel flow schedule for PT6-A27 engine, as shown in figure 10.27. Then the error is processed in the fuel metering system for different control options and thus the new fuel flow is evaluated based on the error and the current engine speed. The output fuel flow is applied to accelerate or decelerate the engine.

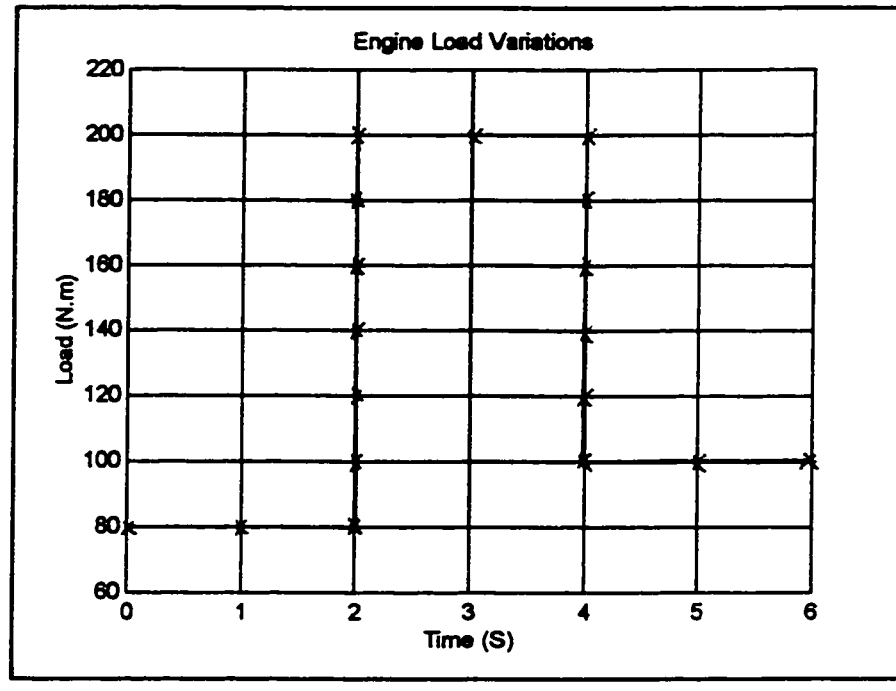

Figure 10.30 The Engine Load Versus Time

Results for the transient response of the engine speed using different control options for an abrupt change in the load (figure 10.30) are shown in figure 10.31. It is assumed that the load increases abruptly by 250% and then after 2 seconds, it reduces by 50%.

According to figure 10.31, the response of the second and the third control options are the fastest . The reason is that in both control options, both valves move in appropriate direction to speed up the fuel flow changes. The first control option which operates as a conventional fuel metering system, has the slowest response and its settling time is 0.5 second longer than the others. The response of the third option results in a little deviation from the engine speed at steady state. Because, after the nozzle flow reaches its 85% of its final value for steady state, the second controller which is controlling the differential pressure, is set on its steady state value. This

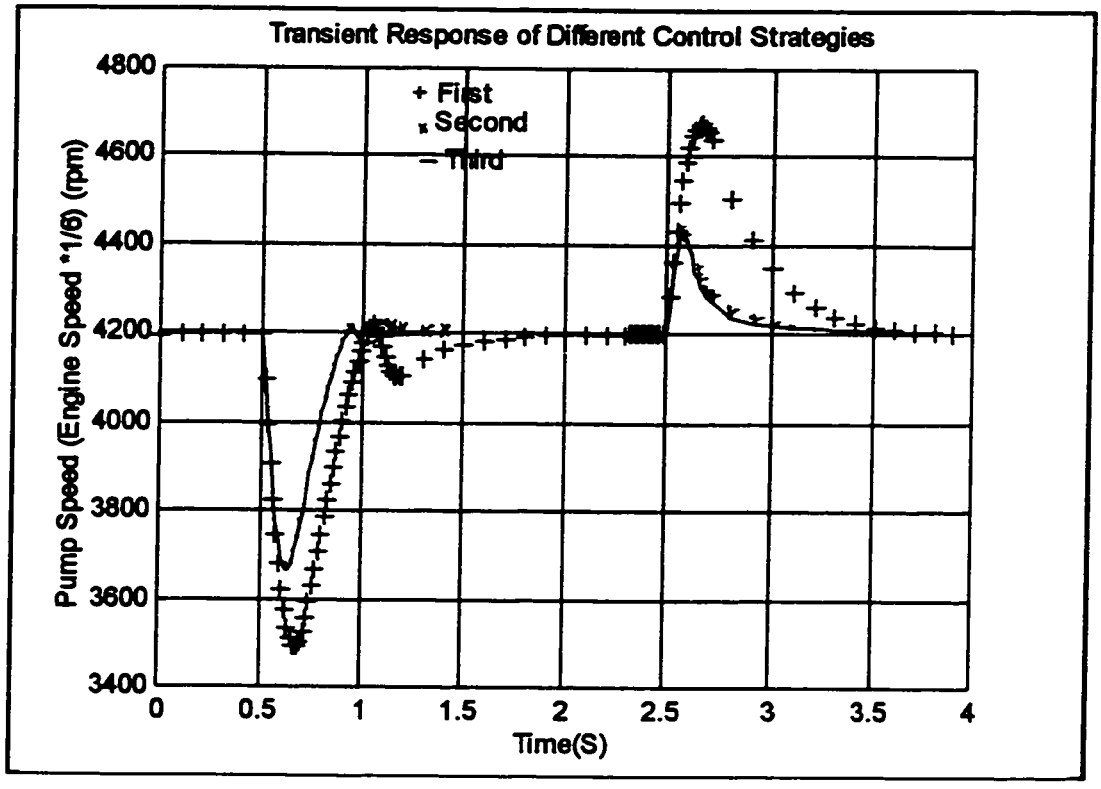

Figure 10.31 The Transient Responses of the Engine Speed For Different Control Options

causes the fuel flow to decrease and thus engine speed is reduced. However, at the same time, the first controller changes the position of the metering valve in order to compensate for the reduced fuel flow.

In general, the second control option, has the best dynamic response. However, due to fact that the dynamic response of the third control option is very similar to the response of the second control option, and also because the second control option does not have a unique positioning of the valves (and thus its response varies depending on the relative positioning of the valves, as explained in section 10.2), the third control option (new control strategy) is considered as the best for the proposed

fuel metering system. In the next section, the steady state and the dynamic response of the different fuel metering systems design configurations will be compared to determine the best configuration.

10.6 Comparison of Different Fuel Metering Systems Design Configurations

In this section, some of the selected low cost fuel metering system design configurations, which have been introduced in the thesis objectives and their mathematical models developed in chapter 6, are analyzed and compared regarding their deviations from fuel flow linearity, dynamic response and cost. These design configurations are:

- Fuel Metering System with Diaphragm Flat-Seat Bypass Valve and Varying Supply Pressure (Configuration 1)
- Fuel Metering System with Differential Pressure Flat-Seat Valve and Constant Supply Pressure (Configuration 2)
- Fuel Metering System with Bendix Bypass Valve and Varying Supply Pressure (Configuration 3)
- Double Plunger Fuel Metering System with Varying Differential Pressure and Back-Up Capabilities (Configuration 4)

Since the characteristics of the pump which is used to deliver the fuel to the injectors through the fuel metering systems has a direct impact on the fuel flow linearity and the cost of the fuel system for a particular engine, therefore, three different pumps which are *Constant Displacement Fuel Pump Driven by the Engine, Constant Displacement Fuel Pump Driven by a DC Electric Motor* and *Constant Displacement Fuel Pump Driven by a Constant Speed Electric Motor,* are considered in this investigation.

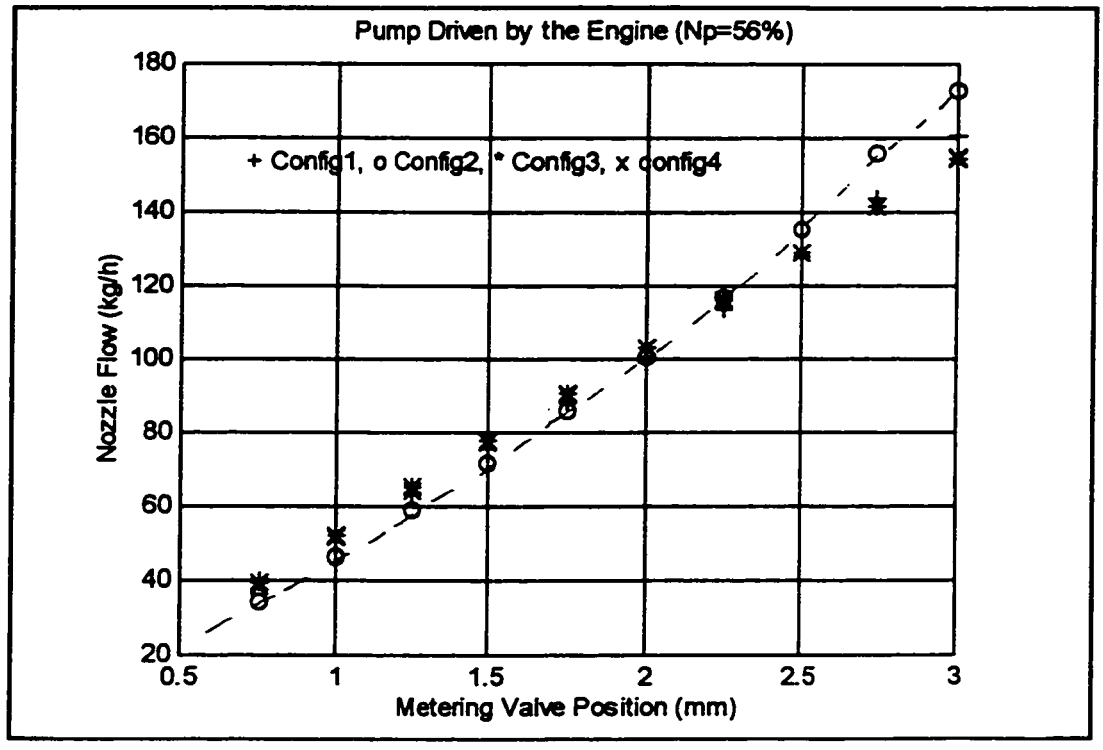

Figure 10.32 The Steady State Simulation Results with Different Design Configurations for the Nozzle Flow

10.6.1 Comparison of The Steady State Results

The steady state simulation results for the full travel of the metering valve of different design configurations and with the fuel pump driven by the engine at the constant speed of 3600 rpm (Np=56 %) are shown in figures 10.32 and 10.33. Based on the definition of the linearity presented in section 9.1.1, the deviation from the fuel flow linearity for each configuration, starting in sequence from the first configuration, is 8.2%, 28.64% , 2.5% and 0.91% respectively. Configuration 4 has the minimum deviation from fuel flow linearity. This is due to the fact that the bypass valve plunger in this configuration is controlled by an additional digital controller so that the differential pressure across the metering valve remains constant.

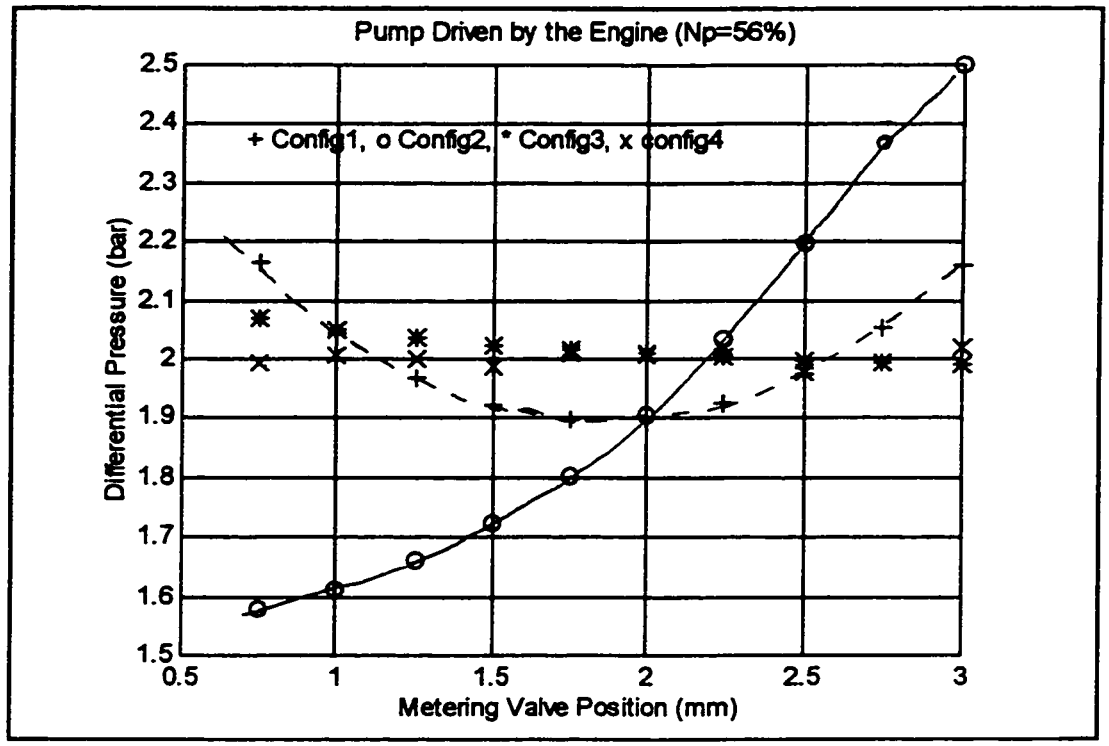

Figure 10.33 The Steady State Simulation Results for the Differential Pressure

The linearity of the third configuration is better than that of the configurations 1 and 2. However, the plunger and barrel of the bypass valve have sophisticated shapes and therefore, this configuration is more expensive to manufacture as compared to the first or second configuration.

Figure 10.32 also shows that for the second configuration, the relation between the metering valve position and the nozzle flow rate is most non-linear. According to reference [33], to maintain a constant differential pressure, the diameter of the inlet manifold controlled by the diaphragm must be as small as possible. Since for the PT6-A27 engine, higher fuel flow is required (the fuel metering system was originally designed for a maximum flow rate of 100 kg/ h), therefore, the diameter of the nozzle manifold was enlarged and consequently the non-linearity has been increased. In

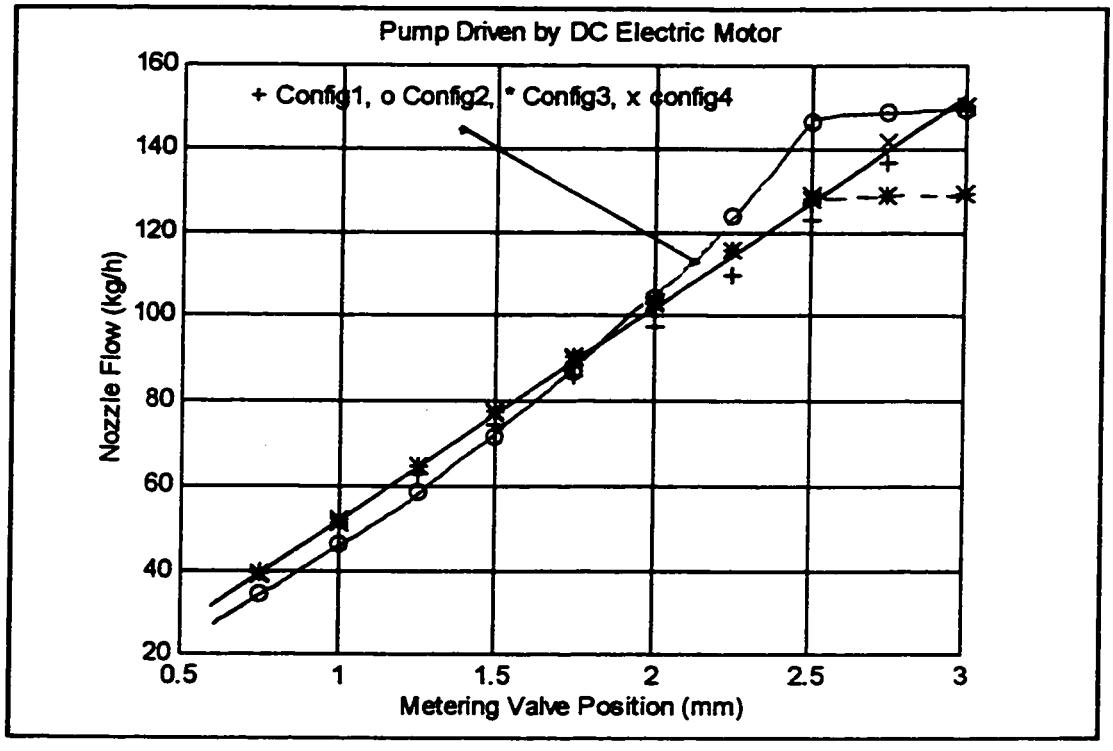

Figure 10.34 The Steady State Simulation Results for the Nozzle Flow

general, this fuel metering system is rather applicable to the engines with maximum fuel consumption less than 100 kg/h [33].

Finally, the figure 10.32 also indicates that the first configuration provides an acceptable linear relation between the metering valve position and the nozzle flow. This is due to the fact that the design parameters for this configuration were optimized

Figure 10.34 shows the fuel flow simulation results for different metering system design configurations which are supplied by a constant displacement pump driven by a DC electric motor. With this type of the pump, as the torque load (nozzle back pressure) increases, the pump speed decreases and, therefore, the pump output flow is reduced. As can be seen, the first and the fourth configurations provide the best linearity, as compared to other configurations. This is due to the fact that as the nozzle pressure increases, the fuel pump output decreases. However, by increasing

the nozzle pressure, the diaphragm in the first configuration and the bypass valve plunger in the fourth configuration restrict the fuel flow through the bypass valve and thus the nozzle flow can increase. Moreover, in these configurations, it is possible to close the bypass valve flow completely. This is not true for the third configuration where, to have a linear relationship between the nozzle flow and the metering valve position, the bypass valve plunger has been designed in such a way that the bypass valve flow has a minimum flow rate of 75 kg/ h. Therefore, as the bypass flow is reduced to 75 kg/ h, the nozzle flow is able to reach only about 130 kg/ h. This value is 20 kg/ h less than the maximum flow rate for the first and the forth configurations.

For the second configuration, the minimum fuel pressure provided by the pump is higher than the pre-set pressure of the pressure regulator and therefore, this configuration can be used with this pump. However, if this configuration is used for engines with the flow rate higher than 100 kg/ h, the linearity will suffer , due to the fact that the ratio of the inlet nozzle diameter to diaphragm diameter would be excessive.

In general, the first and the fourth configurations are more adaptable to this type of pump, i.e. they are less sensitive to the pump flow decline in case of pump speed decrease, caused by the increase of the nozzle back pressure.

The steady state simulation results for the pump driven by a constant speed electric motor is shown in figure 10.35. In this case, the increase of the pump torque (nozzle back pressure) does not have visible impact on the pump output flow which remains almost constant during the full pump operation. For steady state simulation, the pump flow was adjusted to 220 kg/ h. The figure shows that the maximum nozzle flow which could be delivered by the third configuration is about 140 kg/ h, which is 20 kg/ h less than the flow delivered by the other configurations. This means

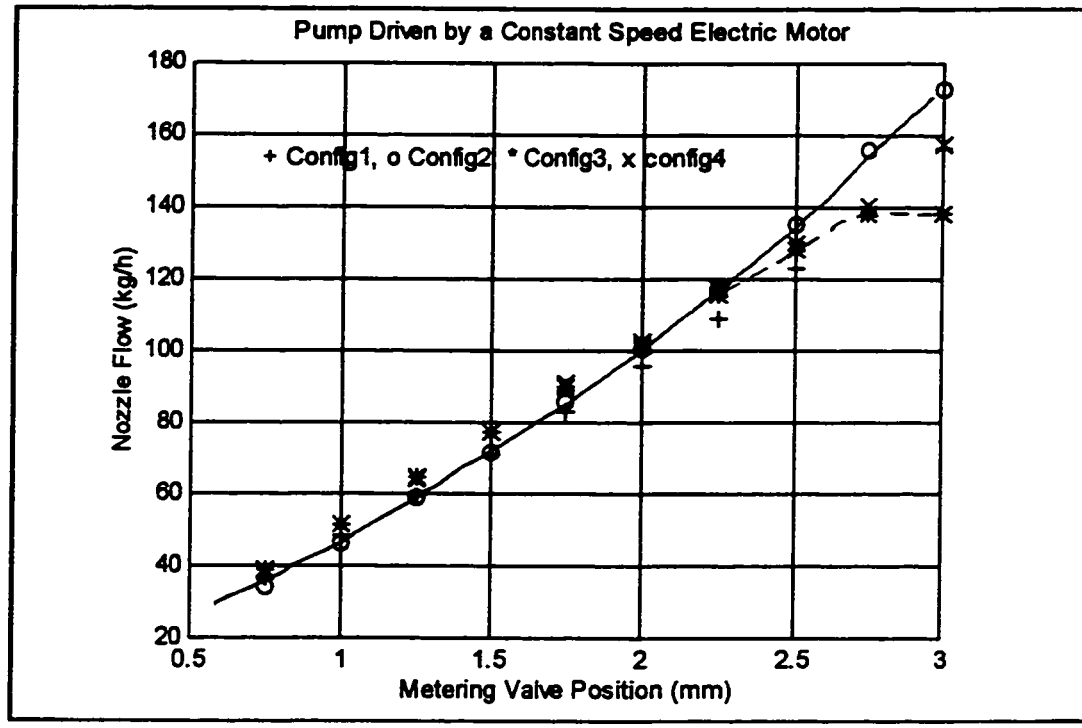

Figure 10.35 The Steady State Simulation Results for the Nozzle Flow

that for other configurations, even a smaller pump output could be accepted.

The response of the second configuration is the same as that for the fuel pump driven by a DC electric motor. This is due to the fact that in both cases, the pump pressures are controlled by the pressure regulator. This means that for this configuration, if the pump pressure produced by any type of pump, reaches the pre-set pressure of the regulator, then, the fuel flow linearity will be equal.

Finally, regarding the steady state operation, all configurations except configuration 2 have an acceptable linearity; however, in case when a fuel pump with smaller output would be used, the first and the forth configurations are rather recommended.

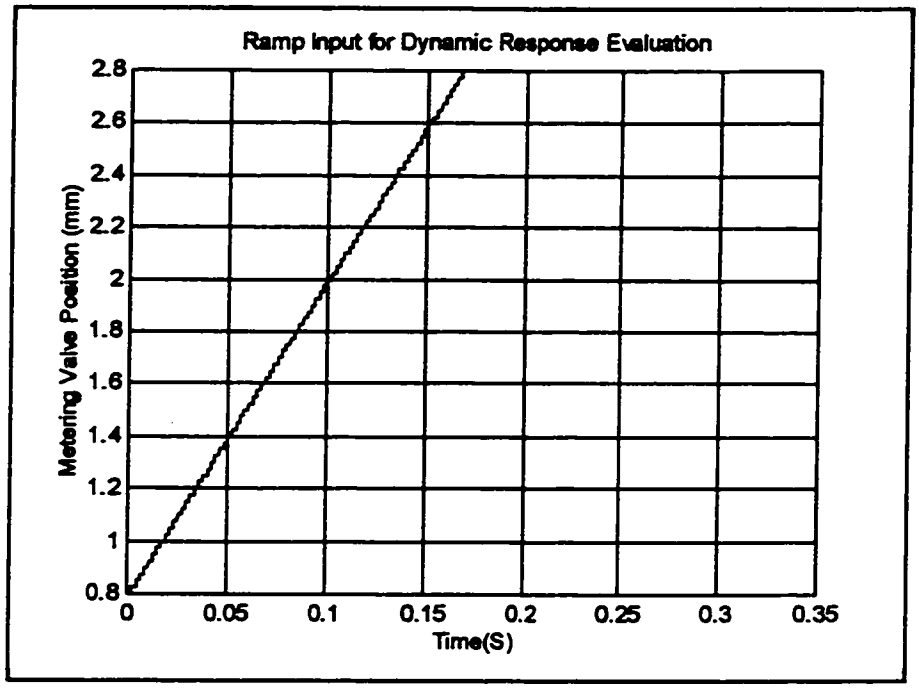

Figure 10.36 The Ramp Input for the Metering Valve Position

10.6.2 Comparison of Transient Responses for Different Design Configurations

To evaluate the dynamic response of the different design configurations, a ramp input was assumed for simulation; the metering valve moved from its initial position to final position in a ramp mode with a step size of 0.025 mm and with the stepping rate of 500 steps /s as shown in figure 10.36. It has to be mentioned here that for a complete comparison, the characteristics of the fuel pump, the metering valve, and the stepper motor, as well as the differential pressure across the metering valve, were considered the same for all configurations during both, the steady state and the transient response investigations.

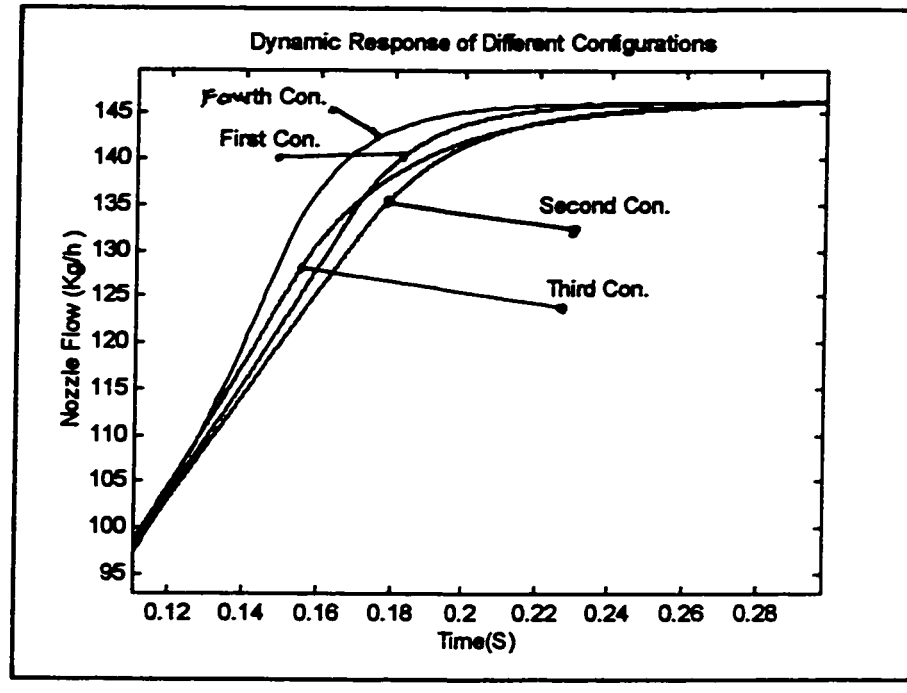

Figure 10.37 The Dynamic Response of the Different Design Configurations

Figure 10.37 shows the simulation results for a ramp input in the metering valve position. As seen, the fourth configuration has the best transient response. This is due to the fact that, the independently controlled bypass valve plunger, moved very fast to decrease the bypass flow in order to speed up the response.

The first configuration also has a faster response in comparison with the next two configurations due to its optimized design parameters and also due to the fast operation of the diaphragm to close the bypass flow. The third configuration has a faster response than the second configuration due to the restriction imposed on the bypass flow by the bypass valve plunger.

Finally, all design configurations have overdamped responses. This means that the response does not show any oscillation or overshoot and, therefore, it is quite appropriate for gas turbine engines. However, the fourth configuration has the best

performance and the most proper response. It shows a linear relation between the metering valve movement and the nozzle flow and also the fastest response as compared to the other configurations. Moreover, it can better comply with various types of fuel pumps and therefore, it provides more flexibility when used in gas turbine engines. Finally, its best advantage is its back-up capability, while none of the other configurations has this feature.

From the cost aspect, the first configuration is the cheapest one. Unlike the second configuration, it does not need any pressure regulator and also it can comply with various types of fuel pumps, especially with the electric fuel pumps which are now emerging in aircraft industry, following their acceptance in the automotive industry, as being more inexpensive in comparison with the other types of pumps. The third configuration, has a complicated plunger and barrel design for the bypass valve, which needs to be manufactured by the crush grinding method. This makes the third configuration more expensive, as compared to the first configuration. It is thus recommended to replace the first configuration with the third configuration due to the its lower cost and also to its satisfactory performance.

The cost comparison of the first and the fourth configurations is rather not simple. The first one acts just with one actuator, meanwhile, the latter acts with two actuators and plungers, therefore, its control is more complicated than for the first one. Moreover, some of the parts of the first configuration are already produced by Bendix Avelex and Bosch and therefore, they would be less expensive. However, the fourth configuration needs just a few parts. This means that from the cost aspect, the fourth configuration is more expensive, however, it provides the fuel metering system with more flexibility and back-up features.

11. CONCLUSIONS AND RECOMMENDATIONS

11.1 Conclusions

Two new, low cost, electronically controlled fuel metering systems for small gas turbine engines were presented and investigated. In the first system, a linear digital actuator was used to change the metering valve flow area, while a constant differential pressure across the metering valve was maintained by a diaphragm flat-seat bypass valve. The mathematical models for both the steady state and transient processes were developed and used for computer simulation. Next, experiments were performed in order to validate the models. It was proved that the models accurately predicted the performance of the first proposed fuel metering system and therefore, it could be used for the design optimization to improve its performance. Three design optimization criteria; the linearity between the nozzle flow versus metering valve travel, low sensitivity to the design parameters changes, and the short dynamic response time, were defined as the design optimization goals; next, a multi-objective optimization technique was developed to obtain the best design variables. The results showed that the first proposed fuel metering system has the ability to correctly manage the fuel flow demands at different operating conditions of the engine and, therefore, it can be proposed as a low cost replacement for the Bendix bypass valve in the DP-F2 and DP-F3 fuel control units.

Next, the feasibility of the second fuel metering system with a single barrel and double concentric plungers which are operated by two independently acting linear digital actuators was investigated. This system has the ability to speed up the dynamic response of the engine by varying the differential pressure across the metering valve.

Due to the flexibility offered by this fuel metering system, different control options were introduced and to compare them, a dynamic model for a gas turbine engine was presented and used. Based on the results obtained from the simulation of the engine with different control options, it was concluded that the best control strategy is provided by the third control option. In this control strategy (option), the differential pressure across the metering valve varied only in the initial part of the transient process and next, it is returned to its steady state value. Moreover, an additional advantage of this fuel metering system is its back-up capability. It was shown that during the failure of either the bypass valve or the metering valve actuator, the system was able to maintain the required fuel flow for the engine in order to return the aircraft home safely.

Finally, several fuel metering systems were compared, regarding their fuel flow linearity, dynamic response and cost when using different fuel pumps. It was concluded that both fuel metering systems (configurations 1 and 4) proposed in this thesis show a quite good linear relation between the nozzle fuel flow and the metering valve position. Moreover, they are able to work with different fuel pumps and in case of a constant displacement pump driven by a simple DC electric motor, they are less sensitive to the flow decline caused by the pump speed decrease as the result of the nozzle back pressure increase. This means that these configurations can be used with less expensive pumps with lower output, as compared to the other remaining configurations.

From the dynamic response aspect, both the proposed fuel metering systems provided a faster response as compared to other configurations. Moreover, their responses were underdamped. All these mean that the proposed fuel metering systems

could be used in small gas turbine engines.

Regarding the cost aspect of the proposed electronic fuel metering systems (EFMS), two types of comparison could be made:

When comparing all of the four configurations, including two previous electronic fuel metering systems (configurations 2 and 3) which have been developed earlier for Bendix Avelex Ltd. (Allied Signal Ltd.) with those of the hydro-mechanical (conventional) fuel control units (FCU) for small gas turbine engines (like Bendix DP-F2 FCU), there is an obvious cost reduction due to the lower number of parts, as well as to the use of some automotive parts which are commercially available at low cost.

When comparing the two presently proposed EFMS's (configuration 1 and 4) with those developed previously (configuration 2 and 3), there is a further reduction of cost, particularly for configuration 1, as compared with configuration 2 and 3, which represent similar control features. Configuration 1 is less expensive than 2 because it does not have a pressure regulator and can operate with less expensive fuel pumps. It is also much less expensive than configuration 3 which is using the Bendix bypass valve which requires much more machining time and tooling due to its complicated plunger-barrel design.

Cost comparison with configuration 4, however, is more difficult, due to the fact that this system is superior over the first three configurations. Despite its simple single barrel design, the need for two digital actuators and an on-off solenoid would increase its cost over that of the first configuration; also, it would cost more than the third configuration. Taking into consideration the additional advantages of faster dynamic response and back-up capability, as well as its small size and weight, it has

to be considered as functionally superior, and thus, as the most cost effective option.

In summary, this thesis has provided several contributions to the engineering knowledge. First, it proposed a new fuel metering system which is simple and less expensive as compared to other fuel metering systems for small gas turbine engines. Next, the impact of different fuel pumps on the behaviour of fuel metering systems was investigated. Then, the concept of a low cost fuel metering system with back-up capabilities for small gas turbine engines of remotely piloted vehicles was proposed and investigated. Finally, a control strategy was developed for controlling the digital linear actuators of a double actuator fuel metering system.

11.2 Recommendations For Future Work

To continue this research, the following work is recommended:

1. In this thesis, a simple dynamic engine model was formulated, in order to investigate the impact of the fuel metering system on the dynamic response of the engine. However, for more accurate results, it would be recommended, first, to model each component of a gas turbine engine such as compressor, turbine, combustion chamber etc and after establishing the interface between these components, the dynamic response of the engine would be investigated. In this way, not only the performance of the engine, but also the function of each component would be evaluated.
2. In this research, the dynamic response of the engine was evaluated using the engine and the fuel metering system models (Chapter 10). For more accurate evaluation of the fuel metering system, it would be recommended to set the fuel metering system to be run on a test bench and to interface it with a digital

computer representing the engine model (figure 11.1). In this case, the fuel pump speed and the linear digital actuator position would be controlled based on the signals from the engine model installed in the digital computer. As a result, the simulation results would be closer to the real operation of the engine and it could help to avoid the engine testing which is very expensive.

3. In this thesis, a PD controller was used to control the digital linear actuators. It is recommended to do more research for choosing the best type of the controller and to optimize its parameters. It is also possible to employ concepts from the modern control theory such as state feedback control and adaptive control to design a dedicated controller for the proposed fuel metering systems.

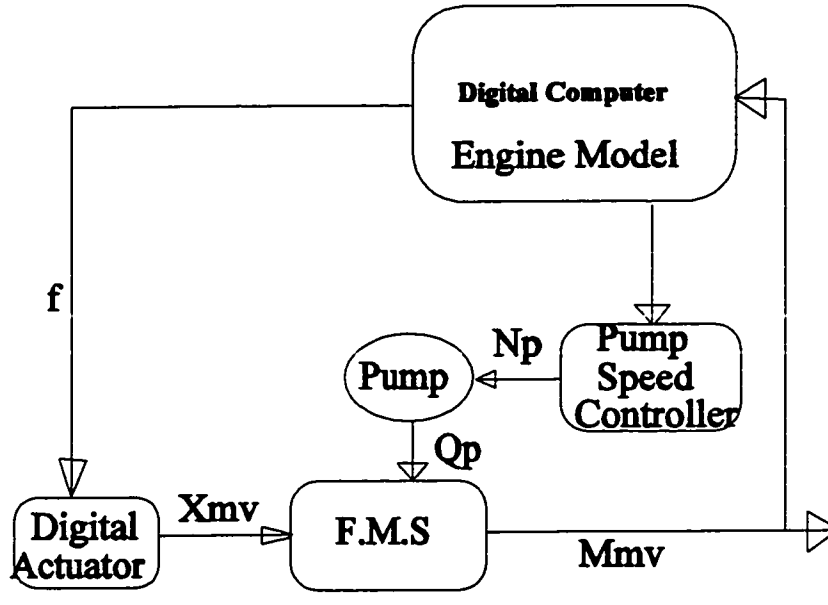

Figure 11.1 Schematic of the Proposed Test Set-Up

12. REFERENCES:

1. R. G. Moore, "Fuel System Requirements for Small Gas Turbine Engines", SAE paper 740381, April 1974.
2. W. C. Peck,"Microelectronics in Fuel Controls", SAE paper 650529, May 1965.
3. R. Falk,"Digital Techniques Applied to the Control of Gas Turbine Engines", SAE paper 650528, May 1965.
4. M. F. Keck, J. J. Fredlake, and G. V. Schwent, "A control Concept Combining the Best of the Current Hydromechanical and Electronic Technologies", SAE paper 740380, April 1974.
5. J. S. Frew and M. F. Keck, "Electronic Control System for a Modern Turboprop Engine", SAE paper 810620, April 1981.
6. A.I. Georgants, and T. Krepec, "Low Cost Electronic Fuel Control Unit for small Gas Turbine Engines of Remotely Piloted Vehicles", Progress Report No. 1. to Bendix, Avelex, Concordia University, 1987.
7. J. J. Fredlake, and M. R. Adams, "Electronic Control System for Executive Jet Aircraft", SAE paper 831478, February 1983.
8. D. J. Hawes, "Electronic Fuel Controls-Who Needs Them?", SAE paper 810619, April 1981.
9. R. D. Porter, "The influence of Microcomputer Technology on Propulsion Management System Design", SAE SP, 1975.
10. J. L. Lockenour and G. P. Layton, "RPRV Research Focus on HiMAT", Astronautics and Aeronautics, Published by the AIAA, New York, April 1976.

11. J. E. Bayati, "The HiMAT RPRV Propulsion Control System", SAE paper 760887, November 1976.

12. J. F. Bussell, "Failure Survival Aspects of a Digital Fuel Control System", SAE paper 751062, November 1975.

13. R. M. Evans, "Hybrid Computer Simulation in Digital Fuel Control Design", SAE paper 821373, October 1982.

14. R. M. Evans and C. Cusson, "Development of a Full Authority Digital Electronic Control For a Gas Turbine Engine Using a Hybrid Computer System as a Design Aid", Summer Computer Simulation Conference, Newport Beach, July 1978.

15. D. Hawes, R. Evans, "NDEC- A Control Concept for Helicopter Gas Turbines 36th Annual Forum of the American Helicopter Society, Washington D.C., May 1980.

16. J. P. Kuhleberg, J. Kniat, D. M. Newirth, J. C. Jamison and J. R. Switalski, "Transport Engine Control Design", 18-th Joint Propulsion Conference, Cleveland, Ohio, 1982.

17. B. A. Barclay, T. G. Lenox and C. J. Bosco, "Full Authority Digital Electronic Control- Highlights of Next Generation Propulsion Control Technology, ASME paper 78-GT-165, April 1978.

18. R. W. Vizzini, T. G. Lenox, and R. J. Miller, "Full Authority Digital Electronic Control Turbofan Engine Demonstration", SAE paper 801199, October 1980.

19. R. W. Vizzini and P. D. Toot, "Full Authority Digital Electronic Control Application to a Variable Cycle Engine", SAE paper 801203, October 1980.

20. K. L. Linebrink and R. W. Vizzini, "Full Authority Digital Electronic Control Augmented Fighter Engine Demonstration, SAE paper 821371, October 1982.

21. M. E. McGlone, R. J. Miller, W. J. Davis, and P. T. Adams, "Full Authority Fault Tolerant Electronic Engine Control Systems for Advanced High Performance Engines (FAFTEEC), SAE paper 821398, October 1982.

22. P. B. Sisson and D. K. Faymon,"Digital Control Brings Large Turbofan Benefits to the Regional Jetliner Turbofan Market", International Gas Turbine and Aero engine Congress and Exposition, The Hague, Netherlands, June 1994.

23. D. H. Middleton, "Avionic Systems", Longman Scientific & Technical, U. K. 1989.

24. A. Solomon, "Full Authority Digital Electronic Control of Pratt & Whitney 305 Turbofan Engine", SAE paper 911018, April 1991.

25. J. F. Kuhlberg and W. Zimmerman, "Flight Test of All-Electronic Propulsion Control System", paper AIAA-80-1147 presented at AIAA-SAE-ASME 16th Joint Propulsion Conference, Hartford, June 30, 1980.

26. J. Kniat and J. A. Bluish, "An Application of Redundancy in Digital Electronic Engine Control", SAE paper 801200, October 1980.

27. F. C. Zuliani, and G. N. Kline, "Microcomputer Brings Digital Power to the Small Gas Turbine", SAE paper 821402, October 1982.

28. Microcomputers Applied to Small Aircraft Gas Turbines, Aerospace Engineering, pp 18-22, March 1983.

29. G. D. Cropper, "Electronic Fuel Controls for Missile and RPV Gas Turbines", SAE paper 751061, November 1975.

30. D. G. Burnell, M. A. Cole, T. B. Morrison, A. H. White, and R. D. Zagranski, "Miniaturized High Speed Controls for Turbine Engines", Technical Report AFAPL-TR-74-93, August 1974.

31. A.I. Georgants, G. Carrese and T. Krepec, "Low Cost Electronic Fuel Control Unit for small Gas Turbine Engines of Remotely Piloted Vehicles", Progress Report No. 3 to Bendix, Avelex, Concordia University, 1989.

32. T. Krepec and A.I. Georgants, "New Family of Low Cost Electronic Fuel Control Units for Small Gas Turbine Engines", SAE paper 901039, April 1990.

33. G. Carrese, T. Krepec and C.H. To, "Simulation, Testing and Optimization of a New Low Cost Electronic Fuel Control Unit for Small Gas Turbine Engines", SAE paper 901027 , April 1990.

34. Bosch, "Automotive Electrical/Electronic System", Robert Bosch, Gmbh, Stuttgart, 1988.

35. A.I. Georgants, T. Krepec, and G. Carrese, "Computer Aided Development of a Simple Electronic Fuel Control Unit for Remotely piloted Flying Vehicles", International Computers in Engineering Conference and Exhibition, ASME, Boston, August 1990.

36. Bendix Corporation, "DP-F2 Gas Turbine Fuel Control" Service Manual 1976.

37. T. Krepec, H. Hong, A. I. Georgants, "Optimization of A Diaphragm Type Differential Pressure Valve Using CAD Techniques", Eighth World Congress on the Theory of Machines and Mechanisms, Prague, Czechoslovakia, August 1991.

38. A.I. Georgants, T. Krepec and R. M. H. Cheng, "Application of a Double Actuator Electronic Fuel Control Unit on a Small Gas Turbine Engine", SAE paper 912160, September 1991.

39. A. I. Georgants, G. Carrese and T. Krepec, "Designing and Tuning the Digital Controller of an Electronic Fuel Control Unit for Small Gas Turbine Engines", SAE paper 892255, September 1989.

40. K. B. Swonger, and M. F. Huffman, "Low Cost Control System for Expandable Turbine Engines", AIAA/ASME/SAE/ASEE, 25th Joint Propulsion Conference, AIAA-89-2586, Monterey, CA, July 10-12, 1989.

41. J. Bennett, Allied Signal Fluid Systems,"Fuel-Metering Valve Design Innovations", Journal of Aerospace Engineering, October 1993.

42. Bosch, "Automotive Handbook", Robert Bosch, Stuttgart, 1986.

43. Digital Linear Actuators, Airpax Catalog, 1983.

44. Intel, "ASM 96 Software Development Package", Reference Guide, 1988.

45. Intel, "EV80C196KB Microcontroller Evaluation Board", User's Manual, Release 001, February 20, 1989.

46. Intel, "16-bit Embeded Controllers", Reference Guide, 1991.

47. Rolls Royce, "The Jet Engine" Derby, England, 1973

48. Sciemetric Instruments Incorporation, "System 200 Hardware User Guide", December 1990.

49. Sciemetric Instruments Incorporation, "Gen 200 Software User Guide", May 1990.

50. The MATH Works Incorporation, "Matlab User's Guide", August 1992.

51. The MATH Works Incorporation, "Simulink User's Guide", April 1993.

52. G.F. Forsythe, M.A. Malcolm, C.B. Moler, "Computer Methods for Mathematical Computations", Prentice Hall, 1977.

53. K. Ogata, "Modern Control Engineering", Prentice Hall, 1982.

54. N. S. Nise, "Control System Engineering", The Benjamin / Cummings Publishing Company Incorporation, 1992.

55. A. Goicoechea, D. R. Hansen, L. Duckstem, "Multiobjective Decision Analysis with Engineering and Business Applications", John Wiley & Sons, 1982.

56. L. A. Zadeh, "Optimality and Non Scaler-Valued Performance Criteria", IEEE Transaction Automatic Control, Vol. Ac-8, p1, 1963.

57. Y. Censor, "Pareto Optimality in Multiobjective Problems", Applied Mathematical Optimization, Vol 4, pp 41-59, 1977.

58. The MATH Works Incorporation, "Optimization Toolbox User's Guide", January 1994.

59. F.W. Gembicki, "Vector Optimization for Control with Performance and Parameter Sensitivity Indices, "Ph.D. Dissertation, Case Western Reserve University, Cleveland, Ohio, 1974.

60. United Technologies Pratt & Whitney Canada, "PT6A-21, 27 and 28 Turboprop Engines, Descriptive Notes", October 1984.

APPENDIX A

CALIBRATION CURVES

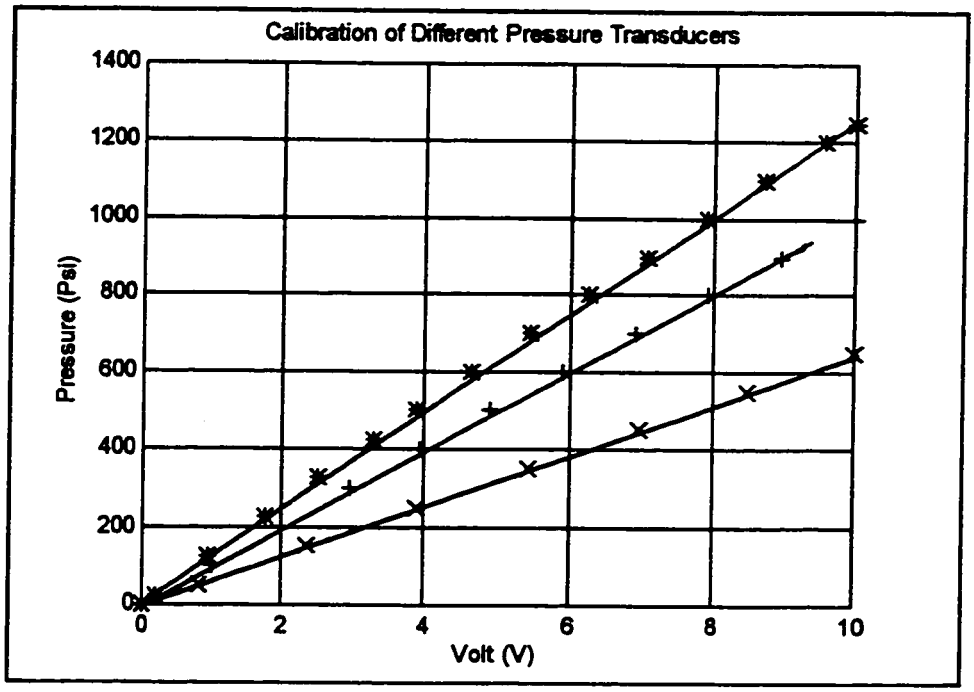

Figure A.1 Calibration Curves for Pressure Transducers

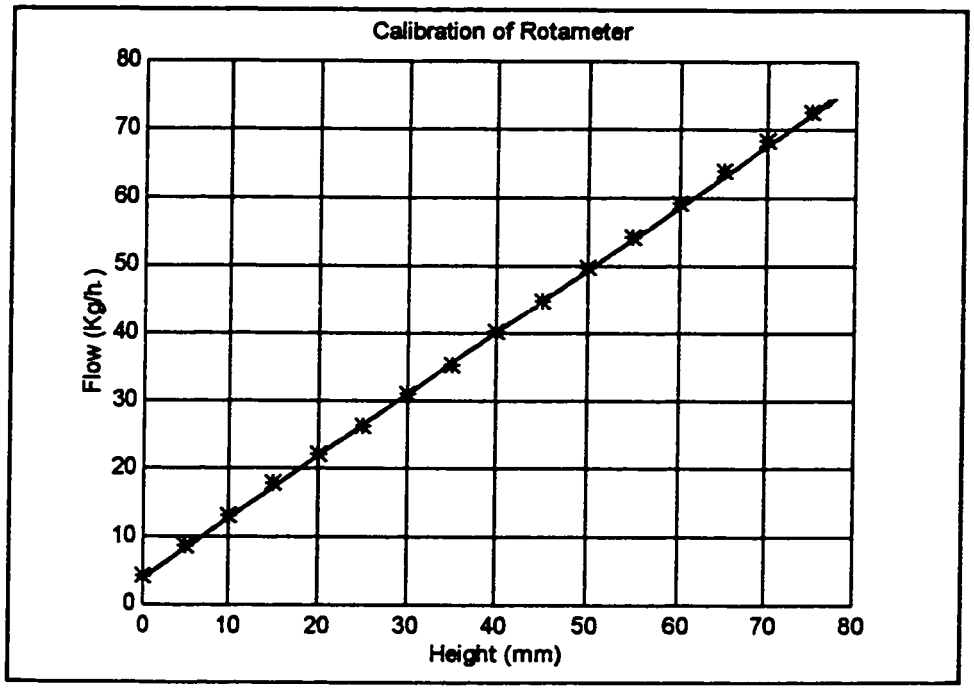

Figure A.2 Calibration of Rotameter

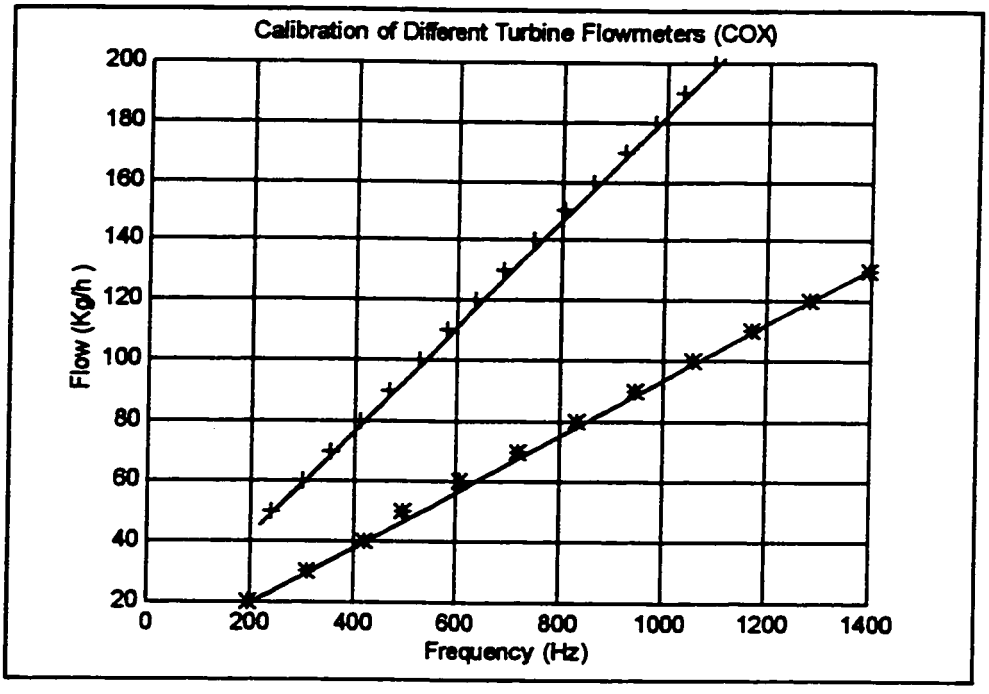

Figure A.3 Calibration of Cox Turbine Flowmeters

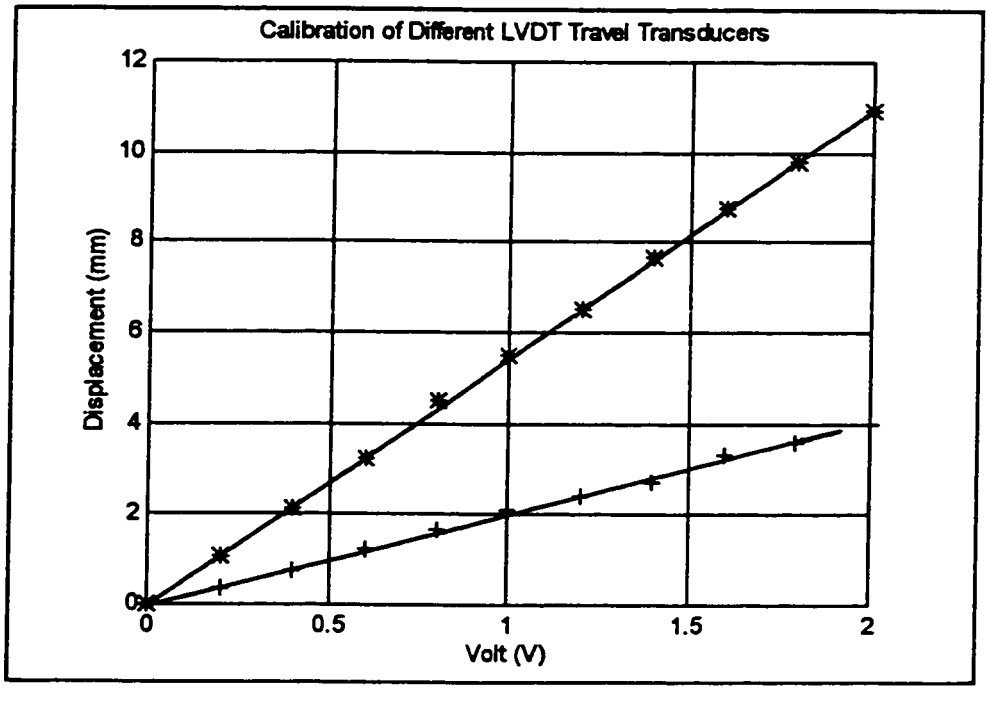

Figure A.4 Calibration of LVDT Travel Transducers

CALIBRATION FLUID

AlliedSignal Aérospatiale Canada Inc.
200 boul. Marcel-Laurin
Montréal, Québec
H4M 2L5

AlliedSignal AEROSPACE

Description:	*REFERENCE ONLY*	Issue No. Prod Code:
CALIBRATING FLUID		[illegible]
		REV DATE: 1995/05/05

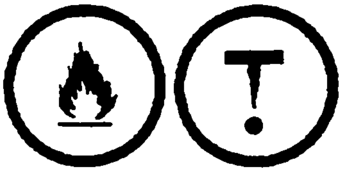

SECTION A: GENERAL INFORMATION

GENERAL..........................THIS MATERIAL IS A CALIBRATING FLUID FOR
AIRCRAFT FUEL SYSTEM COMPONENTS.
AT ASACa IT IS USED SPECIFICALLY AS A FUEL
TEST STAND FLUID.

REFERENCE SPECIFICATION......MATERIAL TO MEET THE REQUIREMENTS OF
MIL-C-7024, TYPE II, LATEST ISSUE
SAMPLE TO BE APPROVED PRIOR TO DELIVERY

SECTION B - APPROVED VENDOR LIST

CASTROL CANADA................CALIBRATING FLUID

HARRISON & CROSFIELD,
MONTREAL, QUEBEC............NAPHTHA SPIRITS

ASHLAND CHEMICAL, 1817 W.
INDIANA AVE., SOUTH BEND,
INDIANA.......................360 CALIBRATING FLUID

SECTION C - PROCUREMENT INSTRUCTIONS

PURCHASE ORDERS...............THE SUPPLIER MUST MEET THE SPECIFICATIONS
DEFINED IN THIS SECTION.
ALL SHIPMENTS WHICH ARE NOT PROPERLY LABELLED
IN ACCORDANCE WITH THE TRANSPORT OF DANGEROUS
GOODS REGULATIONS WILL BE RETURNED, FREIGHT
COLLECT.
THE SUPPLIER MUST FURNISH A VALID MATERIAL
SAFETY DATA SHEET WITH EACH SHIPMENT.

PURCHASE ORDER TO SPECIFY:..MATERIAL TO MEET THE REQUIREMENTS OF
MIL-C-7024, TYPE II, LATEST ISSUE
SAMPLE TO BE APPROVED PRIOR TO DELIVERY

VENDOR DOCUMENTATION
REQUIRED.....................CERTIFICATE OF COMPLIANCE REQUIRED FOR EACH

AlliedSignal Aérospatiale Canada Inc.
200 boul. Marcel-Laurin
Montréal, Québec
H4M 2L5

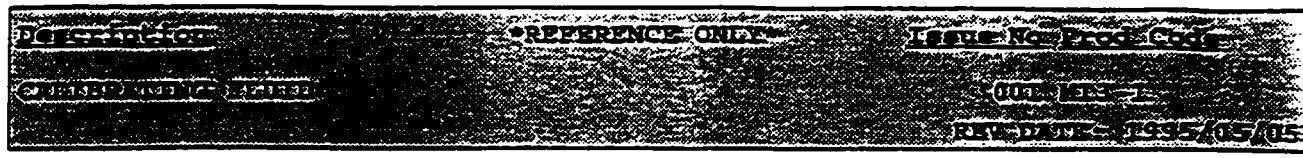

SECTION 6 - PROCUREMENT INSTRUCTIONS (CONT.)

SHIPMENT
PACKAGING INSTRUCTIONS.....BULK DELIVERY BY TANKER TRUCK TO STORAGE AREA

SECTION 7 - MATERIAL ACCEPTANCE

SUBMISSION TO MPE.....SAMPLE TO BE TESTED PRIOR TO DELIVERY - TEST CELL MAINTENANCE BEING INFORMED OF RESULTS BY MEMO IN ORDER TO ACCEPT DELIVERY
RECEIVING REPORT TO BE SUBMITTED FOR COMPLETION AFTER RECEIVING DELIVERY
SHELF LIFE.....INDEFINITE
MPE TEST PROCEDURES.....SPECIFIC GRAVITY AND VISCOSITY PER LP #70
TEST CELL MAINTENANCE TO NOTE RECEIVING REPORT NUMBER, DATE OF DELIVERY, QUANTITY AND INITIAL THE LOG BOOK
SPECIAL STORAGE.....BULK STORAGE LOADING PROCEDURES TO BE FOLLOWED

SECTION 8 - MISCELLANEOUS INFORMATION

REVISION.....NEW SECTION ADDED - SECTION 0
ORIGINATOR.....HANS BROUWER
ORIGINATOR DATE.....1994/08/31
REVIEWED BY.....CONFORM-ACTION DATA SYSTEMS
REVIEW DATE.....1994/09/20
APPROVED BY.....JOE RITLOP
APPROVAL DATE.....1994/10/13
1995/05/05

SECTION 9 - MANUFACTURER INFORMATION

DISCLAIMER.....THE INFORMATION CONTAINED IN THIS MSDS IS BASED ON DATA FROM SOURCES CONSIDERED TO BE RELIABLE, BUT ASACa DOES NOT GUARANTEE THE ACCURACY OR COMPLETENESS THEREOF. THE INFORMATION IS PROVIDED AS A SERVICE TO PERSONS PURCHASING OR USING THE MATERIAL TO WHICH IT REFERS AND ASACa EXPRESSLY DISCLAIMS

AlliedSignal Aérospaciale Canada Inc.
200 boul. Marcel-Laurin
Montréal, Québec
H4M 2L5

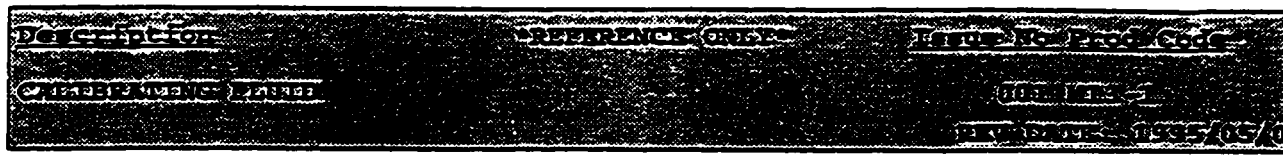

ALL LIABILITY FOR LOSS OR DAMAGE, INCLUDING CONSEQUENTIAL LOSS, OR FOR INJURY TO PERSONS (INCLUDING DEATH) ARISING DIRECTLY OR INDIRECTLY FROM RELIANCE UPON THE INFORMATION OR USE OF THE MATERIAL.

FABRICANT / MANUFACTURER....CASTROL CANADA INC.
3660, LAKESHORE BOUL. WEST
TORONTO, ONTARIO
M8W 1P2

SUPPLIER 24 HOUR PHONE NUMBER.....416-252-5511
CHEMICAL FAMILY.....HYDROCARBON
FIRST AID.....REPORT TO MEDICAL CENTER
DANGER PRECAUTIONS....MAY CAUSE IRRITATION TO SKIN AND/OR EYES - AVOID CONTACT
COMBUSTIBLE - KEEP AWAY FROM HEAT AND FLAMES

HAZARD RATING
HEALTH.....2
FIRE.....2
REACTIVITY.....0

SECTION 2 - HAZARDOUS INGREDIENTS

INGREDIENT	%CONC.	TLV TWA-ACGIH	C.A.S.	LD/50	LC/50
NAPHTHA (PETROLEUM, HYDROTREATED HEAVY	90	NOT KNOWN	64742-48-9	NOT ESTABLISHED	NOT ESTABLISHED

SECTION 3 - PHYSICAL DATA

PHYSICAL STATE.....LIQUID
APPEARANCE & ODOR.....CLEAR COLOURLESS PETROLEUM ODOR
PH (AS IS).....NOT AVAILABLE
ODOR THRESHOLD (PPM).....NOT AVAILABLE
SPECIFIC GRAVITY @ 20°C.....0.772
BOILING POINT (°C).....> 155°C
VAPOUR PRESSURE (MMHG).....2.9
VAPOUR DENSITY (AIR=1).....4.9

AlliedSignal Aérospatiale Canada Inc.
200 boul. Marcel-Laurin
Montréal, Québec
H4M 2L5

AlliedSignal AEROSPACE

[redacted]

SECTION 3 - PHYSICAL DATA (CONT.)

FREEZING/MELTING POINT (°C)	NOT AVAILABLE
EVAPORATION RATE (BUTYL ACETATE = 1)	0.21
VOLATILES (%) BY VOLUME	100
SOLUBILITY IN WATER (%)	NEGLIGIBLE
COEFFICIENT OF WATER/OIL DIST.	NOT AVAILABLE
VOLATILE ORGANIC COMPOUNDS	NOT AVAILABLE

SECTION 4 - FIRE & EXPLOSION DATA

FLAMMABILITY	COMBUSTIBLE
IF YES, UNDER WHICH CONDITIONS?	EXCESSIVE HEAT, SPARKS AND OPEN FLAME
EXTINGUISHING MEDIA	CARBON DIOXIDE, DRY CHEMICAL, FOAM DO NOT USE WATER SAND
SPECIAL PROCEDURES	FIREFIGHTERS SHOULD WEAR THE USUAL PROTECTIVE GEAR COOL EXPOSED CONTAINERS WITH WATER SPRAY
FLASH POINT (°C), METHOD	39°C - TCC
AUTO IGNITION TEMPERATURE	NOT AVAILABLE
UPPER FLAMMABLE LIMIT (% VOL)	6.0
LOWER FLAMMABLE LIMIT (% VOL)	1.0
EXPLOSION DATA	
SENSITIVITY TO STATIC DISCHARGE	IF HEATED, THIS PRODUCT WILL EMIT VAPORS WHICH COULD BE SUSCEPTIBLE TO STATIC DISCHARGE
SENSITIVITY TO IMPACT	NOT EXPECTED
RATE OF BURNING	NOT AVAILABLE
EXPLOSIVE POWER	VAPOUR FORMS EXPLOSIVE MIXTURE WITH AIR BETWEEN UPPER AND LOWER EXPLOSIVE LIMITS CONTAINER MAY EXPLODE UNDER FIRE CONDITIONS
HAZARDOUS COMBUSTION PRODUCTS	OXIDES OF CARBON (CO,CO2) SMOKE

IMAGE EVALUATION
TEST TARGET (QA-3)

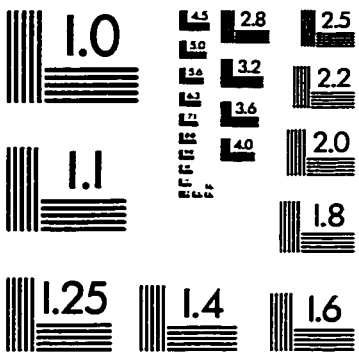

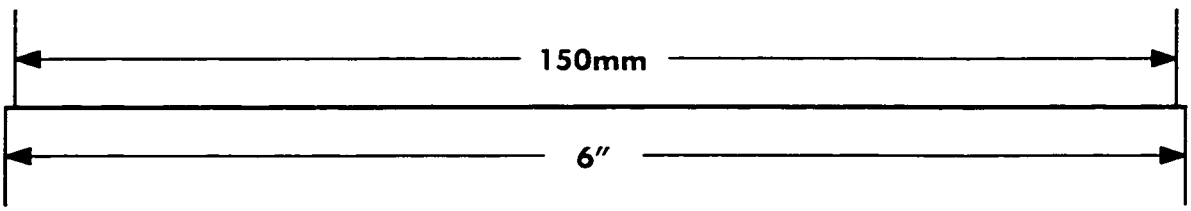

APPLIED IMAGE, Inc
1653 East Main Street
Rochester, NY 14609 USA
Phone: 716/482-0300
Fax: 716/288-5989